UNIVERSIDAD COMPLUTENSE DE MADRID

FACULTAD DE CIENCIAS MATEMÁTICAS

TESIS DOCTORAL

Entrelazamiento y correlaciones en sistemas cuánticos de muchos cuerpos

Entanglement and correlations in quantum many-body systems

MEMORIA PARA OPTAR AL GRADO DE DOCTOR

PRESENTADA POR

Andrea María Cadarso Rebolledo

DIRECTORES

David Pérez García
Juan José García Ripoll

UNIVERSIDAD COMPLUTENSE DE MADRID
FACULTAD DE CIENCIAS MATEMÁTICAS
DEPARTAMENTO DE ANÁLISIS MATEMÁTICO

TESIS DOCTORAL

Entrelazamiento y correlaciones en sistemas cuánticos de muchos cuerpos

Entanglement and correlations
in quantum many-body systems

Memoria para optar al grado de Doctor
presentada por:

Andrea María Cadarso Rebolledo

Bajo la dirección de los doctores:

Dr. David Pérez García
Dr. Juan José García Ripoll

UNIVERSIDAD COMPLUTENSE DE MADRID
SCHOOL OF MATHEMATICS
DEPARTMENT OF MATHEMATICAL ANALYSIS

Entanglement and correlations in quantum many-body systems

Analytical and numerical methods
in quantum information and computation

A thesis submitted in fulfillment
of the requirements for the degree of
Doctor of Philosophy in Mathematics

Andrea María Cadarso Rebolledo

Advisors:

Dr. David Pérez García
Dr. Juan José García Ripoll

A mis padres, Luis y Chelo.

Contents

List of Figures

List of Tables

Agradecimientos

Esta tesis doctoral es fruto del trabajo realizado a lo largo de cuatro años y de la colaboración y el apoyo de muchas personas, a las que debo mi más sincera gratitud.

En primer lugar, quiero dar las gracias a mis directores de tesis, Juan José García Ripoll y David Pérez García, por su tiempo, buenos consejos, generosidad y paciencia. Gracias Juanjo, por tu puerta abierta desde el primer día y por compartir tus amplios conocimientos sobre física. Gracias David, por encontrar siempre un hueco para hablar en la pizarra y por el entusiasmo constante por las matemáticas que siempre transmites. Gracias a ambos por vuestra dedicación, por las muchas preguntas que habéis contestado en detalle y por el inagotable compromiso con vuestro trabajo.

Gracias a los miembros del grupo QUINFOG, en el Instituto de Física Fundamental (CSIC), con los que he compartido comidas en el comedor del CSIC, conversaciones, viajes a congresos y grandes momentos. Gracias a Juan León, Jordi Mur, Jaime Julve, Alejandro Bermúdez, Hans Westman, Andreas Kurcz, Diego G. Olivares, Miguel Montero y Johannes Junemann. Gracias Borja, por las conversaciones en el despacho y por tu buen humor, gracias Marco, por tus perlas de sabiduría pero sobre todo por el insuperable viaje a Malta, gracias Carlos, por las charlas de café, por las cenas en Inglaterra junto a Mencha y Nicolás y por tus extraordinarias imitaciones. Gracias Edu, por tu amistad desde los inicios en Hypatia hasta el día de hoy. Gracias Emilio, por tener siempre a mano una buena palabra o un temazo de música con el que alegrar el día, ha sido un auténtico placer compartir el despacho contigo.

También me gustaría dar las gracias al grupo de Matemáticas e Información Cuántica de la UCM, en especial, gracias a Nacho Villanueva, Carlos Fernández, Carlos González, Carlos Palazuelos, Sofyan Iblisdir, y a los ex-miembros, Angelo Lucía, Toby Cubitt y Tom Cooney.

Durante el desarrollo de esta tesis tuve la oportunidad de visitar el grupo de teoría del Instituto Max Planck de Óptica Cuántica. Me gustaría agradecer a Ignacio Cirac y a Mari Carmen Bañuls la invitación y la posibilidad de conocer el grupo y el instituto. Agradezco también a Gemma de las Cuevas, Michael

Lubasch, a Juan Bermejo Vega y al resto de integrantes del grupo, las agradables conversaciones y tiempo compartido durante mis visitas.

Debo mucho a mis amigos, Miriam, Patri, Marina, Anuka, a los frikimáticos, Alba y Pablo, Jorge y Leire, Cruz, Omar y Vero, por los buenos momentos que hemos pasado juntos en los últimos años y por vuestras numerosas palabras de ánimo y comprensión.

Quiero dar las gracias al equipo de Quantitative Development de BBVA por haberme dado la posibilidad de desarrollar mi carrera profesional mientras elaboraba esta tesis doctoral.

Gracias a mi familia, en especial a mis padres, Luis y Chelo, que siempre me han apoyado, a Alfonso y a Carmen, a mis hermanos, Pablo, Luis y Alejandro, a mis abuelas, Chelo y Maruja, y a mi madrina, Carmen María. Gracias también a Carmen, Antonio y Raquel por hacerme sentir parte de vuestra familia en Madrid.

A todas las personas que formáis parte de mi vida, gracias por vuestro apoyo, esta tesis existe gracias a todos vosotros.

Por último, gracias, Álvaro, por tu apoyo constante, por estar a mi lado durante el tiempo que he dedicado a escribir esta tesis y ayudarme a mejorar cada día, pero sobre todo, por hacerme feliz.

Part I

Introduction

Resumen

Los sistemas cuánticos de muchos cuerpos ofrecen numerosos retos para diversos campos de la física y las matemáticas, como la materia condensada, la teoría de la información cuántica, la teoría de operadores o el análisis numérico. Algunos de estos problemas surgen de la gran complejidad de estos sistemas, que dificulta su estudio mediante métodos clásicos, así como del interés de la comunidad científica por comprender sus propiedades físicas, tales como la dinámica, estructura de correlaciones o comportamiento tanto dentro como fuera del equilibrio. Entre las propiedades más interesantes de estos sistemas se encuentra el entrelazamiento, un cierto tipo de correlación cuántica que carece de análogo en sistemas clásicos y que se ha establecido como un recurso imprescindible en los campos de la información y computación cuántica.

La presente tesis doctoral profundiza en el estudio de correlaciones, localidad y entrelazamiento en sistemas cuánticos. En particular, se enfoca en herramientas matemáticas como redes de tensores, cotas de Lieb-Robinson y algoritmos cuánticos, para obtener resultados originales, tanto analíticos como numéricos, de aplicación directa en teoría de la información cuántica, materia condensada y metrología cuántica.

Los sistemas cuánticos que estudiamos consisten en conjuntos de partículas que interaccionan localmente unas con otras. La localidad de estos sistemas permite establecer una cota superior finita a la velocidad de propagación de las excitaciones, también conocida como cota de Lieb-Robinson. En esta tesis, demostramos que existen cotas de Lieb-Robinson para modelos de espines que interaccionan en una red mediante un campo bosónico que también verifica una cota de Lieb-Robinson en ausencia de acoplamiento espín-bosón. Aplicando estas cotas a sistemas de iones atrapados, observamos que la propagación de las correlaciones de espín mediante los fonones de un cristal iónico puede ser más rápida que el régimen explorado actualmente en los experimentos. Por este motivo, proponemos un esquema experimental para probar las cotas que consiste en medir las funciones de correlación retardadas a través de la fluorescencia del cristal.

La localidad de las interacciones también impone restricciones sobre la estructura del entrelazamiento de los sistemas cuánticos y permite encontrar representaciones matemáticas eficientes denominadas redes de tensores. Las redes

de tensores son conjuntos de tensores interconectados que reflejan la estructura de entrelazamiento del sistema, reducen la complejidad de su representación y capturan las propiedades físicas más relevantes de los estados cuánticos en los que estamos interesados. En esta tesis, utilizamos el caso unidimensional de las redes de tensores, también conocido como estados producto de matriz (MPS), para probar resultados analíticos y realizar simulaciones numéricas. Más específicamente, demostramos que una gran fraccionalización en la magnetización de una cadena de espines o la existencia de interacciones de largo alcance implican una gran cantidad de entrelazamiento en el estado de la cadena.

Las correlaciones y el entrelazamiento se han revelado como recursos de gran utilidad en metrología cuántica, estableciendo nuevas técnicas de medida que mejoran la precisión respecto a los métodos exclusivamente clásicos. En esta tesis, establecemos algoritmos cuánticos para medir las correlaciones temporales que se acumulan en un sistema cuántico tras su interacción con pulsos de luz láser. A partir de esta noción, introducimos el concepto de interferometría cuántica multipulso en el que un átomo o conjunto de átomos pueden actuar como un detector que mide de forma precisa diferencias entre pulsos de luz láser o propiedades de los pulsos. Por último, aplicamos este concepto para caracterizar y estabilizar un peine de frecuencias con una mejora polinomial en la sensibilidad respecto a protocolos clásicos.

Abstract

The study of quantum many-body systems poses a wide range of complex problems in different areas of physics and mathematics, such as condensed matter, quantum information theory, operator theory or numerical analysis. Some of these problems arise due to the high complexity of these systems, which makes their study unfeasible using classical approaches, as well as from the ever-growing interest in understanding their dynamics, physical properties and behaviour both in and out of equilibrium. Among the most interesting properties of these systems lies entanglement, a certain type of quantum correlation which is not present in classical systems and which has proven to be essential for quantum computation and quantum information.

This dissertation deals with the study of correlations, locality and entanglement in quantum systems. It relies on mathematical tools such as tensor network representations, Lieb-Robinson bounds and quantum algorithms in order to obtain original results, both analytical and numerical, with practical applications to quantum information theory, condensed matter and quantum metrology.

We investigate quantum many-body systems which consist on particles interacting locally with each other. Locality gives rise to a finite upper bound to the velocity of propagation for excitations, which is known as Lieb-Robinson bound. In our work, we prove the existence of Lieb-Robinson bounds for spin-boson models, where the spins interact through a bosonic lattice field which satisfies a Lieb-Robinson bound itself in the absence of spin-boson coupling. We apply these bounds to systems of trapped ions and we observe that the propagation of spin correlations may be faster than the speeds currently observed in state-of-the-art experiments. We present an experimental proposal to test the bounds, measuring retarded correlation functions.

The locality of the interactions also restricts the structure of entanglement and makes possible to obtain efficient mathematical representations of quantum systems, also known as tensor network representations. Tensor network states are built from sets of interconnected tensors and they reflect the structure of entanglement of the original states, while reducing the complexity of their representation and capturing the most relevant physical properties. In this thesis, we use the one-dimensional case of tensor networks, also known as matrix product

states (MPS) to prove analytical results and to perform numerical simulations. We quantify the amount of entanglement that exists in a quantum spin chain under certain physical conditions such as the fractionalization of the magnetization or the absence of a local parent Hamiltonian. We prove that a large fractionalization in the magnetization or the need of long-range interactions implies a large amount of entanglement in a quantum spin chain.

Correlations and entanglement have become fundamental resources in quantum metrology, bringing forward new measurement techniques which significantly improve the precision in comparison to classical protocols. In this thesis, we suggest novel quantum algorithms to measure time correlations which accumulate in a quantum system during its interaction with laser pulses. Building from this notion, we introduce the concept of multipulse quantum interferometry in which a single atom or an ensemble of atoms act as a detector that measures accurately differences between pulses of laser light or individual properties of the pulses. Finally, we apply this idea to the characterization and stabilization of a frequency comb, obtaining a polynomial improvement on the sensitivity over classical protocols.

1 Introducción en castellano

1.1 Motivación

Los sistemas cuánticos de muchos cuerpos suscitan preguntas fundamentales en diversos contextos físicos y matemáticos, como la física de altas energías, la materia condensada, la información cuántica, el análisis numérico o la teoría de operadores. Matemáticamente, un sistema cuántico puro constituido por N partículas de dimensión física d se puede representar mediante un vector unitario en un espacio de Hilbert $\mathcal{H} = (\mathbb{C}^d)^{\otimes N}$, también llamado vector *estado del sistema*, de la forma siguiente:

$$|\psi\rangle = \sum_{i_1,\ldots,i_N=1}^{d} \lambda_{i_1,\ldots,i_N} |i_1\rangle \otimes \ldots \otimes |i_N\rangle,\ \lambda_{i_1,\ldots,i_N} \in \mathbb{C} \tag{1.1}$$

donde cada $|i_r\rangle_{i_r=1}^{d}$ es una base ortonormal del espacio de Hilbert $\mathbb{C}^d$. Como se puede observar en la ecuación 1.1, se necesitan d^N coeficientes complejos $\lambda_{i_1,\ldots,i_N}$ para representar el estado $|\psi\rangle$, lo cual significa que la descripción exacta de un sistema de N partículas requiere un número de parámetros que escala exponencialmente con el número de partículas.

Este crecimiento exponencial conlleva que la simulación de los sistemas cuánticos sea sumamente compleja usando recursos clásicos, excepto al restringirnos a sistemas con tamaños suficientemente pequeños. Incluso para una cadena de espín $\frac{1}{2}$ y longitud $N \sim 50$, la caracterización del sistema requiere una cantidad de memoria dedicada superior a la memoria disponible en los ordenadores clásicos actuales.

Una de las propiedades más relevantes de los sistemas cuánticos es el entrelazamiento, un tipo de correlación que carece de análogo en sistemas clásicos. La descripción clásica de un sistema puro multipartito compuesto por n subsistemas se puede escribir como el estado producto de los n sistemas considerados individualmente. Por otra parte, si consideramos el formalismo cuántico, dicho sistema debe describirse usando la ecuación 2.1, que, en general, no es equivalente al producto tensorial de los estados de los subsistemas, es decir, $|\psi\rangle \neq |\psi_1\rangle \otimes |\psi_2\rangle \otimes \ldots \otimes |\psi_n\rangle$.

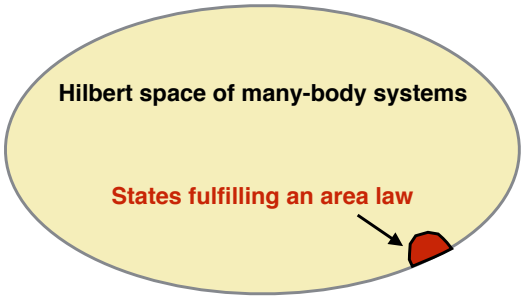

Figura 1.1: El espacio de Hilbert correspondiente a los estados que cumplen una ley de área para la entropía de entrelazamiento es un subconjunto muy pequeño del espacio de Hilbert total de los sistemas cuánticos de muchos cuerpos. El espacio de los estados con una ley de área se ha denominado informalmente como una "pequeña esquina" del estado de Hilbert subyacente.

Los estados puros con entrelazamiento son precisamente aquellos que no se pueden escribir como el producto tensorial de los estados de los subsistemas individuales. Algunos de los ejemplos paradigmáticos de estados puros entrelazados son los pares de *Bell* o los pares de *Einstein-Podolsky-Rosen* [EPR35], que se componen de dos partículas A y B de espín 1/2, con estados posibles $|\uparrow\rangle$ o $|\downarrow\rangle$, tales como:

$$|\psi_{\text{EPR}}\rangle = \frac{1}{\sqrt{2}} \left(|\uparrow\rangle_A \otimes |\downarrow\rangle_B - |\downarrow\rangle_A \otimes |\uparrow\rangle_B \right). \tag{1.2}$$

Si consideramos la clase más general de los estados mixtos, los estados entrelazados son aquellos que no se pueden construir a partir de un producto tensorial utilizando únicamente operaciones locales y comunicación clásica [Wer89]. En la actualidad, el entrelazamiendo se ha convertido en un elemento clave para los campos de la información y computación cuántica, dando lugar a aplicaciones notables como la teleportación cuántica [BBC$^+$93], la criptografía cuántica [Eke91] o la codificación superdensa [BW92].

La representación y caracterización de los estados entrelazados multipartitos es un problema desafiante, entre otros motivos por el crecimiento exponencial del espacio de Hilbert subyacente. Afortunadamente, estamos interesados en sistemas compuestos por un gran número de partículas que interaccionan localmente entre ellas en un conjunto macroscópico. La localidad de las interacciones permite demostrar que los autoestados de baja energía de hamiltonianos locales con gap verifican una ley de área para la entropía de entrelazamiento [1][Has06, Has07a, ALV12, AKLV13, ECP10]. El conjunto de estados que satisfa-

[1]Este resultado se ha demostrado para sistemas unidimensionales y para sistemas en dos

cen una ley de área para la entropía de entrelazamiento es un pequeño subconjunto del espacio de Hilbert total (ver Fig. 1.1). Esto nos permite obtener representaciones matemáticas eficientes para los sistemas cuánticos basadas en la estructura de la entropía del entrelazamiento: las *redes de tensores* [VC04, Vid07]. Estas representaciones están basadas en conjuntos de tensores interdependientes que reflejan la estructura del entrelazamiento y reducen la complejidad de la representación del estado original, mientras capturan las propiedades físicas más relevantes.

Las redes de tensores unidimensionales, también conocidas como *estados producto de matriz* (MPS) se introdujeron inicialmente en el trabajo de Fannes, Nachtergaele y Werner [FNW92]. Se trata de estados puros cuyos coeficientes pueden calcularse como el producto de matrices,

$$|\psi\rangle = \sum_{i_1,\ldots,i_N}^{d} \operatorname{tr}\left[A_{i_1}^{[1]} \ldots A_{i_N}^{[N]}\right] |i_1 \ldots i_n\rangle, \tag{1.3}$$

donde $A_{i_k}^{[k]} \in \mathcal{M}_{D_k \times D_{k+1}}$ son las matrices asociadas al sitio k del sistema unidimensional [PGVWC07]. La relevancia de estos estados se debe a que los MPS son una buena representación de los sistemas en una dimensión que cumplen una ley de área [Has07a, SWVC08, VC06] y capturan toda la física de los sistemas unidimensionales [Has07b, Has06, Vid04]. Los estados producto de matriz permiten explicar el éxito de métodos numéricos como el Density Matrix Renormalization Group (DMRG) propuesto por White [Whi92, Whi93] para simular sistemas unidimensionales fuertemente correlacionados. Por otra parte, los estados mixtos también se pueden representar como redes de tensores usando *operadores de densidad producto de matriz* (MPDO) [VGRC04, PMCV10], y simular su evolución en equilibrio térmico y bajo disipación mediante métodos numéricos basados en este formalismo [VGRC04, PMCV10]. Sin embargo, los operadores de densidad producto de matriz deben superar un fuerte obstáculo, ya que no es posible determinar si el estado global del sistema es positivo semidefinido simplemente estudiando las matrices locales A_i que definen el MPDO [KGE14, DCC$^+$16]. Las purificaciones, un cierto tipo de MPDO, permiten superar esta limitación al estar definidas como un MPS con un entorno local en cada sitio, generando un estado positivo global por construcción. Las descripciones de un estado mixto como MPDO o como purificación no son equivalentes en general [DSPGC13], aunque existen métodos para obtener una purificación a partir de un cierto MPDO [DSPGC13].

Otra consecuencia de la localidad de las interacciones es la existencia de una cota para la velocidad de propagación de las correlaciones, conocida como cota de Lieb-Robinson. Las cotas de Lieb-Robinson [LR72] son una herramienta

dimensiones bajo ciertas hipótesis. Cuando dichas hipótesis no se cumplen en dos dimensiones, la pregunta de si los autoestados de energía más baja para hamiltonianos locales con gap cumplen una ley de área se trata de un problema abierto llamado *la conjetura de la ley de área*, una de las preguntas abiertas más relevantes en el campo.

fundamental para estudiar sistemas en materia condensada y permiten demostrar que, bajo ciertas condiciones, los sistemas cuánticos no relativistas exhiben una estructura causal análoga a la de sistemas descritos por teorías cuánticas de campo [PS95]. Estas cotas también se pueden utilizar para probar propiedades físicas importantes, como leyes de escala para la entropía de entrelazamiento [Has07a, ECP10], el decaimiento exponencial de las correlaciones para el estado fundamental de hamiltonianos con gap [HK06] o la estabilidad del orden topológico [BHV06].

El estudio de los sistemas cuánticos no se centra únicamente en el estudio de sus propiedades, sino que también existen líneas de investigación dedicadas a la búsqueda de nuevas aplicaciones en tecnologías cuánticas [OFV10]. Un ejemplo de ello, es el uso de sistemas cuánticos para obtener métodos más precisos en metrología cuántica [LKD02, GLM11], como la mejora en las técnicas de medida usando entrelazamiento [NKD+11, Mac13] o la obtención de algoritmos cuánticos que mejoran los recursos cuánticos para realizar una cierta tarea.

1.2 Objetivos y resultados principales

Esta tesis doctoral se dedica al estudio de las correlaciones, localidad y entrelazamiento en sistemas cuánticos. Se enfoca en técnicas matemáticas como las representaciones con redes de tensores, cotas de Lieb-Robinson y algoritmos cuánticos para obtener resultados originales analíticos y numéricos con aplicaciones prácticas en información cuántica, materia condensada y metrología cuántica. Los resultados principales de este trabajo se pueden clasificar en tres categorías diferenciadas en las que tratamos de contestar varias preguntas: "Entrelazamiento y estados producto de matriz", "Localidad y cotas de Lieb-Robinson" y "Algoritmos cuánticos para metrología cuántica".

Entrelazamiento y estados producto de matriz

Los estados producto de matriz ofrecen una representación natural para los sistemas cuánticos de muchos cuerpos en términos de la estructura del entrelazamiento del sistema. A pesar de que el entrelazamiento es uno de los recursos fundamentales en física cuántica, todavía se desconocen las condiciones bajo las cuales es posible afirmar que existe una gran cantidad de entrelazamiento [Sre93, ECP10]. Se han obtenido algunos resultados para sistemas unidimensionales, por ejemplo, los estados que sufren una transición resistiva cuántica muestran una gran cantidad de entrelazamiento [Car11], pero la imagen general todavía está incompleta. Nuestro objetivo en los capítulos 5 y 6 consiste en encontrar nuevos escenarios en los que sea posible cuantificar el entrelazamiento, tales como la fraccionalización en la magnetización de una cadena de espines o la imposibilidad de aproximar un

cierto estado por el estado fundamental de un hamiltoniano con interacciones de corto alcance, sin frustración y con gap.

Objetivo 1: Estudiar la relación entre la fraccionalización en la magnetización de una cadena de espines cuántica y la entropía de entrelazamiento del sistema.

En el capítulo 5 utilizamos estados producto de matriz para cuatificar la cantidad de entrelazamiento en una cadena de espines [CSW+13]. En particular, probamos que una gran fraccionalización en la magnetización de dicho estado, implica la existencia de una gran cantidad de entrelazamiento en el sistema. Para poder demostrar rigurosamente esta afirmación, debemos desarrollar la teoría de los estados producto de matriz, extendiendo resultados previos ya presentados en las referencias [PGVWC07, PGWS+08, SWPGC09], y obteniendo resultados nuevos.

Objetivo 2: Estudiar la relación entre la existencia de interacciones de largo alcance en el hamiltoniano padre de una cadena de espines cuántica y la entropía de entrelazamiento del sistema.

En el capítulo 6, obtenemos otro conjunto de condiciones bajo las cuales podemos cuantificar el entrelazamiento para un sistema unidimensional. Cuando un sistema tiene interacciones de largo alcance, intuitivamente esperamos que toda región esté correlacionada con cualquier otra región del estado, lo cual debería reflejarse en la entropía de entrelazamiento. No obstante, no es sencillo transformar esta intuición en un resultado matemático riguroso. En este capítulo establecemos una cota inferior a la entropía de entrelazamiento de un estado producto matriz traslacionalmente invariante, que no es el estado fundamental de ningún hamiltoniano con gap, sin frustración y con interacciones de corto alcance y que se encuentra suficientemente alejado de cualquier otro estado con estas propiedades para cualquier longitud de interacción dada [CSW+13]. Además, demostramos que el entrelazamiento escala linealmente con la longitud de interacción. Para probar este resultado, debemos obtener nuevas cotas que permiten aproximar la matriz de densidad reducida del sistema usando otra matriz de densidad reducida cuyas matrices asociadas tienen una dimensión de enlace inferior.

Localidad y cotas de Lieb-Robinson

La localidad es otra de las propiedades de los sistemas cuánticos que estudiamos en esta tesis, puesto que los sistemas que consideramos se componen de partículas que interaccionan localmente unas con otras. Una consecuencia de la localidad es la existencia de una cota superior finita para la velocidad de propagación de las excitaciones, también denominada cota de Lieb-Robinson. En 1972, Lieb y Robinson demostraron que la velocidad de grupo para la propagación de las correlaciones en sistemas cuánticos de muchos cuerpos con interacciones de

corto alcance está acotada superiormente por una constante finita independiente del tiempo [LR72]. Posteriormente, estas cotas se extendieron a diferentes sistemas físicos, como sistemas con interacciones de largo alcance con un decaimiento exponencial o algebraico, o para ciertos tipos de hamiltonianos no acotados [NRSS07, NRSS09, NS10a, BHV06, PSHKMK09, CSE08]. Numerosos resultados sobre la propagación de las correlaciones y aplicaciones teóricas relevantes se han desarrollado usando las cotas de Lieb-Robinson, como, por ejemplo, el clustering exponencial de las correlaciones [HK06] o la eficiencia de métodos numéricos como el DRMG dependiente del tiempo [Whi92, Whi93]. Nuestro objetivo en esta sección es encontrar nuevas cotas de Lieb-Robinson para modelos de espín-bosón en retículos, que pueden observarse experimentalmente en cristales iónicos.

Objetivo 3: Establecer cotas de Lieb-Robinson para modelos de espín-bosón en retículos.

En el capítulo 7 obtenemos cotas de Lieb-Robinson para un modelo general de sistemas con dimensión finita, interaccionando a través de un campo bosónico que satisface una cota de Lieb-Robinson en ausencia de acoplamiento espín-bosón [JCPG$^+$13]. Estas cotas se pueden aplicar al caso general de modelos de espín-bosón en retículos independientemente de la geometría del retículo y pueden probarse experimentalmente usando tecnología del estado del arte.

Objetivo 4: Obtener cotas de Lieb-Robinson para cristales de iones en diferentes regímenes.

En el capítulo 8, aplicamos las cotas de Lieb-Robinson que hemos obtenido en el capítulo 7 a cristales de iones atrapados, y observamos que la velocidad de propagación de las correlaciones puede ser más rápida que las escalas temporales que se consideran en los experimentos actuales [JCPG$^+$13]. Por otra parte, también derivamos cotas de Lieb-Robinson en el régimen perturbativo, donde la velocidad de las correlaciones es menor, y en el régimen impulsivo, donde las fuerzas actúan localmente sobre los iones separados durante un periodo de tiempo corto y la propagación de las correlaciones depende únicamente de la propagación de los fonones y de la eficiencia del acoplamiento espín-bosón en los espín y bosones correlacionados. En este capítulo obtenemos la velocidad de propagación óptima en el régimen impulsivo, en el que se satura la cota de Lieb-Robinson. Proponemos un esquema experimental para medir las funciones de correlación retardadas a través de la fluorescencia del cristal, lo cual nos permite probar las cotas de Lieb-Robinson que hemos obtenido en el régimen perturbativo.

Algoritmos cuánticos para metrología cuántica

El entrelazamiento y las correlaciones han generado numerosas aplicaciones en tecnologías cuánticas [OFV10], como los sistemas de distribución de clave cuánti-

ca [GT07] en los que se usa el entrelazamiento para garantizar la seguridad de la clave para aplicaciones criptográficas. Por otra parte, también se han utilizado en metrología cuántica [LKD02] para obtener nuevas técnicas de medida que mejoran la precisión respecto a protocolos clásicos [CPHH15]. En esta área, nuestro objetivo se centra en buscar nuevas aplicaciones del uso de correlaciones y algoritmos cuánticos en metrología cuántica, como la caracterización y estabilización de un peine de frecuencias.

Objetivo 5: Los sistemas cuánticos se pueden usar como detectores que miden propiedades de pulsos láser con una alta precisión.

En el capítulo 9, proponemos nuevos algoritmos cuánticos para medir correlaciones temporales que se acumulan en un sistema cuántico durante su interacción con un tren de pulsos láser. A partir de esta idea, introducimos la noción de interferometría cuántica multipulso (MPQI) [CMPGR14], en la que un átomo o un conjunto de átomos actúan como un detector que mide las diferencias entre pulsos de luz láser o propiedades específicas de los pulsos. A continuación, mostramos cómo se pueden utilizar estos algoritmos para caracterizar y estabilizar un peine de frecuencias. Esta aplicación da lugar a una mejor polinomial sobre la sensibilidad de los protocolos clásicos existentes, y puede extenderse para proponer nuevos estándares para la medición de tiempos y frecuencias.

1.3 Estructura de la tesis

Esta tesis está compuesta por un resumen en castellano e inglés, por una introducción en castellano en la que se detallan los objetivos, resultados, conclusiones y líneas futuras de investigación de la tesis y por la tesis completa en inglés. El cuerpo de la tesis se estructura en diez capítulos: el capítulo 2 es una introducción y motivación autocontenida, los capítulos 3 y 4 presentan los requisitos necesarios para dar contexto al resto de la memoria. Estos primeros capítulos tratan temas diversos, como los principios de la mecánica cuántica, la teoría del entrelazamiento, la teoría de las redes de tensores o las cotas de Lieb-Robinson. Los capítulos 5-9 contienen los resultados de la tesis y todos ellos tienen una estructura análoga, compuesta de una introducción, los resultados principales y una conclusión que resume los puntos fundamentales y propone una visión general de las futuras líneas de investigación.

Más específicamente, en el capítulo 2 presentamos el propósito, los resultados principales y la visión general de la tesis; este capítulo ofrece la información necesaria acerca de los objetivos y la estructura de la memoria.

En los capítulos 3 y 4 revisamos la teoría general de varios temas en los que se fundamenta la tesis y que puede ayudar a aquellos lectores que desconozcan alguna de las áreas que tratamos. Estos capítulos ofrecen la notación utilizada

en el resto de la tesis y el conjunto de técnicas que se usan para demostrar los resultados de los capítulos siguientes. El capítulo 3 revisa los conceptos básicos de la mecánica cuántica, la teoría del entrelazamiento y las medidas de entrelazamiento. Posteriormente, discutimos la propagación de la información en los sistemas cuánticos y presentamos las célebras cotas de Lieb-Robinson. El capítulo 4 introduce una herramienta matemática que se usa en el cuerpo de la tesis para representar los sistemas cuánticos de muchos cuerpos: las redes de tensores y, en particular, los estados producto de matriz.

Los capítulos 5 y 6 contienen los resultados relacionados con el entrelazamiento y los estados producto de matriz. Estos capítulos abordan los objetivos 1 y 2 y se han publicado en Physical Review B 87, 035114 (2013).

Los capítulos 7 y 8 tratan sobre las cotas de Lieb Robinson para modelos de espín-bosón en retículos y su aplicación para iones atrapados. Hemos dividido estos resultados en dos capítulos diferentes, ya que en el primero de ellos exponemos los resultados analíticos y las nuevas cotas de Lieb-Robinson, mientras que en el segundo tratamos las propuestas de implementación experimental. En concreto, el capítulo 7 aborda el objetivo 3 y el capítulo 8 trata el objetivo 4. Los resultados presentados en este capítulo se han publicado en Physical Review Letters 111, 230404 (2013).

El capítulo 9 trata sobre el objetivo 5. Los resultados contenidos en este capítulo se han publicado en Physical Review Letters 112, 073603 (2014).

Por último, el capítulo 10 presenta las conclusiones y líneas de trabajo futuras que se discuten en cada uno de los capítulos.

1.4 Conclusiones y trabajo futuro

A continuación mencionaremos las conclusiones de la tesis doctoral, que se encuentran al final de cada uno de los capítulos, y las posibles líneas de investigación futura que surgen a partir de los resultados recogidos en esta memoria.

Fraccionalización en la magnetización y entrelazamiento. En el capítulo 5 de esta tesis doctoral demostramos que en el estado de una cadena de espines cuántica, una gran fraccionalización en la magnetización implica la existencia de una gran cantidad de entrelazamiento. Para hacer esto, hemos establecido una cota inferior para la entropía de entrelazamiento de cualquier región conexa y suficientemente grande de una cadena de espines cuántica. En esta línea de investigación sería interesante extender este resultado a sistemas en más dimensiones, utilizando PEPS [VC04]. Sin embargo, extender nuestros resultados a sistemas en dos dimensiones da lugar a dificultades que son preguntas abiertas en el campo, como la ausencia de una forma canónica para PEPS o la caracterización de la

fraccionalización en estos sistemas. La forma canónica tiene una gran cantidad de usos en el caso de los MPS y una de las más relevantes es la caracterización de simetrías [PGWS$^+$08] y de fases [CGW11, SPGC11]. En sistemas bidimensionales, es posible caracterizar las diferentes simetrías en el caso inyectivo pero este resultado no se puede aplicar en los sistemas más relevantes con orden topológico, como las fases SET [GW09, PBTO12]. Por otra parte, en sistemas unidimensionales la fraccionalización surge de una estructura periódica, que explotamos en el capítulo 5 para demostrar el resultado principal. No obstante, en dimensiones superiores existen teselaciones aperiódicas del plano que pueden dar lugar a sistemas físicos fraccionalizados sin periodicidad ni propiedades topológicas. Creemos que puede ser interesante estudiar hamiltonianos relacionados con teselaciones aperiódicas del plano y determinar si los sistemas asociados dan lugar a fraccionalización. También nos gustaría llevar a cabo simulaciones numéricas para cuantificar la cantidad de entrelazamiento en sistemas concretos que presentan fraccionalización en la magnetización y determinar cómo de buena es la cota que presentamos y si es posible saturarla en algún caso.

Interacciones de largo alcance y entrelazamiento. A continuación, en el capítulo 6 demostramos que, para el estado de una cadena de espines, la imposibilidad de encontrar un estado que la aproxime suficientemente bien y que además sea el estado fundamental de un hamiltoniano local requiere una gran cantidad de entrelazamiento. Este resultado está relacionado con otras muchas preguntas de interés que no contestamos en esta tesis, como, por ejemplo, si es posible demostrar que un estado producto matriz traslacionalmente invariante con una cierta dimensión de enlade D se puede aproximar usando un MPDO traslacionalmente invariante con una dimensión de enlace menor $\tilde{D} \leq D$ y tal que la cota de la distancia entre ambos estados para L partículas escale linealmente con L. Esto daría lugar a cotas rigurosas sobre el error que se comete al usar método numéricos basados en MPS como el iTEBD, que se basan en truncar el resultado de evoluciones temporales infinitesimales. En relación con esta conjetura, hemos realizado simulaciones numéricas para la cadena spin-1 de Heisenberg spin-1, calculando la distancia entre parámetros de orden de cadena (SOP). Hemos encontrado que el scaling entre los observables es lineal en el número de partículas, afianzando nuestra conjetura de que para estados traslacionalmente invariantes el escalado para el error en la aproximación de la matriz de densidad reducida de L partículas es lineal en L.

Otro resultado relacionado con los capítulos 5 y 6, que nos gustaría explorar en el futuro es la versión cuántica de la desigualdad de Wielandt's [SPGWC10], que implica la existencia de una cota en la longitud de interacción para hamiltonianos con un estado fundamental único y que se puede representar de forma exacta como un MPS. La pregunta sobre si existe un teorema de Wielandt en dimensiones superiores sigue abierta y nos gustaría abordarla en investigaciones futuras.

Existen más preguntas interesantes relacionadas con la representación con redes de tensores, como cuándo es posible encontrar métodos numéricos eficientes para construir purificaciones de un operador de densidad producto matriz. Tal y como veremos en la sección 4.2, en general no es posible confirmar localmente la positividad global de un MPDO. Siguiendo con esta línea de investigación, estamos trabajando en desarrollar métodos numéricos basados en el método polinomial de suma de cuadrados [DSPGC13] para construir purificaciones aproximadas eficientemente.

Cotas de Lieb-Robinson para modelos de espín-bosón. En el capítulo 7, derivamos cotas de Lieb-Robinson para un modelo general de sistemas finito-dimensionales que interaccionan a través de una campo bosónico que satisface una cota de Lieb-Robinson. Estas cotas se pueden aplicar a todos los sistemas de espín-bosón en retículos independientemente de la dimensionalidad y de la geometría del sistema. Para continuar en esta línea de trabajo, nos gustaría estudiar otras implicaciones teóricas de estas cotas, como la eficiencia de los métodos DMRG con dependencia temporal o el clustering de correlaciones. Por otra parte, también se podría intentar generalizar estas cotas al límite en el continuo de la red y demostrar si el cono de luz al que dan lugar las cotas de Lieb-Robinson en el continuo se corresponde con el que esperaríamos al tomar el límite del cono de luz que se obtiene en el caso discreto. Esto nos permitiría abordar la propagación de correlaciones en teorías cuánticas de campos que son el límite uniforme de modelos discretos de bosones interaccionando con fermiones.

También nos gustaría explorar otra posible generalización de las cotas de Lieb-Robinson usando una ruta motivada físicamente que complementaría otras técnicas propuestas en la literatura [HK06, NOS06, CSE08, NRSS09, Pou10, PSHKMK09]. Existen ciertos sistemas infinito-dimensionales que no se encuentran bajo las hipótesis de las cotas de Lieb-Robinson existentes, para los que es posible definir estados de temperatura finita. Esta noción de temperatura restringe notablemente el tamaño de la región a la variedad del estado fundamental y su vecindad, y puede considerarse intuitivamente como una medida de para qué operadores se pueden calcular valores esperados a una cierta temperatura. Nos gustaría refinar esta idea para obtener una generalización a las cotas de Lieb-Robinson aplicable a sistemas de interés, como el hamiltoniano de Bose-Hubbard [GK63].

Cotas de Lieb-Robinson para cristales iónicos. Posteriormente, en el capítulo 8 aplicamos las cotas de Lieb-Robinson que hemos obtenido a cristales de iones atrapados. Observamos que en estas cotas de Lieb-Robinson, la velocidad de propagación de las correlaciones de spin depende de las velocidad de propagación de los fonones del cristal así como de la eficiencia con la que los iones emiten y reabsorben las correlaciones de los fonones. También hemos demostrado que la

velocidad para la propagación de las correlaciones dada por nuestras cotas puede ser más rápida que las escalas temporales exploradas por los regímenes experimentales considerados actualmente. Muchos de los experimentos realizados para la simulación del magnetismo cuántico se implementan en el régimen perturbativo con velocidades de propagación más lentas, por lo que hemos extendido las cotas de Lieb-Robinson a dicho régimen, observando que la velocidad de propagación para las correlaciones de espín es al menos dos órdenes de magnitud más lenta que en el caso no perturbativo.

Por otra parte, también aplicamos la cotas de Lieb-Robinson en el régimen impulsivo, en el que las fuerzas actúan localmente sobre los iones alejados durante un corto intervalo de tiempo y la propagación de correlaciones depende únicamente de la propagación de los fonones y de la eficiencia del acoplamiento espín-bosón para correlar espines y bosones. Observamos que la velocidad de propagación óptima se alcanza en el régimen impulsivo, en el que se saturan las cotas de Lieb-Robinson que deducimos.

También se propone un esquema experimental para medir las funciones de correlación retardadas a través de la fluorescencia del cristal y determinar si se alcanzan las cotas de Lieb-Robinson que se derivan en el regimen impulsivo. Este esquema se puede modificar usando fuerzas dependientes del estado para obtener las cotas de Lieb-Robinson armónicas que se introducen en el capítulo. Como investigación adicional, sería interesante obtener esquemas experimentales distintos que permitiesen probar las cotas de Lieb-Robinson en el régimen perturbativo, en el que la propagación de las correlaciones es más lenta. Por otra parte, a pesar de que hemos aplicado las cotas de Lieb-Robinson únicamente a cristales de iones atrapados, nuestros resultados se pueden extender a una gran variedad plataformas experimentales como circuitos superconductores, puntos cuánticos con centros-NV que interaccionas con cavidades acopladas o cristales fotónicos.

Algoritmos cuánticos en metrología cuántica. Por último, en el capítulo 9 presentamos algoritmos interferométricos cuánticos basados en la idea de que un átomo puede acumular el efecto de múltiples pulsos láser, obteniendo sus diferencias a través de una cierta ordenación de los pulsos, puertas intermedias y medidas. A este conjunto de protocolos los llamamos interferometría cuántica multipulso (MPQI) y observamos que da lugar a una mejora polinomial sobre la sensibilidad respecto a la interferometría atómica convencional o interferometría Ramsey. La interferometría cuántica multipulso se puede utilizar para detectar cambios temporales en la fase CEP de un peine de frecuencias, ya que la unitaria implementada por un pulso es sensible a la intensidad y a la fase CEP, pero no es sensible al tiempo de llegada del pulso. Los esquemas que presentamos son adecuados para peines de frecuencias que abarcan menos de una octava (non-octave spanning) y tienen un ruido de fase intrínseco bajo, como por ejemplo los láseres Ti:Sapphire.

Una generalización directa de nuestro trabajo consiste en extender nuestro protocolos más allá de la aproximación de onda rotante (RWA) tal y como mencionamos en la sección 9.3. Además de esto, existen otras propiedades de los peines de frecuencia que podrían estudiarse usando nuestros métodos, como por ejemplo las fluctuaciones de intensidad. Esto se podría hacer modificando los protocolos cuánticos que proponemos para obtener características distintas de un peine de frecuencias, siendo propiedad más interesante la fase absoluta o la fase CEP. La importancia de caracterizar la fase absoluta radica en que esto permitiría corregir cada pulso del tren individualmente, en lugar de depender del desplazamiento entre pulsos consecutivos. Si fuera posible caracterizar la fase absoluta, se obtendrían métodos de estabilización que mejorarían significativamente la escala temporal considerada.

En el capítulo 9 hemos asumido que las fluctuaciones para el desfase son aleatorias por lo que podríamos explorar cuál es el conjunto de hipótesis más débiles que permiten aplicar nuestro método experimentalmente con éxito.

Por último, a diferencia de la interferometría estándar, nuestros métodos permiten interrogar el átomo detector varias veces y aprovechar la repetición, mejorando el proceso de medida. Nuestros métodos pueden aplicarse para mejorar la precisión de otros procesos interferométricos, en particular, nos gustaría explorar la posibilidad de utilizar MPQI para aumentar la precisión del interferómetro utilizado en el experimento LIGO, ideado para detectar ondas gravitacionales.

Sobre esta tesis

Esta tesis se presenta por Andrea Cadarso Rebolledo en el Departamento de Análisis Matemático de la Universidad Complutense de Madrid, para obtener el título de Doctor en Matemáticas en el programa de doctorado en Investigación Matemática. Este trabajo ha sido dirigido por el Dr. David Pérez García, Catedrático en el Departamento de Análisis Matemático de la Universidad Complutense de Madrid, y por el Dr. Juan José García Ripoll, Investigador Científico en el Consejo Superior de Investigaciones Científicas.

1.5 Contribuciones científicas

Los resultados contenidos en esta tesis se han publicado en revistas internacionales de alto impacto revisadas por pares. En particular, se han aceptado tres artículos con los resultados de los capítulos 5, 6, 7, 8 y 9:

- "Phase stabilization of a frequency comb using multi-pulse quantum interferometry" Andrea Cadarso, Jordi Mur-Petit, Juan José García-Ripoll. Phys. Rev. Lett 112, 073603 (2014).
- "Lieb-Robinson bounds for spin-boson lattice models and trapped ions" Johannes Juenemann, Andrea Cadarso, David Pérez-García, Alejandro Bermudez, Juan José García-Ripoll. Phys. Rev. Lett 111, 230404 (2013).
- "Entanglement, fractional magnetization and long-range interactions" Andrea Cadarso, Mikel Sanz, Michael M. Wolf, J. Ignacio Cirac, David Perez-García. Phys. Rev. B 87, 035114 (2013).

Los resultados de esta tesis también se han presentado en seminarios, workshops y conferencias nacionales e internacionales como contribución oral o póster:

- "Lieb-Robinson bounds for spin-boson models and quantum field theories" 1-3 Junio 2015, Workshop Información Cuántica en España, EHU-UPV, Bilbao. (Contribución oral)
- "Phase stabilization of a frequency comb using Multipulse Quantum Interferometry" 30 Junio 2014, Quantum Roundabout, University of Nottingham, UK. (Contribución oral)
- "Phase stabilization of a frequency comb using trapped atoms" 14 Enero 2013, V Encuentro Gases Cuánticos en Madrid, CSIC, Madrid (Contribución oral)

- "Entanglement, fractional magnetization and long-range interactions" 7-9 Noviembre 2012, Quantum Square - Student conference on mathematical and theoretical aspects of quantum mechanics, Nottingham, UK. (Contribución oral)
- "Entanglement, fractional magnetization and long-range interactions" 19-21 Septiembre 2012, Workshop of Young Researchers in Mathematics, UCM, Madrid. (Contribución oral)
- "Entanglement, fractional magnetization and long-range interactions" 17-19 Septiembre 2012, Workshop Información Cuántica en España, CSIC, Madrid. (Contribución oral)
- "Entanglement, fractional magnetization and long-range interactions" Mayo 2012, Networking tensor networks, Benasque, Huesca. (Contribución oral)
- "Entanglement, fractional magnetization and long-range interactions" Septiembre 2011, Workshop of Young Researchers in Mathematics, UCM, Madrid. (Contribución oral)
- "Lieb-Robinson bounds for spin-boson models and quantum field theories" 16-17 Abril 2015, 17th Symposium in Topological Quantum Information, Garching, Alemania. (Póster)
- "Lieb-Robinson bounds for spin-boson models and quantum field theories" 13-15 Abril 2015, Quantum Correlations beyond Entanglement, Bad-Honnef, Alemania. (Póster)
- "Lieb-Robinson bounds for spin-boson lattice models and trapped ions" 24-30 Agosto 2014, Numerical and Analytical methods for Strongly Correlated Systems, Centro de Ciencias de Benasque "Pedro Pascual", Benasque. (Póster)
- "Entanglement, fractional magnetization and long-range interactions" 19-21 Noviembre 2012, Workshop Entangle this: strings, fields and atoms, UAM, Madrid. (Póster)
- "Entanglement, fractional magnetization and long-range interactions" 22-25 Octubre 2012, Workshop on Quantum Simulations, EHU, Bilbao. (Póster)
- "Entanglement, fractional magnetization and long-range interactions" Julio 2012, Workshop in Quantum Information, Seefeld, Austria. (Póster)
- "Entanglement, fractional magnetization and long-range interactions" 24-27 Abril 2012, Quantum Malta 2012: Fundamental Problems in Quantum Physics, Malta. (Póster)

2 Introduction

2.1 Motivation

Quantum many-body systems give rise to fundamental questions in many physical and mathematical contexts, ranging from high energy physics, condensed matter physics and quantum information theory to numerical analysis or operator theory. Mathematically, a pure quantum many-body system formed by N particles, each of them with physical dimension d is described by a vector in the Hilbert space $\mathcal{H} = (\mathbb{C}^d)^{\otimes N}$, the state of the system, as follows:

$$|\psi\rangle = \sum_{i_1,\ldots,i_N=1}^{d} \lambda_{i_1,\ldots,i_N} |i_1\rangle \otimes \ldots \otimes |i_N\rangle,\ \lambda_{i_1,\ldots,i_N} \in \mathbb{C} \tag{2.1}$$

where each $|i_r\rangle_{i_r=1}^{d}$ is an orthonormal basis of the Hilbert space $\mathbb{C}^d$. As extracted from Eq. 2.1, we need d^N different complex coefficientes $\lambda_{i_1,\ldots,i_N}$ to represent the system $|\psi\rangle$, which implies that the exact description of a system of N particles requires a number of parameters which scales exponentially with N. This exponential scaling makes the simulation of many-body systems generally intractable using classical computers unless restricted to small system sizes. Even for a 1/2-spin chain of length $N \sim 50$, the representation of the system would need more memory allocated that the available memory in current classical computers.

One of the most striking features of quantum systems is entanglement, a type of correlation which is not present in classical systems. If we consider a multipartite pure system formed by n subsystems then its classical description is a product state of the n separate systems. Nevertheless, when we consider the quantum formalism, such multipartite system is described by Eq. 2.1, which, in general, cannot be written as a tensor product of the states of the subsystems, that is, $|\psi\rangle \neq |\psi_1\rangle \otimes |\psi_2\rangle \otimes \ldots \otimes |\psi_n\rangle$. Pure states displaying entanglement are precisely those which cannot be written as a tensor product of the states of the individual subsystems. Some paradigmatic examples of entangled pure states are the so-called *Bell states* or *Einstein-Podolsky-Rosen pairs* [EPR35] which are composed of two particles A and B of spin 1/2, with possible states either $|\uparrow\rangle$ or $|\downarrow\rangle$, such as

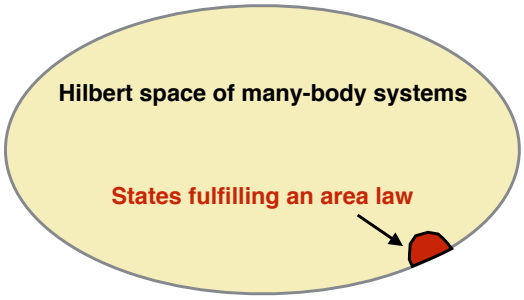

Figure 2.1: The Hilbert space corresponding to those states fulfilling an area law for the entanglement entropy is a very small subset of the total Hilbert space of quantum many body systems. The space of area-law states has been informally labelled as a "tiny corner" of the underlying Hilbert space.

$$|\psi_{\text{EPR}}\rangle = \frac{1}{\sqrt{2}} \left(|\uparrow\rangle_A \otimes |\downarrow\rangle_B - |\downarrow\rangle_A \otimes |\uparrow\rangle_B \right) \tag{2.2}$$

If we consider the more general class of mixed states, entangled states are those states which cannot be produced from a tensor product state using only local operations and classical communication [Wer89]. Nowadays, entanglement has become a centerpiece in the fields of quantum information and computation, and its study has led to remarkable applications such as quantum teleportation [BBC$^+$93], quantum cryptography [Eke91] or superdense coding [BW92].

The representation and characterization of many-body entangled states is a challenging problem, also due to the exponential growth of the underlying Hilbert space. However, we are interested in systems comprised of a large number of particles interacting locally which each other in a macroscopic ensemble. The locality of interactions leads to several consequences such as that the low energy eigenstates of gapped Hamiltonians with local interactions fulfill an area law for the entanglement entropy [1][Has06, Has07a, ALV12, AKLV13, ECP10]. The set of states that satisfy an area law for the entanglement entropy is a small subset of the whole Hilbert space (see Fig. 2.1) which allows to obtain efficient mathematical representations of quantum systems based on their entanglement structure. This idea led to the definition of *tensor network states* [VC04, Vid07]: sets of interdependent tensors which reflect the structure of entanglement and reduce the complexity of the state representation, while capturing the most relevant physi-

[1]This result is true in full generality for one-dimensional systems. It is also true for two-dimensional systems under certain hypothesis. When these hypothesis are not met, it is an open problem called *the area law conjecture*, one of the most important open questions in the field.

cal properties. One-dimensional tensor networks, also known as *matrix product states* (MPS) were already introduced in the work of Fannes, Nachtergaele and Werner [FNW92]. They are pure states whose coefficients can be calculated as a product of matrices,

$$|\psi\rangle = \sum_{i_1,\ldots,i_N}^{d} \operatorname{tr}\left[A_{i_1}^{[1]} \ldots A_{i_N}^{[N]}\right] |i_1 \ldots i_n\rangle, \tag{2.3}$$

where $A_{i_k}^{[k]} \in \mathcal{M}_{D_k \times D_{k+1}}$ are the matrices associated to the site k of the one-dimensional system [PGVWC07]. Their relevance stems from the fact that MPS are an accurate representation of one-dimensional systems fulfilling an area law [Has07a, SWVC08, VC06] and capture all the physics in one-dimensional systems [Has07b, Has06, Vid04]. Matrix product states also explain the success of several numerical methods such as the Density Matrix Renormalization Group (DMRG) proposed by White [Whi92, Whi93] to simulate one-dimensional strongly correlated systems. On the other hand, mixed states can be represented in terms of tensor networs using *matrix product density operators* [VGRC04, PMCV10], which give rise to numerical methods to simulate the evolution of one-dimensional quantum systems in thermal equilibrium and under dissipation [VGRC04, PMCV10]. Matrix product density operators must overcome a major limitation, since it is not possible to decide if the global state is positive semidefinite simply by inspecting the local matrices A_i that define the MPDO [KGE14, DCC$^+$16]. Purifications, a certain type of MPDO, help overcome this problem since they are defined by an MPS with a local environment on each site, which yields a positive global state by construction. The descriptions of a mixed state as a MPDO or as a purification are generally inequivalent [DSPGC13], but there exist several methods to obtain a purification from a given MPDO[DSPGC13].

Another consequence of the locality of interactions is the existence of a bound for the propagation speed of correlations, also known as Lieb-Robinson bound. Lieb-Robinson bounds [LR72] are a fundamental tool to study condensed matter systems and they may be used to show that, under certain conditions, non-relativistic quantum systems exhibit a causal structure which is analogous to quantum field theories [PS95]. These bounds may be also used to prove other important physical properties, such as scaling laws for the entanglement entropy [Has07a, ECP10], the exponential decay of correlations for the ground state of local Hamiltonians with gap [HK06] or the stability of topological order [BHV06].

Although we have only discussed quantum many-body systems to understand their properties, they are also extensively studied in order to find novel applications in quantum technologies [OFV10]. For instance, quantum systems may be exploited to find applications in quantum metrology [LKD02, GLM11], such as the improvement of measurement techniques using entanglement [NKD$^+$11,

Mac13] or quantum algorithms which improve over classical resources.

2.2 Objectives and main results

This thesis is devoted to the study of correlations, locality and entanglement in quantum systems. It focuses on mathematical techniques such a tensor network representations, Lieb-Robinson bounds and quantum algorithms to obtain original analytical and numerical results with practical applications in quantum information theory, condensed matter and quantum metrology. The main results of this work may be classified into three main categories in which we try to give answers to differents problems: "Entanglement and matrix product states", "Locality and Lieb-Robinson bounds" and "Quantum algorithms for quantum metrology".

Entanglement and matrix product states

Matrix product states provide a natural representation of quantum many-body systems in terms of the entanglement structure of the system. While entanglement is one of the most fundamental resources in quantum physics, it is not well known under which conditions there exists a large amount of entanglement [Sre93, ECP10]. Some results have been obtained for one-dimensional systems, such as that states which undergo a quantum quench display a large amount of entanglement [Car11] but the general picture is yet incomplete. Our objective in Chapters 5 and 6 is finding new physical settings to quantify entanglement, such as the fractionalization in the magnetization of a spin chain or the impossibility of approximating a given state by the ground state of a short-range gapped and frustration-free Hamiltonian.

Objetive 1: Study the relationship between the fractionalization in the magnetization of a quantum spin chain and the entanglement entropy of the system.

In Chapter 5 we use matrix product states to quantify the amount of entanglement between two disjoint regions of a one-dimensional spin chain, in terms of the fractionalization in the magnetization of the system [CSW$^+$13]. We prove that a large fractional magnetization in such state must imply a large amount of entanglement in the system. In order to rigorously prove this statement, we have to further develop the theory of matrix product states, extending previous results presented in Refs. [PGVWC07, PGWS$^+$08, SWPGC09], and deriving new ones.

Objetive 2: Study the relationship between the existence of long-range interactions in the parent Hamiltonian of a quantum spin chain and the entanglement entropy of the system.

In Chapter 6, we obtain a different setting in which it is possible to give a lower bound for the amount of entanglement for a one-dimension quantum many-body system. When a system has long-range interactions, it is intuitively expected that any region will be correlated to any othe region of the state, which should be reflected accordingly in the entanglement entropy. Nevertherless, it not easy to obtain a rigorous result to back up this intuition. We establish a lower bound for the entanglement entropy of a translationally invariant MPS, which is not the ground state of any short-range gapped and frustration-free Hamiltonian and such that it is sufficiently far away from any other state with this property for any given interaction length [CSW$^+$13]. Furthermore, we show that the entanglement scales linearly with the range of the interaction. In order to derive this result, we must obtain new bounds to approximate the reduced density matrix of the system using another reduced density matrix whose matrices have a smaller bond dimension.

Locality and Lieb-Robinson bounds

Locality is another of the properties that we study extensively in this thesis, since the systems that we deal with are comprised of particles interacting locally with each other. A consequence of locality is the existence of a finite upper bound for the speed of propagation for excitations, also known as Lieb-Robinson bound. In 1972, Lieb and Robinson proved that the group velocity for the propagation of correlations in quantum many-body systems with short-range interactions is upper bounded by a finite constant in time [LR72]. Afterwards, these bounds were extended to numerous settings, ranging from systems with long-range interactions but with a power-law or for certain types of unbounded Hamiltonians [NRSS07, NRSS09, NS10a, BHV06, PSHKMK09, CSE08]. Many results about the spread of correlations and interesting theoretical applications have been developed using Lieb-Robinson bounds such as the exponential clustering of correlations [HK06] or the efficiency of the time-dependent density matrix renormalization group methods [Whi92, Whi93]. Our objetive is finding new Lieb-Robinson bounds for spin-boson lattice models which describe the physics of ion crystals.

Objetive 3: Establish Lieb-Robinson bounds for spin-boson lattice models.

In Chapter 7, we obtain Lieb-Robinson bounds for a general model of finite dimensional systems interacting through a bosonic field that satisfies a Lieb-Robinson bound itself in the absence of spin-boson coupling [JCPG$^+$13]. These

bounds apply to the general case of spin-boson lattice models independently of the geometry of the lattice and they can be tested using state-of-the-art technology.

Objetive 4: Obtain Lieb-Robinson bounds for ion crystals in different regimes.

In Chapter 8, we apply the Lieb-Robinson bounds that we have obtained in Chapter 7 to crystals of trapped ions and we find that the velocity for the spread of correlations can be faster than the time scales in the experimental regimes currently considered [JCPG+13]. We also derive Lieb-Robinson bounds in the perturbative regime, with slower correlation speeds, and in the impulsive regime, where the forces act locally on the distant ions for a short interval of time and the propagation of correlations only depends on the bare propagation of the phonons and on the efficiency of the spin-boson coupling in correlating spins and bosons. We obtain the optimal propagation spread in the impulsive regime when the original Lieb-Robinson bound is saturated. We propose an experimental scheme to measure retarded correlation functions via the crystal fluorescence, which allows us to test the Lieb-Robinson bounds that we have derived in the impulsive regime.

Quantum algorithms for quantum metrology

Entanglement and correlations have given rise to groundbreaking applications in quantum technologies [OFV10, Par09], such as quantum key distribution systems [GT07] in which entanglement is used to assure the secrecy of keys for cryptographic applications. They have also been used in quantum metrology [LKD02] to obtain new measurement techniques which improve the precision in comparison to classical protocols [CPHH15]. In this area, our objetive is looking for new applications of correlations in quantum metrology such as the characterization and stabilization of a frequency comb.

Objetive 5: Quantum systems may be used as detectors that measure properties of laser pulses with high precision

In Chapter 9, we propose new quantum algorithms to measure the time correlations which accumulate in a quantum system during its interaction with a train of laser pulses. Using this idea, we introduce the notion of multipulse quantum interferometry (MPQI)[CMPGR14], where a single atom or an ensemble of atoms act as a detector that measures differences between pulses of laser light or specific properties of the pulses. Afterwards, we show how these algorithms can be used to characterize and stabilize the train of pulses that form a frequency comb. This application exhibits a polynomial enhancement over the sensitivity of classical protocols and could be used to build new time and frequency standards.

2.3 Overview

This thesis is composed of an abstract in Spanish and in English, and the complete work in English. The body of the thesis is structured in ten chapters: the first of them, Chapter 2, is a self-contained introduction and motivation, Chapters 3 and 4 introduce the required concepts to give context and to successfully navigate through the rest of the memory. These chapters cover different topics, such as the principles of quantum mechanics, entanglement theory, tensor network theory or Lieb-Robinson bounds. Chapters 5-9 contain the main results of the dissertation and all of them have an analogous structure comprised of an introduction, the main results and a conclusion which summarizes the results and presents an outlook on future lines of research.

More specifically, in chapter 2 we present the purpose, the main results and the overview of this thesis; this chapter provides the necessary information about the guidelines of the thesis, the main results and the structure of this work.

Chapters 3 and 4 review some background information which will be helpful to those readers who are unfamiliar with some parts of the field of research. These chapters provide a unified language and the set of techniques needed to address the results contained in the body of the thesis. Chapter 3 reviews the basic concepts of quantum mechanics, entanglement theory and entanglement measures. Later on, we discuss the propagation of information in quantum systems, dwelving into the famed Lieb-Robinson bounds. Chapter 4 introduces a mathematical tool which will be used in the body of this thesis to represent quantum many-body systems: tensors networks and, in particular, matrix product states.

Chapters 5 and 6 contain the results related to entanglement and matrix product states. They concern objectives 1 and 2 and have been published in Physical Review B 87, 035114 (2013).

Chapters 7 and 8 deal with Lieb Robinson bounds for spin boson lattice models and its application to trapped ions. We have divided these results into two different chapters, since we present mathematical results and experimental implementation proposals. In particular, Chapter 7 addresses objective 3 and Chapter 8 addresses objective 4. The results presented in these chapters have been published in Physical Review Letters 111, 230404 (2013).

Chapter 9 addresses objetive 5. The results contained in this chapter have been published in Physical Review Letters 112, 073603 (2014).

Finally, in Chapter 10 we present the main conclusions and future lines of work discussed in each chapter.

About this thesis

This thesis is submitted by Andrea Cadarso Rebolledo to the Department of Mathematical Analysis of Universidad Complutense of Madrid, in partial fulfillment of the requirements for the degree of Doctor of Philosophy in Mathematics. It has been directed by Dr. David Pérez García, Full Professor of Mathematics at Universidad Complutense of Madrid, and by Dr. Juan José García Ripoll, Researcher at the Spanish National Research Council (CSIC), for the doctoral program in Mathematical Research at Universidad Complutense of Madrid.

2.4 Scientific contributions

The results contained in this thesis have been partially published in international peer-reviewed papers. In particular, three articles have been accepted, corresponding to chapters 5, 6, 7, 8 and 9:

- "Phase stabilization of a frequency comb using multi-pulse quantum interferometry" Andrea Cadarso, Jordi Mur-Petit, Juan José García-Ripoll. Phys. Rev. Lett 112, 073603 (2014).
- "Lieb-Robinson bounds for spin-boson lattice models and trapped ions" Johannes Juenemann, Andrea Cadarso, David Pérez-García, Alejandro Bermudez, Juan José García-Ripoll. Phys. Rev. Lett 111, 230404 (2013).
- "Entanglement, fractional magnetization and long-range interactions" Andrea Cadarso, Mikel Sanz, Michael M. Wolf, J. Ignacio Cirac, David Perez-García. Phys. Rev. B 87, 035114 (2013).

They have also been presented in several seminars, workshops and conferences as either a poster or an oral contribution:

- "Lieb-Robinson bounds for spin-boson models and quantum field theories" 1-3 June 2015, Workshop Información Cuántica en España, EHU-UPV, Bilbao, Spain. (Oral contribution)
- "Phase stabilization of a frequency comb using Multipulse Quantum Interferometry" 30 June 2014, Quantum Roundabout, University of Nottingham, UK. (Oral contribution)
- "Phase stabilization of a frequency comb using trapped atoms" 14 January 2013, V Encuentro Gases Cuánticos en Madrid, CSIC, Madrid, Spain. (Oral contribution)

- "Entanglement, fractional magnetization and long-range interactions" 7-9 November 2012, Quantum Square - Student conference on mathematical and theoretical aspects of quantum mechanics, Nottingham, UK. (Oral contribution)
- "Entanglement, fractional magnetization and long-range interactions" 19-21 September 2012, Workshop of Young Researchers in Mathematics, UCM, Madrid, Spain. (Oral contribution)
- "Entanglement, fractional magnetization and long-range interactions" 17-19 September 2012, Workshop Información Cuántica en España, CSIC, Madrid, Spain. (Oral contribution)
- "Entanglement, fractional magnetization and long-range interactions" May 2012, Networking tensor networks, Benasque, Huesca, Spain. (Oral contribution)
- "Entanglement, fractional magnetization and long-range interactions" September 2011, Workshop of Young Researchers in Mathematics, UCM, Madrid, Spain. (Oral contribution)
- "Lieb-Robinson bounds for spin-boson models and quantum field theories" 16-17 April 2015, 17th Symposium in Topological Quantum Information, Garching, Germany. (Poster)
- "Lieb-Robinson bounds for spin-boson models and quantum field theories" 13-15 April 2015, Quantum Correlations beyond Entanglement, Bad-Honnef, Germany. (Poster)
- "Lieb-Robinson bounds for spin-boson lattice models and trapped ions" 24-30 August 2014, Numerical and Analytical methods for Strongly Correlated Systems, Centro de Ciencias de Benasque "Pedro Pascual", Benasque, Spain. (Poster)
- "Entanglement, fractional magnetization and long-range interactions" 19-21 November 2012, Workshop Entangle this: strings, fields and atoms, UAM, Madrid, Spain. (Poster)
- "Entanglement, fractional magnetization and long-range interactions" 22-25 October 2012, Workshop on Quantum Simulations, EHU, Bilbao, Spain. (Poster)
- "Entanglement, fractional magnetization and long-range interactions" July 2012, Workshop in Quantum Information, Seefeld, Austria. (Poster)
- "Entanglement, fractional magnetization and long-range interactions" 24-27 April 2012, Quantum Malta 2012: Fundamental Problems in Quantum Physics, Malta. (Poster)

3 Entanglement and locality in quantum many-body systems

In this chapter we present the basic concepts that will be needed in the rest of the Thesis, regarding the mathematical description of quantum many-body systems, entanglement and locality. In section 3.1 we provide the mathematical notation and background information for quantum many-body systems. Afterwards, in section 3.2, we introduce the notion of entanglement, probably the most striking feature of quantum mechanics. In section 3.3, we bring up the idea of locality and we explain what Lieb-Robinson bounds are. Advanced readers may skip this chapter.

3.1 Quantum many-body systems

In what follows we define a quantum state as a complete representation of a quantum physical system. Systems whose state is known exactly correspond to *pure states* and they are described by unit vectors in a Hilbert space $\mathcal{H}$, known as the *state space* of the system. We use the notation $|\psi\rangle$ for the unit vectors in the Hilbert space $\mathcal{H}$, also known as *kets*.

A Hilbert space is a vector space endowed with an inner product and complete (recall that completeness means that every Cauchy sequence in $\mathcal{H}$ converges in $\mathcal{H}$ with the norm induced by the inner product in $\mathcal{H}$). In the following chapters we consider that $\mathcal{H}$ is a finite dimensional complex vector space, that is, $\mathcal{H} = \mathbb{C}^d$. We define $\mathcal{B}(\mathcal{H})$ as the set of (bounded) linear operators acting on $\mathcal{B}(\mathcal{H})$. We consider the set of orthonormal vectors $\{|i\rangle, 1 \leq i \leq d\}$ as the computational basis in $\mathcal{H} = \mathbb{C}^{\mathrm{d}}$ where we assume that

$$\begin{aligned} |1\rangle^T &= \begin{bmatrix} 1 & 0 & \dots & 0 \end{bmatrix} \\ |2\rangle^T &= \begin{bmatrix} 0 & 1 & \dots & 0 \end{bmatrix} \\ &\vdots \\ |d\rangle^T &= \begin{bmatrix} 0 & 0 & \dots & 1 \end{bmatrix} \end{aligned} \tag{3.1}$$

In this basis we write ket vectors as follows

$$|\psi\rangle^T = \psi_1|1\rangle + \psi_2|2\rangle + \ldots + \psi_d|d\rangle \tag{3.2}$$

$$= \begin{bmatrix}\psi_1 & \psi_2 & \ldots & \psi_d\end{bmatrix} \tag{3.3}$$

The Hermitian transposition of a ket vector $|\phi\rangle$ with respect to the computational basis is called a *bra* vector $\langle\phi|$.

$$\langle\phi| = \begin{bmatrix}\phi_1^* & \phi_2^* & \ldots & \phi_d^*\end{bmatrix} \tag{3.4}$$

Bras are linear maps from the Hilbert space $\mathcal{H}$ to the complex field $\mathbb{C}$, and we have the following relation:

$$\langle\phi|(|\psi\rangle) = \langle\phi|\psi\rangle \tag{3.5}$$

Performing a measurement in the computational basis is done taking into account that the probability of obtaining a given result is the absolute value squared of the corresponding vector entry, that is,

$$Pr(i) = \langle\psi_i|\psi_i\rangle = |\psi_i|^2. \tag{3.6}$$

The time evolution of a closed quantum system is described by a unitary transformation. The state of the system $|\psi\rangle_{t_0}$ at a time t_0 is related to the state of the system $|\psi\rangle_{t_1}$ at a time t_1 by a unitary operator U which depends only on times t_0 and t_1 :

$$|\psi\rangle_{t_1} = U_{t_0,t_1}|\psi\rangle_{t_0} \tag{3.7}$$

This statement is roughly equivalent to postulating that the evolution of the system can be predicted using Schrödinger's equation

$$i\hbar\frac{d|\psi\rangle}{dt} = H|\psi\rangle, \tag{3.8}$$

where $\hbar$ is Planck's constant and H is an Hermitian operator known as the Hamiltonian of the closed system.

In physical systems, we are mostly concerned with measuring certain properties or physical quantities, which can be observed for all the available states. In particular, we will use a particular case of measurements called *projective measurements* which are described by the corresponding observable. Observables are Hermitian linear operators on the state space that is observed [NC11]. Every observable O has a spectral decomposition

$$O = \sum_m \lambda_m P_m, \tag{3.9}$$

where P_m is the projector onto the eigenspace of O with eigenvalue λ_m. The eigenvalues $\{\lambda_m\}$ of the observables O are the possible outcomes of the measurement process. Once we measure the state $|\psi\rangle$ to obtain the value of an observable O, the probability of obtaining λ_m is

$$Pr(\lambda_m) = \langle\psi|P_m|\psi\rangle. \tag{3.10}$$

Given that we have obtained λ_m as the result of the measurement, then we can affirm that the state of the quantum system after the measurement is

$$|\psi'\rangle = \frac{P_m|\psi\rangle}{\sqrt{Pr(\lambda_m)}}, \tag{3.11}$$

and the average value of the projective measurement is given by

$$\mathbb{E}(O) = \sum_m \lambda_m Pr(\lambda_m) = \langle\psi|O|\psi\rangle. \tag{3.12}$$

Sometimes we need to describe quantum systems whose state is not completely known, such as in a real experiment or in a system not isolated from the environment. Suppose that the quantum system may be in one of a number of pure states $\{|\psi_i\rangle\}_i$ with certain probabilities $\{p_i\}_i$, such that $|\psi_i\rangle \in \mathcal{H}$, $p_i \geq 0$ for all i and $\sum_i p_i = 1$. The set $\{p_i, |\psi_i\rangle\}$ is called an *ensemble of pure states*. The density operator of the system ρ is defined as a convex combination of rank-one projectors as follows:

$$\rho = \sum_i p_i |\psi_i\rangle\langle\psi_i| \tag{3.13}$$

where p_i is a probability distribution, $p_i \geq 0$ for all i, $\sum_i p_i = 1$ and $|\psi_i\rangle \in \mathcal{H}$. The set of density operators or density matrices is denoted as $\mathcal{D}(\mathcal{H}) = \{\rho \in \mathcal{B}(\mathcal{H}) | \rho \geq 0, \mathrm{Tr}\rho = 1\} \subset \mathcal{B}(\mathcal{H})$, and it corresponds to the set of bounded linear positive semi-definite operators with unit trace on the Hilbert space $\mathcal{H}$. In the computational basis, the elements of $\mathcal{D}(\mathcal{H})$ may be written as $d \times d$ matrices with complex elements, $M_{d\times d}$. We note that the description in Eq. 3.13 of a given density operator is generally not unique and also that different ensembles may give rise to the same density operator.

In terms of the density operator description, a pure state can be written as

$$\rho_{|\psi\rangle} = |\psi\rangle\langle\psi|, \tag{3.14}$$

where $|\psi\rangle \in \mathcal{H}$ is a unit vector. Otherwise, we say that the state is in a mixture of the pure states in the ensemble $\{p_i, |\psi_i\rangle\}$ or that it is a *mixed state.* The representation of quantum systems as density operators implies that the calculation of observables may be carried out as follows

$$\mathbb{E}(O) = \mathrm{Tr}\left[O\rho\right]. \tag{3.15}$$

The postulates of quantum mechanics may be written equivalently in terms of state vectors or in terms of density operators. We use one notation or the other depending on the problem that we need to solve; for instance, density operators are specially useful in systems whose state is not known, such as in the preparation of experiments, in systems undergoing dissipation, or in the description of subsystems of composite quantum systems.

Composite quantum systems which are comprised of subsystems A_1, A_2, ..., A_n may be represented in a Hilbert space $\mathcal{H}$ with a tensor product structure $\mathcal{H} = \mathcal{H}_1 \otimes \ldots \otimes \mathcal{H}_n$ where $\mathcal{H}_i$ is the Hilbert space of the subsystem i.

3.2 Entanglement

Correlations among random variables measure the relationships of dependence that exist between them. For instance, in statistical physics, correlations functions are a measure of the relationship among microscopic variables which are located either at different spatial or time positions. On the other hand, quantum many-body systems display a richer correlation structure than classical systems, since they may exhibit quantum correlations, such as entanglement, apart from purely classical correlations.

The non-local correlations predicted by quantum mechanics were initially discussed by Einstein, Podoslky and Rosen in their seminal work of 1935 [EPR35], in which they conclude that the mere existence of such exotic properties would necessarily invalidate the completeness of quantum mechanics and its capability to successfully describe Nature. However, later that same year, Schrödinger coined the phenomenon with the German word *verschränkung*, which he translated as *entanglement*. While rejected and considered unphysical by Einstein, Schrödinger [Sch35] and Bohr [Boh35] acknowledged entanglement as the defining trait of quantum theories, which led them to revisit the idea of reality and the character of physical phenomena. In Schrödinger's words:

Entanglement is not one but rather the characteristic trait of quantum mechanics, the one that enforces its entire departure from classical lines of thought. [Sch35]

A very simple case in which we may observe this phenomenon is in a system composed of two particles A and B of spin $\frac{1}{2}$, with possible states either $|\uparrow\rangle$ or $|\downarrow\rangle$. This system is completely described by the singlet state:

$$|\psi_{\text{EPR}}\rangle = \frac{1}{\sqrt{2}} \left(|\uparrow\rangle_A \otimes |\downarrow\rangle_B - |\downarrow\rangle \, d_A \otimes |\uparrow\rangle_B \right). \tag{3.16}$$

Despite $|\psi_{\text{EPR}}\rangle$ being a pure state, the state of any of the two individual subsystems for particles A and B is random and correlated to the other, which is reflected in the measurement of any observable on the state. For instance, if

we measure the spin of any of the two particles independently, we observe that while any one of them may *randomly* be either $|\uparrow\rangle_A$ or $|\downarrow\rangle_A$ with probability $\frac{1}{2}$, the other must necessarily point in the opposite direction.

Entanglement and separability of quantum states

Let us consider a bipartite quantum system, that is, a system composed of two different subsystems A and B described by a Hilbert space $\mathcal{H} = \mathcal{H}_A \otimes \mathcal{H}_B$.

Definition 3.1 (Separability of pure states)**.** *A pure state $|\psi\rangle \in \mathcal{H}_A \otimes \mathcal{H}_B$ is a separable state if it can be written as a product of pure states*

$$|\psi\rangle = |\psi_A\rangle \otimes |\psi_B\rangle, \tag{3.17}$$

where $|\psi_A\rangle \in \mathcal{H}_A$ and $|\psi_B\rangle \in \mathcal{H}_B$.

Definition 3.2 (Separability of mixed states)**.** *A mixed state $\rho \in \mathcal{D}(\mathcal{H}_A \otimes \mathcal{H}_B)$ is a separable state if it admits a convex decomposition as follows*

$$\rho = \sum_i p_i \rho_A^{(i)} \otimes \rho_B^{(i)}, \ \sum_i p_i = 1, \ p_i \geq 0, \tag{3.18}$$

where $\rho_A^{(i)} \in \mathcal{D}(\mathcal{H}_A)$ and $\rho_B^{(i)} \in \mathcal{D}(\mathcal{H}_B)$.

In the multipartite case, we consider the Hilbert space $\mathcal{H} = \mathcal{H}_1 \otimes \ldots \otimes \mathcal{H}_n$ where there are many ways of defining separability. Any separable state can be produced by Local Operations and Classical Communication (LOCC) starting from a product state [Wer89]

$$|\psi\rangle = |\psi_1\rangle \otimes \ldots \otimes |\psi_n\rangle \tag{3.19}$$

that is, they can be created by parties in separate laboratories exchanging only classical information.

Entangled states are those which are not separable, and deciding whether a given state is entangled or not, that is, whether it has quantum correlations or only classical correlations is called the *separability problem*. The problem of determining whether a general state $\rho \in \mathcal{D}(\mathcal{H})$ is separable or not is not trivial and, even in the bipartite case, is NP-hard [Gur03].

If we consider a bipartite system in a Hilbert space $\mathcal{H} = \mathcal{H}_A \otimes \mathcal{H}_B$ we obtain the following definitions of entangled states:

Definition 3.3 (Entanglement of pure states)**.** *A pure state $|\psi\rangle \in \mathcal{H}_A \otimes \mathcal{H}_B$ is entangled if and only if it is not separable, that is, if there are no local states $|\psi_A\rangle \in \mathcal{H}_A$ and $|\psi_B\rangle \in \mathcal{H}_B$ such that the state of the system $|\psi\rangle$ can be written as a product of pure states*

$$|\psi\rangle = |\psi_A\rangle \otimes |\psi_B\rangle. \tag{3.20}$$

The criterion for deciding whether pure states in a bipartite system are entangled or not is quite simple in terms of the Schmidt decomposition [NC11].

Theorem 1 (Schmidt decomposition)**.** *Let us suppose that $|\psi\rangle \in \mathcal{H}_A \otimes \mathcal{H}_B$ is a pure state of a composite system, AB. Then there exist orthonormal states $\{|i_A\rangle\} \in \mathcal{H}_A$ for system A, and orthonormal states $\{|i_B\rangle\} \in \mathcal{H}_B$ of system B such that*

$$|\psi\rangle = \sum_i \lambda_i |i_A\rangle |i_B\rangle, \tag{3.21}$$

where λ_i are non-negative real numbers satisfying $\sum_i \lambda_i^2 = 1$ known as Schmidt coefficients. If there is no degeneracy, this decomposition is unique up to arbitrary opposite phases in $|i_A\rangle$ and $|i_B\rangle$.

Definition 3.4 (Schmidt rank)**.** *The Schmidt rank, $r(|\psi\rangle)$, is defined as the number of non-vanishing Schmidt coefficients.*

Taking into account the notion of Schmidt decomposition and the definition of Schmidt rank, we obtain the following criterion of separability for pure states:

Proposition 1. *A bipartite pure state $|\psi\rangle \in \mathcal{H}$ is separable if and only if it has Schmidt rank one, $r(|\psi\rangle) = 1$.*

Proposition 1 readily implies that a bipartite pure state is entangled if and only if $r(|\psi\rangle) > 1$. In the mixed case, there exists an analogous definition of entangled states. However, it is not as simple to find a criterium to determine whether a given bipartite mixed state is separable.

Definition 3.5 (Entanglement of mixed states)**.** *A mixed state $\rho \in \mathcal{D}(\mathcal{H}_A \otimes \mathcal{H}_B)$ is entangled if and only if it is not separable, that is, if there is no convex decomposition such that*

$$\rho = \sum_i p_i \rho_A^{(i)} \otimes \rho_B^{(i)}, \ \sum_i p_i = 1, \ p_i \geq 0, \tag{3.22}$$

where $\rho_A^{(i)} \in \mathcal{D}(\mathcal{H}_A)$ and $\rho_B^{(i)} \in \mathcal{D}(\mathcal{H}_B)$.

The Schmidt decomposition may be generalized to mixed states, giving rise to the Schmidt number of a mixed state, s, [TH00],

$$s = \inf_{\{p_i, |\psi_i\rangle\}_i} \max_i r(|\psi_i\rangle) \tag{3.23}$$

using the convex roof extension. From Eq. 3.23 we observe that the Schmidt number of the mixed state ρ is the minimum over all ensembles that generate ρ of the maximal Schmidt rank of the pure states in the ensemble. We obtain an analogous criterium of separability for mixed states in terms of the Schmidt number:

Proposition 2. *A bipartite mixed state $\rho \in \mathcal{D}(\mathcal{H}_A \otimes \mathcal{H}_B)$ is separable if and only if it has Schmidt rank one, $s(\rho) = 1$.*

The question of separability of mixed states is generally quite complex, although there are several operational criteria to test this property in certain cases [HHHH09], such as the positive partial transpose (PPT) criterion [Per96], separability via positive (but not c.p.) maps [HHH96] or criteria based on entanglement witnesses [HHH96, Ter00].

Entanglement measures

The measurement and quantification of entanglement is a very relevant problem in quantum information. In order to approach it, we introduce the idea of entanglement measure:

Definition 3.6 (Entanglement (monotone) measure)**.** *An entanglement (monotone) measure over the set of pure states of a quantum system $\mathcal{H}_1 \otimes \ldots \otimes \mathcal{H}_n$ is a nonnegative real-valued function*

$$E : \mathcal{H}_1 \otimes \ldots \otimes \mathcal{H}_n \to \mathbb{R}^+ \tag{3.24}$$

which is zero for separable states and cannot increase under local operations and classical communication (LOCC).

The definition of entanglement measure can be immediately extended to mixed states simply by changing the domain of the function E, that is,

Definition 3.7 (Entanglement (monotone) measure)**.** *An entanglement (monotone) measure over the set of mixed states of a quantum system $\mathcal{D}(\mathcal{H}_1 \otimes \ldots \otimes \mathcal{H}_n)$ is a nonnegative real-valued function*

$$E : \mathcal{D}(\mathcal{H}_1 \otimes \ldots \otimes \mathcal{H}_n) \to \mathbb{R}^+ \tag{3.25}$$

which is zero for separable states and cannot increase under local operations and classical communication (LOCC).

The entanglement of a pure bipartite state $|\psi\rangle \in \mathcal{H}_A \otimes \mathcal{H}_B$ can be measured by the entropy of entanglement $E(|\psi\rangle)$, which represents the amount of uncertainty present in any of the subsystems A or B. For a pure bipartite state which can be written as

$$|\psi\rangle = \sum_i p_i |\psi_A^i\rangle \otimes |\psi_B^i\rangle, \tag{3.26}$$

its entropy of entanglement is

$$E(|\psi\rangle) = S(\rho_A) = S(\rho_B) \tag{3.27}$$

and it may be computed as the entropy of any of the subystems considered alone, where $\rho_A = \mathrm{Tr}_B |\psi\rangle \langle\psi|$ is the reduced density matrix for system A, after tracing over the degrees of freedom of system B, $\rho_B = \mathrm{Tr}_A |\psi\rangle \langle\psi|$ and $S(\rho)$ is the von Neumann entropy [Sha48].

Definition 3.8 (Von Neumann entropy of quantum states [Sha48]). *Let $\rho \in \mathcal{B}(\mathcal{H})$ be a density matrix, the von Neumann entropy is defined as*

$$S(\rho) := -Tr(\rho \log_2 \rho). \tag{3.28}$$

If we consider $\{\lambda\}_{i=1}^n$ the eigenvalues of the density matrix ρ, then the von Neumann entropy can be computed taking into account that

$$S(\rho) = -\sum_i (\lambda_i \log_2 \lambda_i). \tag{3.29}$$

Note that if ρ_A and ρ_B describe pure states then $E(|\psi\rangle) = S(\rho_A) = S(\rho_B) = 0$. Another measure of entanglement comes from the Renyi entropy of order α, where $\alpha \geq 0$ and $\alpha \neq 1$:

Definition 3.9 (Renyi entropy of a probability distribution [Rén61]). *Let $\mathcal{P} = (p_1, p_2, \ldots, p_n)$ be a finite discrete probability distribution, $\alpha \geq 0$ and $\alpha \neq 1$, then the Renyi entropy of order α of the distribution $\mathcal{P}$ is defined as*

$$H_\alpha(\mathcal{P}) := \frac{1}{1-\alpha} \log \sum_{i=1}^n p_i^\alpha. \tag{3.30}$$

The corresponding entropy of entanglement is written as

$$E_\alpha(|\psi\rangle) = S_\alpha(\rho_A) = S_\alpha(\rho_B) \tag{3.31}$$

where $S_\alpha(\rho)$ is the $\alpha-$Renyi entropy of the density matrix ρ.

Definition 3.10 ($\alpha-$Renyi entropy of quantum states). *Let $\rho \in \mathcal{B}(\mathcal{H})$ be a density matrix, the $\alpha-$Renyi entropy is defined as*

$$S_\alpha(\rho) = \frac{1}{1-\alpha} \log Tr(\rho^\alpha). \tag{3.32}$$

Let $\mathcal{P}' = \{\lambda\}_{i=1}^n$ be the eigenvalues of the density matrix ρ, then the $\alpha-$Renyi entropy can be computed as follows

$$S_\alpha(\rho) = H_\alpha(\mathcal{P}') = \frac{1}{1-\alpha} \log \sum_{i=1}^n \lambda_i^\alpha. \tag{3.33}$$

For both pure states and mixed states there are other measures of entanglement, and the choice of one measure over the rest depends on the specific application. See Refs. [PV05, HHHH09] for a review of entanglement measures and entanglement theory.

3.3 Locality and propagation of correlations. Lieb-Robinson bounds.

Many of the quantum systems that we are interested in are governed by Hamiltonians (see Eq. 3.8) with local interactions on a lattice. We follow an approach very similiar to the works of B. Nachtergaele et al. [NOS06, NS06, NS10a, NS10b]; we define a lattice as an undirected graph $G = (E, L)$ with a set of vertices L, where the physical degrees of freedom are defined, and an edge set E, which describes neighbourhood relations in the lattice. We consider a metric $d : L \times L \to \mathbb{R}^+$ such that for $x, y \in L$, $d(x, y)$ it represents the distance between the subsystems which are located in vertices x and y. We associate a Hilbert space $\mathcal{H}_x$ to each $x \in L$ and the bounded linear operators over the Hilbert space $\mathcal{H}_x$ are given by $\mathcal{B}(\mathcal{H}_x)$. For any finite set Λ, the Hilbert space of the subsystems is given by $\mathcal{H}_\Lambda = \otimes_{x\in\Lambda}\mathcal{H}_x$ and the algebra of observables is $\mathcal{A}_\Lambda = \otimes_{x\in\Lambda}\mathcal{B}(\mathcal{H}_x)$. We identify $A \in \mathcal{A}_\Lambda$ with $A \otimes \mathbb{1} \in \mathcal{A}_L$ which implies that $\mathcal{A}_\Lambda \subset \mathcal{A}_L$. If we consider an increasing sequence of finite subsets $\{\Lambda_n\}_n \subset L$, the algebra of local observables is given by the inductive limit $\mathcal{A}_{\text{loc}} = \cup_n \mathcal{A}_{\Lambda_n}$. We define the support of an observable $A \in \mathcal{A}_{\text{loc}}$, as the minimal set $\Lambda \subset L$ such that A belongs to the subalgebra $\mathcal{A}_\Lambda$, that is, $A = A' \otimes \mathbb{1}$ with $A' \in \mathcal{A}_\Lambda$.

The local Hamiltonians for these systems are defined in terms of interactions. The global Hamiltonian is generally denoted using an uppercase letter H, and interactions are mappings h from the set of finite subsets of L into $\mathcal{A}_{\text{loc}}$ such that for each finite $X \subset L$,

$$h_X^* = h_X \in \mathcal{A}_X. \tag{3.34}$$

where the subscript indicates the sites the local Hamiltonian h acts on nontrivially and each h_X can be identified with $h_X \otimes \mathbb{1}_{L\setminus X} \in \mathcal{A}_{\text{loc}}$. For subsets that contain a single vertex of the graph, i.e. $X = \{x\}$, the mapping h is called an on-site interaction whereas, when this is not the case, the mapping h is called a local interaction. A local (finite-range) Hamiltonian H on the finite set $\Lambda \subset L$ is defined as

$$H = \sum_{X\subset\Lambda} h_X \,. \tag{3.35}$$

A simple one-dimensional Hamiltonian with this structure is the Ising Hamiltonian with a transverse magnetic field

$$H_{\text{Ising}} = -J \sum_i \sigma_i^x \sigma_{i+1}^x - h \sum_i \sigma_i^z, \tag{3.36}$$

which is written as a sum of nearest-neighbour interactions and on-site interactions.

For local Hamiltonian H, the Heisenberg dynamics are well-defined and the time evolution of an observable $A \in \mathcal{A}_{\mathrm{loc}}$ can be written as

$$A(t) = e^{itH_\Lambda} A e^{-itH_\Lambda}. \tag{3.37}$$

and forms a group of automorphisms.

If the set L is infinite, we must assume that there is a non-increasing, real-valued function $F : [0, \infty) \to (0, \infty)$, with the following properties [NS10a, NS10b, NRSS09]:

1. F must be uniformly integrable over L :

$$\|F\| = \sup_{x \in L} \sum_{y \in L} F(d(x, y)) \, < \, \infty \, . \tag{3.38}$$

2. F must have the convolution property, that is, there exists a number $C > 0$ such that for any pair $x, y \in L$,

$$\sum_{z \in L} F(d(x, z)) F(d(z, y) \leq C F(d(x, y)) \, . \tag{3.39}$$

We can assume that $C = 1$ without loss of generality simply by replacing F by $C^{-1}F$.

Proposition 3 ([NOS06, NS10b])**.** *If there exists a function F on L satisfying i) and ii), then for any $\mu \geq 0$, the function F_μ defined by setting $F_\mu(r) = e^{-\mu r} F(r)$ also satisfies i) and ii) with $\|F_\mu\| \leq \|F\|$ and $C_\mu \leq C$.*

Theorem 2 (Lieb-Robinson bounds [NOS06, NS10b])**.** *For any $\mu \geq 0$, we denote by $\mathcal{B}_\mu(L)$ the set of interactions h for which*

$$\|h\|_\mu = \sup_{x, y \in \Gamma} \frac{1}{F_\mu(d(x, y))} \sum_{\substack{X \subset \Gamma; \\ x, y \in X}} \|h_X\| \, < \infty \, . \tag{3.40}$$

If $h \in \mathcal{B}_\mu(\Gamma)$, then a Lieb-Robinson bound of the form

$$\|[A(t), B(0)]\| \leq 2\|A\|\|B\| C_\mu^{-1} \, (e^{2C_\mu \|h\|_\mu |t|} - 1) \sum_{x \in X} \sum_{y \in Y} F_\mu(d(x, y)) \tag{3.41}$$

holds for all $A \in \mathcal{A}_X$, $B \in \mathcal{A}_Y$, $X \cap Y = \emptyset$, and $t \in \mathbb{R}$.

If $\mu > 0$, then the double sum that appears in 2 can be bounded by an exponentially decaying factor $C\|F\|e^{-\mu d(X,Y)}$, which gives rise to the following version of the bound [NOS06, NS10b]:

$$\|[A(t), B(0)]\| \leq 2\|A\|\|B\| C e^{-\mu(d(X,Y) - v|t|)} \, . \tag{3.42}$$

In this case, $v = 2\mu^{-1}C_\mu\|h\|_\mu$ is the Lieb-Robinson velocity and we can take $C = C_\mu^{-1}\min(|X|, |Y|)$ or, in the case of interactions of finite range R,

$$C = RC_\mu^{-1}\min(|\partial X|, |\partial Y|) \tag{3.43}$$

where $|\partial Z|$ is the size of the boundary of Z.

As we haven seen in Eq. 3.42, the locality of the interactions in the Hamiltonian, under certain additional conditions, gives rise to the existence of an upper bound for the speed of propagation of excitations and an effective light cone with exponentially decaying tails. In 1972, Lieb and Robinson proved a slightly weaker form of Theorem 2, concluding that there exists a bound on the group velocity in quantum spin dynamics generated by a short-range Hamiltonian [LR72]. This result has been generalized to many other physical setups, such as finite-dimensional models, anharmonic oscillators or master equations [HK06, NOS06, CSE08, NRSS09, Pou10].

Lieb-Robinson bounds imply that non-relativistic quantum many-body systems, under certain conditions, show a causal structure analogous to relativistic quantum field theories. On the other hand, Lieb-Robinson bounds are a fundamental technique to prove the existence of relevant properties in quantum many-body systems, such as the exponential decay of correlations in the ground-state of gapped local Hamiltonians [HK06] or the scaling area laws for entanglement entropy [Has07a, ECP10].

4 Tensor Network States

In this chapter we present the basic notions that we will use in the rest of the Thesis, concerning matrix product states, matrix product density operators and numerical methods which exploit these representations. In Section 4.1 we introduce the concept of matrix product states and we state some of the most relevant results based on the MPS theory. Then, in Section 4.2, we extend the concept of tensor networks to mixed states through matrix product density operators and purifications. In Section 4.3 we present several numerical methods which use matrix product states and matrix product density operators to calculate the evolution in real time and in imaginary time of pure states and of mixed states. Advanced readers may skip this chapter.

4.1 Matrix product states

As we have already discussed in Chapter 3, pure states of N particles, each of them corresponding to a $d-$dimensional Hilbert space, can be described as vectors in a complex Hilbert space, using the notation $|\psi\rangle \in \mathbb{C}^{\otimes d^N}$. The matrix product state representation [FNW92, PGVWC07] of a one-dimensional system of size N may be written as follows

$$|\psi\rangle = \sum_{i_1,\ldots,i_N=1}^{d} \mathrm{tr}\left[A_{i_1}^{[1]} A_{i_2}^{[2]} \ldots A_{i_N}^{[N]}\right] |i_1,\ldots,i_N\rangle \tag{4.1}$$

where d is the dimension of the Hilbert space corresponding to the physical system, $\{A_{i_j}^{[j]}\}_j \subset \mathcal{M}_{D_j \times D_{j+1}}$ are matrices associated to the site j of the one-dimensional system. We consider that $|i_1,\ldots,i_N\rangle = |i_1\rangle \otimes \ldots \otimes |i_N\rangle$ and $|i_r\rangle$ are the elements of the computational basis. In Eq. 4.1, $|\psi\rangle$ is not necessarily normalized and it is important to note that the MPS representation is not unique. This class of states offers a local description of quantum states, since every state can be represented as a matrix product state if each bond dimension D_k is sufficiently large. Nevertheless, once we fix the bond dimension of the state, it is only necessary to use a polynomial number of parameters to describe the state, in sharp contrast to the exponential growth of the underlying Hilbert space. Generally, we consider quantum states to be matrix product states if they have a matrix

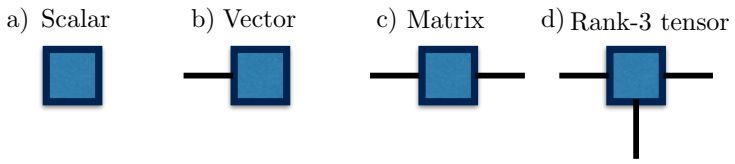

Figure 4.1: Tensor networks have a simple diagrammatic representation. In these pictures: (a) is a scalar, (b) is a vector, (c) is a matrix and (d) is a rank-3 tensor.

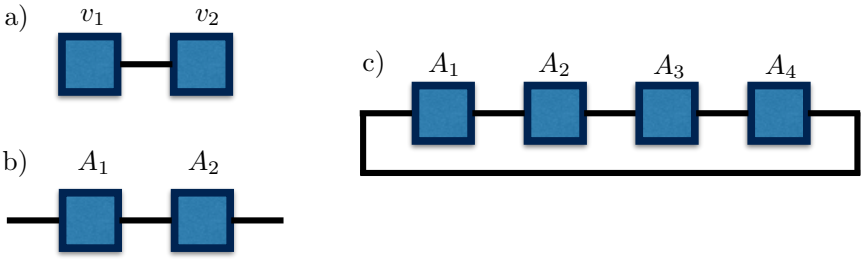

Figure 4.2: Tensor networks diagrams can represent tensor operations in a visual and simple way. In these pictures: (a) is a vector product, (b) is a matrix product, (c) is the trace of the product of four matrices.

product state representation with a small bond dimension $D = \max_k D_k$ which does not grow with the system size N.

Tensor networks and, in particular, MPS can be represented graphically using tensor network diagrams. In these diagrams, a square depicts a tensor, lines (legs) which emerge from the squares represent the indices in the tensors. Lines that connect the squares among each other represent contraction rules between the tensors and unconnected lines which emerge from squares represent open indices in the tensor network (see Fig. 4.1).

Calculations involving tensor networks can be translated to tensor network diagrams, which allow to handle complicated algebraic manipulations in a much more visual way. Some examples of the diagrams for calculations are represented in Fig. 4.2, such as the vector product, the matrix product or the trace of the product of several matrices. See Ref. [Orú14] for a review of tensor networks and the diagrammatic notation.

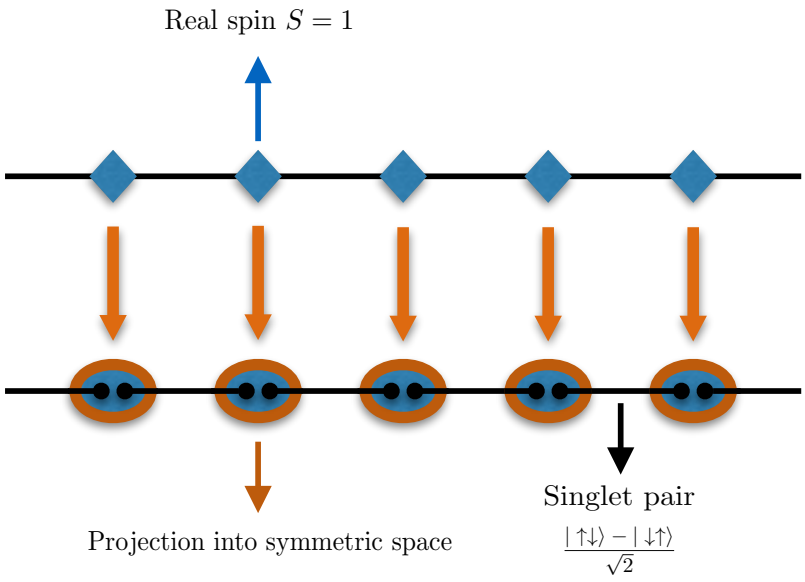

Figure 4.3: Diagram of the construction of the AKLT model using the Valence Bond State (VBS) picture. This construction relies on partial projections on bipartite singlets.

Matrix product states and the AKLT model

The AKLT model was proposed by Afflect, Kennedy, Lieb and Tasaki in 1972 [AKLT87, AKLT88] as a representation of an antiferromagnetic spin-1 chain with quantum fluctuations. This model has an exact solution and it is possible to prove the existence of a Haldane gap rigorously. We will revisit the construction of the AKLT ground state as a paradigmatic example of matrix product states. In fact, the main objetive of the original paper on matrix product states by Fannes, Nachtergaele and Werner [FNW92] was extending the valence bond picture of the AKLT model to the largest possible family of states.

The AKLT Hamiltonian represents an isotropic one-dimensional spin chain, it is gapped, it has a unique ground state in the thermodynamic limit, a continuous $SO(3)$ symmetry and an exponential decay of the correlation functions in the ground state. It can be written as follows

$$H = \sum_i \left[\frac{1}{2} \vec{S}_i \cdot \vec{S}_{i+1} + \frac{1}{6} \left(\vec{S}_i \cdot \vec{S}_{i+1} \right)^2 + \frac{1}{3} \right]. \tag{4.2}$$

In order to find its ground state, we consider a spin-1 chain of N particles, and we associate two virtual spin-$\frac{1}{2}$ to each site of the chain. A spin-1 can be

interpreted as the symmetric part of the tensor product of two spin-$\frac{1}{2}$, so we will use this observation to construct a state in the so-called valence bond picture. The state is constructed by creating a singlet between a virtual spin-$\frac{1}{2}$ from site i and a virtual spin-$\frac{1}{2}$ from site $i+1$, and symmetrizing the two virtual spin-$\frac{1}{2}$ in each site to obtain a spin-1 afterwards, as shown in Fig. 4.3. That is, two spin-$\frac{1}{2}$ form a singlet state on neighbouring sites:

$$\frac{|\uparrow\downarrow\rangle - |\downarrow\uparrow\rangle}{\sqrt{2}}, \tag{4.3}$$

and the entangled bond state at a given site is identified with a pair of spin-$\frac{1}{2}$ which has been symmetrized

$$|s_{\alpha,\beta}\rangle := \frac{1}{\sqrt{2}}\left(|\alpha\rangle|\beta\rangle + |\beta\rangle|\alpha\rangle\right) \tag{4.4}$$

where $\alpha, \beta \in \{\uparrow, \downarrow\}$ and clearly $|s_{\alpha,\beta}\rangle$ and $|s_{\beta,\alpha}\rangle$ give rise to the same state. We can associate an orthonormal basis of the real space of spin-1 particles to the virtual space of the singlet states generated by the product of virtual spin-$\frac{1}{2}$ particles, simply by identifying

$$|+1\rangle = \frac{|s_{\uparrow,\uparrow}\rangle}{\sqrt{2}} = |\uparrow\uparrow\rangle\,, \tag{4.5}$$

$$|0\rangle = |s_{\downarrow,\uparrow}\rangle = |s_{\uparrow,\downarrow}\rangle = \frac{1}{\sqrt{2}}\left(|\uparrow\downarrow\rangle + |\downarrow\uparrow\rangle\right), \tag{4.6}$$

$$|-1\rangle = \frac{|s_{\downarrow,\downarrow}\rangle}{\sqrt{2}} = |\downarrow\downarrow\rangle\,. \tag{4.7}$$

We will show that for a chain of length N this state can be written as a matrix product state with bond dimension $D = 2$ as follows [Sch11]

$$|\psi\rangle = \sum_{\mathbf{a}}\sum_{\mathbf{b}} c_{\mathbf{ab}}\,|\mathbf{ab}\rangle\,, \tag{4.8}$$

where $|\mathbf{a}\rangle = |a_1 \ldots a_N\rangle$ represents the first spin-$\frac{1}{2}$ particle of each site and $|\mathbf{b}\rangle = |b_1 \ldots b_N\rangle$ represents the second spin-$\frac{1}{2}$ particle. The singlet state which connects the sites i and $i+1$ can be represented as

$$|\phi^{[i]}\rangle \sum_{b_i a_{i+1}} \hat{\phi}_{b_i a_{i+1}}\,|b_i\rangle\,|a_{i+1}\rangle \tag{4.9}$$

where $\hat{\phi}$ corresponds to the matrix

$$\hat{\phi} = \begin{pmatrix} 0 & \frac{1}{\sqrt{2}} \\ -\frac{1}{\sqrt{2}} & 0 \end{pmatrix} \tag{4.10}$$

and the state which has singlet bonds in all the sites and periodic boundary conditions can be written as

$$|\psi\rangle = \sum_{\mathbf{a}} \sum_{\mathbf{b}} \hat{\phi}_{b_1 a_2} \hat{\phi}_{b_2 a_3} \dots \hat{\phi}_{b_{N-1} a_N} \hat{\phi}_{b_N a_1} |\mathbf{ab}\rangle . \tag{4.11}$$

On the other hand, a state with open boundary conditions can be represented as

$$|\psi\rangle = \sum_{\mathbf{a}} \sum_{\mathbf{b}} \hat{\phi}_{b_1 a_2} \hat{\phi}_{b_2 a_3} \dots \hat{\phi}_{b_{N-1} a_N} |\mathbf{ab}\rangle . \tag{4.12}$$

We consider the following mapping from the state to the real spin-1 Hilbert space $\{|\sigma\rangle\}$

$$\mathcal{A} = \sum_{\sigma \in \{-1,0,+1\}} \sum_{\mathbf{ab}} M^{\sigma_1}_{a_1 b_1} M^{\sigma_2}_{a_2 b_2} \dots M^{\sigma_N}_{a_N b_N} |\sigma\rangle \langle \mathbf{ab}| \tag{4.13}$$

where

$$M^{+} = \begin{pmatrix} 1 & 0 \\ 0 & 0 \end{pmatrix}, \qquad M^{0} = \begin{pmatrix} 0 & \frac{1}{\sqrt{2}} \\ \frac{1}{\sqrt{2}} & 0 \end{pmatrix}, \qquad M^{-} = \begin{pmatrix} 0 & 0 \\ 0 & 1 \end{pmatrix} \tag{4.14}$$

Let us apply the mapping $\mathcal{A}$ to the state $|\psi_\phi\rangle$, so that we obtain

$$\begin{aligned} |\psi\rangle &= \mathcal{A} |\psi_\phi\rangle & (4.15)\\ &= \sum_{\sigma} \sum_{\mathbf{ab}} M^{\sigma_1}_{a_1 b_1} \hat{\phi}_{b_1 a_2} M^{\sigma_2}_{a_2 b_2} \hat{\phi}_{b_2 a_3} \dots \hat{\phi}_{b_{N-1} a_N} M^{\sigma_N}_{a_N b_N} \hat{\phi}_{b_N a_1} |\sigma\rangle & (4.16)\\ &= \sum_{\sigma} \mathrm{tr} \left(M^{\sigma_1}_{a_1 b_1} \hat{\phi} M^{\sigma_2}_{a_2 b_2} \hat{\phi} \dots \hat{\phi} M^{\sigma_N}_{a_N b_N} \hat{\phi} \right) |\sigma\rangle & (4.17) \end{aligned}$$

If we denote $\hat{A}^\sigma = M^\sigma \hat{\phi}$, then the AKLT ground state can be written as an MPS as follows

$$|\psi_{\mathrm{AKLT}}\rangle = \sum_{\sigma} \mathrm{tr} \left(\hat{A}^{\sigma_1} \hat{A}^{\sigma_2} \dots \hat{A}^{\sigma_N} \right) |\sigma\rangle , \tag{4.18}$$

where

$$\hat{A}^{+} = \begin{pmatrix} 0 & \frac{1}{\sqrt{2}} \\ 0 & 0 \end{pmatrix}, \; \hat{A}^{0} = \begin{pmatrix} -\frac{1}{2} & 0 \\ 0 & \frac{1}{2} \end{pmatrix}, \; \hat{A}^{-} = \begin{pmatrix} 0 & 0 \\ -\frac{1}{\sqrt{2}} & 0 \end{pmatrix} . \tag{4.19}$$

As we can see in Eq. 4.18, the ground state of the AKLT Hamiltonian can be written as an exact matrix product state. Some other states which can be represented as MPS are cluster states [BR01], W-states and GHZ-states [GHZ89]. However, these are very special cases since it is generally not possible to write the ground state of a Hamiltonian as a matrix product state and we normally construct them as an approximation or through a numerical method, for instance, to compute time evolution (see Section 4.3).

Figure 4.4: In these pictures: (a) represents an MPS with periodic boundary conditions and three sites and (b) represents an MPS with open boundary conditions and three sites.

Boundary conditions and canonical form

Given a quantum state $|\psi\rangle$ in terms of an MPS with open boundary conditions, there is a choice of tensors called canonical form of the MPS, which is very convenient. The canonical form depends on the boundary conditions, which can be open boundary (OBC) or periodic boundary (PBC).

An MPS has open boundary conditions (OBC) if the first and last matrices are vectors, that is, if it can written as

$$|\psi\rangle = \sum_{i_1,\ldots,i_N=1}^{d} \mathrm{tr}(A_{i_1}^{[1]} A_{i_2}^{[2]} \ldots A_{i_{N-1}}^{[N-1]} A_{i_N}^{[N]}) |i_1, \ldots, i_N\rangle \tag{4.20}$$

where $A_{i_m}^{[m]}$ are $D_m \times D_{m+1}$ matrices and $D_1 = D_{N+1} = 1$ (see Fig. 4.4)). If we can find $D = \max_m D_m$, then the MPS has bond dimension D. We can obtain the canonical form for an MPS with open boundary conditions as explained in the following theorem.

Theorem 3 (Canonical form of an MPS-OBC [PGVWC07])**.** *Any state* $|\psi\rangle \in (\mathbb{C}^d)^{\otimes N}$ *may be described as an MPS with open boundary conditions of the form Eq. 4.20 with bond dimension* $D \leq D \leq d^{\lfloor N/2 \rfloor}$ *and*

1. $\sum_i A_i^{[m]} A_i^{[m]\dagger} = \mathbb{1}_{D_m}$ *for all* $1 \leq m \leq N$.
2. $\sum_i A_i^{[m]\dagger} \Lambda^{[m-1]} A_i^{[m]} = \Lambda^{[m]}$, *for all* $1 \leq m \leq N$,
3. $\Lambda^{[0]} = \Lambda^{[N]} = 1$ *and each* $\Lambda^{[m]}$ *is a* $D_{m+1} \times D_{m+1}$ *diagonal matrix which is positive, full rank and with* $Tr[\Lambda^{[m]}] = 1$.

Nevertheless, if all the matrices which compose the MPS in Eq. 4.1 are identical (i.e. $A_i^{[m]} = A_i$) then the state is translationally invariant (TI) with periodic boundary conditions (see Fig. 4.4). The reciprocal statement is also true, that is, every translationally invariant state has an MPS representation using a translationally invariant MPS.

Theorem 4 (Representation of an MPS-PBC with site-independent matrices [PGVWC07]). *A translational invariant pure state with periodic boundary conditions on a finite chain has an MPS representation with site-independent matrices* $A_i^{[m]} = A_i$, *that is,*

$$|\psi\rangle = \sum_{i_1,\ldots,i_N=1} tr(A_{i_1} A_{i_2} \ldots A_{i_N}) |i_1, \ldots, i_N\rangle \tag{4.21}$$

If we start from an OBC MPS representation, in general one has to increase the bond dimension from D *to* ND *to get site-independent matrices.*

Injectivity is a relevant property of MPS and it means that for regions larger than a given length, different boundary conditions give rise to different states. The characterization of injectivity may be done as follows:

Definition 4.1 (Injective MPS [PGVWC07]). *An MPS* $|\psi\rangle$ *defined by the set of Kraus operators* $\{A_i \in \mathcal{M}_D\}_{i=1}^d$ *is called injective if there exists an* L *such that for regions of size* L *or larger, different boundary conditions give rise to different states; that is, if and only if the map* $\Gamma(X) : \mathcal{M}_D \to \left(\mathbb{C}^d\right)^{\otimes N}$

$$\Gamma(X) = \sum_{i_1,\ldots,i_L} \mathrm{tr}\left[X A_{i_1} \cdots A_{i_L}\right] |i_1 \cdots i_L\rangle \tag{4.22}$$

is an injective map.

There is a relation between the concept of injectivity and the canonical form of an MPS [PGVWC07], since injectivity is equivalent to the fact that, after a suitable transformation of the form $A_i \mapsto X A_i X^{-1}$, one obtains a *canonical form* fulfilling the following conditions:

1. $\sum_i A_i A_i^\dagger = \mathbb{1}$
2. $\sum_i A_i^\dagger \Lambda_A A_i = \Lambda_A$ for a diagonal positive full rank matrix Λ_A
3. the cp map $\mathbb{E}_A$ defined as

$$\mathbb{E}_A(X) = \sum_i A_i X A_i^\dagger \tag{4.23}$$

   has 1 as its unique non-degenerate eigenvalue of maximal modulus.

This canonical form is unique in the following sense:

Proposition 4 (Relation between different canonical representations of an injective MPS [PGVWC07]). *If* A *and* B *are matrices giving rise to different canonical representations of the same injective MPS, then they must be related by a unitary* U *according to* $e^{i\theta} A_i = U B_i U^\dagger$.

Non-injective MPS also possess a canonical form where the matrices are block-diagonal and the cp map associated to each block verifies conditions (1), (2) and (3) above, except for the existence of other eigenvalues of modulus 1.

Parent Hamiltonian and energy gap

In this section we will consider translationally invariant local Hamiltonians (see Eqs. 3.35, 3.8), that is, Hamiltonians defined as a sum of local terms corresponding to local interactions,

$$H = \sum h_X \tag{4.24}$$

where X is the set in which the mapping h acts on non-trivially.

A very relevant concept in MPS theory is the notion of *parent Hamiltonian*, a local translationally invariant Hamiltonian which can be constructed from a given MPS and such that the MPS is the ground state of the parent Hamiltonian. We will now state the rigorous definitions for the concepts of parent Hamiltonian, local interaction, frustration-free Hamiltonian and energy gap.

Definition 4.2 (PBC translation operator)**.** *The translation operator with periodic boundary conditions, τ, is defined as*

$$\tau\left(\otimes_{i=1}^{N} x_i\right) = \otimes_{i=1}^{N} x_{i+1} \tag{4.25}$$

where we have identified sites 1 *and* $N+1$.

Definition 4.3 (Parent Hamiltonian)**.** *Let $|\psi\rangle$ be a translationally invariant MPS of N particles, and ρ^n its reduced density matrix for $n < N$ particles. Let $\{|v_i\rangle\}_{i=1}^{r}, r \geq 1$ be an orthonormal basis for $Ker[\rho^n]$. If we consider any positive linear combination of projectors $\{|v_i\rangle\langle v_i|\}_{i=1}^{r}$, we can construct the following operator for local interactions*

$$h(\vec{a}) = \sum_{i=1}^{r} a_i |v_i\rangle\langle v_i| \tag{4.26}$$

with $\vec{a} = (a_1, \ldots, a_r)$ and $a_i > 0$. Let τ be the translation operator with periodic boundary conditions, as in Eq. 4.25, then the parent Hamiltonian is defined as

$$H = \sum_{i=1}^{N} \tau_i(h) \otimes \mathbb{1} \tag{4.27}$$

Note that Ker[h] corresponds with the support of ρ^n. The interaction length of the parent Hamiltonian is n, the number of particles in the support of $\rho^{(n)}$.

Definition 4.4 (L-local Hamiltonian)**.** *Let us consider a translationally invariant Hamiltonian on a ring of N $d-$dimensional quantum systems*

$$H = \sum_{i=1}^{N} \tau^i(h) \tag{4.28}$$

where τ is the translation operator with periodic boundary conditions, as in Eq. 4.25. The interaction is $L-$ local if h acts non-trivially only on $L-$neighbouring sites.

Definition 4.5 (Frustration-free Hamiltonian)**.** *Let us consider a translationally invariant n-local Hamiltonian on a ring of N $d-$dimensional quantum systems, as in Eq. 4.28. We say that H is frustration-free with respect to its ground state $|\psi_0\rangle$, if the ground state minimizes the energy locally, that is, if*

$$\langle\psi_0|H|\psi_0\rangle = \inf_{\psi}\langle\psi|H|\psi\rangle = N \inf_{\psi}\langle\psi|h\otimes\mathbb{1}|\psi\rangle. \tag{4.29}$$

Definition 4.6 (Energy gap of a Hamiltonian)**.** *Let us consider a Hamiltonian H with a one-dimensional ground space, with eigenvalues $\{\lambda_i\}_i$, and such that $\lambda_0 < \lambda_1, \ldots$ then the energy gap between the ground space and the first excited state is*

$$\epsilon_0 = \lambda_1 - \lambda_0. \tag{4.30}$$

Lemma 1 (Energy gap of a Hamiltonian)**.** *Let H be a Hamitonian with a one-dimensional ground space and with ground state energy $\lambda_0 = 0$. Then, the energy gap above the ground space ϵ_0 is the largest constant γ such that*

$$H^2 \geq \gamma H, \tag{4.31}$$

that is, $\epsilon_0 = \sup_\gamma\{\gamma | H^2 - \gamma H \geq 0\}$.

Theorem 5 (Injectivity implies the existence of an energy gap [FNW92])**.** *Let us consider the parent Hamiltonian H of a translationally invariant injective MPS $|\psi\rangle$ of N particles, such that $H|\psi\rangle = 0$. Then the energy gap of the Hamiltonian, ϵ_0, is positive.*

As we have seen in Eq. 4.27 any matrix product state $|\psi\rangle$ can be regarded as the ground state of a local Hamiltonian. However, the reciprocal question is far from answered, that is, the precise set conditions under which the ground state of a local Hamiltonian is a matrix product state has not been characterized yet.

4.2 Matrix product density operators

In analogy to pure states, the representation of mixed states requires an exponential number of coefficients. However, it is possible to put forward a parametrization of the state, called matrix product density operator (MPDO) [VGRC04], which allows to use a polynomial number of coefficients in the representation of the state as follows

$$\rho = \sum_{i_1,\ldots,i_N,i'_1,\ldots,i'_N=1}^{d} \mathrm{tr}\left[M^{[1]}_{i_1,i'_1} M^{[2]}_{i_2,i'_2} \ldots M^{[N]}_{i_N,i'_N}\right] |i_1,\ldots,i_N\rangle\langle i'_1,\ldots,i'_N| \quad (4.32)$$

where $M^{[k]}_{i_k,i'_k}$ is a $D_k^2 \times D_{k+1}^2$ matrix associated to the site k and the basis states $|i_k\rangle$ and $|i'_k\rangle$, and d is the dimension of the Hilbert state corresponding to the physical system.

For a given mixed state we may associate a pure state called purification [NC11, VGRC04], which we present in the following definition.

Definition 4.7 (Purification of a mixed state [VGRC04])**.** *Let $\rho_A \in \mathcal{D}(\mathcal{H}_A)$ be a mixed state, then it is possible to introduce a reference system $\mathcal{H}_R$ and a pure state in the joint system $|\psi_{AR}\rangle \in \mathcal{H}_A \otimes \mathcal{H}_R$ such that*

$$\rho_A = Tr_R\left(|\psi_{AR}\rangle\langle\psi_{AR}|\right) \quad (4.33)$$

For a given mixed state ρ it is clear that there exists an infinite number of possible purifications, which hinders the characterization of the state using purifications. Let us consider the class of mixed states ρ for which the purification can be represented as an MPS,

$$|\psi\rangle = \sum_{i_1,\ldots,i_N,a_1,\ldots,a_N=1}^{d,d_k} \mathrm{Tr}(A^{[1]}_{i_1,a_1} A^{[2]}_{i_2,a_2} \ldots A^{[N]}_{i_N,a_N})|i_1 a_1,\ldots,i_N a_N\rangle \quad (4.34)$$

where $|a_k\rangle$ is the ancillary state of physical dimension d_k associated to the physical system $|i_k\rangle$. In this case, the ancillary systems constitute the reference system $R \in \mathcal{H}_R$ and the MPDO ρ is obtained after tracing over the ancillary systems,

$$\rho = \mathrm{Tr}_a|\psi\rangle\langle\psi|. \quad (4.35)$$

The matrices of the MPDO (see Eq. 4.32), $M^{[k]}_{i_k,i'_k}$, may be computed from the purified state taking into account that

$$M^{[k]}_{i_k,i'_k} = \sum_{a=1}^{d_k} A^{[i]}_{i_k,a} \otimes \overline{A}^{[i]}_{i'_k,a}. \quad (4.36)$$

The ancillary matrices $A^{[i]}_{i_k,a}$ can also be recovered from the matrices $M^{[k]}_{i_k,{i'}_k}$ using an eigenvalue decomposition.

However, for an arbitrary mixed state ρ that has a representation as an MPDO with bond dimension D given by Eq. 4.32, is it generally not possible to give an upper-bound for the bond dimension of its local purification form [DSPGC13] which means that the local purification may be considerably more costly to compute than the MPDO. In addition to this, it is not always possible to obtain a purification for a given matrix product density operator. As proven in Ref. [DCC+16], there are mixed states which may be written as a translationally invariant matrix product density operators for all system sizes and such that it is not possible to find a translational invariant purification for all system sizes. However, some constructive methods to obtain purifications have been developed (see Ref. [DSPGC13]) which suggest that under certain conditions it is possible to obtain a purification for a given matrix product density operator.

4.3 Numerical methods using tensor networks

Matrix product states give rise to several numerical methods to simulate quantum many-body systems and analyse their properties, such as their ground state or their time evolution. In this section, we will explain two of the most established numerical methods to find the ground state of a system, namely the variational method and the imaginary time evolution method. After introducing these techniques, we will address the time evolution of mixed states using matrix product density operators.

Variational optimization

One of the most powerful methods for the study of one-dimensional strongly interacting systems is the DMRG [Whi92, Whi93, WF04], an iterative variational method initially conceived to study ground-state properties. This method can be reformulated in terms of matrix product states and, in this case, the objetive in the DMRG method is finding the matrices of an MPS for a given bond dimension D such that the energy is minimized [Sch11].

Let H be the local Hamiltonian of the system that we are interested in studying with ground state energy E_0. Then, for a given quantum state $|\psi\rangle$ it holds that

$$\frac{\langle\psi| H |\psi\rangle}{\langle\psi|\psi\rangle} \geq E_0, \tag{4.37}$$

The minimization problem of finding the matrices of an MPS with bond di-

mension D such that the energy is minimized is then

$$\min_{|\psi_{\mathrm{MPS}}\rangle} \left(\langle \psi_{\mathrm{MPS}}| H |\psi\rangle - \gamma \langle \psi_{\mathrm{MPS}}|\psi_{\mathrm{MPS}}\rangle \right), \tag{4.38}$$

where γ is the Lagrange multiplier and we may add the constraint that ψ_{MPS} has norm 1. If the method converges to the absolute minimum, we expect ψ_{MPS} to be the ground state of the Hamiltonian H and γ, its ground state energy.

In order to minimize Eq. 4.38, we start by minimizing with respect to a given tensor fixing the rest of the tensors in the chain. Once this is done, we will repeat the same procedure for the next tensor of the chain. We sweep over each tensor of the chain, starting from the first one to the last one and we repeat this method several times until we reach convergence to the minimum of the expectation value.

When we minimize with respect to one tensor A, whose coefficients are the parameters in the optimization, we must fix the rest of the tensors which define the state. The minimization can be written as

$$\min_{A} \left(\langle \psi| H |\psi\rangle - \gamma \langle \psi|\psi\rangle \right) = \min_{A} \left(\vec{A}^{\dagger} \mathcal{H}_{\mathrm{eff}} \vec{A} - \gamma \vec{A}^{\dagger} \mathcal{N} \vec{A} \right). \tag{4.39}$$

In Eq. 4.39, $\vec{A}$ is the tensor A written as a vector, $\mathcal{H}_{\mathrm{eff}}$ is an effective Hamiltonian which corresponds to the MPS for $\langle \psi| H |\psi\rangle$ without the tensors A and A^*, and $\mathcal{N}$ is a normalization matrix which corresponds to $\langle \psi|\psi\rangle$ without tensors A and A^* [Sch11, Orú14]. The minimization is achieved when the following derivative is zero,

$$\frac{\partial}{\partial \vec{A}^{\dagger}} \left(\vec{A}^{\dagger} \mathcal{H}_{\mathrm{eff}} \vec{A} - \gamma \vec{A}^{\dagger} \mathcal{N} \vec{A} \right) = 0, \tag{4.40}$$

which gives rise to an eigenvalue problem

$$\mathcal{H}_{\mathrm{eff}} \vec{A} = \gamma \mathcal{N} \vec{A}\,. \tag{4.41}$$

This eigenvalue problem can be solved numerically using linear algebra methods and both $\mathcal{H}_{\mathrm{eff}}$ and $\mathcal{N}$ can be computed exactly using tensor networks.

Imaginary time evolution

The *time-evolving block decimation* (TEBD) is another method which is widely used to study the time evolution of one-dimensional systems [Vid03, Vid04, WF04, DKSV04]. The evolution in imaginary time of a system consists in evolving an initial state $|\psi(0)\rangle$ in imaginary time with the Hamiltonian of the system H as follows

$$|\psi(\tau)\rangle = e^{-\tau H} |\psi(0)\rangle\,, \tag{4.42}$$

where $\tau = it$ is the imaginary time. After performing the imaginary time evolution, we would expect the initial state to converge to the ground state $|\psi_{\mathrm{GS}}\rangle$ of the system,

$$|\psi_{\mathrm{GS}}\rangle = \lim_{\tau\to\infty} \frac{e^{-\tau H}\,|\psi(0)\rangle}{\sqrt{|\,\langle\psi(\tau)\rangle\,\psi(\tau)|}} \tag{4.43}$$

if the Hamiltonian of the system is gapped and the initial quantum state $|\psi(0)\rangle$ fulfills that $\langle\psi(0)|\psi_{\mathrm{GS}}\rangle \neq 0$.

In order to implement the evolution in imaginary time for an MPS we must discretize the time period and also split the imaginary-time evolution operator into imaginary-time steps,

$$e^{-\tau H} = \left(e^{-\delta\tau H}\right)^m, \tag{4.44}$$

where $m = \tau/\delta\tau \gg 1$. We compute the evolution operator 4.44 using a Suzuki-Trotter expansion [HS05], in which the Hamiltonian is decomposed into a sum and the evolution operator is split into a product of exponentials. For instance, let us assume that the Hamiltonian H is a nearest-neighbor interaction, then

$$H = \sum_i h_{i,i+1}, \qquad H = H_{\mathrm{even}} + H_{\mathrm{odd}} \tag{4.45}$$

$$H_{\mathrm{even}} = \sum_k h_{2k,2k+1}, \qquad H_{\mathrm{odd}} = \sum_k h_{2k-1,2k}, \tag{4.46}$$

Taking this into account, we may approximate the time evolution to first order in $\delta\tau$ using a first-order Suzuki-Trotter expansion [HS05]

$$U(\delta\tau) = e^{-\delta\tau H} \approx e^{-\delta\tau H_{\mathrm{even}}} e^{-\delta\tau H_{\mathrm{odd}}} + O(\delta\tau^2). \tag{4.47}$$

We may also consider a Suzuki-Trotter expansion of higher order in case it is necessary to reduce the error associated to this approximation, such as

$$e^{-\delta\tau H} \approx e^{-\frac{\delta\tau}{2} H_{\mathrm{even}}} e^{-\delta\tau H_{\mathrm{odd}}} e^{-\frac{\delta\tau}{2} H_{\mathrm{even}}} + O(\delta\tau^3). \tag{4.48}$$

Both operators $e^{-\delta\tau H_{\mathrm{even}}}$ and $e^{-\delta\tau H_{\mathrm{even}}}$ can be written as tensor products, since all the terms which compose each Hamiltonian commute, that is

$$e^{-\delta\tau H_{\mathrm{even}}} = \bigotimes_k e^{-\delta\tau h_{2k,2k+1}} \tag{4.49}$$

$$e^{-\delta\tau H_{\mathrm{odd}}} = \bigotimes_k e^{-\delta\tau h_{2k-1,2k}} \tag{4.50}$$

and each $e^{-\delta\tau h_{i,i+1}}$ can be represented as an MPO [Sch11].

Therefore, the imaginary-time evolution operator can be approximated using $m \gg 1$ repetitions of the operator $U(\delta\tau)$ on an initial MPS. There are several

possible ways to apply the previous operator to a given MPS, such as performing an infinitesimal evolution and truncating the state afterwards. We start by applying the operator $U(\delta\tau)$ on a given MPS $|\psi\rangle$ with bond dimension D, obtaining a new MPS

$$|\widetilde{\psi}\rangle = U(\delta\tau)\,|\psi\rangle \tag{4.51}$$

with bond dimension $\tilde{D} \geq D$. Once we have the state $|\widetilde{\psi}\rangle$ with bond dimension $\tilde{D}$, we approximate it using a new MPS $|\psi'\rangle$ with bond dimension D. This approximation can be addressed minimizing error in squared distance

$$\text{Error} = \left|\left||\psi'\rangle - |\widetilde{\psi}\rangle\right|\right|^2. \tag{4.52}$$

This minimization is done again using the strategy that we introduced in the previous subsection, that is, fixing all the tensors in $|\psi'\rangle$ except for a certain tensor A and then sweeping over each tensor in the state. The minimization over the tensor A is then

$$\min_A \left|\left||\psi'\rangle - |\widetilde{\psi}\rangle\right|\right|^2 = \min_A \left(\vec{A}^\dagger \mathcal{N} \vec{A} - \vec{A}^\dagger \vec{M} - \vec{M}^\dagger \vec{A} + c\right), \tag{4.53}$$

where $\vec{A}$ is the vectorization of tensor A, $\mathcal{N}$ is normalization matrix that we introduced in Eq.(4.39), $\vec{M}$ is a vector corresponding to the environment of tensor A in $\langle\psi'|\widetilde{\psi}\rangle$, and $c = \langle\widetilde{\psi}|\widetilde{\psi}\rangle$ is a scalar. The minimization can be written as follows

$$\frac{\partial}{\partial \vec{A}^\dagger}\left(\vec{A}^\dagger \mathcal{N} \vec{A} - \vec{A}^\dagger \vec{M} - \vec{M}^\dagger \vec{A} + c\right) = 0, \tag{4.54}$$

which implies that

$$\mathcal{N}\vec{A} = \vec{M}. \tag{4.55}$$

The previous expression is a linear system of equations for the components of A. This system can be solved taking into account that

$$\vec{A} = \mathcal{N}^{-1}\vec{M} \tag{4.56}$$

and this is easily done for small bond dimensions D.

The TEBD method is very useful to simulate a wide range of systems, however, its practical application depends heavily on how well it converges despite of the potencial sources of error, such as the truncation step after performing an infinitesimal time evolution. It would relevant to obtain rigorous mathematical criteria to prove the efficiency and stability of these methods. We have addressed this question in the course of this thesis as we mention in the outlook of Chapter 6.

Simulation of the time evolution for mixed states

If instead of considering a one-dimensional pure state we need to study the properties of a mixed state, such as its time evolution in real or in imaginary time, we may explore the numerical methods for matrix product density operators [VGRC04].

Let us start from a purified MPS $|\psi(0)\rangle$ of the mixed state, then we may compute the next purification $|\psi(\Delta t)\rangle$ exactly using the infinitesimal evolution that was put forward in Eq. 4.51. We generally find that the bond dimension of the state $|\psi(\Delta t)\rangle$ increases so we need to truncate the state, finding another MPS of a lower or equal bond dimension which approximates $|\psi(\Delta t)\rangle$ well enough. We compute the approximation for a given bond dimension $\hat{D}$ minimizing the squared distance between the original MPS and the approximation as in Eq. 4.52. As we already explained in the previous subsection, the truncation method is iterative and it is based on several sweeps as in the DMRG method. Once we find the truncated purification, we take it as our next initial state and we repeat the infinitesimal evolution and the truncation until we reach convergence. Once we finish, the purification can be used to construct the matrix product density operator simply by tracing over the ancillary systems.

This method to simulate the time evolution of mixed states is based on the assumption that there exists a purification of the mixed state in study with a given bond dimension, but this is not always the case, as shown in Refs. [DSPGC13, KGE14, DCC$^+$16]. Several proposals to obtain a purification from a certain matrix product density operator have been set forth [DSPGC13] but there is a lack of efficient numerical methods to obtain an approximate purification when the system size increases. We have addressed this problem in the course of this thesis and we mention further ideas in this direction in the outlook of Chapter 6.

Part II

Body

5 Entanglement and fractional magnetization

5.1 Introduction

Entanglement plays a central role in many-body quantum systems as it can be used to understand the structure of the quantum states that appear in nature. In systems governed by short-range interactions, low energy states possess very little entanglement. In contrast, states evolved after quenches display large amounts of entanglement. These different behaviors, which are supported by abundant numerical evidence, have been recently established on solid grounds in one spatial dimension [Car11, Sre93, ECP10]. Nevertheless, apart from these cases, there exists practically no other physical situation where the existence of large or small amounts of entanglement can be rigorously established.

In this chapter, we explore an application of Matrix Product States [FNW92, PGVWC07] to the foundations of quantum magnetism in spin systems as well as to the quantification of entanglement. We establish a relationship between the fractionalization of a state's magnetization and the entanglement between two disjoint regions of such a state, and we find that the more fractional the magnetization of the state, the larger the expected entanglement.

5.2 Fractional magnetization in spin chains

Fractionalization is a striking phenomenon that arises whenever certain observables, which are expected to take integer expectation values, appear to be fractional-valued instead. The most prominent example of such behavior is the celebrated fractional quantum Hall effect [STG99, TSG82, Lau83] which occurs in certain setups when a two-dimensional electron gas is exposed to a very low temperature and a very high magnetic field. Under these conditions, the Hall conductance is quantized and it may display fractional values of $\frac{e^2}{h}$, where e is the charge of the electron and h is Planck's constant (see Figure 6.1).

Fractionalization has attracted a lot of attention in the last years, since it

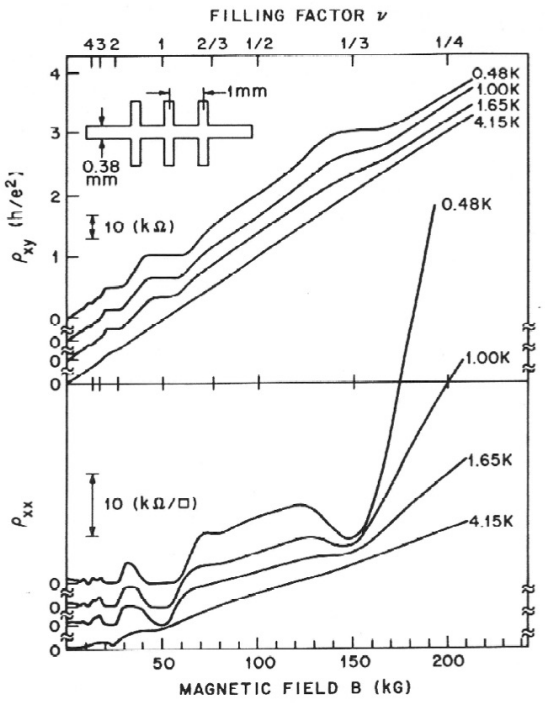

Figure 5.1: This picture shows the results from the original fractional quantum Hall effect experiment, carried out by D. C. Tsui, H. L. Störmer, and A. C. Gossard. In this graph, the Hall resistence has a plateau of $\rho_{x,y} = \frac{3h}{e^2}$ when the filling factor is $\frac{1}{3}$ and at low temperatures ($T < 5K$). (Source: [TSG82], p. 2).

has shown to be connected to most of the fundamental concepts in condensed matter physics, as conductivity, topological order, degeneracy or criticality. Because of this, it has been extensively studied in many systems, including spin chains [OYA97, Hid94], where the magnetization per particle is fractionalized as a function of the external magnetic field.

Fractional magnetization in a spin chain occurs whenever we have a $U(1)$ symmetry, in our case, generated by an operator J_z, and the expectation value of the generator $m = \langle J_z \rangle / N$, the magnetization per particle, fulfills that $J - m = q/p$, where p and q are coprime, J represents the spin number of the state and N is the number of spins in the chain. When we change some external parameter, such as a magnetic field, the value of m generally changes in discrete steps, giving rise to typical plateaus in the magnetization (see Figure 5.2).

In [OYA97], Oshikawa et al. studied the behaviour of quantum spin chains at zero-temperature in a uniform magnetic field pointing along the z-axis. They found out that for integer or half-integer spin, J, the magnetization curve may have plateaus and they argued that the magnetization per site, m, is topologically

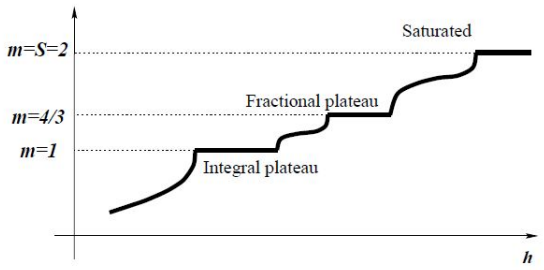

Figure 5.2: Scheme of the possible magnetization curve for a spin chain with $J = 2$ as depicted in [OYA97]. We can see plateaus, both integer and fractional, at certain values of the magnetization m.

quantized. They also discovered that fractional magnetization could occur if the previous conditions were accompanied by explicit or spontaneous breaking of the translational symmetry, such as the existence of periodic components in the representation of the spin chain.

Our aim is to show that whenever a translationally and $U(1)$ invariant MPS displays a fractional magnetization defined using the previous notation, the entanglement entropy of any sufficiently large region is greater than $\log(p)$. That is, the value of p imposes some lower bound on the entanglement present in the system.

5.3 A toy example

We start out with a trivial example that will help us build an intuition about the main statement of this chapter, and then we will generalize this claim to arbitrary states.

Let us consider the half-integer spin $J = 1/2$ and any two numbers q, p which are coprime. We construct a state of np spins, where n and p are both integers, grouped in $2n$ alternating domains with q spins down and $(p - q)$ spins up. In order to do this, we consider a p-particle state of the form $|a\rangle = |\uparrow\uparrow \cdots \uparrow\downarrow\downarrow \cdots \downarrow\rangle$, with q spins down. Then, we take n copies of such state and we build an equal superposition of the p possible different translations of $|a\rangle^{\otimes n}$,

$$|\psi\rangle = \frac{1}{\sqrt{p}} \sum_{m=0}^{p-1} \tau^m |a\rangle^{\otimes n} \tag{5.1}$$

where τ is the translation operator. This state is translationally invariant, it has a $U(1)$ symmetry generated by the operator $J_z = \sum s_n^z$, where s_z is the

single-spin operator $s_z = \frac{1}{2}\left(|\uparrow\rangle\langle\uparrow| - |\downarrow\rangle\langle\downarrow|\right)$, and it holds that $J_z|\psi\rangle = np(1/2 - q/p)|\psi\rangle$, and, thus, exhibits fractional magnetization with $m = J - \frac{p}{q}$. Following the prescriptions of Oshikawa et al. [OYA97] that we mentioned in the previous section, this example contains "periodic components" in order to display such a phenomenon.

As one can see by simple inspection, if we take any region A of size $L = kp$, with $k \in \{1, \ldots, n\}$, the reduced density operator can be written as

$$\rho_L = \frac{1}{p}\sum_{m=0}^{p-1} |\varphi_m\rangle\langle\varphi_m| \tag{5.2}$$

where φ_m are mutually orthogonal. Thus, the entropy of ρ_L and, consequently, the entanglement entropy between the region A and the rest is $\log(p)$.

As we will see in the following sections, this toy model presenting such entropy is connected to the fact that, in this case, fractional magnetization arises because the ground state is a linear superposition of p-particle states which are both locally orthogonal and related through a translation.

5.4 A large fractional magnetization implies large entanglement

In what follows, we consider the richer family of translationally invariant MPS, that is $A_i[n] = A_i$ independently of the site n (see Section 4 and references [FNW92, PGVWC07]) in order to prove a general result. For that, we realize that the previous toy example is contained in the family of MPS just by considering the matrices

$$A_\downarrow = \sum_{i=1}^{q} |i\rangle\langle i+1| \ , \ A_\uparrow = \sum_{i=q+1}^{p} |i\rangle\langle i+1|. \tag{5.3}$$

However, extending the previous example to all translationally invariant MPS is quite challenging. The main reason is that finding a characterization of all MPS displaying fractional magnetization is hard and, even if an MPS is a superposition of states related by a translation, nothing ensures that the reduced states are sums of few pure and mutually orthogonal states. Nevertheless, we can prove the following result:

Theorem 5.1 (Large fractional magnetization implies large entanglement)**.** *Let $|\psi\rangle$ be a translationally and $U(1)$ invariant MPS of spin J, with magnetization per particle m, and verifying $J - m = \frac{q}{p}$, where p and q are coprime. Then there exists a constant $\gamma \in \mathbb{N}$ such that the entropy of the reduced density matrix of any*

region of size $L = k\gamma p$ $(\forall k \in \mathbb{N})$ *verifies* $S(\rho_L) \geq \log(p)$, *up to a exponentially small correction in* $N - L$ *and in* k.

In order to prove this theorem, we rely on several lemmas that we present in the following subsection. We need to consider a characterization of symmetries for injective MPS [PGWS+08], as well as an extension of the Lieb-Schultz-Mattis (LSM) theorem [LSM61] for a $U(1)$ symmetry. The characterization of symmetries in [PGWS+08] allows to assert that all injective MPS corresponding to blocks must have the same symmetry and the same magnetization m. The extension of the LSM theorem implies that all these blocks should have a period multiple of p. Moreover, we also have to prove that states corresponding to different blocks are necessarily different.

Preliminary results

Our first objective is to state and prove a couple of lemmas formalizing the claim that different injective MPS are orthogonal to each other.

Lemma 5.1 (For injective MPS, different means orthogonal)**.** *Given two translationally invariant and injective MPS,* $|\psi_A\rangle$ *and* $|\psi_B\rangle$, *then* $\||\psi_A\rangle\| = 1, \||\psi_B\rangle\| = 1$ *up to an exponentially small correction in* N. *Moreover, either both are equal for all* N, *or* $tr_{N-L}|\psi_A\rangle\langle\psi_B| = 0$ *up to an exponentially small correction in* $N - L$. *In particular, if they are not equal then* $|\langle\psi_A|\psi_B\rangle| = 0$ *up to an exponentially small correction in* N.

Proof. It is easy to see that $\langle\psi_B|\psi_A\rangle = \mathrm{tr}\left[\mathcal{E}_{A,B}^N\right]$, where $\mathcal{E}_{A,B} = \sum_i A_i \otimes \bar{B}_i$. Moreover, it is clear that the eigenvalues of $\mathcal{E}_{A,B}$ are the same as those of the map $\mathbb{E}_{A,B}(X) = \sum_i A_i X B_i^\dagger$, which gives $\||\psi_A\rangle\|, \||\psi_B\rangle\| = 1$ up to a exponentially small correction (see Section 4 for a more detailed account of the properties of MPS).

To complete the proof, it is enough to see that all eigenvalues λ of $\mathbb{E}_{A,B}$ verify that $|\lambda| < 1$. We will use the conditions verified by the canonical form of an injective MPS, that is: (i) $\sum_i A_i A_i^\dagger = \mathbb{1}$, (ii) $\sum_i A_i^\dagger \Lambda_A A_i = \Lambda_A$ for a diagonal positive full rank matrix Λ_A, and (iii) the completely positive map $\mathbb{E}_A$ defined as

$$\mathbb{E}_A(X) = \sum_i A_i X A_i^\dagger \tag{5.4}$$

has 1 as its unique non-degenerate eigenvalue of maximal modulus.

Let us take X such that $\sum_i A_i X B_i^\dagger = \lambda X$, using (i) for A and (ii) for B we get

$$|\lambda| \left|\mathrm{tr}\left[X\Lambda_B X^\dagger\right]\right| = \left|\sum_i \mathrm{tr}\left[A_i X B_i^\dagger \Lambda_B X^\dagger\right]\right|$$

$$\begin{aligned} &\leq \left[\sum_i \mathrm{tr}\left[XB_i^\dagger \Lambda_B B_i X^\dagger\right]\right]^{1/2} \left[\sum_i \mathrm{tr}\left[A_i^\dagger X \Lambda_B X^\dagger A_i\right]\right]^{1/2} \\ &= \left|\mathrm{tr}\left[X\Lambda_B X^\dagger\right]\right|, \end{aligned} \tag{5.5}$$

where we have used the Cauchy-Schwarz inequality and $\mathrm{tr}\left[X\Lambda_B X^\dagger\right] > 0$. So, if $|\lambda| \geq 1$, we must have an equality and, therefore,

$$\alpha \Lambda_B^{1/2} X^\dagger A_i = \Lambda_B^{1/2} B_i X^\dagger$$

Multiplying by the adjoint expression, summing in i, taking traces and using (i) and (ii) again we get that $|\alpha| = 1$ and, hence, $\alpha = e^{i\theta}$.

Finally, since Λ_B is invertible, we get $\sum_i B_i X^\dagger X B_i^\dagger = X^\dagger X$ which, by (iii), leads to $X^\dagger X = \mathbb{1}$ and implies that $e^{i\theta} A_i = X B_i X^\dagger$. This means that $|\psi_A\rangle$ and $|\psi_B\rangle$ are equal up to a global phase, for all N. □

It is also necessary to prove a lemma for the reduced density matrix of states which are a linear combination of injective MPS:

Lemma 5.2 (Injectivity and reduced density matrix)**.** *Given an MPS of the form $|\psi\rangle = \sum_{r=1}^n \lambda_r |\psi_r\rangle$ such that the $|\psi_r\rangle$ are different injective MPS, then $\mathrm{tr}\left[\rho_r^L \rho_s^L\right] \propto \delta_{rs} + O(e^{-L}) + O(e^{-(N-L)})$, being ρ_r^L the reduced density matrix for L particles associated to $|\psi_r\rangle$.*

Proof. The proof follows straightforwardly from the previous lemma. □

The next thing we need is the following modification of Theorem 5 in [PGVWC07].

Lemma 5.3 (Representation of MPS as a superposition of injective β-periodic MPS)**.** *Consider any MPS $|\psi_A\rangle \in \mathbb{C}^{d\otimes N}$ which has only one block in its canonical form with $D \times D$ matrices $\{A_i\}$ and such that $\mathbb{E}_A$ has β eigenvalues of modulus one. If β is a factor of N, then the state can be written as a superposition of β β-periodic* different and injective *MPS with equal coefficients and bonds D_i (also with the property that $\sum_i D_i = D$). Otherwise, if β is not a factor of N, then $|\psi_A\rangle = 0$.*

Proof. The only thing to verify is that the β-periodic states are injective and different among them. In the proof of Theorem 5 in [PGVWC07], based on [FNW92], one proves the existence of a set of orthogonal projectors $\{P_k\}$ with $\sum_k P_k = \mathbb{1}$ such that

$$\mathbb{E}_A^\beta(X) = \sum_{j,k} P_j \mathbb{E}_A^\beta(P_j X P_k) P_k, \tag{5.6}$$

$\mathbb{E}_A^\beta$ has 1 with degeneracy exactly β as the only eigenvalue of modulus 1, and each block in the block-diagonal form of the Kraus operators of $\mathbb{E}_A^\beta$ given by (5.6) corresponds to one of the β-periodic states. Moreover, the space of fixed points is generated by P_k and the space of fixed points of the adjoint map is generated by $P_k \Lambda P_k$.

The cp maps associated to the β-periodic states are then

$$\mathbb{E}_k(X) = P_k \mathbb{E}^\beta(P_k X P_k) P_k$$

when restricted to inputs with $X = P_k X P_k$. It is clear that P_k is its only fixed point, $P_k \Lambda P_k$ the only fixed point of the adjoint map, and there is no other eigenvalue of modulus 1, which shows that all β-periodic states are injective. Now, if two of them were equal, we would reach a contradiction in the following way. For simplicity, we reason in the case of 2 2-periodic states but the argument can be adapted straightforwardly to the general case. $\mathbb{E}_A^2$ has block-diagonal Kraus operators of the form $B_i \otimes |0\rangle\langle 0| + C_i \otimes |1\rangle\langle 1|$. By the hypotheses and the uniqueness of the canonical form for injective MPS, $B_i = e^{i\theta} U C_i U^\dagger$ for all i. Then, apart from $\mathbb{1} \otimes |0\rangle\langle 0|$ and $\mathbb{1} \otimes |1\rangle\langle 1|$, we also get $U \otimes |0\rangle\langle 1|$ as an eigenvector of $\mathbb{E}_A^\beta$ with eigenvalue of modulus 1, from where the contradiction follows. □

Finally, we need the following version of the Lieb-Schultz-Mattis theorem for a $U(1)$ symmetry. It is interesting to note that it does not use any MPS structure, so it is valid in full generality and for any spatial dimension. Let us recall that, in the Lemma 17 of [PGSGG+10], it has been shown that any quantum state with a $U(1)$ symmetry given by the canonical generator of spin $S_z^{(J)}$ verifies that

$$u_g^{\otimes N} |\psi\rangle = e^{igNm} |\psi\rangle \tag{5.7}$$

with $u_g = e^{igS_z^{(J)}}$ and a magnetization per particle m.

Lemma 5.4 (Lieb-Schultz-Mattis for a $U(1)$ symmetry)**.** *Let m be any rational number and $p \in \mathbb{N}$ such that there exist two quantum states of (local spin J and) pN and $(N+1)p$ particles respectively, for some N, having both of them magnetization per particle m. Then $p(J-m) = q$ with q integer.*

Proof. By expanding equation (5.7) in the canonical basis, we get

$$\sum_{k_1 \cdots k_{pN}} c_{k_1 \cdots k_{pN}} e^{ig \sum_j k_j} |k_1 \cdots k_{pN}\rangle = \sum_{k_1 \cdots k_{pN}} e^{igpNm} c_{k_1 \cdots k_{pN}} |k_1 \cdots k_{pN}\rangle$$

Since it is a basis and the state is not zero, there must exist $k_1, \cdots, k_{pN} \in \{-J, -J+1, \ldots J-1, J\}$ such that $\sum_j k_j = Npm$. For the same reason, there must exist $k'_1, \cdots, k'_{pN+p} \in \{-J, -J+1, \ldots J-1, J\}$ such that $\sum_j k'_j = (Np+p)m$. Subtracting, we get that $mp = \sum_j k'_j - \sum_j k_j$ has the same character (integer or semi-integer) as pJ. □

With this at hand, if we consider an MPS $|\psi\rangle$ of spin J and pN particles with a $U(1)$ symmetry, given by the canonical generator of spin $S_z^{(J)}$, we have the following lemma.

Lemma 5.5 (Generalized Lieb-Schultz-Mattis)**.** *Let p be the smallest integer such that, after blocking p sites together, $|\psi\rangle$ has a block-diagonal representation with injective blocks. Then $p(J-m) = q$, with q an integer.*

Proof. To see it we consider blocks of p-sites. From Theorem 5 in [PGWS+08], we know that each block is an injective MPS with the same symmetry. Since, by Lemma 5.1, states corresponding to different blocks are equal or linearly independent, all of them must have also magnetization m. Now, by the characterization of symmetries for injective MPS [PGWS+08], we know that the matrices defining each block inherit the symmetry and therefore the associated MPS has magnetization m for all system sizes that are multiple of p. Lemma 5.4 finishes the argument. □

We also get a reciprocal result:

Lemma 5.6 (Reciprocal of the Lieb-Schultz-Mattis)**.** *Let us assume that $J-m = \frac{q}{p}$ with $\gcd(p,q) = 1$ in a $U(1)$ symmetric MPS, then there exists $\gamma \in \mathbb{N}$ such that the MPS has only γp-periodic blocks. Moreover (trivially from Lemma 5.3), states belonging to blocks of different periods are different.*

Proof. As above, all injective MPS corresponding to the blocks must have the same symmetry and the same magnetization m. Therefore, Lemma 5.4 shows that only blocks of period multiple of p can appear. □

Proof of the main theorem

We are finally ready to prove Theorem 5.1:

Proof. Let $|\psi\rangle$ be a MPS, which is translational and $U(1)$ invariant. We also impose that this MPS has spin J and magnetization per particle m, verifying $J - m = \frac{q}{p}$, where p and q are coprime, and consider its canonical form.

If the state has a single block, due to Lemma 5.6, it must be γp-periodic, where $\gamma \in \mathbb{N}$. This means that all the eigenvalues of magnitude one corresponding to the cp-map $\mathbb{E}_A$ are the γp-roots of unity. Consequently, if we block γp spins, then we can write the new matrices A_i as block-diagonal, with each block being injective and different (see Lemma 5.3). We have now that the state $|\psi\rangle$ can be written as linear combination with equal coefficients of γp different injective MPS, each of them being a translation of each other.

In Lemma 5.1, we show that different injective MPS are orthogonal in the thermodynamic limit. Let $L = k\gamma p$ ($k \in \mathbb{N}$), using Jensen's inequality we have that $S(\rho_L) \geq -\log(\mathrm{tr}(\rho_L^2))$ which, by Lemma 5.2 implies $S(\rho_L) \geq \log(\gamma p) \geq \log(p)$, up to an exponentially small correction in $N - L$ and k, as in the example proposed above.

If the MPS has many blocks in its canonical form, we will show that one can treat each of these blocks as in the single block case, obtaining an extension of the last result. Lemma 5.6 gives us $\gamma \in \mathbb{N}$ such that all the blocks of the canonical form of $|\psi\rangle$ have period γp. Let $L = k\gamma p$, where $k \in \mathbb{N}$. We observe that the reduced density operator of a region comprising L sites verifies

$$\rho_L = \oplus_{i=1}^{n} \mu_i \rho_i, \tag{5.8}$$

up to a correction exponentially small in $N - L$ and k (see Lemma 5.2). The ρ_i's are the reduced density matrices corresponding to single blocks, where repeated blocks are simply reflected in the μ_i's. Using the single block case, we can ensure again that $S(\rho_i) \geq \log(p)$ for all i. It is clear, from (5.8) and the subadditivity of the entropy, that $S(\rho_L) \geq \log(p)$ up to another exponentially small correction in $N - L$ and k, yielding the desired result. □

5.5 Conclusions and outlook

Summing up, we have shown that for the state of a quantum spin chain, a large fractionalization in the magnetization demands large entanglement. In order to prove this, we have established a lower bound for the entanglement entropy of any connected and sufficiently large region of a quantum spin chain in terms of the fractionalized magnetization. Moreover, since MPS seem to be the right representation for the low energy sector of 1D systems, we postulate this result being true in full generality.

In this line of work, it would be interesting to extend this result to higher dimensions, using PEPS [VC04]. However, extending the results of this chapter to two-dimensional systems poses several difficulties which are still open questions in the field, such as the lack of a canonical form for PEPS or the characterization of fractionalization. The canonical form has a wide array of applications for MPS, and one of the most important is the classification of symmetries [PGWS$^+$08] and the classification of phases in one-dimensional systems [CGW11, SPGC11]. In two-dimensional systems, it is possible to characterize the different symmetries in the injective case but this result does not apply to the most relevant systems with topological order, such as SET phases [GW09, PBTO12].

On the other hand, in one-dimensional systems fractionalization arises from a periodical structure, which we have exploited to prove the main result of the chapter. However, in two-dimensional systems there exist aperiodical tilings of

the plane which may allow for fractionalized physical setups without periodicity or topological properties. We believe it could be interesting to study Hamiltonians related to aperiodical tilings of the plane and find out whether these systems display fractionalization.

As future work, we would also like to perform numerical simulations to quantify the amount of entanglement in terms of the fractionalization of the magnetization in particular examples of spin chains and find out how good the bound is for concrete physical systems.

6 Entanglement and long-range interactions

6.1 Introduction

The existence of interactions influences the behaviour of spin systems in different ways and gives rise to a variety of interesting phenomena. For instance, an isolated spin chain with disorder may undergo a metal-insulator transition in the presence of interactions [BAA06, CFIM12]. While interactions are typically local and each constituent of the system interacts mainly with nearest neighbours, they may also be long-range. In this case, the area law for the entanglement entropy does not apply. Intuitively, we expect that in presence of long-range interactions, any specific region will be correlated to any other part of the chain, giving rise to large amounts of entanglement.

However, it is quite difficult to transform this intuitive idea into a rigorous result. The main reason is that the ground state of a Hamiltonian containing long-range interactions may coincide with, or be very similar to the ground state of another Hamiltonian containing short-range ones and, therefore, fulfilling the area law. As an example, if we consider an Ising model with decaying interactions and in the absence of a transverse magnetic field, the ground state will be still a product state, which in turn is also the ground state of the Ising model with nearest-neighbor couplings. Such state does not display any entanglement at all. Hence, we can only expect to have large amounts of entanglement whenever such examples do not exist; that is, whenever our state is, in some sense, not close to any other state corresponding to the ground state of a Hamiltonian with short-range interactions.

In this chapter, we will establish a rigorous lower bound for the entanglement entropy of a translationally invariant MPS, $|\psi_A\rangle$, which is not the ground state of any short-range gapped and frustration-free Hamiltonian and such that it is sufficiently far away from any other state with this property for any given interaction length. We will show that, under these conditions, the entanglement entropy of this state must be large and that it will scale with the range of the interaction. In order to prove this statement, we have to further develop the theory of MPS, ex-

tending previous results presented in Refs. [PGVWC07, PGWS+08, SWPGC09], and deriving new ones.

6.2 Main result: large interaction length implies large entanglement

We begin discussing the main result of the chapter and providing a brief scheme of the steps and lemmas which eventually lead to the proof. In order to do this, let us consider a translationally invariant MPS, $|\psi_A\rangle$, which is not the ground state of any short-range gapped and frustration-free Hamiltonian. Furthermore, let us assume that this MPS is also far away, as specified below, from any other state with this property for any given interaction length. We would like to prove that as a consequence its entanglement entropy will be large and, indeed, that it will scale with the range of the interaction.

More specifically, if we denote by ρ_A^L the reduced density operator of $|\psi\rangle$ for a connected region containing L spins, we prove the following theorem:

Theorem 6.1 (Long-range interactions imply large entanglement)**.** *Let $|\psi_A\rangle$ be an MPS such that every state $|\tilde{\psi}\rangle$ which is the unique ground state of a gapped frustration-free Hamiltonian with interaction length L verifies $\|\rho_A^L - \tilde{\rho}^L\|_1 \geq \epsilon$. Then, for sufficiently large regions R, we have that the α-Renyi entropy $S_\alpha(\rho_A^R) \geq aL + b\log\epsilon + c$, for $\alpha \leq \frac{1}{6}$ and where a, b, c are constants depending only on the local physical dimension d of $|\psi_A\rangle$.*

This claim is proved by contradiction. We suppose that for every connected region and for $\alpha \leq \frac{1}{6}$ the α-Renyi entropy is upper bounded by an expression of the form $aL + b\log\epsilon + c$, for $\alpha \leq \frac{1}{6}$, where a, b, c are constants depending on the physical dimension of $|\psi_A\rangle$. It is enough to prove that this implies the existence of a state, the unique ground state of a gapped frustration-free Hamiltonian with interaction length L, such that $\|\rho_A^L - \tilde{\rho}^L\|_1 < \epsilon$, to reach a contradiction.

The hypothesis on S_α being small implies that we can find another MPS with a sufficiently small bond dimension, $\tilde{D}$ (in particular, $\tilde{D} \leq d^{(L-1)/2}$) that is close enough to the original one. In order to do this, we will rely on [VC06, Lemma 2] and on a new bound for reducing the bond dimension of an MPS that we explain in Section 6.3. More precisely, this bound will be of the form

$$\|\rho_A^L - \rho_{\tilde{A}}^L\|_1 \leq 2\sqrt{2}d^{L/2}\sqrt{L}\delta^{1/4} + (2L+3)\delta,$$

where $\rho_{\tilde{A}}^L$ will be the reduced density matrix which can be constructed from ρ_A^L by substituting the Kraus operators A_i by PA_iP and $\Lambda = P\Lambda P$, where $P = \sum_{i_1}^{\tilde{D}} |i\rangle\langle i|$. These steps will be explained in further detail in 6.3.

Now, arbitrarily close to the MPS associated to the reduced density matrix $\rho_{\tilde{A}}^L$, there exists another which is the unique ground state of a Hamiltonian with gap and interaction length L. Taking into account that the interaction length is closely related to the bond dimension at which the MPS reaches injectivity, this will be deduced from proving that all MPS (except for a set with measure zero) reach injectivity fast enough. Standard Algebraic Geometry, as explained in Lemma 11 of 6.4 and [Har77, GH11], reduces this problem to finding the existence of a single MPS displaying this property. The existence of such an example can be obtained using quantum expanders, as explained also in 6.4.

In the following sections, we present the aforementioned statements as lemmas and theorems with their proofs and we explain in detail how they yield the main result.

6.3 Approximation of quantum states using matrix product states

In this section, we derive a new bound for approximating a translationally invariant MPS by another MPS with a smaller bond dimension. This bound is written in terms of the normalized reduced density matrices of both states where we consider the notation and concepts about MPS theory that we defined in Chapter 4.

Let $A_i \in \mathcal{M}_D$ be the canonical Kraus operators defining an injective and translationally invariant MPS (see Chapter 4), with Λ as its fixed point. We define the normalized reduced density matrix for L particles ρ_A^L, up to a correction exponentially small in $N - L$, by

$$\rho_A^L = \sum_{\substack{i_1,\ldots,i_L \\ j_1,\ldots,j_L}} \operatorname{tr}\left[A_{j_L}^\dagger \cdots A_{j_1}^\dagger \Lambda A_{i_1} \cdots A_{i_L}\right] |i_1 \cdots i_L\rangle\langle j_1 \cdots j_L| \tag{6.1}$$

We also introduce a different density matrix $\rho_{\tilde{A}}^L$, which results from projecting the Kraus operators and the fixed point into a subspace of dimension $\tilde{D} \leq D$. In other words, this state is a matrix product density operator (see Chapter 4) with smaller matrices $\tilde{A}_i = PA_iP$ and a new fixed point $\tilde{\Lambda} = P\Lambda P$ where $P = \sum_{i=1}^{\tilde{D}} |i\rangle\langle i|$, that is,

$$\begin{aligned}
\rho_{\tilde{A}}^L &= \sum_{\substack{i_1,\ldots,i_L \\ j_1,\ldots,j_L}} \operatorname{tr}\left[\tilde{A}_{j_L}^\dagger \cdots \tilde{A}_{j_1}^\dagger \tilde{\Lambda} \tilde{A}_{i_1} \cdots \tilde{A}_{i_L}\right] |i_1 \cdots i_L\rangle\langle j_1 \cdots j_L| \\
&= \sum_{\substack{i_1,\ldots,i_L \\ j_1,\ldots,j_L}} \operatorname{tr}\left[PA_{j_L}^\dagger P \cdots PA_{j_1}^\dagger P\Lambda PA_{i_1}P \cdots PA_{i_L}P\right] |i_1 \cdots i_L\rangle\langle j_1 \cdots j_L|
\end{aligned}$$

In this case, $\mathbb{E}$ is the completely positive map associated to A_i and $\tilde{\mathbb{E}}$ the one associated to $\tilde{A}$.

Taking all this into account, we can state and prove the following theorem:

Theorem 6.2 (Bound for the reduced density matrix)**.** *Let $\rho_A^L, \rho_{\tilde{A}}^L$ be the reduced density matrices for the original and truncated state. We can bound the distance between the reduced density matrices as follows:*

$$\|\rho_A^L - \rho_{\tilde{A}}^L\|_2 \leq 2\mathrm{tr}\left[\tilde{\Lambda}^{1/2}\right]\sqrt{L}\delta^{1/4} + (2L+3)\delta,$$

$$\|\rho_A^L - \rho_{\tilde{A}}^L\|_1 \leq 2\sqrt{2}\tilde{D}\sqrt{L}\delta^{1/4} + (2L+3)\delta$$

where $\delta = \mathrm{tr}\left[\Lambda - \tilde{\Lambda}\right]$.

In order to do this, we must prove two lemmas as preliminary results. In the first place, we show that the original fixed point of the state ψ_A is approximately the fixed point of the truncated channel.

Lemma 6.1. *The original fixed point of the state $|\psi_A\rangle$ is approximately the fixed point of the truncated channel $\tilde{\mathbb{E}}^L$*

$$\|\tilde{\mathbb{E}}^L(\Lambda) - \Lambda\|_1 \leq 2L\delta.$$

In particular,

$$\mathrm{tr}\left[\tilde{\mathbb{E}}^L(\Lambda)\right] \geq 1 - 2L\delta.$$

Proof. Using both the definition of δ and that $\mathbb{E}$ is contractible for the 1-norm, we get that $\|\Lambda - \mathbb{E}(P\Lambda P)\|_1 \leq \delta$. The map $P \bullet P$ is also contractible for the 1-norm, so

$$\begin{aligned} & \|\Lambda - P\mathbb{E}(P\Lambda P)P\|_1 \\ \leq\ & \|\Lambda - P\Lambda P\|_1 + \|P\Lambda P - P\mathbb{E}(P\Lambda P)P\|_1 \\ \leq\ & 2\delta \end{aligned}$$

This means that $\|\Lambda - \tilde{\mathbb{E}}(\Lambda)\|_1 \leq 2\delta$, since $\tilde{\mathbb{E}}(\Lambda) = P\mathbb{E}(P\Lambda P)P$. However, $\tilde{\mathbb{E}}$ is also contractible respect to the 1-norm, so

$$\begin{aligned} \|\Lambda - \tilde{\mathbb{E}}^2(\Lambda)\|_1 &\leq \|\Lambda - \tilde{\mathbb{E}}(\Lambda)\|_1 + \|\tilde{\mathbb{E}}(\Lambda) - \tilde{\mathbb{E}}^2(\Lambda)\|_1 \\ &\leq 4\delta \end{aligned}$$

The result can be obtained by induction. □

We will now define, under the previous notation for the Kraus operators and the fixed point, the following operators

$$\sigma_A = \sum_{\substack{i_1,\ldots,i_L \\ j_1,\ldots,j_L}} \mathrm{tr}\left[A^\dagger_{j_L}\cdots A^\dagger_{j_1}\tilde{\Lambda}A_{i_1}\cdots A_{i_L}\right]|i_1\cdots i_L\rangle\langle j_1\cdots j_L|$$

$$\sigma_{A,P} = \sum_{\substack{i_1,\ldots,i_L \\ j_1,\ldots,j_L}} \mathrm{tr}\left[PA^\dagger_{j_L}\cdots A^\dagger_{j_1}\tilde{\Lambda}A_{i_1}\cdots A_{i_L}P\right]|i_1\cdots i_L\rangle\langle j_1\cdots j_L|$$

where it is important to note that $\sigma_{A,P}$ is a positive operator. The second lemma reads:

Lemma 6.2. *$\|\rho_A - \rho_{\tilde{A}}\|_2 \leq \|\sigma_{A,P} - \phi_{\tilde{A}}\|_2 + (2L+3)\delta$, where $\phi_{\tilde{A}} = \mathrm{tr}\left[\tilde{\mathbb{E}}^L(\Lambda)\right]\rho_{\tilde{A}}$ is the not normalized reduced density matrix generated by $\tilde{A}_i$. The same holds changing the 2-norm by the 1-norm in both sides of the inequality.*

Proof. By using the triangle inequality and the fact that $\|\cdot\|_2 \leq \|\cdot\|_1$,

$$\begin{aligned}\|\rho_A - \rho_{\tilde{A}}\|_2 &\leq \|\rho_A - \sigma_A\|_1 + \|\sigma_A - \sigma_{A,P}\|_1 \\ &+ \|\sigma_{A,P} - \phi_{\tilde{A}}\|_2 + \|\phi_{\tilde{A}} - \rho_{\tilde{A}}\|_1 \,.\end{aligned}$$

The first term can be calculated exactly

$$\begin{aligned}\|\rho_A - \sigma_A\|_1 &= \sum_{i_1,\ldots,i_L} \mathrm{tr}\Big[\mathrm{A}^\dagger_{\mathrm{i_L}}\cdots\mathrm{A}^\dagger_{\mathrm{i_1}}(\Lambda-\tilde{\Lambda})\mathrm{A}_{\mathrm{i_1}}\cdots\mathrm{A}_{\mathrm{i_L}}\Big] \\ &= \delta\,.\end{aligned}$$

The first equality holds because the operator is positive and the 1-norm can be replaced by a trace and the second one holds because $\mathbb{E}$ is trace preserving. The second term can be bounded in a similar way.

$$\begin{aligned}\|\sigma_A - \sigma_{A,P}\|_1 &= \mathrm{tr}\left[P^\perp \sum_{i_1,\ldots,i_L} A^\dagger_{i_L}\cdots A^\dagger_{i_1}\tilde{\Lambda}A_{i_1}\cdots A_{i_L}P^\perp\right] \\ &\leq \delta + \mathrm{tr}\left[P^\perp \sum_{i_2,\ldots,i_L} A^\dagger_{i_L}\cdots A^\dagger_{i_2}\Lambda A_{i_2}\cdots A_{i_L}\right].\end{aligned}$$

This holds because

$$\|\Lambda - \mathbb{E}(\tilde{\Lambda})\|_1 = \|\mathbb{E}(\Lambda - \tilde{\Lambda})\|_1 = \delta,$$

since $\mathbb{E}$ is trace preserving and $\mathbb{E}(\Lambda) = \Lambda$. Therefore,

$$\|\sigma_A - \sigma_{A,P}\|_1 \leq \delta + \mathrm{tr}\left[P^\perp\Lambda\right] = 2\delta.$$

Finally, the last term can be bounded using Lemma 6.1 because

$$\|\phi_{\tilde{A}} - \rho_{\tilde{A}}\|_1 = -1 + \mathrm{tr}\left[\tilde{\mathbb{E}}^L(\Lambda)\right] \leq 2\delta L.$$

We obtain the result by collecting all bounds above. □

Now

$$\begin{aligned} & \|\sigma_{A,P} - \phi_{\tilde{A}}\|_2^2 \\ \leq\ & \left[\left(\mathrm{tr}\left[Q(\mathcal{E}^*)^L(\tilde{\Lambda}\otimes\tilde{\Lambda})\mathcal{E}^L Q\right] - \mathrm{tr}\left[Q(\mathcal{F}^*)^L(\tilde{\Lambda}\otimes\tilde{\Lambda})\mathcal{F}^L Q\right]\right)\right. \\ +\ & \left.\left(\mathrm{tr}\left[Q(\mathcal{F}^*)^L(\tilde{\Lambda}\otimes\tilde{\Lambda})\mathcal{F}^L Q\right] - \mathrm{tr}\left[Q(\tilde{\mathcal{E}}^*)^L(\tilde{\Lambda}\otimes\tilde{\Lambda})\tilde{\mathcal{E}}^L Q\right]\right)\right] \end{aligned}$$

where $\mathcal{E} = \sum_i A_i \otimes \bar{A}_i$, $Q = P \otimes P$ and $\mathcal{F} = (\mathbb{1}\otimes P)\mathcal{E}(\mathbb{1}\otimes P)$.

We may now approach the main theorem of this section:

Proof of the Theorem. We start by bounding the term

$$\mu = \left|\mathrm{tr}\left[Q(\mathcal{E}^*)^L(\tilde{\Lambda}\otimes\tilde{\Lambda})\mathcal{E}^L Q\right] - \mathrm{tr}\left[Q(\mathcal{F}^*)^L(\tilde{\Lambda}\otimes\tilde{\Lambda})\mathcal{F}^L Q\right]\right|.$$

This can be done by adding and subtracting terms such that they differ in one projector, i.e.

$$\begin{aligned} \mu\ &\leq\ \sum_{r=1}^{L-1}\left|\mathrm{tr}\left[\mathcal{F}^L Q(\mathcal{F}^*)^{r-1}\mathcal{E}^*(\mathbb{1}\otimes P^\perp)(\mathcal{E}^*)^{L-r}(\tilde{\Lambda}\otimes\tilde{\Lambda})\right]\right| \\ &+\ \sum_{s=1}^{L-1}\left|\mathrm{tr}\left[\mathcal{E}^s(\mathbb{1}\otimes P^\perp)\mathcal{E}\mathcal{F}^{L-s-1}Q(\mathcal{E}^*)^L(\tilde{\Lambda}\otimes\tilde{\Lambda})\right]\right| \\ &=\ \sum_r \mu_r + \sum_s \nu_s. \end{aligned}$$

Let us bound the first family of terms. By applying the Cauchy-Schwarz inequality

$$\left|\mathrm{tr}\left[\sum_i A_i B_i\right]\right| \leq \left|\mathrm{tr}\left[\sum_i A_i^\dagger A_i\right]\right|^{\frac{1}{2}}\left|\mathrm{tr}\left[\sum_i B_i B_i^\dagger\right]\right|^{\frac{1}{2}}$$

This bound allows us to prove the following bound for μ_r

$$\mu_r\ =\ \left|\mathrm{tr}\left[\sum_{\substack{k_1,\ldots,k_L\\ i_1,\ldots,i_r\\ j_1,\ldots,j_{L-r}}}\left(\sqrt{\tilde{\Lambda}}A_{k_1}\cdots A_{k_L}PA_{i_1}^\dagger\cdots A_{i_r}^\dagger A_{j_1}^\dagger\cdots A_{j_{L-r}}^\dagger\tilde{\Lambda}^{1/4}\otimes\tilde{\Lambda}^{1/4}\right)\right.\right.\cdot$$

$$\left(\overline{\tilde{\Lambda}^{1/4}\otimes\tilde{\Lambda}^{1/4}\tilde{A}_{k_1}\cdots\tilde{A}_{k_L}\tilde{A}^\dagger_{i_1}\cdots\tilde{A}^\dagger_{i_{r-1}}A^\dagger_{i_r}P^\perp A^\dagger_{j_1}\cdots A^\dagger_{j_{L-r}}\sqrt{\tilde{\Lambda}}}\right)\Bigg]\Bigg|$$

$$\leq \Bigg|\mathrm{tr}\Bigg[\sum_{\substack{k_1,\ldots,k_L\\ i_1,\ldots,i_r\\ j_1,\ldots,j_{L-r}}}(\tilde{\Lambda}^{1/4}A_{j_{L-r}}\cdots A_{j_1}A_{i_r}\cdots A_{i_1}PA^\dagger_{k_L}\cdots A^\dagger_{k_1})\cdot$$

$$\cdot(\tilde{\Lambda}A_{k_1}\cdots A_{k_L}PA^\dagger_{i_1}\cdots A^\dagger_{i_r}A^\dagger_{j_1}\cdots A^\dagger_{j_{L-r}}\tilde{\Lambda}^{1/4}\otimes\tilde{\Lambda}^{1/2})\Bigg]\Bigg|^{\frac{1}{2}}\cdot$$

$$\cdot\Bigg|\mathrm{tr}\Bigg[\sum_{\substack{k_1,\ldots,k_L\\ i_1,\ldots,i_r\\ j_1,\ldots,j_{L-r}}}(\tilde{\Lambda}^{1/2}\otimes\tilde{\Lambda}^{1/4}\tilde{A}_{k_1}\cdots\tilde{A}_{k_L}\tilde{A}^\dagger_{i_1}\cdots\tilde{A}^\dagger_{i_{r-1}}A^\dagger_{i_r}P^\perp)\cdot$$

$$\cdot(A^\dagger_{j_1}\cdots A^\dagger_{j_{L-r}}\tilde{\Lambda}A_{j_{L-r}}\cdots A_{j_1}P^\perp A_{i_r}\tilde{A}_{i_{r-1}}\cdots\tilde{A}_{i_1}\tilde{A}^\dagger_{k_L}\cdots\tilde{A}^\dagger_{k_1}\tilde{\Lambda}^{1/4}\Bigg]\Bigg|^{\frac{1}{2}}.$$

The first term is equal to

$$\begin{aligned}&\mathrm{tr}\left[\tilde{\Lambda}^{1/2}\right]^{1/2}\mathrm{tr}\left[P\mathbb{E}^L(\tilde{\Lambda})P\tilde{\mathbb{E}}^L(\tilde{\Lambda}^{1/2})\right]^{1/2}\\ \leq\ &\mathrm{tr}\left[\tilde{\Lambda}^{1/2}\right].\end{aligned}$$

The second term is equal to

$$\begin{aligned}&\mathrm{tr}\left[\tilde{\Lambda}^{1/2}\right]^{1/2}\mathrm{tr}\left[\tilde{\mathbb{E}}^{r-1}\circ\mathbb{E}\left(P^\perp\mathbb{E}^{L-r}(\tilde{\Lambda})P^\perp\right)\tilde{\mathbb{E}}^L(\tilde{\Lambda}^{1/2})\right]^{1/2}\\ \leq\ &\delta^{1/2}\mathrm{tr}\left[\tilde{\Lambda}^{1/2}\right]\end{aligned}$$

where we have used that $\tilde{\Lambda}\leq\Lambda$ (hence, $\mathrm{tr}\left[P^\perp\mathbb{E}^{L-r}(\tilde{\Lambda})P^\perp\right]\leq\delta$), and that both $\mathbb{E}$ and $\tilde{\mathbb{E}}$ are contractible for the trace norm. Therefore, $\mu_r\leq\mathrm{tr}\left[\tilde{\Lambda}^{1/2}\right]^2\sqrt{\delta}$. The result for the ν_s is exactly the same, so it follows that $\mu\leq 2L\mathrm{tr}\left[\tilde{\Lambda}^{1/2}\right]^2\sqrt{\delta}$.

The other term can be calculated in the same way, by replacing $\mathcal{E}\to\mathcal{F}$ and $\mathcal{F}\to\tilde{\mathcal{E}}$, and it gives exactly the same estimate.

The second inequality follows from the first one, $\mathrm{tr}\left[\tilde{\Lambda}^{1/2}\right]\leq\sqrt{\tilde{D}}\mathrm{tr}\left[\Lambda\right]$, and the fact that $\sigma_{A,P}-\phi_{\tilde{A}}$ has rank $\leq 2\tilde{D}$, which then gives

$$\|\sigma_{A,P}-\phi_{\tilde{A}}\|_1\leq\sqrt{2\tilde{D}}\|\sigma_{A,P}-\phi_{\tilde{A}}\|_2.$$

□

6.4 Injectivity can be reached fast

In this section we prove that all MPS of a certain form reach injectivity fast enough, as stated in the following technical lemma:

Lemma 6.3 (Injectivity can be reached fast)**.** *Every MPS (with the exception of a zero-measure set) of the form*

$$|\tilde{\psi}\rangle = \sum_{\substack{i_1,\ldots,i_L \\ i_{L+1},\ldots,i_N}} tr\left(A_{i_1}\cdots A_{i_L}B_{i_{L+1}}C_{i_{L+2}}\cdots C_{i_N}\right)|i_1\cdots i_N\rangle \tag{6.2}$$

where $A_i, B_j, C_k \in \mathcal{M}_{D\times D}$ and $L \geq \frac{2\log D}{\log d}$ reaches injectivity in every region of length $L-1$.

Proof. Since the set of MPS failing this property is clearly a projective algebraic subvariety of $\left(\mathbb{C}^D\otimes\mathbb{C}^D\otimes\mathbb{C}^d\right)^{\otimes 3}$, standard algebraic geometry tells us that, if this set is non-empty, since $\left(\mathbb{C}^D\otimes\mathbb{C}^D\otimes\mathbb{C}^d\right)^{\otimes 3}$ is irreducible then both projective varieties must be equal. This is a straightforward conclusion after relating the following ideas concerning projective sets such that $X\subset Y$ (which always implies $\dim X\leq\dim Y$). On the one hand, if X is a non-empty open subset of Y, then $\dim X=\dim Y$. On the other hand, if $\dim X=\dim Y$ and Y is irreducible then $X=Y$ [Har77, GH11].

Therefore, it is enough to find a single MPS reaching injectivity as stated in this lemma, which has been verified numerically up to $D=200$ and $d=50$, and also analytically in the next lemma using quantum expanders. Note that our analytical proof gives a slightly worse condition for the L needed to reach injectivity, in terms of D and d, but suffices, nevertheless, to prove the main theorem. □

It is proven in [Has07c] that for all $d\geq 4$, there exists a Hermitian trace-preserving completely positive map

$$\mathbb{E}(X)=\sum_{i=1}^{d}A_i^\dagger X A_i$$

such that $|\lambda_2|\leq\left(\frac{2\sqrt{d-1}}{d}\right)\left(1+O\left(\log(D)D^{\frac{-2}{15}}\right)\right)$, where $A_i\in M_D$. If we take the MPS $|\psi\rangle$ generated by the matrices A_i and consider the map

$$\Gamma_n(X)=\sum_{i_1\cdots i_n}\mathrm{tr}\left[XA_{i_1}\cdots A_{i_n}\right]|i_1\cdots i_n\rangle,$$

we want to find a lower bound for n such that Γ_n is injective, as stated in the following result:

Theorem 6.3. *Assuming D is large enough, Γ_n is an injective map for*

$$n \geq \left\lceil \frac{k \log(D)}{\log(d)} \right\rceil + 1,\ K = 8, d > 16$$

Note that in this theorem, k can be made arbitrarily close to 4 at the price of enlarging d. This theorem is a consequence of the following lemma:

Lemma 6.4.

$$\sup_{\mathrm{tr}\left[X^\dagger X\right]=1} \left| \Gamma_n(X)^\dagger \Gamma_n(X) - \frac{1}{D} \mathrm{tr}\left[X^\dagger X\right] \right| \leq D|\lambda_2|^n$$

Proof. Considering in $\mathcal{M}_D$ the usual Hilbert-Schmidt Hilbert structure, it is easy to see that the left hand side is equal to

$$\left\| \Gamma_n^* \Gamma_n - \frac{1}{D} \mathbb{1} \right\|_{\mathrm{op}}$$

for the usual operator norm on the Hilbert space $\mathcal{M}_D$.

Moreover, in coordinates, calling $\mathcal{E} = \sum_i A_i \otimes \bar{A}_i$, we have that

$$\Gamma_n^* \Gamma_n - \frac{1}{D} \mathbb{1} = \sum_{abcd} \left(\langle cd|\mathcal{E}^n|ab\rangle - \frac{1}{D} \delta_{ab}\delta_{cd} \right) |bd\rangle\langle ac| \ .$$

just identifying $\mathcal{M}_D = \mathbb{C}^D \otimes \mathbb{C}^D$ and calling $|ij\rangle$ to the canonical (matrix) basis there.

Since for each operator on an n dimensional Hilbert space, $\|\cdot\|_{op} \leq \|\cdot\|_2 \leq \sqrt{n}\|\cdot\|_{op}$, being $\|\cdot\|_2$ the Hilbert-Schmidt norm, and using that the Hilbert-Schmidt norm is invariant under arbitrary rearrangements of the coordinates, we get that

$$\begin{aligned} & \left\| \Gamma_n^* \Gamma_n - \frac{1}{D} \mathbb{1} \right\|_{\mathrm{op}} \\ \leq\ & D \left\| \sum_{abcd} \left(\langle cd|\mathcal{E}^n|ab\rangle - \frac{1}{D} \delta_{ab}\delta_{cd} \right) |ab\rangle\langle cd| \right\|_{op} \\ =\ & D\|\mathcal{E}^n - \frac{1}{D}|\mathbb{1}\rangle\langle\mathbb{1}|\|_{op} = D\|\mathcal{E}^n - \mathcal{E}^\infty\|_{op} \\ =\ & D\|\mathbb{E}^n - \mathbb{E}^\infty\|_{op} = D|\lambda_2|^n \end{aligned}$$

where we have used in the last step that $\mathbb{E}$ is Hermitian and $|\mathbb{1}\rangle$ denotes the unnormalized vector $\sum_{i=1}^D |ii\rangle$.

□

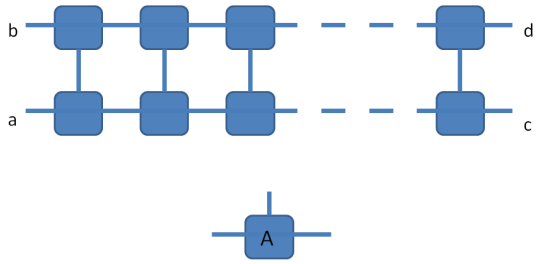

Figure 6.1: Given the tensor $A = (\langle\alpha|A_i|\beta\rangle)_{i\alpha\beta}$ which defines the MPS, and with the usual convention that rotating means complex conjugation, we can represent the map $\Gamma_n^*\Gamma_n$ as the map in the figure from systems ac to systems bd and the map $\mathbb{E}^n$ as the same figure but now mapping systems cd to systems ab

Proof of Theorem 6.3. Γ_n must be injective as long as

$$|\lambda_2|^n < \frac{1}{D^2}. \tag{6.3}$$

Otherwise, taking a (normalized) X such that $\Gamma_n(X) = 0$, we would get a contradiction to Lemma 6.4. Since we know from [Has07c] that

$$|\lambda_2| \leq \left(\frac{2\sqrt{d-1}}{d}\right)\left(1 + O\left(\log(D)D^{\frac{-2}{15}}\right)\right)$$

it suffices to take n such that

$$\left(\frac{2\sqrt{d-1}}{d}\right)^n \left(1 + O\left(\log(D)D^{\frac{-2}{15}}\right)\right)^n < \frac{1}{D^2}\,.$$

Taking logarithms

$$2\log(D) + n\log\left[\left(\frac{2\sqrt{d-1}}{d}\right)\left(1 + O\left(\log(D)D^{\frac{-2}{15}}\right)\right)\right] < 0$$

which is equivalent to

$$n > \frac{2\log(D)}{\log\left[\left(\frac{d}{2\sqrt{d-1}}\right)\right] - \log\left(1 + O\left(\log(D)D^{\frac{-2}{15}}\right)\right)}$$

It is clear that taking D large enough we can upper-bound the RHS by

$$\left\lceil \frac{2\log(D)}{\log\left(\left(\frac{d}{2\sqrt{d-1}}\right)\right)} \right\rceil + 1$$

But now

$$\begin{aligned}\frac{2\log(D)}{\log\left(\left(\frac{d}{2\sqrt{d-1}}\right)\right)} &= \frac{4\log(D)}{2\log(d) - \log(4) - \log(d-1)} \\ &\leq \frac{4K\log(D)}{\log(d)}\end{aligned}$$

as long as $\frac{1}{K} \leq 1 - \frac{2}{\log d}$, which finishes the proof of the theorem. □

6.5 Results for non-translationally invariant matrix product states

In this section, we prove that for a given reduced density matrix ρ_A^L of the form that we presented in Section 6.3, there exists a non-translationally invariant MPS with the following structure

$$|\psi\rangle = \sum_{\substack{i_1,\ldots,i_L \\ i_{L+1},\ldots,i_N}} \operatorname{tr}\left(A_{i_1}\ldots A_{i_L}B_{i_{L+1}}C_{i_{L+2}}\ldots C_{i_N}\right)|i_1,\ldots i_N\rangle \tag{6.4}$$

such that ρ_A^L is its reduced density matrix. We formalize this result in the next lemma:

Lemma 6.5. *Let $A_i, \Lambda \in \mathcal{M}_D$, then there exist $B_i, C_i \in \mathcal{M}_D$ such that if we consider the state*

$$|\psi\rangle = \sum_{\substack{i_1,\ldots,i_L \\ i_{L+1},\ldots,i_N}} tr\left(A_{i_1}\ldots A_{i_L}B_{i_{L+1}}C_{i_{L+2}}\ldots C_{i_N}\right)|i_1,\ldots i_N\rangle \tag{6.5}$$

then the reduced density matrix for L particles (particles 1-L) is

$$\rho_{1\ldots L} = \sum_{\substack{i_1,\ldots,i_L \\ j_1,\ldots,j_L}} tr\left(A_{j_L}^\dagger\ldots A_{j_1}^\dagger \Lambda A_{i_1}\ldots A_{i_L}\right)|i_1,\ldots i_N\rangle\langle j_1,\ldots j_L| \tag{6.6}$$

Proof. We consider the channel defined as

$$\mathbb{E}(X) = \sum_{i=1}^{d} V_i X V_i^\dagger, \tag{6.7}$$

where $V_1\sqrt{D}$ is a diagonal unitary matrix with different incommensurable eigenvalues such that V_1^k still has different eigenvalues for all $k \in \mathbb{N}$, $V_2\sqrt{D}$ is a random unitary matrix with non-zero entries and $V_i = 0_D, i \in \{3, ..., d\}$. This channel is trace preserving and unital. On the one hand, it is trivial to see that the only matrices that commute with V_1 are diagonal matrices. On the other hand, to find which of these diagonal matrices commute with V_2 it is enough to consider the algebraic system of equations in coordinates for $[V_2, X] = 0$ from where we get that, since $(V_2)_{ij} \neq 0$, and $(X)_{ij} = 0$ if $i \neq j$, then $(X)_{ii} - (X)_{jj} = 0$ for all $i \neq j$. From this, we deduce that the only matrices that commute with all of the Kraus operators for our channel are multiples of the identity matrix. Lüders' Theorem [BJKW00] guarantees that our channel has the identity as its unique fixed point. Since $\mathbb{E}$ is an irreducible channel [Wol12], all its eigenvalues of modulus 1 are k-roots of unity, where $k \in \{1, \ldots, D^2\}$. Let Y be such that $\mathbb{E}(Y) = \alpha Y$ for $|\alpha| = 1$. It is clear that $\mathbb{E}^k(Y) = Y$ and, again by Lüders' Theorem, $[V_1^k, Y] = 0 = [V_2 V_1^{k-1}, Y]$. Reasoning as above, Y is a multiple of the identity, which implies that $\alpha = 1$; hence, the channel is primitive [Wol12].

We can define now

$$\begin{cases} B_j & = \sqrt{\Lambda} V_j \\ C_k & = V_k \end{cases} \tag{6.8}$$

where V_i are the Kraus operators for our channel. If we consider the state

$$|\psi\rangle = \sum_{\substack{i_1,\ldots,i_L \\ i_{L+1},\ldots,i_N}} \operatorname{tr}\left(A_{i_1} \ldots A_{i_L} B_{i_{L+1}} C_{i_{L+2}} \ldots C_{i_N}\right) |i_1, \ldots i_N\rangle \tag{6.9}$$

and compute the reduced density matrix for particles $1...L$, we obtain

$$\rho_L = \sum_{\substack{i_1,\ldots,i_L \\ j_1,\ldots,j_L}} \left(\sum_{\alpha,\beta} \langle\alpha| \left[A_{i_1} \ldots A_{i_L} \mathbb{E}_B \mathbb{E}_C^{N-(L+1)}(|\alpha\rangle\langle\beta|) A_{j_L}^\dagger \ldots A_{j_1}^\dagger \right] |\beta\rangle \right) \cdot$$
$$\cdot \quad |i_1, \ldots i_N\rangle\langle j_1, \ldots j_L|$$

It is clear that $\mathbb{E}_C^{N-(L+1)}(|\alpha\rangle\langle\beta|) = \delta_{\alpha\beta}\mathbb{1}$, up to an exponentially small correction. This leads us to

$$\begin{aligned} \rho_L &= \sum_{\substack{i_1,\ldots,i_L \\ j_1,\ldots,j_L}} \left(\sum_{\alpha} \langle\alpha| \left[A_{j_L}^\dagger \ldots A_{j_1}^\dagger \mathbb{E}_B(\mathbb{1}) A_{i_1} \ldots A_{i_L} \right] |\alpha\rangle \right) |i_1, \ldots i_N\rangle\langle j_1, \ldots j_L| \\ &= \sum_{\substack{i_1,\ldots,i_L \\ j_1,\ldots,j_L}} \left(\sum_{\alpha} \langle\alpha| \left[A_{j_L}^\dagger \ldots A_{j_1}^\dagger \Lambda A_{i_1} \ldots A_{i_L} \right] |\alpha\rangle \right) |i_1, \ldots i_N\rangle\langle j_1, \ldots j_L| \\ &= \sum_{\substack{i_1,\ldots,i_L \\ j_1,\ldots,j_L}} \operatorname{tr}\left(A_{j_L}^\dagger \ldots A_{j_1}^\dagger \Lambda A_{i_1} \ldots A_{i_L} \right) |i_1, \ldots i_N\rangle\langle j_1, \ldots j_L| \end{aligned}$$

once again, up to a exponentially small correction, as we wanted to prove. □

6.6 Proof of the main theorem

In the previous sections, we have presented all the necessary tools to prove Theorem 6.1, which we will demonstrate as follows:

Proof. Let us call λ_i the ordered eigenvalues of ρ_A^R, which can be taken as close as wanted to those of $\Lambda \otimes \Lambda$ by enlarging region R (see Lemma 2 in [VC06]). In this case, it is not difficult to see that, if we call μ_i the ordered elements of Λ, then $\sum_{i=\tilde{D}+1}^{\infty} \mu_i \leq \sum_{i=\tilde{D}+1}^{\infty} \lambda_i =: \delta$.

Suppose that, for $\alpha = \frac{1}{6}$ and for all R, we can upper-bound the α-Renyi entropy by

$$S_\alpha(\rho_A^R) \leq \frac{4}{5} \log \epsilon + \frac{1}{10}(L \log d - \log L) - \log \frac{d}{4} \tag{6.10}$$

In Section 6.4, we have shown that we can always construct a state $|\tilde{\psi}\rangle$ of the form

$$|\tilde{\psi}\rangle = \sum_{\substack{i_1,\ldots,i_L \\ i_{L+1},\ldots,i_N}} \operatorname{tr}\left(\tilde{A}_{i_1} \cdots \tilde{A}_{i_L} B_{i_{L+1}} C_{i_{L+2}} \cdots C_{i_N}\right) |i_1 \cdots i_N\rangle \tag{6.11}$$

where $\tilde{A}_i, B_j, C_k \in \mathcal{M}_{\tilde{D}\times\tilde{D}}$, $\tilde{A}_i = PA_iP$ (being A_i the Kraus operators defining the original MPS), with bond dimension $\tilde{D} \leq d^{(L-1)/2}$ and such that the fixed point for the associated channel is $\tilde{\Lambda} = P\Lambda P$, where we are considering that $P = \sum_i^{\tilde{D}} |i\rangle\langle i|$.

In Section 6.4, we have also proved that all states of this form, except for a set of measure zero, reach injectivity in $L-1$ sites. Therefore, the one we have constructed in Eq. (6.11) is the unique ground state of a frustration-free Hamiltonian with interaction length L [PGVWC07, FNW92]. Using a straighforward adaptation of [FNW92, Section 6], this Hamiltonian is also gapped. Even though this state is not exactly translational invariant, it verifies that its normalized reduced density matrix for particles $1 \ldots L$ is of the form

$$\rho_{\tilde{A}}^L = \sum_{\substack{i_1,\ldots,i_L \\ j_1,\ldots,j_L}} \operatorname{tr}\left(\tilde{A}_{j_L}^\dagger \ldots \tilde{A}_{j_1}^\dagger \tilde{\Lambda} \tilde{A}_{i_1} \ldots \tilde{A}_{i_L}\right) |i_1, \ldots i_N\rangle\langle j_1, \ldots j_L| \tag{6.12}$$

up to a exponentially small correction (see Section 6.5).

This allows us to use a bound, which is proved in Section 6.3, which states that

$$\|\rho_A^L - \rho_{\tilde{A}}^L\|_1 \leq 2\sqrt{2} d^{L/2} \sqrt{L} \delta^{1/4} + (2L+3)\delta$$

$$\leq 4\sqrt{2}d^{L/2}\sqrt{L}\delta^{1/4} =: \epsilon',$$

since the first term in the sum is clearly larger than the second. It only remains to show that $\epsilon' \leq \epsilon$, or equivalently, that $\delta \leq \frac{\epsilon^4}{2^{10}d^{2L}\sqrt{L}}$. Since we have taken R large enough, then up to a exponentially small correction in R, we can state that

$$\log(\delta) \leq \frac{1-\alpha}{\alpha}\left(S_\alpha(\rho_A^R) - \log\frac{\tilde{D}}{1-\alpha}\right).$$

Using this and the fact that that $\tilde{D} \geq d^{(L-2)/2}$, it is enough to prove

$$\begin{aligned} S_\alpha(\rho_A^R) &\leq \frac{4\alpha}{1-\alpha}\log\epsilon + \frac{\log d}{2}\left(1 - \frac{4\alpha}{1-\alpha}\right)L \\ &\quad - \frac{\alpha}{(1-\alpha)}(10 + \frac{1}{2}\log L) - \log(1-\alpha) - \log d \\ &= \frac{4}{5}\log\epsilon + \frac{1}{10}(L\log d - \log L) - \log\frac{5}{6} - \log\frac{d}{4} \end{aligned}$$

where, in the last step, we have set $\alpha = \frac{1}{6}$. This is given by hypothesis in Eq. (6.10) and taking into account that the α-Renyi is monotonically increasing in α. Therefore, there exists a state $|\tilde{\psi}\rangle$, which is the unique ground state of a gapped frustration-free Hamiltonian with interaction length L, such that $\|\rho_A^L - \tilde{\rho}^L\|_1 < \epsilon$, as we wanted to prove. □

6.7 Conclusions and outlook

In this chapter, we have shown how matrix product states are powerful enough to provide formal proofs of certain believed statements on strongly correlated spin systems that were lacking a mathematical treatment. In particular, we have stated and proved that, for the state of a quantum spin chain, the impossibility of being well approximated by the ground state of a local Hamiltonian demands large entanglement.

This chapter opens the door to many interesting questions that have not been answered. For instance, it would be very relevant to prove that a translational invariant matrix product state with a certain bond dimension D may be approximated using a translational invariant MPDO with a smaller bond dimension $\tilde{D} \leq D$ and such that the bound on the distance for the reduced density matrix for L particles scales linearly with the range of the interaction. This would allow us to give rigourous bounds on the accuracy of numerical algorithms for these types of states, such as the TEBD or the iTEBD which rely on truncating the outcome of each infinitesimal evolution. This is achieved approximating an MPS with a given bond dimension by another MPS with a lower bond dimension, as we have seen in Section 4.3. If we use the techniques of Ref. [VC06] we obtain a

bound which scales as d^L for the physical dimension d and the interaction length L. On the other hand, by considering that the states associated to the reduced density matrices are not translationally invariant, we obtain the desired linear bound in L as in the bounds that we presented in Theorem 6.2. We would like to explore if there are better bounds when the truncated state is translationally invariant. We have performed numerical simulations for the Heisenberg spin-1 chain, calculating the distance between observables such as string order parameters. We have found that the scaling between these observables is linear on the number of particles, supporting our conjecture that for translationally invariant states the scaling for the reduced density matrix for L particles is also linear in L.

Another result which is related to our proof is the quantum version of Wielandt's inequality [SPGWC10] which implies a bound on the interaction-range of Hamiltonians with a unique MPS ground state. The question of whether there exists a Wielandt's theorem in higher dimensions is still open and it would be interesting to explore it.

There are other interesting questions related to the tensor network representation of quantum many-body systems, such as whether it is possible to put forward efficient numerical methods to obtain the purifications of a given matrix product density operator. As we discussed in Section 4.2, it is generally unfeasible to confirm locally the existence of global positivity for MPDO and finding a purification [VGRC04] could help overcome this limitation. Along this line, we are currently developing a numerical method based on the sum of squares polynomial (sos) method [DSPGC13] to construct approximate purifications to MPDO efficiently.

7 Lieb-Robinson bounds for spin-boson models

7.1 Introduction

Causality is one of the most fundamental concepts in modern physics. It limits how local measurements and perturbations, described by an operator O_X in region X, affect later measurements of another operator O_Y in a separate region Y [PS95]. In analogy to Heisenberg's principle [Rob29], this uncertainty is quantified by a commutator $C_{Y,X}(t) = \langle [O_Y(t), O_X(0)] \rangle$. Lorentz invariance and the mathematical structure of relativistic theories guarantee causality. Thus, $C_{Y,X}(t) = 0$ when the distance $d_{XY} > ct$ places both regions outside the light cone defined by the speed of light c. Nevertheless, causality is not part of the axioms of non-relativistic quantum mechanics, and it is violated at the few particle level [PS95, Heg98]. Remarkably, in the many-body regime, an approximate light cone emerges, outside of which non-causal correlations are vanishingly small. This phenomenon, first demonstrated by Lieb and Robinson for a lattice of locally-interacting spins [LR72], has been generalized to finite-dimensional models, anharmonic oscillators and master equations [HK06, NOS06, CSE08, NRSS09, Pou10].

In this chapter, we address the role of bosons as mediators of interactions between particles in the light of Lieb-Robinson bounds. This is done for a general model of finite dimensional systems interacting through a bosonic field that satisfies a Lieb-Robinson bound itself. We derive new bounds for these kind of models, which are then applied in Chapter 8 to a crystal of trapped atomic ions, where the spins and the bosons map to the atom's internal states and the ion crystal's phonons, respectively. These Lieb Robinson bounds work for all spin-boson lattice models of any dimensionality and geometry realized with state-of-the-art technology [BSK+12, FSG+08, KCK+10, IEK+11, BOC+11, HLB+11, SRW+14].

7.2 Model and motivation

We start by defining the system under study, which we refer to as the *spin-boson lattice model* (SBL). This consists on a lattice model of bosons interacting locally with a collection of finite-dimensional quantum systems. We consider a lattice described by an undirected graph $G = (L, E)$ with a set of vertices L, where the physical degrees of freedom are defined, and an edge set E, which describes neighbourhood relations in the lattice. The physical degrees of freedom of each vertex $i \in L$ are defined in the Hilbert space $\tilde{\mathcal{H}}_i = \mathcal{L}^2(\mathbb{R}) \otimes \mathcal{H}_i$, which combines an infinite-dimensional Hilbert space for the bosons, $\mathcal{L}^2(\mathbb{R})$, with a Hilbert space $\mathcal{H}_i$ of finite dimension d_i for the "spins" (see Fig. 7.1).

The bosons are represented by adimensionalized harmonic oscillators, with positions and momenta $\mathbf{R}_i^T = (x_i, p_i)$ satifying the usual canonical commutation relations in coordinates

$$[\mathbf{R}_i, \mathbf{R}_j^T] = -\delta_{ij}\sigma^y, \tag{7.1}$$

where we consider $\hbar = 1$, δ_{ij} is the Kronecker delta, σ^y is a Pauli matrix and $i, j \in L$.

The spin degrees of freedom are represented by a set of dimensionless operators $\mathbf{S}_i = (S_i^1, \ldots, S_i^m)$ that form a Lie algebra. For concreteness, we start by assuming that they form a representation of $\mathfrak{su}(2)$ with commutation relations

$$[S_i^\alpha, S_j^\beta] = \mathrm{i}\delta_{ij} \sum_\gamma f^{\alpha\beta\gamma} S_i^\gamma, \tag{7.2}$$

where $\alpha, \beta, \gamma \in \{1, 2, 3\}$ label the different spin components, and $f^{\alpha\beta\gamma} = 2\epsilon^{\alpha\beta\gamma}$ is defined in terms of the completely antisymmetric Levi-Civita symbol $\epsilon^{\alpha\beta\gamma}$. However, the LRB derived in this chapter also applies to more general Lie algebras, provided the structure constants $f^{\alpha\beta\gamma}$ are completely antisymmetric.

Motivated by its applicability in different physical contexts, such as condensed matter, we consider that bosons at distant lattice sites are coupled by a matrix $Q_{ij}(t) \in \mathcal{M}_{2\times 2}(\mathbb{R})$ whose elements have the units of frequency (let us recall that $\hbar = 1$), and fulfill $Q_{ij}(t) = Q_{ji}(t) \neq 0$ whenever the two vertices $i, j \in L$ are connected through an edge of the graph. The spins precess under a general magnetic field $\mathbf{B}_i^T(t) = (B_i^1(t), B_i^2(t), B_i^3(t))$, which might be time-dependent $B_i^\alpha(t) \in \mathbb{R}$, and also has the units of frequency. Finally, the coupling between spins and bosons is purely local, taking place exclusively at the vertices of the graph, and it is defined through the matrices $G_i(t) \in \mathcal{M}_{2\times 3}(\mathbb{R})$ that also have the units of frequency. Altogether, the Hamiltonian of the spin-boson lattice model is

$$H_{\mathsf{SBL}}(t) = \frac{1}{2}\sum_{i,j} \mathbf{R}_i^T Q_{ij}(t) \mathbf{R}_j + \sum_i \mathbf{B}_i(t)^T \cdot \mathbf{S}_i + \sum_i \mathbf{R}_i^T \cdot G_i(t) \cdot \mathbf{S}_i. \tag{7.3}$$

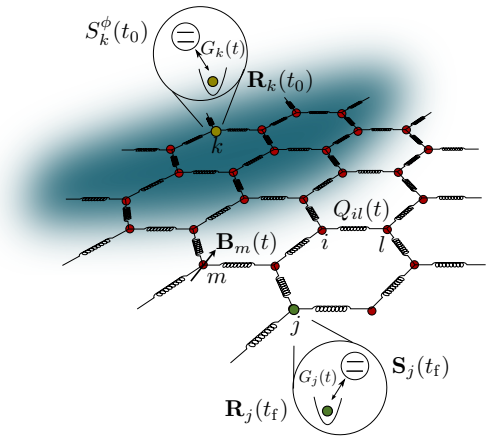

Figure 7.1: **Scheme of the spin-boson lattice model:** Scheme of a graph corresponding to a honeycomb lattice with vertices $i, j, k, l \in L$ represented by red, green and yellow dots. In the two insets, we depict the spin $\mathbf{S}_j$ and bosonic $\mathbf{R}_j$ physical degrees of freedom by discrete levels and a quadratic well, respectively. The links of the lattice correspond to the edges of the graph E, and are represented as springs leading to the coupling $Q_{ij}(t)$ between distant oscillators. We also represent the on-site magnetic-field $\mathbf{B}_j(t)$ under which the spin precess, and the spin-boson coupling $G_j(t)$. The blue region mimics the propagation of a spin perturbation at $S_k^\phi(t_0)$, until it reaches a distant spin $\mathbf{S}_j(t_\mathrm{f})$.

Our objective is to understand how correlations are established between distant spins in the lattice, and to derive a bound on how fast this process can take place. Since distant spins do not interact directly, spin-spin interactions and thus spin correlations can only be mediated by the exchange of bosons, which form an array of coupled oscillators. This situation is common in physics, where bosons act as carriers of the fundamental interactions between particles.

7.3 Main result: Spin-boson Lieb-Robinson bounds

Following the tradition of Lieb-Robinson bounds [Has09], we study the so-called Lieb-Robinson commutators, whose expectation value corresponds to a retarded spin-spin correlation function for a particular state. Such a commutator relates a perturbation at site $k \in L$ and instant $t_0 = 0$, with an observable at a distant site $j \in L$ and $t > t_0$, namely

$$\mathbf{Z}_{jk}(t) := [\mathbf{S}_j(t), S_k^\phi(0)], \tag{7.4}$$

for $\phi \in \{1, 2, 3\}$. Since the spins are coupled to the bosons, we also have to consider the correlations between spin and bosonic operators, which are related

to the following commutator

$$\mathbf{C}_{jk}(t) := [\mathbf{R}_j(t), S_k^{\phi}(0)]. \tag{7.5}$$

We would like to derive a bound for the norm of the spin commutator

$$\|\mathbf{Z}_{jk}(t)\| \leq \xi(d_{jk}, v_{\mathrm{LR}}t), \tag{7.6}$$

where $\xi(d_{jk}, v_{\mathrm{LR}}t)$ is a certain function that depends on the distance d_{jk} between the two lattice sites and on time. Since the retarded spin correlation function fulfills

$$|C_{S_j^{\alpha},S_k^{\phi}}(t)| = |\langle [S_j^{\alpha}(t), S_k^{\phi}(0)]\rangle| \leq \|\mathbf{Z}_{jk}(t)\|_{\infty} := \max_{\beta} \left\| Z_{jk}^{\beta}(t) \right\|, \tag{7.7}$$

we can also interpret that the function $\xi(d_{jk}, v_{\mathrm{LR}}t)$ in the LRB (7.6) contains information on how fast the spin correlations are established as the perturbation travels with a certain speed v_{LR} across the distance d_{jk}.

We state the main result as follows:

Theorem 7.1. *Let us assume that the propagator W of the free bosonic lattice without spins ($G_i = 0$) satisfies a Lieb-Robinson bound*

$$\|[\mathbf{R}_j(t), \mathbf{R}_k(0)]\| \leq \|W_{jk}(t,0)\| \leq \alpha\, e^{\nu_{\mathrm{LR}}t} f(d_{jk}), \tag{7.8}$$

characterized by a Lieb-Robinson speed v_{LR}, a normalization $\alpha > 0$, and a function of the lattice distance such that

$$a_0 := \max_{ik} \left[f(d_{ik})^{-1} \sum_j f(d_{ij}) f(d_{jk}) \right] < +\infty. \tag{7.9}$$

Under these conditions, assuming bounded interactions $\|G_j(t)\| \leq g$ and spins $\|\mathbf{S}\| \leq S$, a a Lieb-Robinson bound emerges for the spin correlations $\mathbf{Z}_{jk}(t) := [\mathbf{S}_j(t), S_k^{\phi}(0)]$, $\phi \in \{1,2,3\}$

$$\|\mathbf{Z}_{jk}(t)\| \leq \alpha\, e^{\nu_{\mathrm{LR}}t} f(d_{jk}) \times \frac{2S^2}{a_0} \left(\mathrm{e}^{(g^2/v_{\mathrm{LR}})2S\alpha a_0 t} - 1 \right). \tag{7.10}$$

Intuitively, since bosons mediate interactions, the bosonic velocity v_{LR} limits the propagation speed of spin correlations. This is precisely the first term of the above expression, which duplicates the bosonic LRB. Additionally, the efficiency with which distant spins excite and reabsorb a propagating boson affects the LRB. This is the second term in Eq. (7.10), which depends on the rate $\sim g^2/v_{\mathrm{LR}}$ at which bosons are emitted or absorbed by spins. This nonperturbative correction

shows that the buildup of correlations is suppressed if bosons are much faster than spins $g \ll v_{\mathrm{LR}}$, an adiabatic-type argument.

Note that Eqs. (7.8) and (7.9) include a very large family of bounds

$$e^{\nu_{\mathrm{LR}} t} f(d_{jk}) = e^{\nu_{\mathrm{LR}} t - \mu d_{jk}} (1 + d_{jk})^{-\eta}, \tag{7.11}$$

with appropriate $\mu \geq 0$ and $\eta > 0$. For nearest-neighbor or short-range interactions $\mu > 0$ yields a light cone, $\mu d_{jk} - v_{\mathrm{LR}} t \sim 0$, outside of which correlations are exponentially suppressed. For algebraically decaying interactions, $\mu = 0$, and the lines of constant correlation are only straight at short distances and times.

For this result to be useful, the bound of Eq. (7.8) must be sufficiently tight. Whereas the bosonic LR speed has been studied for nearest-neighbor [NRSS09] and algebraically decaying [CSE08] time-independent couplings Q, we have developed a tighter bound for such models. Our LR speed only relies on the off-diagonal couplings, using a recursion similar to that in Ref. [CSE08], but eliminating the diagonal terms with unitary transformations. The case relevant for trapped ions involves long-range interactions

$$\left\| Q_{jk}(t) \right\|_{j \neq k} \leq \kappa (1 + d_{jk})^{-\eta} \tag{7.12}$$

with a strength κ that bounds the couplings and a decay power $\eta \geq 0$. We then recover Eq. (7.8) with $f(d) = (1+d)^{-\eta}$, $\alpha = (1+a_0)/a_0$, and a bosonic LR speed $v_{\mathrm{LR}} = \kappa a_0$.

7.4 Preliminary results

Differential equations for the Lieb-Robinson commutators

In order to study the commutators in Eq. (7.4), we will work with the Heisenberg picture. In this picture, the time evolution of any operator A is given by the differential equation $\frac{\mathrm{d}}{\mathrm{d}t} A(t) = -\mathrm{i}[A(t), H_{\mathsf{SBL}}(t)]$. Using the commutation relations in Eqs. (7.1) and (7.2), we arrive at the following system of ordinary differential equations (ODEs) for the boson and spin operators

$$\dot{\mathbf{R}}_j = -\sum_k J \cdot Q_{jk}(t) \cdot \mathbf{R}_k - J \cdot G_j(t) \cdot \mathbf{S}_j, \tag{7.13}$$

$$\dot{\mathbf{S}}_j = \mathrm{i} K_j(t) \cdot \mathbf{S}_j, \tag{7.14}$$

where $K_j(t)$ is a matrix of operators depending on the representation for the spins. For our particular choice, it can be written as

$$K_j^{\alpha\beta}(t) = -\mathrm{i} \sum_\gamma \left(\mathbf{B}_j(t) + \mathbf{R}_j^T \cdot G_j(t) \right)^\gamma f^{\alpha\gamma\beta}, \tag{7.15}$$

which can be easily shown to be Hermitian $K_j(t) = K_j^\dagger(t)$.

Evolution of the bosons

The first equation (7.13) describes a set of coupled harmonic oscillators, where the spins act as a "source" term for the bosonic operators. In order to formally integrate this equation we present an improvement on the LRB for free bosonic lattice models found by M. Cramer *et al.* [CSE08] and we show how this bound enters in the full spin-boson lattice model both for free oscillators and for oscillators with source.

Harmonic lattice Lieb-Robinson bounds for free oscillators

Let use rewrite the bosonic part of the full spin-boson Hamiltonian (7.3) by separating the diagonal and off-diagonal terms

$$H_\mathrm{b} = \frac{1}{2}\sum_i \omega_i(t)\left(p_i^2 + x_i^2\right) + \frac{1}{2}\sum_{i\neq j}\mathbf{R}_i^T Q_{ij}(t)\mathbf{R}_j, \tag{7.16}$$

where $\omega_i(t) = Q_{ii}(t)$, and we impose that the coupling matrices $Q_{ij}(t)$ between different lattice sites $i \neq j$ decay with the distance. Moreover, we also assume that the norm of such matrices can be upper bounded by

$$\|Q_{ij}(t)\| \leq \frac{\kappa \mathrm{e}^{-\mu d_{ij}}}{(1+d_{ij})^\eta}, \tag{7.17}$$

where we use the exponent $\eta \in \mathbb{Z}$, and a constant $\kappa \in \mathbb{R}$ with the units of frequency. For $\mu > 0$, the couplings are more than exponentially suppressed; for $\mu = 0$, we face an algebraic decay.

We can now get rid of the diagonal terms by changing into a frame in which the phase space coordinates rotate with angular speed $\omega_j(t)$

$$\mathbf{R}_j(t) = U_j(t)\tilde{\mathbf{R}}_j(t), \quad U_j(t) = \mathrm{e}^{-\int_{t_0}^t \mathrm{d}\tau \omega_j(\tau) J} \tag{7.18}$$

In this frame, the system of ODEs for the free bosonic operators (7.13) only includes the off-diagonal couplings

$$\frac{\mathrm{d}\tilde{\mathbf{R}}_j}{\mathrm{d}t} = -\sum_{k\neq j} U_j^{-1}(t)\cdot J \cdot Q_{jk}(t)\cdot U_k(t)\cdot \tilde{\mathbf{R}}_k, \tag{7.19}$$

which can be alternatively written in terms of the free bosonic propagator $\tilde{\mathbf{R}}(t) = \tilde{W}(t,t_0)\tilde{\mathbf{R}}(t_0)$ in the rotated frame, such that the full propagator corresponds to $W_{jk}(t,t_0) = U_j(t,t_0)\tilde{W}_{jk}(t,t_0)$. This propagator satisfies the Dyson series

$$\tilde{W}_{jk}(t,t_0) = \delta_{jk}\mathbb{1} - \sum_{l\neq j}\int_{t_0}^t \mathrm{d}\tau U_j^{-1}(t)\cdot J\cdot Q_{jl}(t)\cdot U_l(t)\cdot \tilde{W}_{l,k}(\tau,t_0), \tag{7.20}$$

where we used $\tilde{W}(t_0, t_0) = \mathbb{1}$ for all t_0. Let us calculate the norm of this operator, and use the identities $\|A + B\| \leq \|A\| + \|B\|$, and $\|AB\| \leq \|A\| \, \|B\|$. Moreover, since $U_j(t)$, and J are unitary operators, it follows that

$$\|W_{jk}(t, t_0)\| \leq \delta_{jk} + \sum_{l \neq j} \int_{t_0}^{t} \mathrm{d}\tau \, \|Q_{jl}(t)\| \, \|W_{lk}(\tau, t_0)\| \, . \tag{7.21}$$

By using the bound on the off-diagonal couplings (7.17), we find the expression

$$\|W_{jk}(t, t_0)\| \leq \delta_{jk} + \sum_{l \neq j} \frac{\kappa \mathrm{e}^{-\mu d_{jl}}}{(1 + d_{jl})^{\eta}} \int_{t_0}^{t} \mathrm{d}\tau \, \|W_{lk}(\tau, t_0)\| \, , \tag{7.22}$$

which can be iterated once to obtain

$$\begin{aligned} \|W_{jk}(t, t_0)\| \quad &\leq \quad \delta_{jk} + \sum_{l \neq j} \frac{\kappa \mathrm{e}^{-\mu d_{jl}}}{(1 + d_{jl})^{\eta}} \int_{t_0}^{t} \mathrm{d}\tau_1 \delta_{lk} \\ &+ \quad \sum_{l \neq j} \sum_{l' \neq l} \frac{\kappa \mathrm{e}^{-\mu d_{jl}}}{(1 + d_{jl})^{\eta}} \frac{\kappa \mathrm{e}^{-\mu d_{ll'}}}{(1 + d_{ll'})^{\eta}} \int_{t_0}^{t} \mathrm{d}\tau_1 \int_{t_0}^{\tau_1} \mathrm{d}\tau_2 \, \|W_{l'k}(\tau_2, t_0)\| \, . \end{aligned}$$

In analogy to Eq. (7.29), by introducing the geometric factor

$$\tilde{a}_0 = \max_{jl'} \left\{ e^{\mu d_{jl'}} (1 + d_{jl'})^{\eta} \sum_{l \neq j} e^{-\mu d_{jl}} (1 + d_{jl})^{-\eta} e^{-\mu d_{ll'}} (1 + d_{ll'})^{-\eta} \right\}, \tag{7.23}$$

we find directly that

$$\begin{aligned} \|W_{jk}(t, t_0)\| \quad &\leq \quad \delta_{jk} + (\kappa \tilde{a}_0) \frac{\mathrm{e}^{-\mu d_{jk}}}{\tilde{a}_0 (1 + d_{jk})^{\eta}} \int_{t_0}^{t} \mathrm{d}\tau_1 \\ &+ \quad (\kappa \tilde{a}_0)^2 \sum_{l' \neq l} \frac{\mathrm{e}^{-\mu d_{jl'}}}{\tilde{a}_0 (1 + d_{jl'})^{\eta}} \int_{t_0}^{t} \mathrm{d}\tau_1 \int_{t_0}^{\tau_1} \mathrm{d}\tau_2 \, \|W_{l'k}(\tau_2, t_0)\| \, . \end{aligned}$$

By iterating this recursion to infinite order, we can now see that the free boson propagator can be expressed as

$$\begin{aligned} \|W_{jk}(t, t_0)\| \quad &\leq \quad \delta_{jk} + \frac{\mathrm{e}^{-\mu d_{jk}}}{\tilde{a}_0 (1 + d_{jk})^{\eta}} \sum_{n=1}^{\infty} (\kappa \tilde{a}_0)^n \tilde{T}_n \\ \tilde{T}_n \quad &= \quad \int_0^t \mathrm{d}\tau_1 \int_0^{\tau_1} \mathrm{d}\tau_2 \cdots \int_0^{\tau_{n-1}} \mathrm{d}\tau_n . \end{aligned}$$

In this case, we find exactly that $\tilde{T}_n = t^n / n!$, such that the series can be summed to infinite order yielding

$$\|W_{jk}(t, t_0)\| \quad \leq \quad \delta_{jk} + \frac{\mathrm{e}^{\kappa \tilde{a}_0 t - \mu d_{jk}}}{\tilde{a}_0 (1 + d_{jk})^{\eta}} \leq \frac{(1 + \tilde{a}_0)}{\tilde{a}_0} \frac{\mathrm{e}^{\kappa \tilde{a}_0 t - \mu d_{jk}}}{(1 + d_{jk})^{\eta}} .$$

This is precisely the LRB for the free bosonic lattice model that has been used in Eq. (7.28), where we note that the propagator can be directly related to the Lieb-Robinson retarded commutators of position-momentum operators [CSE08]. We also observe that the bound inherits the decay structure of the couplings. Regarding algebraically decaying couplings ($\mu = 0$), this bound presents certain improvements with respect to the work of M. Cramer *et al.* [CSE08]. The first and most important one is that the Lieb-Robinson speed $v_{\mathrm{LR}} = \kappa\tilde{a}_0$ only depends on the bound of the off-diagonal couplings (7.17) thorough κ. As expected from a physical reasoning, the maximum speed with which the bosonic correlations are build up cannot increase with the on-site frequencies, but must be rather limited by the off-diagonal couplings between distant oscillators. The second reason for the improvement is that our bound applies to more general bosonic lattice models, where the coupling matrix $Q_{ij}(t)$ might depend on time, and have all types of couplings, namely position-position, position-momentum, and momentum-momentum couplings.

Harmonic lattice Lieb-Robinson bounds for oscillators with source

We may also consider the system of ODEs for the oscillators with an additional source term $\mathbf{F}(t)$

$$\dot{\mathbf{R}}_j = -\sum_k J \cdot Q_{jk}(t) \cdot \mathbf{R}_k + \mathbf{F}(t). \tag{7.24}$$

We can solve it with the following ansatz

$$\mathbf{R}(t) = W(t, t_0)[\mathbf{R}(t_0) + \mathbf{X}(t)]$$

where $W(t, t_0)$ is the propagator of the free bosonic system, which is a homogeneous system of ODEs, previously bounded in Eq. (7.24). It is important to remark that we need both the starting time and the final time in W because $Q(t)$ is time dependent: we have lost translational invariance in time. When we introduce this ansatz into the previous equation and impose that W is the propagator of the free bosonic system, $\frac{d}{dt}W(t, t_0) = Q(t)W(t, t_0)$, we obtain $W(t, t_0)\frac{d}{dt}\mathbf{X}(t) = \mathbf{F}(t)$. This leads to the solution

$$\mathbf{R}(t) = W(t, t_0)\mathbf{R}(t_0) + W(t, t_0)\int_{t_0}^{t} \mathrm{d}\tau W(\tau, t_0)^{-1}\mathbf{F}(\tau). \tag{7.25}$$

Using the fact that the operators can be composed, that is

$$W(t, t_0) = W(t, \tau)W(\tau, t_0)$$

which follows from the properties of the solution of the homogeneous system of ODEs, we can simplify the previous expression

$$\mathbf{R}_j(t) = \sum_k W_{jk}(t, t_0)\mathbf{R}_k(t_0) + \int_{t_0}^{t} \sum_k W_{jk}(t, \tau)\mathbf{F}_k(\tau)\mathrm{d}\tau. \tag{7.26}$$

Integration of the boson differential equation

If we consider the particular spin-dependent source term, $\mathbf{F}_k(\tau) = -J \cdot G_k(\tau) \cdot \mathbf{S}_k(\tau)$ and we apply it to the result obtained in Subsection 7.4, the equation can be formally integrated as

$$\mathbf{R}_j(t) = \sum_k W_{jk}(t,0)\mathbf{R}_k(0) - \int_0^t \mathrm{d}\tau \sum_k W_{jk}(t,\tau) \cdot J \cdot G_k(\tau) \cdot \mathbf{S}_k(\tau), \tag{7.27}$$

where we have used the propagator for the free bosons $W(t_1, t_2)$. According to the notation above, we may regard $W(t_1, t_2)$ as an $N \times N$ block matrix, such that each of the blocks is a 2×2 matrix $W_{jk}(t_1, t_2)$ that couples the oscillators at sites j and k.

The norm of these propagators can be bounded by

$$\|W_{jk}(t,t_0)\| \leq e^{\nu_{\mathrm{LR}}|t-t_0|}\alpha \frac{e^{-\mu d_{jk}}}{[1+d_{jk}]^{\eta}} =: \alpha e^{\nu_{\mathrm{LR}}|t-t_0|} f(d_{jk}), \tag{7.28}$$

where v_{LR} is the so-called Lieb-Robinson speed, which determines the maximum rate of propagation of bosonic perturbations in the lattice. Note that this expression includes a more than exponential suppression for $\mu > 0$ and a long-distance attenuation of $\|W_{jk}(t,t_0)\|$ for $\mu = 0$ due to the possibly long-range interactions in the oscillator couplings $Q_{jk}(t)$, a situation that will become evident when discussing the trapped-ion realisation.

The only property that we will use is the fact that the spatial modulation $f(d)$ can be summed in the following way

$$a_0 := \max_{ik} \left[f(d_{ik})^{-1} \sum_j f(d_{ij}) f(d_{jk}) \right] < +\infty, \tag{7.29}$$

which can be interpreted as a bound on the convolution function and is used in different proofs of LRBs [CSE08, NOS06]. For instance, if $\mu = 0$ and one selects d_{ij} as the graph distance (i.e. number of edges forming the shortest path connecting the two vertices $i, j \in L$), it is possible to estimate $\tilde{a}_0 = \alpha c_{\mathrm{D}} 2^{\eta+1} \zeta(1 - D + \eta)$, where $\zeta(s)$ is the Riemann zeta function, and c_{D} is a constant that depends on the particular graph of dimension D [CSE08]. Such a constant can be determined by bounding the maximum number of vertices $\sup_i |S_r(i)| \leq c_D r^{D-1}$ in a sphere of radius $r \in \mathbb{N}$, namely $S_r(i) = \{j \in L : d_{ij} = r\}$. Let us remark, however, that the LRB can be made tighter for the type of lattices realised by the ion crystals, where the Euclidean distance arises naturally, and will allow us to substitute $\tilde{a}_0 \to a_0 < \tilde{a}_0$.

Evolution of the spins

The second equation (7.14) describes the precession of the spins under the operator K_j which, in addition to the effects of the external magnetic field, includes

also the feedback from the bosonic subsystem. An important property used below is that the hermiticity of K_j implies that this operator can be regarded as the generator of unitary rotations $O_j(t)$, namely

$$\frac{\mathrm{d}}{\mathrm{d}t}O_j(t) = \mathrm{i}K_j(t)O_j(t), \quad O_j^{-1}(t) = O_j^{\dagger}(t). \tag{7.30}$$

This crucial property relies on the particular $\mathfrak{su}(2)$ commutation relations. In a more general case, where the matrices $\mathbf{S}_i$ have arbitrary dimension d_i, we may regard these matrices as acting on a subspace of a larger Hilbert space, $\mathbb{C}^{2^m}$, $m \geq \lceil \frac{\log d}{\log 2} \rceil$. In this even-sized space, we can find a set of Hermitian generators $S_i^{\alpha} \in \mathcal{M}_{2^m \times 2^m}(\mathbb{C})$, that form a complete basis for the observable. The commutator of any two generators will depend, once more, on an antisymmetric tensor (see Ref. [Alt04]), which results from the composition of Levi-Civita symbols. Thanks to this fact, we can still prove that the operator $K_j(t)$ is the product of Hermitian operators $(x_n,\, p_n)$ and a set of Hermitian matrices, obtaining, once more, that $O_j(t)$ is unitary.

Evolution of the Lieb-Robinson commutators

Since we are actually interested in the commutators in Eqs. (7.4)-(7.5), we will write down their corresponding time-evolution equations. Note that $\mathbf{C}_{jk}(t)$ is not zero since the source terms in Eq. (7.27) introduce feedback of the spins onto the oscillators, which thus become correlated as the time evolves. Moreover, the opposite effect happens through the $K_j(t)$, complicating the solution of the differential equations

$$\dot{\mathbf{C}}_{jk} = -\sum_l J \cdot Q_{jl}(t) \cdot \mathbf{C}_{lk} - J \cdot G_j(t) \cdot \mathbf{Z}_{jk} \tag{7.31}$$

$$\dot{\mathbf{Z}}_{jk} = \mathrm{i}\sum_n C_{jk}^n A_j^n(t) \cdot \mathbf{S}_j + \mathrm{i}K_j(t) \cdot \mathbf{Z}_{jk}, \tag{7.32}$$

where we have introduced the index $n \in \{x, p\}$ to label the position/momentum spin-boson couplings, and the matrices $A_j^n(t) \in \mathcal{M}_{3\times 3}(\mathbb{C})$, which have the following expression $A_j^n(t) = -\mathrm{i}\sum_\gamma G_j^{n\gamma}(t) f^{\alpha\gamma\beta}$.

It is clear that the last term in Eq. (7.32), namely $\mathrm{i}K_j(t)\mathbf{Z}_{jk}$, cannot be responsible for the propagation of spin correlations, as it is just a local evolution of the spins that would be present even in the case of uncoupled oscillators. Fortunately, we have already shown that this local term can be regarded as the generator of a unitary rotation (7.30). Hence, we may eliminate this term by defining a new set of spin-spin commutators $\mathbf{D}_{jk} := O_j^{-1}\mathbf{Z}_{jk}$, which share the norm with the original ones $\|\mathbf{D}_{jk}\| = \|\mathbf{Z}_{jk}\|$. The time-evolution for these spin commutators becomes

$$\dot{\mathbf{D}}_{jk} = \mathrm{i}O_j^{-1}(t) \cdot \left[\sum_n C_{jk}^n\, A_j^n(t)\right] \cdot \mathbf{S}_j, \tag{7.33}$$

which is simple enough such that we can derive the desired Lieb-Robinson bound for the spin-boson lattice model.

Lieb-Robinson bounds for the spin-boson lattice model

In analogy with the time-evolution of the bosonic operators (7.27), the system of differential equations for the spin-boson commutator (7.31) can be formally integrated. Using the initial condition $\mathbf{C}_{jk}(0) = \mathbf{0}$, which assumes that the spins and bosons are initially uncorrelated, we arrive at

$$\mathbf{C}_{jk}(t) = -\int_0^t \mathrm{d}\tau \sum_l W_{jl}(t,\tau) \cdot J \cdot G_l(\tau) \cdot O_l(\tau) \cdot \mathbf{D}_{lk}(\tau). \tag{7.34}$$

Upon substitution of this result in the system of ODEs for the spin-spin commutators (7.33), we find

$$\dot{\mathbf{D}}_{jk}(t) = \mathrm{i} \sum_{l,n} O_j^{-1}(t) \cdot \int_0^t \mathrm{d}\tau \left[W_{jl}(t,\tau) \cdot J \cdot G_l(\tau) \cdot O_l(\tau) \cdot \mathbf{D}_{lk}(\tau)\right]^n \cdot A_j^n(t) \cdot \mathbf{S}_j(t). \tag{7.35}$$

Integrating this equation leads to a Dyson-type recurrence that only contains spin operators

$$\begin{aligned} \mathbf{D}_{jk}(t) \;=\; & \mathbf{D}_{jk}(0) + \mathrm{i} \int_0^t \mathrm{d}\tau_1 \int_0^{\tau_1} \mathrm{d}\tau_2 \left(\sum_{l,n} O_j^{-1}(\tau_1) \cdot \right. \\ & \left. \cdot \left[W_{jl}(\tau_1,\tau_2) \cdot J \cdot G_l(\tau_2) \cdot O_l(\tau_2) \cdot \mathbf{D}_{lk}(\tau_2)\right]^n \cdot A_j^n(\tau_1) \cdot \mathbf{S}_j(\tau_1) \right) \end{aligned}$$

We can now upper-bound the norm of the Lieb-Robinson commutator $\mathbf{D}_{jk}(t)$ by using two properties of the operator norm, namely $\|A+B\| \leq \|A\| + \|B\|$, and $\|AB\| \leq \|A\|\,\|B\|$. Additionally, we will exploit the fact that O_j is a unitary operator, $\|O_j(t)\| = 1$, and use the bound for the norm of the free bosonic propagator. After introducing the upper bounds $g = \max_{t,j} \|G_j(t)\| = \max_{t,j,n} \left\|A_j^n(t)\right\|$, and $S = \max_{t,j} \|\mathbf{S}_j(t)\|$, we obtain

$$\|\mathbf{D}_{jk}(t)\| \leq \|\mathbf{D}_{jk}(0)\| + \chi \sum_l \int_0^t \mathrm{d}\tau_1 \int_0^{\tau_1} \mathrm{d}\tau_2 \mathrm{e}^{v_{\mathrm{LR}}(\tau_1-\tau_2)} f(d_{jl}) \left\|\mathbf{D}_{lk}(\tau_2)\right\|. \tag{7.36}$$

where we have introduced the constant $\chi = 2g^2 S\alpha$. We now interchange the integration order, noting that the initial integration limits are $0 \leq \tau_2 \leq \tau_1$ and $0 \leq \tau_1 \leq t$, and defining the same integration region as $\tau_2 \leq \tau_1 \leq t$ and $0 \leq \tau_2 \leq t$. Hence,

$$\|\mathbf{D}_{jk}(t)\| \leq \|\mathbf{D}_{jk}(0)\| + \chi \sum_l \int_0^t \mathrm{d}\tau_2 \int_{\tau_2}^t \mathrm{d}\tau_1 \mathrm{e}^{v_{\mathrm{LR}}(\tau_1-\tau_2)} f(d_{jl}) \left\|\mathbf{D}_{lk}(\tau_2)\right\|. \tag{7.37}$$

Integrating the exponential term, we now find

$$\|\mathbf{D}_{jk}(t)\| \leq \|\mathbf{D}_{jk}(0)\| + \frac{\chi}{v_{\mathrm{LR}}} \sum_l \int_0^t \mathrm{d}\tau_2 \mathrm{e}^{v_{\mathrm{LR}}(t-\tau_2)} f(d_{jl}) \|\mathbf{D}_{lk}(\tau_2)\| . \tag{7.38}$$

Let us now iterate this recurrent expression, which leads us to

$$\begin{aligned} \|\mathbf{D}_{jk}(t)\| \leq & \|\mathbf{D}_{jk}(0)\| + \frac{\chi}{v_{\mathrm{LR}}} \sum_l \int_0^t \mathrm{d}\tau_2 e^{v_{\mathrm{LR}}(t-\tau_2)} f(d_{jl}) \|\mathbf{D}_{lk}(0)\| + \\ & + \left(\frac{\chi}{v_{\mathrm{LR}}}\right)^2 \sum_{l,l'} \int_0^t \mathrm{d}\tau_2 \int_0^{\tau_2} \mathrm{d}\tau_3 e^{v_{\mathrm{LR}}(t-\tau_3)} f(d_{jl}) f(d_{ll'}) \|\mathbf{D}_{l'k}(\tau_3)\| . \end{aligned} \tag{7.39}$$

We now use the relation $\sum_l f(d_{jl}) f(d_{ll'}) \leq a_0 f(d_{jl'})$ and we get

$$\begin{aligned} \|\mathbf{D}_{jk}(t)\| \leq & \|\mathbf{D}_{jk}(0)\| + \left(\frac{\chi a_0}{v_{\mathrm{LR}}}\right) \sum_l \int_0^t \mathrm{d}\tau_2 e^{v_{\mathrm{LR}}(t-\tau_2)} \frac{1}{a_0} f(d_{jl}) \|\mathbf{D}_{lk}(0)\| + \\ & + \left(\frac{\chi a_0}{v_{\mathrm{LR}}}\right)^2 \sum_{l'} \int_0^t \mathrm{d}\tau_2 \int_0^{\tau_2} \mathrm{d}\tau_3 e^{v_{\mathrm{LR}}(t-\tau_3)} \frac{1}{a_0} f(d_{jl'}) \|\mathbf{D}_{l'k}(\tau_3)\| . \end{aligned} \tag{7.40}$$

It is possible to iterate the above expression for $j \neq k$, using the equality $\|\mathbf{D}_{jk}(0)\| = 2\|\mathbf{S}_j\| \left\|S_k^\phi\right\| \delta_{jk}$, together with $\|\mathbf{S}_j\| = \|\mathbf{S}_k\|$ and $j \neq k$ which implies $\|\mathbf{D}_{jk}(0)\| = 0$. As an example, the first three steps read

$$\begin{aligned} \|\mathbf{D}_{jk}(t)\| &\leq \|\mathbf{D}_{jk}(0)\| + \left(\frac{\chi a_0}{v_{\mathrm{LR}}}\right) \sum_l \int_0^t \mathrm{d}\tau_2 \frac{e^{v_{\mathrm{LR}}(t-\tau_2)} f(d_{jl})}{a_0} \|\mathbf{D}_{lk}(0)\| \\ &+ \left(\frac{\chi a_0}{v_{\mathrm{LR}}}\right)^2 \sum_{l'} \int_0^t \mathrm{d}\tau_2 \int_0^{\tau_2} \mathrm{d}\tau_3 \frac{e^{v_{\mathrm{LR}}(t-\tau_3)} f(d_{jl'})}{a_0} \|\mathbf{D}_{l'k}(\tau_3)\| \\ &\leq 2\|\mathbf{S}_j\| \left\|S_k^\phi\right\| \left(\frac{\chi a_0}{v_{\mathrm{LR}}}\right) \frac{f(d_{jk})}{a_0} \int_0^t e^{v_{\mathrm{LR}}(t-\tau_2)} \mathrm{d}\tau_2 \\ &+ \left(\frac{\chi a_0}{v_{\mathrm{LR}}}\right)^2 \sum_{l'} \int_0^t \mathrm{d}\tau_2 \int_0^{\tau_2} \mathrm{d}\tau_3 \frac{e^{v_{\mathrm{LR}}(t-\tau_3)} f(d_{jl'})}{a_0} \|\mathbf{D}_{l'k}(0)\| \\ &+ \left(\frac{\chi a_0}{v_{\mathrm{LR}}}\right)^3 \sum_{l',l''} \int_0^t \mathrm{d}\tau_2 \int_0^{\tau_2} \mathrm{d}\tau_3 \int_0^{\tau_3} \mathrm{d}\tau_4 \frac{e^{v_{\mathrm{LR}}(t-\tau_4)} f(d_{jl''})}{a_0} \|\mathbf{D}_{l''k}(\tau_4)\| \\ &\leq 2\|\mathbf{S}_j\| \left\|S_k^\phi\right\| \left(\frac{\chi a_0}{v_{\mathrm{LR}}}\right) \frac{f(d_{jk})}{a_0} \int_0^t e^{v_{\mathrm{LR}}(t-\tau_2)} \mathrm{d}\tau_2 \\ &+ 2\|\mathbf{S}_j\| \left\|S_k^\phi\right\| \left(\frac{\chi a_0}{v_{\mathrm{LR}}}\right)^2 \frac{f(d_{jk})}{a_0} \int_0^t \mathrm{d}\tau_2 \int_0^{\tau_2} \mathrm{d}\tau_3 e^{v_{\mathrm{LR}}(t-\tau_3)} \\ &+ \left(\frac{\chi a_0}{v_{\mathrm{LR}}}\right)^3 \sum_{l''} \int_0^t \mathrm{d}\tau_2 \int_0^{\tau_2} \mathrm{d}\tau_3 \int_0^{\tau_3} \mathrm{d}\tau_4 \frac{e^{v_{\mathrm{LR}}(t-\tau_4)} f(d_{jl''})}{a_0} \|\mathbf{D}_{l''k}(\tau_4)\| \end{aligned}$$

The total sum up to infinite order reads

$$\|\mathbf{D}_{jk}(t)\| \leq \sum_{n=1}^{\infty} 2\,\|\mathbf{S}_j\|\,\left\|S_k^{\phi}\right\|\left(\frac{\chi a_0}{v_{\mathrm{LR}}}\right)^n \frac{\mathrm{e}^{-\mu d_{jk}} f(d_{jk})}{a_0} T_n(j,k), \tag{7.41}$$

with

$$T_n = \int_0^t \mathrm{d}\tau_1 \int_0^{\tau_1} \mathrm{d}\tau_2 \cdots \int_0^{\tau_{n-1}} \mathrm{d}\tau_n\, e^{v_{\mathrm{LR}}(t-\tau_n)} \leq e^{v_{\mathrm{LR}}t} \int_0^t \mathrm{d}\tau_1 \int_0^{\tau_1} \mathrm{d}\tau_2 \cdots \int_0^{\tau_{n-1}} \mathrm{d}\tau_n \tag{7.42}$$

By direct integration, we find that $T_n \leq e^{v_{\mathrm{LR}}t}\frac{t^n}{n!}$ which results in

$$\|\mathbf{D}_{jk}(t)\| \leq \sum_{n=1}^{\infty} 2\,\|\mathbf{S}_j\|\,\left\|S_k^{\phi}\right\|\left(\frac{\chi a_0 t}{v_{\mathrm{LR}}}\right)^n \frac{1}{n!}\frac{\mathrm{e}^{v_{\mathrm{LR}}t}}{a_0} f(d_{jk}). \tag{7.43}$$

The previous series can be summed up to infinite order yielding the desired Lieb-Robinson bound (7.6) for the spin-boson lattice model

$$\|\mathbf{Z}_{j,k}(t)\| = \|\mathbf{D}_{j,k}(t)\| \leq 2\,\|\mathbf{S}_j\|\,\left\|S_k^{\phi}\right\| \frac{e^{v_{\mathrm{LR}}t} f(d_{jk})}{a_0}\left(\mathrm{e}^{\frac{\chi a_0}{v_{\mathrm{LR}}}t} - 1\right), \quad \chi = 2g^2 S\alpha. \tag{7.44}$$

Interestingly, we find that the LRB for this composite system contains two contributions. On the one hand, the first exponential gives the maximum propagation speed for the bosons. Since the spin correlations are built by the exchange of bosons, it is natural that the speed of propagation of spin perturbations has an upper bound given by the speed of propagation of the carriers. On the other hand, the second exponential determines the efficiency with which distant spins can excite and reabsorb a propagating boson. Accordingly, this process should be proportional to g, the maximum spin-boson coupling strength. Moreover, if the bosons travel much faster than the time-scale related to such a spin-boson coupling, an adiabatic-type argument tells us that the efficiency of excitation/reabsorption of bosons by distant spins should be reduced. Therefore, we can expect that, in addition, the process should also be proportional to g/v_{LR}. These arguments based on a physical reasoning are confirmed by the rigorous LRB, as we have found that the argument of the second exponential is $\chi a_0/v_{\mathrm{LR}} \propto g^2/v_{\mathrm{LR}}$.

7.5 Proof of the theorem

We may use the previous results to prove the main result 7.1:

Proof. The Heisenberg equations of motion are $\dot{\mathbf{R}}_j = -\sum_k JQ_{jk}(t)\mathbf{R}_k - JG_j(t)\mathbf{S}_j$ and $\dot{\mathbf{S}}_j = \mathrm{i}K_j(t)\mathbf{S}_j$, with a Hermitian matrix $K_j(t)$ that depends on the couplings,

boson operators, and spin structure constants. The first equation is formally integrated

$$\mathbf{R}_j(t) = \sum_k W_{jk}(t,0)\mathbf{R}_k(0) - \int_0^t \mathrm{d}\tau \sum_k W_{jk}(t,\tau) J G_k(\tau)\mathbf{S}_k(\tau)$$

In this notation, the free boson propagator W is an $N \times N$ block matrix, where each block $W_{jk}(t_1,t_2) \in \mathbb{R}^{2\times 2}$ spreads correlations between sites j and k.

The bosonic bound (7.8) influences the spin-spin correlations through the spin-boson correlators

$$\mathbf{C}_{jk}(t) := [\mathbf{R}_j(t), S_k^{\phi}(0)]$$

This is seen in $\dot{\mathbf{Z}}_{jk} = i\sum_{n\in\{x,p\}} C_{jk}^n A_j^n(t)\mathbf{S}_j + \mathrm{i}K_j(t)\mathbf{Z}_{jk}$, where the matrices $A_j^n(t)$ are defined in terms of the spin-boson couplings. To eliminate the local precession of the spins, we change variables $\mathbf{D}_{jk}(t) := O_j^{-1}(t)\mathbf{Z}_{jk}(t)$ with a unitary $O_j(t)$ obtained by solving $\dot{O}_j(t) = iK_j(t)O_j(t)$. Thus,

$$\dot{\mathbf{C}}_{jk} = -\sum_l JQ_{jl}(t)\mathbf{C}_{lk} - JG_j(t)O_j(t)\mathbf{D}_{jk}, \tag{7.45}$$

$$\dot{\mathbf{D}}_{jk} = iO_j^{-1}(t)\sum_n C_{jk}^n\, A_j^n(t)\mathbf{S}_j \tag{7.46}$$

describe the buildup of spin-boson correlations (7.45) and the conversion of spin-boson into spin-spin correlations (7.46). Some remarks are in order: (i) the equation for $\mathbf{C}_{jk}$ is solved formally in terms of $\mathbf{D}_{jk}$, creating a recursion; (ii) the operator O_i absorbing the unbounded local rotations does not influence the LRB because (iii) $\mathbf{D}_{jk}$ and $\mathbf{Z}_{jk}$ have the same operator norms.

Equations (7.45) and (7.46), with the upper bounds $\|G_j(t)\|, \|A_j^n(t)\| \le g$, $\|\mathbf{S}_j(t)\| \le S$, the bosonic LRB (7.8), and the geometric factor a_0, provide a Dyson-type recursion for the commutators norms

$$\begin{aligned}\|\mathbf{D}_{jk}(t)\| \le \|\mathbf{D}_{jk}(0)\| + \\ + 2g^2 S\alpha \sum_l \int_0^t d\tau_1 \int_0^{\tau_1} d\tau_2 f(d_{jl}, v_{\mathrm{LR}}(\tau_1-\tau_2))\|\mathbf{D}_{lk}(\tau_2)\|.\end{aligned} \tag{7.47}$$

After summing this recursion to infinite order, the desired LRB (7.10) for the spin-boson lattice is recovered. □

7.6 Conclusions and outlook

In this chapter, we have derived new Lieb-Robinson bounds for a general model of finite dimensional systems interacting through a bosonic field that satisfies a Lieb-Robinson bound itself. These bounds apply to all spin-boson lattice models of any dimensionality and geometry realized with state-of-the-art technology. To continue with this line of work, we would like to study further theoretical implications of these bounds, such as the efficiency of time-dependent density matrix renormalization group methods or the clustering of correlations, which might be of interest to recent studies [PISK12].

On the other hand, a fruitful generalization of this work would be to extend these bounds to the continuous limit of the lattice and to prove whether the light cone implied by the Lieb-Robinson bound in the continuous is exacty the expected limit of the light cone obtained in the discrete case. This would allow us to address the propagation of quantum correlations in quantum field theories that are the uniform limit of discrete models of bosons interacting with fermions. Such models and limits are often affected by infrared and ultraviolet divergences and we would like to show that such divergences do not affect the propagation of correlations and that we can define the corresponding light cone of the system.

We would also like to explore a further generalization of the Lieb-Robinson bounds using a physically motivated route that is complementary to other generalizations [HK06, NOS06, CSE08, NRSS09, Pou10, PSHKMK09] and which could apply to many interesting models. A further generalization of Lieb-Robinson bounds could rely on the fact that even for many infinite-dimensional problems for which the existing bounds do not apply, we may still define finite temperature states. This notion of temperature restricts the size of the region explored by the system to the ground state manifold and its surroundings, and it is itself a measure of which operators are reasonable, namely all those whose expectation values can be computed in practice. We would like to exploit this idea to obtain an extension of Lieb-Robinson bounds which could apply to physical systems of interest, such as the Bose-Hubbard Hamiltonian [GK63].

8 Lieb-Robinson bounds in trapped-ion crystals

8.1 Introduction

Correlation spread after quantum quenches is a growing area of active theoretical and experimental research [RGL+14, NOS06, HT13, CBP+12]. In this context, Lieb-Robinson bounds [LR72, NS10a] are a fundamental tool to prove whether there is a finite velocity of the propagation of information in a quantum many-body system. While they were initially conceived to prove the finite group velocity of spin systems [LR72], they have been extended to other physical settings such as the spin-boson Hamiltonian that we presented in Chapter 7.

The first experimental test of Lieb-Robinson bounds was achieved by Cheneau et al [CBP+12], by quenching a quantum gas in a one-dimensional optical lattice. This proved that the spread of correlations by quasiparticle pairs displays a finite velocity, which gives rise to an effective light cone for the dynamics. After this, several experimental proposals have been put forward to obtain the Lieb-Robinson velocity in different systems.

In this chapter, we argue that the results we obtained in Chapter 7 are of quantitative importance for crystals of trapped ions, a system in the field of quantum optics that has been proved to be a prominent architecture for quantum information [HRB08] and which offers a playground where our ideas can be tested experimentally. We provide a detailed description of the applicability of the Lieb-Robinson bound for spin-boson lattice models in a trapped-ion system. Afterwards, we analyze these bounds and find that the propagation of spin correlations, as mediated by the phonons of the ion crystal, can be faster than the regimes currently explored in experiments. We then propose a scheme to test the bounds by measuring retarded correlation functions via the crystal fluorescence.

8.2 Lieb-Robinson bounds for spin correlations in trapped-ion crystals

In the previous chapter, we proved that for the spin-boson Hamiltonian, $H_{\mathsf{SBL}}(t) = \frac{1}{2}\sum_{i,j}\mathbf{R}_i^T Q_{ij}(t)\mathbf{R}_j + \sum_i \mathbf{B}_i(t)^T\cdot\mathbf{S}_i + \sum_i \mathbf{R}_i^T\cdot G_i(t)\cdot\mathbf{S}_i$ (see Chapter 7) and given the assumptions and notation of Theorem 7.1, there is a Lieb Robinson bound for the spin correlations $\mathbf{Z}_{jk}(t) := [\mathbf{S}_j(t), S_k^{\phi}(0)]$, $\phi\in\{1,2,3\}$ given by (7.10)

$$\|\mathbf{Z}_{jk}(t)\| \leq \alpha\, e^{\nu_{\mathrm{LR}}t} f(d_{jk}) \times \frac{2S^2}{a_0}\left(\mathrm{e}^{(g^2/v_{\mathrm{LR}})2S\alpha a_0 t} - 1\right). \tag{8.1}$$

In this section, we provide a detailed description of the applicability of the Lieb-Robinson bound (LRB) for spin-boson lattice models in a trapped-ion system [HRB08].

Spin-boson lattice models with crystals of trapped ions

The spin boson model of Eq. (7.3) can be implemented on top of state-of-the-art technology, such as laser-cooled ions in radio-frequency or Penning traps [HRB08]. In order to do so, we consider a collection of N atomic ions of mass m, and charge e, confined in either *(i)* a linear Paul trap (see Figure 8.1), *(ii)* a Penning trap (see Figure 8.2), or *(iii)* a micro-fabricated surface trap (see [WL11]). For low-enough temperatures, the ions crystallise forming either *(i)* a one-dimensional chain, a *(ii)* triangular lattice in the rotating laboratory frame, or *(iii)* any desired two-dimensional lattice. The equilibrium positions of the ions are labelled, $\mathbf{r}_i^0$ for $i\in\{1,\ldots,N\}$, and correspond to the physical realization of the set of vertices L of the graph G (see Fig. 7.1). As we will see below, because of long-range interactions, the set of edges E is determined by all the possible links for each lattice.

The physical degrees of freedom of each vertex $i\in L$ correspond to the small transverse vibrations of the ions around the equilibrium positions (i.e. bosons), defined in $\mathcal{L}^2(\mathbb{R})$, and to a pair of internal levels of the atomic level structure (i.e. pseudospins), defined in $\mathcal{H}_i = \mathbb{C}^2$.

Bosonic degrees of freedom

The small transverse vibrations will be denoted as $\delta r_{i,\mathrm{t}}$. They correspond to *(i)* one of the two directions perpendicular to the axis of the linear Paul trap, or to *(ii)-(iii)* the direction perpendicular to the crystal plane in the Penning or surface traps. For any of these configurations, the transverse vibrations decouple from the remaining vibrations of the ion crystal, and can be thus described by

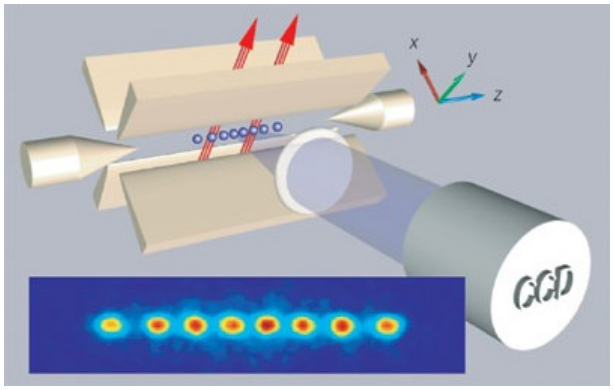

Figure 8.1: Scheme of a Paul ion trap containing 40 Ca+ ions which are arranged in a string (depicted in blue). The ions are cooled using laser beams (depicted in red). Afterwards, the ions are imaged using a charge-coupled device (labelled as CCD in the picture). (Source: [BW08]).

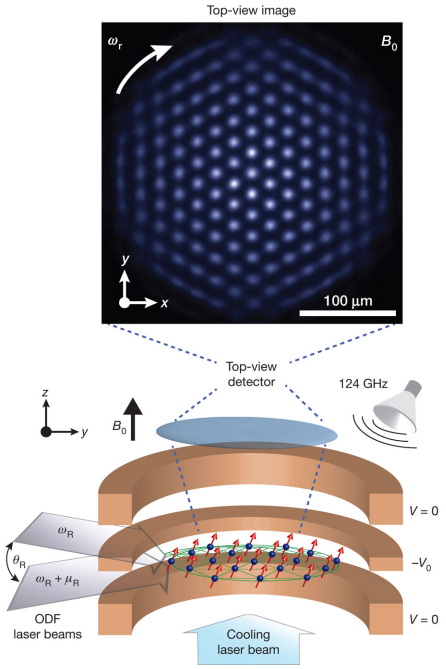

Figure 8.2: Scheme of a Penning ion trap, which confines ions in three dimensions using a combination of a weak electrostatic electric and a strong homogeneous magnetic field. (Source: [BSK+12])

the same harmonic Hamiltonian, namely

$$H_{\mathrm{b}} = \sum_i \left(\frac{p_{i,\mathrm{t}}^2}{2m} + \frac{m}{2}\omega_{\mathrm{t}}^2 \delta r_{i,\mathrm{t}}^2 \right) + \frac{1}{2}\sum_{i,j} \mathbb{V}_{ij}\delta r_{i,\mathrm{t}}\delta r_{j,\mathrm{t}}. \tag{8.2}$$

Here, the couplings between distant ions are obtained by expanding the Coulomb potential to second order in the small transverse displacements, which leads to $\mathbb{V}_{ij} = e_0^2/|\mathbf{r}_i^0 - \mathbf{r}_j^0|^3$ for $i \neq j$, and $\mathbb{V}_{ii} = -\sum_{j\neq i}\mathbb{V}_{ij}$, where $e_0^2 = e^2/4\pi\epsilon_0$. Note also that the origin of the trap frequency ω_{t} shall depend on the particular trap (i.e. for *(i)-(iii)* ω_{t} is proportional to the r.f. frequency, whereas for *(ii)* it is proportional to the d.c. potential). By rescaling the position and momentum operators, $x_i = \sqrt{m\omega_{\mathrm{t}}}\delta r_{i,\mathrm{t}}$ and $p_i = p_{i,\mathrm{t}}/\sqrt{m\omega_{\mathrm{t}}}$, we can define the bosonic operators $\mathbf{R}_i^T = (x_i, p_i)$ with the commutation relations in Eq. (7.1). Moreover, the Hamiltonian for the transverse vibrations (8.2) can be rewritten as

$$H_{\mathrm{b}} = \frac{1}{2}\sum_{i,j} \mathbf{R}_i^T \cdot Q_{ij} \cdot \mathbf{R}_j, \quad Q_{ij} = \begin{pmatrix} \omega_{\mathrm{t}}\delta_{ij} + \frac{\mathbb{V}_{ij}}{m\omega_{\mathrm{t}}} & 0 \\ 0 & \omega_{\mathrm{t}}\delta_{ij} \end{pmatrix}, \tag{8.3}$$

which yields a transparent realization of the free bosonic part (7.3). It is also worth pointing out that the trap frequencies could be modified dynamically in the experiment to study e.g. quenches, leading to a time-dependent $Q_{ij}(t)$ also captured by our LRB.

Spin degrees of freedom

Let us now turn into the spin degrees of freedom, which correspond to a pair of atomic levels $\{|\uparrow_i\rangle, |\downarrow_i\rangle\}$ with a sufficiently long coherence time. For the sake of concreteness, we select two states from the hyperfine ground-state manifold of a certain ion (e.g. $^9\mathrm{Be}^+$ or $^{25}\mathrm{Mg}^+$), although we emphasise that the LRB would equally apply to optical or Zeeman spins (e.g. $^{40}\mathrm{Ca}^+$ or $^{88}\mathrm{Sr}^+$). By defining the Pauli matrices $\sigma_i^x = |\uparrow_i\rangle\langle\downarrow_i| + \mathrm{H.c.}$, $\sigma_i^y = -\mathrm{i}\,|\uparrow_i\rangle\langle\downarrow_i| + \mathrm{H.c.}$, and $\sigma_i^z = |\uparrow_i\rangle\langle\uparrow_i| - |\downarrow_i\rangle\langle\downarrow_i|$, it follows directly that the desired commutation relations (7.2) are fulfilled. We define ω_0 as the transition frequency between the two atomic states, and use electromagnetic radiation (e.g. a Raman configuration with two co-propagating laser beams, or a single microwave in a traveling-wave configuration), such that its frequency fulfills $\nu \approx \omega_0$, and $|\nu - \omega_0| \ll \omega_0$. Then, the light-matter interaction reads as follows

$$H_{\mathrm{s}} = \sum_i \mathbf{B}_i^T(t)\cdot\sigma_i, \qquad B_i^x(t) = \Omega\cos(\nu t - \varphi),\ B_i^y(t) = \Omega\sin(\nu t - \varphi),\ B_i^z(t) = \frac{\omega_0}{2}, \tag{8.4}$$

where $\sigma_i = (\sigma_i^x, \sigma_i^y, \sigma_i^z)^T$. Here, $\Omega \in \mathbb{R}$ is the Rabi frequency of the transition [SZ97], and φ depends on the phases of the electromagnetic wave and the atomic dipole element. The above expression corresponds to the free spin part of Eq. (7.3).

Spin-boson coupling

The only missing ingredient of the target lattice Hamiltonian (7.3) is the spin-boson coupling. This requires a light-matter interaction that couples the internal states of the ions to the transverse vibrations, which can be achieved via the so-called state-dependent dipole forces. Such forces are nowadays routinely used for quantum-information processing in the trapped-ion community. When we encode the pseudospin in the hyperfine states of an ion, we can use the gradient of either a travelling wave in a Raman configuration with non-co-propagating lasers [SM10], or an oscillating magnetic field in the near-field of a microwave source [OLA$^+$08, OWC$^+$11], to obtain

$$H_{\mathrm{sb}} = \sum_i g x_i \sigma_i^z \sin(\tilde{\nu} t - \tilde{\varphi}). \tag{8.5}$$

In this expression, $g = \sqrt{2}\tilde{\Omega}\gamma$ is the coupling strength between the ion and the propagating wave of light, γ is the Lamb-Dicke parameter and $\tilde{\Omega}$ is the crossed-beam ac-Stark shift that originates from the Raman laser beams, or an ac-Zeeman shift in the near-field of an oscillating microwave source. This coupling is what we refer to as "the force" and it has the units of frequency since the rescaled position operator is dimensionless and $\hbar = 1$. We have also introduced the so-called Lamb-Dicke parameter $\gamma \ll 1$, which depends on the gradient of the modulation of the electric (magnetic) field of the laser (microwave) at the position of the ion, and the zero-point motion of the ions. In order to get such state-dependent force, we have to consider that $\tilde{\nu} \approx \omega_{\mathrm{t}}$, such that $|\tilde{\nu} - \omega_{\mathrm{t}}| \ll \omega_{\mathrm{t}}$ and $|\tilde{\Omega}| \ll \omega_{\mathrm{t}}$, in order to make the gradient of the light-matter interaction dominant, which leads to Eq. (8.5) as opposed to the case in Eq. (8.4). We can rewrite the state-dependent forces using the notation in Eq. (7.3) as follows

$$H_{\mathrm{sb}} = \sum_i \mathbf{R}_i^T \cdot G_i(t) \cdot \sigma_i, \quad G_i(t) = \begin{pmatrix} 0 & 0 & g\sin(\tilde{\nu} t - \tilde{\varphi}) \\ 0 & 0 & 0 \end{pmatrix}, \tag{8.6}$$

Note how this yields a transparent realisation of the spin-boson coupling of Eq. (7.3) while Eqs. (8.3),(8.4), and (8.6) provide the remaining ingredients for the trapped-ion realization of the full spin-boson lattice model

$$H_{\mathsf{SBL}}(t) = H_{\mathrm{b}} + H_{\mathrm{s}} + H_{\mathrm{sb}}. \tag{8.7}$$

As the form of the trapped-ion Hamiltonian $H_{\mathsf{SBL}}(t)$ coincides exactly with the general model in Eq. (7.3), we can use directly the LRB derived in the previous sections. This will allow us to estimate the maximum speed at which spin correlations can build up in a trapped-ion experiment. Before closing this section, let us remark once more that the spin-boson dynamics of all these ion crystals in the different traps (i.e. linear Paul trap, Penning trap, or surface trap) is described

by the same Hamiltonian. Therefore, the LRB may find a broad application in a variety of ion-trap setups. We should also point out that, although the state-dependent force (8.5) corresponds to the so-called σ^z-force, other configurations lead to state-dependent forces in the σ^x-, or σ^y-bases [SM10]. Note that our LRB would apply equally to any of these cases.

Lieb-Robinson bounds for non-perturbative spin-boson models

In this section, we evaluate the LRB for the trapped-ion spin-boson lattice model (7.10), obtaining a power-law behavior (7.11).

We start by considering the bosonic part of the evolution. The phonon coupling $Q_{ij} = \mathrm{diag}\{\omega_{\mathrm{t}}\delta_{i,j} + \mathbb{V}_{ij}(m\omega_{\mathrm{t}})^{-1},\ \omega_{\mathrm{t}}\delta_{i,j}\}$ contains the ions' mass m, the transverse trap frequency ω_t, and a dipolar interaction. The following upper bound holds

$$\|Q_{ij}\|_\infty \leq \frac{8\beta\omega_{\mathrm{t}}}{(1+d_{ij})^3},\ \forall i \neq j \tag{8.8}$$

The off-diagonal couplings thus satisfy Eq. (7.12) with algebraic decay $\eta = 3$, where d_{ij} is the Euclidean distance between two vertices $i, j \in L$ of a perfect Bravais lattice, which has unit primitive vectors, and shares the geometry with the ion crystal (i.e. note that ion crystals are usually characterised by an inhomogeneous lattice spacing). The interaction strength $\kappa = 4\beta\omega_t$ is defined in terms of the stiffness parameter [PC04], $\beta = e^2/4\pi\epsilon_0 m\omega_t^2 d_m^3$, which measures the ratio of the Coulomb repulsion to the trapping energy and depends on the minimal separation between two ions in the crystal, $d_{\mathrm{m}} = \min_{i,j}\{|\mathbf{r}_i^0 - \mathbf{r}_j^0|\}$. We note that $\beta \ll 1$ for the setups considered in this chapter, which corresponds to a tight transverse confinement.

Introducing the maximum force $g = \max_t |F_z(t)|$ and considering the supremum norms

$$\|G_i(t)\|_\infty \leq g, \quad \|\sigma_i\|_\infty \leq S = 1\ \forall i \neq j. \tag{8.9}$$

then the LRB for the spin-boson lattice model in an ion crystal is given by

$$\left\|[\sigma_i(t), \sigma_j^\phi(0)]\right\|_\infty \leq \frac{2}{a_0(1+d_{ij})^3} \mathrm{e}^{8a_0(\beta\omega_{\mathrm{t}})t}\left(e^{\alpha\left(\frac{g}{\beta\omega_{\mathrm{t}}}\right)^2(\beta\omega_{\mathrm{t}})t} - 1\right), \tag{8.10}$$

$$\alpha = \frac{1}{4}\left(\frac{1+a_0}{a_0}\right), \tag{8.11}$$

where $\beta\omega_{\mathrm{t}}$ is the typical order of magnitude for the tunneling of vibrational excitations between neighbouring ions. Therefore, the LR speed for the bosons is related to this tunneling, which is in fact the underlying mechanism responsible for the spread of correlations in both the free bosonic system, and the spin-boson

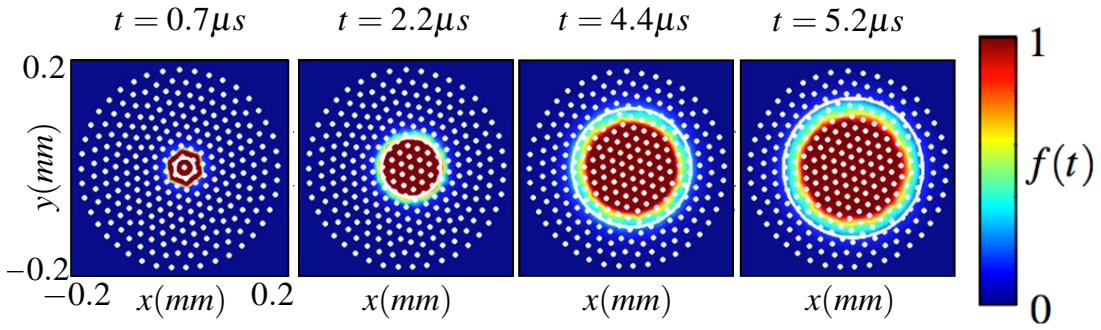

Figure 8.3: **Spin correlation spread in the impulsive regime.** In this regime, we evaluate numerically the bound $\|[\sigma_i^x(t), \sigma_j^x(0)]\|_\infty \leq f(t)$, where $f(t) = \max_{\tau \leq t}\{8|\sin(W_{ij}^{xp}(\tau, 0))|\} \times \theta_i\theta_j$ is obtained from the exact time-evolution of the impulsive regime. We consider a crystal of $N = 253$ $^9Be^+$ ions [BSK+12], assuming pulse areas of $\theta_l = 1$. The white circle corresponds to a wavefront advancing at a speed of $3d_m\beta\omega_t$.

model. However, if we do not allow for a time that is sufficiently long such that bosons can be exchanged between the spins (i.e. $t > (g^2/\beta\omega_t)^{-1}$), no correlations can build up regardless of how fast the vibrational excitations propagate (i.e. the term between brackets makes the correlations negligible, see Fig. 8.4 **(a)**). As anticipated in the proof, the LRB depends fundamentally on the maximum group velocity of the phonon branch, given by $\beta\omega_t$, and on the efficiency of the force in exciting and absorbing a propagating phonon, $(g^2/\beta\omega_t)$.

Let us now evaluate evaluate the LRB by considering realistic parameters for the different ion crystals of interest. First of all, we need to obtain the constant a_0, which is defined through the following bound of the convolution $\sum_l (1 + d_{il})^{-3}(1 + d_{lj})^{-3} \leq a_0(1 + d_{ij})^{-3}$, $\forall\, i, j \in L$. Alternatively, we can define

$$a_0 = \max_{i,j}\left\{\sum_{l\in L} \frac{(1 + d_{il})^{-3}(1 + d_{lj})^{-3}}{(1 + d_{ij})^{-3}}\right\}, \tag{8.12}$$

a maximisation problem that will be solved for the crystals of interest.

Ion chain in a linear Paul trap

In this case, the perfect Bravais lattice associated to the inhomogeneous ion chain is spanned by $\mathbf{a}_1 = \mathbf{e}_z$, such that $\tilde{\mathbf{r}}_i^0 = i\mathbf{a}_1$, where $i \in \mathbb{Z}$. Hence, the Euclidean distance is simply $d_{ij} = |i - j|$, and we can maximise the above expression (8.12) numerically to find that $a_0 = 2.9$. Let us note that this constant differs from the generic estimate [CSE08] based on the graph distance $\tilde{a}_0 = c_1 2^4 \zeta(3) = 38.5$ by an order of magnitude, a fact that will make our LRB much tighter.

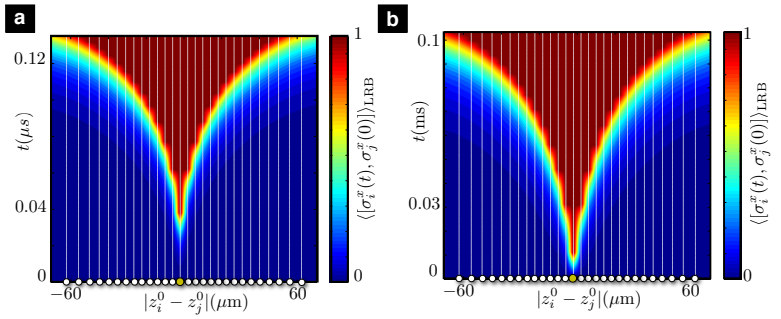

Figure 8.4: **LRB for the spin correlations in an ion chain: (a)** Evaluation of the spin-boson LRB in Eq. (8.11) for a linear chain with $N = 30$ $^{25}\text{Mg}^+$ ions in a linear Paul trap (see the text for the specific parameters). The spin excitation initially localised at the middle of the chain, $j = N/2$, propagates towards the edges giving rise to a quasi-LR cone. We also observe that the cone requires a finite time to arise, which corresponds to the required time to create/annihilate bosons at distant sites. **(b)** Evaluation of the spin LRB in Eq. (8.19) for a linear chain with $N = 30$ $^{25}\text{Mg}^+$ ions in a linear Paul trap (see the text for the specific parameters). We observe an analogous quasi-LR cone, where one must appreciate the very different time-scale of correlation spread as compared to the spin-boson LRB in Eq. (8.11) displayed in **(a)**.

We now consider realistic parameters at reach of current ion-trap experiments. We consider $^{25}\text{Mg}^+$ ions in a linear Paul trap with frequencies $\omega_{\text{ax}}/2\pi = 0.25\,\text{MHz}$, and $\omega_{\text{t}}/2\pi = 5\,\text{MHz}$ (see e.g. [FSG+08]). This trap confines $N = 30$ ions forming a linear chain of length $\ell \approx 140\,\mu\text{m}$, such that the minimum ion distance occurs at the centre of the trap $d_{\text{m}} \approx 4\,\mu\text{m}$, and the tunneling rate of vibrational excitations is $\beta\omega_{\text{t}}/2\pi \approx 450\,\text{kHz}$. Finally, we need to estimate the value of the state-dependent force, $g = \sqrt{2}\tilde{\Omega}\gamma$. Considering that $\gamma \approx 0.14$, and that $|\tilde{\Omega}| \ll \omega_{\text{t}}$, it seems reasonable to consider that the force can be pushed towards $g/2\pi = 100\,\text{kHz}$. In this regime, we find that the LRB (8.11) corresponds to the spin correlation spread displayed in Fig. 8.4 **(a)**. Due to the long range of the vibrational couplings, instead of a perfect Lieb-Robinson cone, we recover a quasi-LR-cone. In any case, it is clear that there is a maximum propagation speed for spin correlations in such a spin-boson medium, and distant spins require a certain minimal time after which correlations can start building up. It is important to note that the timescale of correlation propagation of the LRB is in the μs range even for long chains of $N = 30$, a timescale that is short enough such that other sources of noise (e.g. magnetic-field noise or heating) can be safely neglected.

Although we have considered the particular case of $^{25}\text{Mg}^+$ ion chains, we emphasise that similar experiments can be carried out with other ion species. In fact, linear chains with up to $N = 6$ ions of $^{40}\text{Ca}^+$ [LHN+11], and $N = 3$ [KPS+12]

or $N = 16$ [ISC+13] ions of $^{171}Yb^+$ have already been used in experiments for digital and analog quantum simulations of transverse Ising models. These models arise from spin-boson Hamiltonians equivalent to Eq. (8.7), in a certain regime where the boson can be traced out (see Sect. 8.2). Therefore, in order to test the bound displayed in Fig. 8.4 **(a)**, one would need to consider larger ion chains, and non-perturbative regimes where the ion crystal forms a spin-boson medium.

Triangular lattice in a Penning or surface trap

In this case, the equivalent Bravais lattice is spanned by $\mathbf{a}_1 = \mathbf{e}_x$, and $\mathbf{a}_2 = \mathbf{e}_x/2 + \sqrt{3}\mathbf{e}_y/2$, such that $\tilde{\mathbf{r}}^0_{\mathbf{i}} = i_1\mathbf{a}_1 + i_2\mathbf{a}_2$ and $\mathbf{i} = (i_1, i_2) \in \mathbb{Z} \times \mathbb{Z}$. By maximising (8.12) with the Euclidean distance $d_{\mathbf{ij}} = |\tilde{\mathbf{r}}^0_{\mathbf{i}} - \tilde{\mathbf{r}}^0_{\mathbf{j}}|$, we find $a_0 = 8.5$. Once again, the estimate based on the graph distance would give give $\tilde{a}_0 = c_2 2^4 \zeta(4) = 103.9$ overestimating the LR speed by one order of magnitude. A more accurate approach is to use the bound (7.8) to fit the numerical evolution of the bosonic lattice model. This leads to $a_0 \approx 3/8$, a tighter bound that accounts for the finite size of the lattice and the non-uniformity of the Coulomb crystal.

These ions, confined with a transverse trap frequency of $\omega_t/2\pi \approx 0.8\,\mathrm{MHz}$, form a triangular crystal of $N \sim$100-300 lattice sites characterized by a minimal distance $d_m \sim 20\,\mu\mathrm{m}$. In such experiments, the maximum phonon group velocity is currently $\beta\omega_t/2\pi \approx 60\,\mathrm{kHz}$, and oscillating state-dependent forces with $g/2\pi \approx 0.6\,\mathrm{kHz}$ have been obtained from two non-copropagating laser beams in a Raman configuration.

Let us now specify the remaining parameters to evaluate the LRB. We start by considering the experimental values for a $^9Be^+$ crystal in a Penning trap [BSK+12], where the transverse trap frequency is $\omega_\mathrm{t}/2\pi \sim 0.8\,\mathrm{MHz}$, and the ions form a triangular crystal of $N \sim$100-300 lattice sites characterized by a minimal distance $d_m \sim 20\,\mu\mathrm{m}$. For these parameters, we can estimate that the tunneling of transverse vibrational excitations is on the order of $\beta\omega_\mathrm{t}/2\pi \approx 60\,\mathrm{kHz}$. As a direct consequence of the larger inter-ion spacing d_m, this tunneling is much smaller than in linear Paul traps. However, since there are more neighbours in the triangular lattice (i.e. the value of a_0 is bigger than for linear chains), the LR speed of propagation of spin correlations will not be much slower than the one found for linear Paul traps. Let us now address the strength of the state-dependent dipole force. In the experiment [BSK+12], these forces are obtained from the gradient of a moving optical lattice formed by a couple of non-copropagating laser beams in a Raman configuration. For the incident angles of these beams allowed by the experimental apparatus [BSK+12], these forces correspond to $g/2\pi \approx 0.6\,\mathrm{kHz}$. By evaluating the LRB in Eq. (8.11), we find that the correlations can spread over a whole crystal of $N \sim$ 100-300 ions in a minimum time-scale of 1μs (see Fig. 8.5). In particular, the spins in a crystal of $N \approx 200$ ions can get correlated in timescales of $10\,\mu$s, an amount of time significantly shorter than ex-

perimental sources of decoherence, such as photon-scattering decoherence rates $\sim 10\,\mathrm{ms}$ [BSK$^+$12]. A clear advantage of Penning traps is that they can confine a sufficiently-large number of ions, such that the propagation of correlations becomes a real many-body problem very difficult to tackle even with the most sophisticated numerical methods. For this reason, the advent of a trapped-ion test of our LRB would constitute a quantum simulation that overcomes the capabilities of classical computers.

Micro-fabricated surface traps

Let us now consider another promising architecture, the so-called micro fabricated surface traps [SPS12]. By appropriately designing a planar electrode, it is possible to confine the ions above the electrode surface according to any desired geometry [SWL09]. So far, in order to minimise the heating, the ions have been held sufficiently far away from the electrodes, such that typical ion-ion distances are much larger than in linear or Penning traps (e.g. $d_\mathrm{m} \sim$ 40-50 μm for linear surface traps with $^9\mathrm{Be}^+$ ions [BOC$^+$11] or $^{40}\mathrm{Ca}^+$ ions [HLB$^+$11]). For such larger distances, the Coulomb couplings and thus the tunneling of vibrational excitations is reduced considerably. For instance, for $^9\mathrm{Be}^+$ crystals with $d_\mathrm{m} \approx 40\,\mu\mathrm{m}$, and transverse trap frequency of $\omega_\mathrm{t}/2\pi \sim 10\,\mathrm{MHz}$, we get $\beta\omega_\mathrm{t}/2\pi \approx 0.6\,\mathrm{kHz}$. According to the LRB (8.11), we understand that the transport of correlations will be much slower in this case. For moderate state-dependent forces $g/2\pi \approx 0.4\mathrm{kHz}$, we find that the transport of correlations in the surface trap is two orders of magnitude slower with respect to the LRB of the linear chain in Fig. 8.4 **(a)**. For the recent experiments [SRW$^+$14], where the fluorescence of a triangular crystal of $^{171}\mathrm{Yb}^+$ ions in a surface trap has been observed for the first time, the estimated phonon tunneling $\beta\omega_\mathrm{t}/2\pi \approx 0.03\,\mathrm{kHz}$ for trapping frequencies of $\omega_\mathrm{t}/2\pi \approx 3.3\,\mathrm{MHz}$ leads to a slower transport of correlations.

Bounds for perturbative interacting spin models.

Whereas our LRB (8.11) gives the fastest timescale of correlation, many experiments for the simulation of quantum magnetism [FSG$^+$08, BSK$^+$12, KCK$^+$10, IEK$^+$11] are implemented in the so-called perturbative regime, which leads to significantly slower correlation speeds. In the far-detuned regime of the spin-boson lattice model (8.7) the effect of the bosons as carriers of spin correlations can be described neatly, since the oscillating forces that are much weaker than their detuning from the trap frequency, $g \ll \delta_t$, thus the spin-boson coupling (8.6) is weak enough and the bosons can only be created/annihilated virtually. In this perturbative limit, one traces out the bosons to obtain an effective algebraically decaying spin-spin interaction [PC04, PC06], $H_\mathrm{eff} = \sum_{ij} J_{ij}\sigma_i^z\sigma_j^z$ due to the virtual boson exchange between distant ions.

In order to trace out the bosons, it is more convenient to diagonalise first the

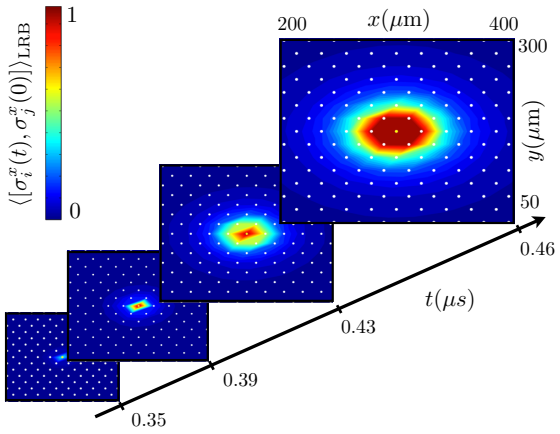

Figure 8.5: **LRB for the spin correlations in a triangular ion crystal in a Penning trap:** . Evaluation of the spin-boson LRB in Eq. (8.11) for a triangular crystal $^9Be^+$ ions in triangular Penning trap (see the text for the specific parameters). We observe the evolution of a spin perturbation initially localised in the centre of the crystal, and spreading toward its boundary as the time evolves.

harmonic crystal Hamiltonian (8.2). This can be done by the following canonical transformation

$$\delta r_{i,\mathrm{t}} = \sum_n \sqrt{\frac{1}{2m\omega_n}}\mathcal{M}_{in}(a_n^\dagger + a_n), \quad p_{i,\mathrm{t}} = \mathrm{i}\sum_n \sqrt{\frac{m\omega_n}{2}}\mathcal{M}_{in}(a_n^\dagger - a_n), \tag{8.13}$$

where $a_n^\dagger(a_n)$ create(annihilate) phonons in the crystal, and $\mathcal{M}_{in}$ are the elements of an orthogonal matrix that leads to the normal-mode frequencies of the crystal $\omega_n = \omega_{\mathrm{t}}(1+\beta\tilde{\mathcal{V}}_n)^{1/2}$. Here, $\tilde{\mathcal{V}}_n = \sum_{ij}\mathcal{M}_{in}\tilde{\mathbb{V}}_{ij}\mathcal{M}_{jn}$, and $\tilde{\mathbb{V}}_{ij} = 1/|\tilde{\mathbf{r}}_i^0 - \tilde{\mathbf{r}}_l^0|^3$ are the rescaled oscillator couplings, where the equilibrium distances have been divided by the minimum distance of the crystal $\tilde{\mathbf{r}}_i^0 = \mathbf{r}_i^0/d_m$. Hence, the harmonic crystal Hamiltonian (8.2) becomes $H_{\mathrm{b}} = \sum_n \omega_n a_n^\dagger a_n$.

Let us now move to the interaction picture with respect to $H_0 = \sum_i B^z\sigma_i^z + \sum_n \omega_n a_n^\dagger a_n$. We assume that *(i)* the on-site spin terms (8.4) fulfil $\nu = \omega_0$, and $\varphi = 0$, and $\Omega \ll \omega_0$, *(ii)* the state-dependent force (8.5) fulfils $\tilde{\nu} \approx \omega_n$, and $\tilde{\Omega}\gamma_n \ll \omega_n$, such that $\gamma_n = \gamma(\omega_{\mathrm{t}}/\omega_n)^{1/2}$. In this case, after a rotating-wave approximation, we can describe the interaction-picture Hamiltonian as

$$H(t) = \sum_i h\sigma_i^x + \sum_{in}\mathcal{F}_{in}\sigma_i^z a_n^\dagger \mathrm{e}^{\mathrm{i}\tilde{\delta}_n t} + \mathrm{H.c.}, \tag{8.14}$$

where $h = \Omega/2$, $\mathcal{F}_{in} = \mathrm{i}\tilde{\Omega}\gamma_n \mathrm{e}^{\mathrm{i}\tilde{\varphi}}\mathcal{M}_{in}/2$, and $\tilde{\delta}_n = \omega_n - \tilde{\nu}$ is the detuning of the state-dependent force. In the far-detuned regime $|\mathcal{F}_{in}| \ll \tilde{\delta}_n \ll \omega_n$, the force can only create/annihilate phonons virtually giving rise to an effective interaction

between the spins. Assuming that the phonons are initially in a thermal state $\rho(t_0) = |\psi_s\rangle\langle\psi_s| \otimes \rho_{th}$, whereas the spins are in an arbitrary pure state $|\psi_s\rangle$, it is possible to trace out the phonons by means of a canonical transformation [PC04] or via the Magnus expansion [Mag54]. The latter leads to an effective time evolution operator for the spins that reads as follows

$$U_{\text{eff}}(t) = \mathrm{e}^{-\mathrm{i}tH_{\text{eff}}} + \mathcal{O}\big((g/\tilde{\delta}_t)^2(\bar{n}_t + 1/2)\big), \tag{8.15}$$

where $g = \sqrt{2}\tilde{\Omega}\gamma$ is the strength of the spin-boson coupling, $\tilde{\delta}_t$ is the detuning with respect to the center-of-mass mode, and $\bar{n}_t$ is its thermal occupation. Thus, if the detuning is large enough, and the crystal is laser-cooled to sufficiently low temperatures $(g/\tilde{\delta}_t)^2(\bar{n}_t + 1/2) \ll 1$, the residual terms can be neglected. We thus obtain the effective transverse-field Ising model

$$H_{\text{eff}} = \sum_{i\neq j} J_{ij}\sigma_i^z\sigma_j^z + \sum_i h\sigma_i^x, \quad J_{ij} = -\sum_n \frac{\mathcal{F}_{in}^*\mathcal{F}_{jn}}{\tilde{\delta}_n}. \tag{8.16}$$

For the transverse modes, where $\beta = e_0^2/m\omega_t^2 d_m^3 \ll 1$, it is possible to show that the leading-order term for the spin-spin couplings decays algebraically with distance. In particular, if $\beta \ll 2\tilde{\delta}_t/\omega_t$, we obtain the following a dipolar law

$$J_{ij} = \frac{J_0}{|\tilde{\mathbf{r}}_i^0 - \tilde{\mathbf{r}}_j^0|^3}, \quad J_0 = \frac{1}{16}\left(\frac{g}{\tilde{\delta}_t}\right)^2 \beta\omega_t \tag{8.17}$$

At this point, it is important to remark that the force is constrained to $(g/\tilde{\delta}_t)^2 \ll 1$, which follows from the need to neglect residual spin-boson couplings in the evolution (8.15). Therefore, the spin couplings $J_0 \ll \beta\omega_t$ are much smaller than the tunneling of phonons, which is consistent with the fact that the interactions are carried by the phonons via perturbative virtual exchange. Although in this work we have focused on the regime of dipolar decaying interactions $\beta \ll 2\tilde{\delta}_t/\omega_t$, let us also note that if $\beta\omega_t \approx 2\tilde{\delta}_t$, other algebraic decays can be found (e.g. Coulomb-like, monopole-dipole, etc). To achieve this regime, one may either reduce the detunings $\tilde{\delta}_t$ [BSK+12], or change the vibrational bandwidth $\beta\omega_t$ modifying the axial trap frequency [ISC+13]. The latter method does not compromise the spin couplings, since the residual error $\mathcal{O}((g/\tilde{\delta}_t)^2)$ can be fixed without decreasing the forces.

In the dipolar regime, we can thus derive a LRB for the spin model following similar steps as in Chapter 7, that is finding a Dyson-type recursion for the LR commutator, bounding its norm, and resuming the expressions to infinite order. This derivation depends on the bound of the spin-spin couplings, and since they share the same distance-dependence with the oscillator couplings Q_{ij} (see Eq. (8.9)), we require analogous bounds on the supremum norms

$$\|\sigma_i\|_\infty \leq S = 1, \quad \|J_{ij}\|_\infty = J_{ij} \leq \frac{8J_0}{(1+d_{ij})^3}, \ \forall i \neq j, \tag{8.18}$$

where d_{ij} is again the Euclidian distance of a perfect Bravais lattice that shares the geometry with the ion crystal. We can then establish the following LRB for the effective spin model

$$\left\|[\sigma_i(t),\sigma_j^{\phi}(0)]\right\|_{\infty} \leq \frac{2}{a_0(1+d_{ij})^3}\left(e^{\tilde{\alpha}\left(\frac{g}{\tilde{\delta}_t}\right)^2(\beta\omega_t)t}-1\right),\ \ \tilde{\alpha}=a_0 \tag{8.19}$$

where a_0 is again defined by the maximisation of the convolution (8.12). We note that this bound coincides with the formal result of [NOS06] applied to our case. Let us emphasise that the parameter dependence of this spin-LRB resembles the spin-boson-LRB found in Eq. (8.11). There are, however, two main differences: *(i)* As the bosons have been traced out by a sort of adiabatic elimination, their propagation (i.e. first exponential in Eq. (8.11)) does not appear in the spin-LRB. *(ii)* The term in brackets, which accounts for the spin-spin coupling by virtual boson exchange, scales with $(g/\tilde{\delta}_t)^2$ as opposed to $(g/\beta\omega_t)^2$ for the spin-boson-LRB (8.11). Let us now discuss realistic values for different setups.

Ion chain in a linear Paul trap

We consider $^{25}Mg^+$ ions confined in a trap with the same parameters as discussed for the spin-boson LRB. The only parameter that we have to modify is the strength of the state-dependent force to fulfil the far-detuned-regime condition, such that the effective spin model is an accurate description. Let us first fix a large detuning $\tilde{\delta}_t/2\pi \approx 0.5\,\mathrm{MHz}$, which fulfils $\tilde{\delta}_t \ll \omega_t$. To reach the far-detuned regime $g \ll \tilde{\delta}_t$, we choose $g/2\pi \approx 50\,\mathrm{kHz}$. By substituting the previously-found value $a_0 = 2.9$, and considering again a chain of $N = 30$ ions, the corresponding spin-LRB (8.19) leads to the correlation transport displayed in Fig. 8.4 **(b)**. In contrast to the speed of correlations predicted by the spin-boson LRB (see Fig. 8.4 **(a)**), we find that the LR bound for the effective spin model predicts a much slower spread of correlations in the 0.1 ms range.

Triangular lattice in a Penning or surface trap

Let us now discuss the orders of magnitude for the propagation speed in the far-detuned regime of Penning traps and surface traps. For $^9Be^+$ ions in Penning traps, we fix again the detuning $\tilde{\delta}_t/2\pi \approx 80\,\mathrm{kHz}$. For the weak forces attained in the experiment $g/2\pi \approx 0.6\,\mathrm{kHz}$ [BSK+12], and recalling that $\beta\omega_t/2\pi \approx 60\,\mathrm{kHz}$, the LRB predicts a propagation of spin correlations in the milliseconds range. By allowing for larger incident angles of the laser beams responsible for the force, it is expected to achieve stronger forces $g/2\pi \approx 4\,\mathrm{kHz}$ [BSK+12] that would allow for LRB in the 0.1 ms range. Achieving such propagation speeds is important, as other sources of noise (e.g. magnetic field fluctuations) lead to decoherence times in 1-10 ms timescales. Let us now address a surface trap loaded with $^9Be^+$ ($^{171}Yb^+$) ions forming a triangular lattice. Let us recall that the ion spacing

in this case was much larger, such that $\beta\omega_{\rm t}/2\pi \approx 0.6\,{\rm kHz}$ ($\beta\omega_{\rm t}/2\pi \approx 0.03\,{\rm kHz}$). Considering the same detunings and forces as for the Penning trap, this leads to a propagation in 0.1-1 s (1-10 s), far too slow with respect to existing sources of noise. According to this discussion, we can conclude that the transport of spin correlations in the far-detuned regime can be sometimes hindered by existing sources of noise in the experiment. From a pragmatic point of view, it would be very interesting to study how to approach the faster spin-boson LRB (8.11) experimentally.

Bounds for impulsive spin-boson models

The above evaluation of the bounds has shown that the speed of propagation of spin correlations in the far-detuned regime is at least two orders of magnitude slower than the prediction of the spin-boson LRB (compare Figs. 8.4 **(a)** and **(b)**). Interestingly, by abandoning the far-detuned regime such that bosons cannot be eliminated from the dynamics, our new LRB (8.11) predicts that there is plenty of room for enhancement of the propagation speed. In fact, it seems possible that the spin correlations approach the optimal prediction of the LRB and spread with the maximum possible speed: the speed of the bare bosons propagating in the lattice. However, the LR theory does not tell us how to achieve this bound in practice, that is, it does not specify the particular spin-boson coupling or the time-modulation of the Hamiltonian parameters that would allow us to reach the aforementioned LRB (8.11). Finding the optimal regime of the spin-boson lattice model poses a many-body problem much more difficult to tackle, even numerically, than the effective spin model (see e.g. [HT13, SLRD13]). Hence, the possibility of exploring the LRB experimentally would be an instance of a quantum simulator that overcomes the power of the most sophisticated algorithms with classical computers.

As a guiding principle, we now study a simplified scenario that suggests that the optimal propagation speed (8.11) could also be achieved in the truly many-body problem (7.3). Let us consider the trapped-ion Hamiltonian (8.14) for $h = 0$. In this limit, $\sigma_i^z(t) = \sigma_i^z(t_0)$ is a conserved quantity, and the dynamics of the spin-boson lattice model can be integrated exactly. By using the free boson propagator $W_{ij}(\tau_1, \tau_2)$ in Eq. (7.27), it is possible to find the following bound for the LR commutator

$$\left\|[\sigma_i^x(t_{\rm f}), \sigma_j^x(t_0)]\right\|_\infty \leq 8 \sin\left(\int_{t_0}^{t_{\rm f}} {\rm d}\tau_1 \int_{t_0}^{\tau_1} {\rm d}\tau_2 F_{z,i}(\tau_1) W_{ij}^{xp}(\tau_1, \tau_2) F_{z,j}(\tau_2)\right), \quad (8.20)$$

which involves the state-dependent forces acting on the two ions $F_{z,i}(\tau_1), F_{z,j}(\tau_2)$ at different time-ordered instants $\tau_1 > \tau_2$. Let us remark that this expression does not require summing the Dyson series to infinite order as we did for the spin-boson LRB (8.11). It rather follows from the exact integrability of the dynamics, and thus serves as a test-bed for the validity of Eq. (8.11). We will focus on the

impulsive regime, where the forces act locally on the distant ions for a very short interval of time $\delta t \sim 1/g$, such that $\delta t \ll (\beta\omega_{\rm t})^{-1}$. Under this constraint, the phonons do not propagate during the time where the pulsed forces are active, and we can approximate the forces as Dirac delta functions

$$F_{z,i}(\tau_1) = \theta_i \delta(\tau_1 - t_{\rm f}),\ \ F_{z,j}(\tau_2) = \theta_j \delta(\tau_2 - t_0), \quad \theta_l = \int_{t_0}^{t_{\rm f}} {\rm d}\tau F_{z,l}(\tau). \tag{8.21}$$

Here, the pulse area θ_l is related to the number of local vibrational excitations created by each force (i.e. $\bar{n}_l = |\theta_l|^2 \sim (g\delta t)^2$). In this impulsive regime, we obtain

$$\left\|[\sigma_i^x(t_{\rm f}), \sigma_j^x(t_0)]\right\|_\infty \leq 8 \sin\left(W_{ij}^{xp}(t_{\rm f}, t_0)\theta_i\theta_j\right) \leq 8|W_{ij}^{xp}(t_{\rm f}, t_0)| \times |\theta_i\theta_j|. \tag{8.22}$$

We have thus obtained that the propagation of correlations in this impulsive regime is given by two contributions: the bare propagation of the phonons, and a term that depends on the efficiency of the spin-phonon coupling in correlating spins and phonons. This is exactly the form of the more general spin-boson LRB (8.11). This result is also intuitively correct, as we are *(i)* using a fast force to excite the phonons correlating them to the spin state at $t = t_0$, *(ii)* letting the bosons evolve under no additional force for $t \in (t_0, t_{\rm f})$, and *(iii)* performing another fast force to correlate the propagated phonons to a distant ion at $t = t_{\rm f}$.

Let us now go back to the state-dependent force of strength $g = \sqrt{2}\tilde{\Omega}\gamma$ in Eq. (8.5), and address the possibility of reaching the impulsive regime $g \sim (\delta t)^{-1} \gg \beta\omega_{\rm t}$ in ion-trap experiments. As argued below this equation, to achieve this force, the frequency of the radiation must be tuned $\tilde{\nu} \approx \omega_{\rm t}$, and its strength constrained to $\tilde{\Omega} \ll \omega_{\rm t}$ as we want to make the gradient of the radiation dominant with respect to other sidebands. For Lamb-Dicke parameters $\gamma \sim 0.1$, this poses a constraint on the achievable forces $g \lesssim 10^{-2}\omega_{\rm t}$. Moreover, considering the stiffness parameters of the above experimental realizations $\beta(^{25}{\rm Mg}^+, {\rm Linear}) \approx 0.09$, $\beta(^9{\rm Be}^+, {\rm Penning}) \approx 0.08$, $\beta(^9{\rm Be}^+, {\rm Surface}) \approx 0.06 \cdot 10^{-3}$, it is clear that the impulsive regime $g \gg \beta\omega_{\rm t}$ could only be attained for surface traps using this implementation of the forces. We now discuss two possible alternatives to reach the impulsive regime:

(i) By concatenating pairs of short resonant laser pulses coming from different directions, it is possible to implement much stronger state-dependent forces in the σ_x-basis without the requirement of resolving the sidebands [GRZC03]. As shown in recent experiments [MSN+13], this allows for very fast state-dependent forces $\delta t \approx 3\,{\rm ns}$ that create $\bar{n} \approx 10$ phonons. Therefore, one would obtain very strong and fast forces $g \sim \sqrt{\bar{n}}/\delta t \approx 2\pi \times 170$ MHz, which would clearly fulfil the impulsive-regime constraint for any of the above realizations. However, one should also note the technical overhead of this method, as it requires the use of pulsed trains of ultrafast picosecond laser pulses [MSN+13].

(ii) We now discuss an alternative without these experimental requirements which, although not allowing for such strong forces, can still reach the impulsive regime for $^9Be^+$ in Penning traps. The main message is that one can alleviate the condition of the resolution of the sidebands $\tilde{\Omega} \ll \omega_t$ to $\tilde{\Omega}\gamma \ll 4\omega_t$. Under this condition, in addition to the gradient (8.14), we should also consider the homogeneous terms as they can no longer be neglected. On the contrary, all the higher sidebands of the spin-phonon coupling can be neglected, and for $h = 0$ and $\tilde{\nu} \approx \omega_t$, we obtain

$$H(t) = \sum_i \frac{\tilde{\Omega}}{2}\sigma_i^z e^{-i\tilde{\nu}t} + \sum_{in} \mathcal{F}_{in}\sigma_i^z a_n^\dagger e^{i\tilde{\delta}_n t} + \text{H.c.}. \tag{8.23}$$

Another factor that typically limits the strength of the state-dependent forces in experiments is the compensation of ac-Stark shifts whereby photons are absorbed and reemitted into the same laser beam [BSK+12]. It is important to compensate such shifts when the forces are applied for a long period of time, as fluctuations in the laser intensities would lead to decoherence. However, for the short pulses required in the impulsive regime, these ac-Stark shifts need not be compensated as they can be refocused by a simple spin echo provided that the laser intensities do not fluctuate during $\delta t \sim g^{-1}$. We thus incorporate possible ac-Stark shifts to the spin-boson Hamiltonian

$$H(t) = \sum_i \frac{1}{4}\Delta\omega_{ac}\sigma_i^z + \sum_i \frac{\tilde{\Omega}}{2}\sigma_i^z e^{-i\tilde{\nu}t} + \sum_{in} \mathcal{F}_{in}\sigma_i^z a_n^\dagger e^{i\tilde{\delta}_n t} + \text{H.c.}. \tag{8.24}$$

The problem can still be integrated exactly, leading to an evolution operator $U(\delta t) = e^{-i\sum_i(\frac{1}{2}\Delta\omega_{ac}\delta t + \frac{\tilde{\Omega}}{\tilde{\nu}}\sin(\tilde{\nu}\delta t))\sigma_i^z} U_{\mathsf{SBL}}(\delta t)$, where $U_{\mathsf{SBL}}(t)$ is the evolution operator leading to the LRB in the impulsive regime (8.22). We first impose that $\nu\delta t = 2\pi n$, where $n \in \mathbb{Z}$. Additionally, at the middle of the evolution we apply a spin-echo pulse consisting of a π-pulse $\sigma_i^z \to -\sigma_i^z$, and $\tilde{\Omega} \to -\tilde{\Omega}$. The π-pulse is routinely achieved in trapped-ion experiments by driving the carrier transition [HRB08], whereas the inversion of the Rabi frequency can be achieved by controlling the laser phase [TGB+13]. In this way, $U(\delta t) = U_{\text{SBL}}(\delta t)$, and we can overcome the effects of the spurious terms. In this new regime, taking into account the parameters of $^9Be^+$, and the larger incident angles planned in the experiment [BSK+12], we find that the forces can be as large as $g/2\pi \approx 0.3\,\text{MHz}$, such that $\beta\omega_t/g \approx 0.2$ and we achieve the desired impulsive. Note that the pulsed forces are applied for time intervals of $\delta t \sim$0.1-1 μs, which is considerably shorter in comparison to the propagation of the spin correlations.

Let us close this section by reminding that this impulsive regime should serve as a guiding principle to test experimentally how the LRB (8.11) can be attained. However, we should keep in mind that the interesting many-body problem would be the one where the forces are non-perturbative and also non-impulsive.

8.3 Probing Lieb-Robinson bounds through fluorescence measurements

We discuss how to exploit the high accuracies in controlling and measuring the quantum state of a collection of trapped ions [HRB08] to probe LRBs. Note that single-time observables, $\langle\sigma_i^\alpha(t)\rangle, \langle\sigma_i^\alpha(t)\sigma_j^\beta(t)\rangle$, are already being measured with trapped ions [RLR$^+$04] or atoms in optical lattices [ECF$^+$11, KKG$^+$13]. Our aim is to measure retarded correlation functions $\langle\sigma_i^\alpha(t)\sigma_j^\beta(0)\rangle$. Let us emphasise that the experimental scheme, which has been depicted in Fig. 8.6, consists of a sequence of operations that are standard in several trapped-ion laboratories dedicated to quantum-information processing. This sequence can be divided in three steps: initialization, evolution and measurement that we will explore in the following subsections.

Initialization

The first step is the initialization, namely to prepare a localized spin excitation in a certain region of the ion crystal at $t = t_0$. Considering the trapped-ion realization of the spin-boson coupling (8.6), and the effective Ising interaction in the perturbative limit (8.16), we will study the following initial state $\rho(t_0) = |\psi_{\rm s}\rangle\langle\psi_{\rm s}| \otimes \rho_{\rm th}$, where $\rho_{\rm th}$ is the thermal state of the vibrational excitations after laser cooling, and $|\psi_{\rm s}\rangle = U_j|\downarrow\cdots\downarrow\rangle$ is obtained by optical pumping $\mathcal{P}$ to a state where all spins pointing down $|\downarrow\cdots\downarrow\rangle$, and subsequently implementing a $\pi/2$-pulse at a certain ion j, namely $U_j = \exp\{{\rm i}\frac{\pi}{2}\sigma_j^y\}$. Ideally, $|\psi_{\rm s}\rangle = |\downarrow\cdots\downarrow+_j\downarrow\cdots\downarrow\rangle$, where $|+_j\rangle = (|\uparrow_j\rangle + |\downarrow_j\rangle)/\sqrt{2}$ is the spin excitation. However, we remark that the LRB would also apply if the initial perturbation is delocalised around j, as far as it does not have an overlap with the distant lattice site i where the measurement takes place. Therefore, the experiment does not require individual addressability. Moreover, we also emphasise that laser cooling to the vibrational ground-state is not required, as the general LRB (8.11) is valid for any temperature of the ions (provided that the crystal is stable, and only small excursions from the equilibrium positions take place). This is a clear advantage with respect to the effective spin models (8.16), which are obtained by tracing out the vibrational excitations, and whose validity relies on minimising residual spin-phonon couplings. This requires either cooling closer to the vibrational ground-state, or using larger detunings such that the couplings become weaker, and other sources of noise may start contributing. In our case, Doppler cooling to modest temperatures (e.g. $\bar{n}_i = {\rm Tr}\{a_i^\dagger a_i\rho_{\rm th}\}$ ∼10-20) will suffice to test the validity of the LRB. Finally, note also that unitaries analogous to U_j correspond to single-qubit gates for quantum computation, which have been accomplished with very high fidelities [HRB08]. Due to all these properties, the initialisation step can be achieved with accuracies above 99%.

Evolution

After state preparation, the following step in Figs. 8.6**(a)** and **(b)** would be the *evolution* for $t \in [t_0, t_\mathrm{f})$, where we switch on the spin-boson lattice Hamiltonian $H_{\mathsf{SBL}}(t)$ (8.7) continuously (Fig. 8.6**(a)**) or in a couple of short uses (Fig. 8.6**(b)**). We let the spin excitation propagate in time $\rho(t_\mathrm{f}) = U_{\mathsf{total}}(t_\mathrm{f}, t_0)\rho(t_0)U^\dagger_{\mathsf{total}}(t_\mathrm{f}, t_0)$, where $U_{\mathsf{total}}(t_\mathrm{f}, t_0) = U_{\mathsf{SBL}}(t_\mathrm{f}, t_0)$ in the continuous regime of Fig. 8.6**(a)**, and $U_{\mathsf{total}}(t_\mathrm{f}, t_0) = U_{\mathsf{SBL}}(t_\mathrm{f}, \frac{1}{2}(t_\mathrm{f} - t_0))U_{\mathsf{SE}}U_{\mathsf{SBL}}(\frac{1}{2}(t_\mathrm{f} - t_0), t_0)$ in the pulsed regime of Fig. 8.6**(b)**. Here, we have introduced the evolution operator under the spin-boson lattice model (8.7), namely

$$U_{\mathsf{SBL}}(t_\mathrm{f}, t_0) = \mathcal{T}\left\{\mathrm{e}^{-\mathrm{i}\int_{t_0}^{t_\mathrm{f}} \mathrm{d}\tau H_{\mathsf{SBL}}(\tau)}\right\}, \tag{8.25}$$

and the corresponding spin echo U_{SE} that acts at the middle of the evolution. Let us note that the use of state-dependent dipole forces, such as the force in the z-basis (8.7) or in x, y-bases, has become a frequent tool in different laboratories [SM10]. Such forces underlie a wide variety of quantum-information experiments, such as the creation of Schrödinger cat states with single ions, conditional phase gates for quantum computing with two ions, or quantum simulations of magnetic interactions with several ions. Therefore, we expect that the evolution step can also be conducted with very high accuracies.

Measurement

Once the state of the system has evolved in time $\rho(t_0) \to \rho(t_\mathrm{f})$, the measurement step of the protocol starts (Fig. 8.6). In order to test the LRB (8.11), we need to measure the retarded correlation function

$$C_{\sigma_i^x, \sigma_j^x}(t_\mathrm{f} - t_0) = \langle[\sigma_i^x(t_\mathrm{f}), \sigma_j^x(t_0)]\rangle \tag{8.26}$$

However, the usual trapped-ion measurements $\mathcal{M}$ based on state-selective fluorescence only allow for measurements of single-time observables ($\langle\sigma_i^z(t)\rangle$, $\langle\sigma_i^z(t)\sigma_j^z(t)\rangle$) [HRB08]. In the following, we describe a modification of these schemes for the measurement of the above retarded correlation function. The main idea is to encode the information of the retarded correlator in the measurement of a single-time observable by means of a certain perturbation applied during the evolution step (i.e. a linear-response-type scheme [BF04]). To maintain the generality, let A_i be the single-spin observable that can be measured at $t = t_\mathrm{f}$. At $t = t_0$, we let the system evolve under a perturbed spin-boson lattice Hamiltonian $H(t) = H_{\mathsf{SBL}}(t) + V(t)$, where $V(t) = \lambda_\mathrm{B} B_j \delta(t - t_0)$ with $\lambda_\mathrm{B} \ll 1$ is a dimensionless perturbative parameter, B_j is a certain operator localised around j, and $\delta(t - t_0)$ is the Dirac delta function. At $t = t_\mathrm{f}$, we switch off the perturbed spin-boson lattice Hamiltonian, and perform an additional unitary operator $\tilde{U}_i$ localised around the site i (see Fig. 8.6), consisting of single-spin rotations (i.e. single-qubit gates).

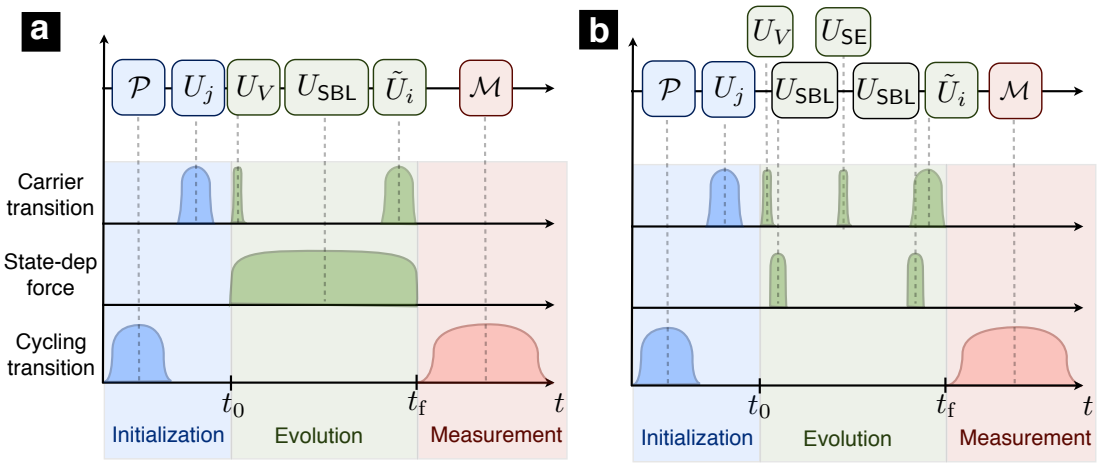

Figure 8.6: **Experimental sequence to test the LRB: (a)** Always-on and **(b)** pulsed spin-phonon forces. We represent the *initialization* step in blue, which consists of laser cooling followed by optical pumping $\mathcal{P}$ and leads to $|\downarrow\cdots\downarrow\rangle\langle\downarrow\cdots\downarrow| \otimes \rho_{\rm th}$, where $\rho_{\rm th}$ is a thermal state of the phonons after Doppler cooling. We then apply a $\pi/2$-pulse $U_j = \exp\{\mathrm{i}\frac{\pi}{2}\sigma_j^y\}$ by driving the carrier transition [HRB08]. In the *measurement* step in red, one collects the state-dependent fluorescence $\mathcal{M}$ during a continuous driving of the cycling transition [HRB08]. At the beginning of the *evolution* step $t = t_0$, we apply the unitary U_V associated to the impulsive perturbation $V(t)$ described in the main text. This is followed by the actual evolution under the state-dependent forces: **(a)** in the always-on regime, the forces should be switched on continuously during the evolution, or **(b)** in the impulsive regime, we apply two pulsed forces. Additionally, at the middle of the evolution, we apply the spin-echo sequence $U_{\rm SE}$ $\sigma_i^z \to -\sigma_i^z$ and $\tilde{\Omega} \to -\tilde{\Omega}$ to refocus uncompensated ac-Stark shifts. Before measuring, we apply another $\pi/2$-pulse $\tilde{U}_i = \exp\{-\mathrm{i}\frac{\pi}{2}\sigma_i^y\}$.

Using the interaction-picture formalism, the total time-evolution operator can be thus written as follows

$$U = \tilde{U}_i U_{\rm total}(t_{\rm f}, t_0) U_V(t_{\rm f}, t_0), \quad U_V(t_{\rm f}, t_0) = \mathcal{T}\left\{\mathrm{e}^{-\mathrm{i}\int_{t_0}^{t_{\rm f}} \mathrm{d}\tau \hat{V}(\tau)}\right\}, \tag{8.27}$$

where $\hat{V}(\tau) = U_{\rm total}^\dagger(\tau, t_0) V(\tau) U_{\rm total}(\tau, t_0)$. Due to the impulsive and perturbative nature of the perturbation, we can approximate this evolution operator as $U \approx \tilde{U}_i U_{\rm total}(t_{\rm f}, t_0)(\mathbb{1} - \mathrm{i}\hat{V}(t_0))$.

Finally, the measurement of the observable gives us

$$\begin{aligned} & \langle A_i(t_{\rm f})\rangle_{\rm pert} \\ = \; & \mathrm{Tr}\{(\tilde{U}_i U_{\rm total}(t_{\rm f}, t_0)(\mathbb{1} - \mathrm{i}\lambda_{\rm B} B_j(t_0)))^\dagger A_i \tilde{U}_i U_{\rm total}(t_{\rm f}, t_0)(\mathbb{1} - \mathrm{i}\lambda_{\rm B} B_j(t_0))\rho(t_0)\} \end{aligned} \tag{8.28}$$

Using linear-response theory, we find that to linear order in the perturbation strength

$$\langle A_i(t_\mathrm{f})\rangle_\mathrm{pert} = \langle \tilde{A}_i(t_\mathrm{f})\rangle_\mathrm{unpert} - \mathrm{i}\lambda_\mathrm{B}\langle[\tilde{A}_i(t_\mathrm{f}), B_j(t_0)]\rangle_\mathrm{unpert}, \tag{8.29}$$

where we have defined $\tilde{A}_i = \tilde{U}_i^\dagger A_i \tilde{U}_i$, and the subindex $\langle\cdot\rangle_\mathrm{unpert}$ refers to the expectation value for the time-evolved state with respect to the unperturbed Hamiltonian, namely the spin-boson lattice model $U_\mathsf{total}(t_\mathrm{f}, t_0)$ in the continuous or pulsed regimes. Therefore, by letting the system evolve with and without the perturbation, we can measure

$$f(\lambda_\mathrm{B}) = \langle A_i(t_\mathrm{f})\rangle_\mathrm{pert} - \langle \tilde{A}_i(t_\mathrm{f})\rangle_\mathrm{unpert}, \tag{8.30}$$

and thus estimate the retarded correlator. To be more precise, $\mathrm{d}f/\mathrm{d}\lambda_\mathrm{B}|_{\lambda_\mathrm{B}=0} = -\mathrm{i}\langle[\tilde{A}_i(t_\mathrm{f}), B_j(t_0)]$, so we would need to modify the perturbative parameter λ_B, such that we can estimate its derivative for very weak couplings. We note that the use of measurement unitaries $\tilde{U}_i$ has been already demonstrated in the measurement of single-time observables in different basis (e.g. $\langle {\sigma_i}^\alpha(t)\rangle, \langle\sigma_i^\alpha(t)\sigma_j^\beta(t)\rangle$) for state tomography [RLR+08], or to recover the position operator of a trapped ion [GKZ+10]. By including a perturbation at $t = t_0$, we get access to two-time observables, and in particular to the desired information about the Lieb-Robinson commutator.

Application of the scheme to the dynamics under study

In this case, the state-dependent fluorescence allows us to measure $A_i = \sigma_i^z$. Typical fidelities for this type of measurements are above 99% for photon-collection times on the millisecond range [HRB08]. Although the spin correlation transport occurs on a much faster time-scale, the fact that we switch off the spin-phonon coupling at $t = t_\mathrm{f}$ (Fig. 8.6) implies that the spin-populations will be frozen for $t > t_\mathrm{f}$. Thus, this scheme allows for the required photon-collection times without compromising the information about the transport of correlations. The perturbation that must be applied to recover the desired correlator is $B_j = \sigma_j^x$, which can be achieved by driving the so-called carrier transition of the ions, such that $\lambda_\mathrm{B} = \Omega\delta t/2$. We can reach the perturbative regime by simply driving the carrier with a sufficiently small intensity. Therefore, the Rabi frequency Ω must be much smaller than any other coupling strength in the problem $\Omega \ll \{g, \beta\omega_\mathrm{t}\}$. Moreover, the impulsive regime will be a good approximation when the time during which the perturbation is applied, δt, is much smaller than any other time-scale of the problem $\delta t \ll \{g^{-1}, (\beta\omega_\mathrm{t})^{-1}\}$. Finally, the measurement unitary corresponds to $\tilde{U}_i = \mathrm{e}^{-\mathrm{i}\frac{\pi}{2}\sigma_i^y}$, which leads to the desired correlator $C_{\sigma_i^x,\sigma_j^x}(t_\mathrm{f} - t_0)$ encoded in the resonance fluorescence of the ion

$$\langle\sigma_i^z(t_\mathrm{f})\rangle_\mathrm{pert} = \langle\sigma_i^x(t_\mathrm{f})\rangle_\mathrm{unpert} - \mathrm{i}\lambda_\mathrm{B}\langle[\sigma_i^x(t_\mathrm{f}), \sigma_j^x(t_0)]\rangle_\mathrm{unpert}. \tag{8.31}$$

As announced previously, by measuring a single-time observable in the presence of a perturbation, we can recover the retarded correlator and test the validity of

the LRB. At this point, it is worth commenting on the following points. First, let us note that the unitary $\tilde{U}_i$ could also be delocalised around the site j, such that individual addressability is not required. Second, we remark that other choices of $B_j, \tilde{U}_i$, which are equally accessible in an experiment, would allow us to estimate any other correlator $\langle[\sigma_i^\alpha(t), \sigma_j^\beta(t_0)]\rangle$, which might be important when the state-dependent forces act in a different basis, or if we combine them to produce Heisenberg-type Hamiltonians. Moreover, the use of state-dependent forces in $\tilde{U}_i$ can also allow for measurements of the LR commutators for the free bosonic lattice to test the harmonic LRB (7.24).

8.4 Conclusions and outlook

In this chapter, we have applied the Lieb-Robinson bounds for spin-boson lattice models to crystals of trapped ions. In these LRB the spread of spin correlations depends on the propagation speed of the phonons of the crystal as well as on the the efficiency with which the ions emit and reabsorb correlations from the phonons. We have also found that the speed for the spread of correlations given by our bounds can be faster than the time scales in the experimental regimes currently considered.

Since many experiments for the simulation of quantum magnetism are implemented in the perturbative regime with slower correlation speeds, we have derived the Lieb-Robinson bounds in this regime and we have found that the speed of propagation for the spin correlation is at least two orders of magnitude slower than in the non-perturbative case.

We have also studied the bounds in the impulsive regime, where the forces act locally on the distant ions for a short interval of time and the propagation of correlations only depends on the bare propagation of the phonons and on the efficiency of the spin-boson coupling in correlating spins and bosons. We have obtained the optimal propagation spread in this regime when the original Lieb-Robinson bound is saturated.

In the following table, we recall the orders of magnitude of the speed of propagation for spin correlations for the different regimes and two trapped-ion setups:

	Paul trap	Penning trap / surface trap
Impulsive regime	$1\,\mu s$	$10\,\mu s$
Non-perturbative regime	$1\,\mu s$	$10\,\mu s$
Perturbative regime	$0.1\,ms$	$0.1\,ms$

Finally, we have proposed an experimental scheme to measure retarded correlation functions via the crystal fluorescence, which allows to test the Lieb-

Robinson bounds that we have derived in the impulsive regime. This scheme can be modified using state-dependent forces to test the harmonic Lieb-Robinson bound (7.24) that we have proposed in Section 7.4. As a further investigation, it would be interesting to find other experimental schemes that could test the Lieb-Robinson bounds in other regimes. The most interesting regime would be the non-perturbative and non-impulsive (8.11), although we would also like to explore the perturbative regime, where the spread of correlations is slower.

While we have applied the LRB to trapped ion crystals, our results immediately extend to a variety of fields, such as superconducting quantum circuits and quantum dots or NV-centers interacting with coupled cavities or photonic crystals.

9 Quantum algorithms for quantum metrology

9.1 Introduction

Quantum metrology and quantum sensing are some of the fields which have benefited greatly from the incresing progress in the control and observation of individual quantum systems, with accurate atomic clocks assisted by quantum gates [SRL+05, CHK+10] or the use of atomic squeezing for enhanced magnetometry [WJK+10, NKD+11]. The basic problem in quantum metrology is the estimation of an unknown parameter using quantum strategies to improve precision over classical methods [GLM06, GLM11, Par09], such as entanglement [CEB+05, HMM16] or the interaction with a quantum system [NKD+11]. The measurement of a parameter has three differents parts: first, the probe must be prepared, secondly, the probe interacts with the system and finally the probe must be measured in order to obtain the parameter estimate. The possible errors that arise in this process may be minimized classically by computing the average of several independent measurements of the parameter. In this case, the error scales as $O(N^{-1/2})$, where N is the number of measurements, as a result of the central limit theorem and giving rise to the "standard quantum limit" [GLM06, GLM11]. However, this scaling can improve using quantum effects to assist a certain step of the measurement process until the limits in precision predicted by quantum mechanics, or "Heisenberg bounds", are reached [GLM04].

In this chapter, we introduce the notion of "multi-pulse quantum interferometry" (MPQI), where an atom acts as a nonlinear, fast-response detector that efficiently measures the differences between ultrashort laser pulses. Modelling the atom-pulse interaction as a sequence of unitaries, $\{U_i\}_{i=1}^{N}$, through a suitable reordering of the pulses, additional gates and measurements, we build quantum algorithms to accurately determine the differences among the pulses, or the properties of individual pulses themselves. Compared with continuous wave (CW) laser interferometry, this approach provides a polynomial enhancement of the sensitivity because a single atom accumulates many interferometric events. We propose as a direct application of this idea the characterization and stabilization

of a frequency comb [UHH02, YC05].

9.2 The frequency comb. Classical stabilization.

A frequency comb is a device that produces a train of laser pulses with a fixed duration, τ, and a regular spacing, T (see Figure 9.1). Stabilizing a comb is ensuring that the offset frequency, ν_0, remains a constant and well-known value, and that the spectrum is a collection of regularly spaced teeth with frequencies $f_n = n/T + \nu_0$ (see Figure 9.1). Haensch and Hall solved this problem [RHUH99, JDR$^+$00] in frequency space, interferometrically comparing different teeth in the limit of many pulses, which requires a comb whose spectrum spans at least an octave, or broadening the light with a nonlinear fiber. This stabilization enables direct frequency comb spectroscopy, accurately revealing the atomic level structure of neutral atoms [MSL$^+$04, WZU$^+$05] and ions [WvdBUE09, WMK$^+$11].

If instead of considering the frequency space, we study the time-domain image of the pulse train, we observe that the effect of the offset frequency is to change the relative phase between the electric field carrier wave and the peak of the pulse envelope from pulse to pulse. This phase is also known as the carrier-envelope offset phase (CEP) (see Figure 9.1), which is related to the offset frequency ν_0 as follows

$$\phi_{n+1} - \phi_n = \Delta\phi = \nu_0 T \tag{9.1}$$

The first direct observation of CEP effects was reported in the spatial asymmetry of above-threshold ionization from Kr gas [PGW$^+$01] and in x-ray emission from Ne [BUU$^+$03]. The direction of photocurrents injected in semiconductors is also controlled by the CEP phase [FRJ$^+$04, RLS$^+$05] and the absolute CEP of single pulses was recently measured [WHH$^+$09]. The study of the CEP has been generally centered on its spectral components [WD09], while only a few reports have addressed time-domain measurements of the relative phase of successive pulses in a train [XSP$^+$96, OGGS07].

9.3 Quantum protocols for stabilization.

To address the problem of comb stabilization we introduce multipulse quantum interferometry (MPQI), designing protocols that detect the phase difference between pulses with the greatest accuracy possible. We begin by determining the unitaries associated to the laser pulses emitted by the comb, which depend on the carrier-envelope offset phase (CEP). We then use these unitaries to propose

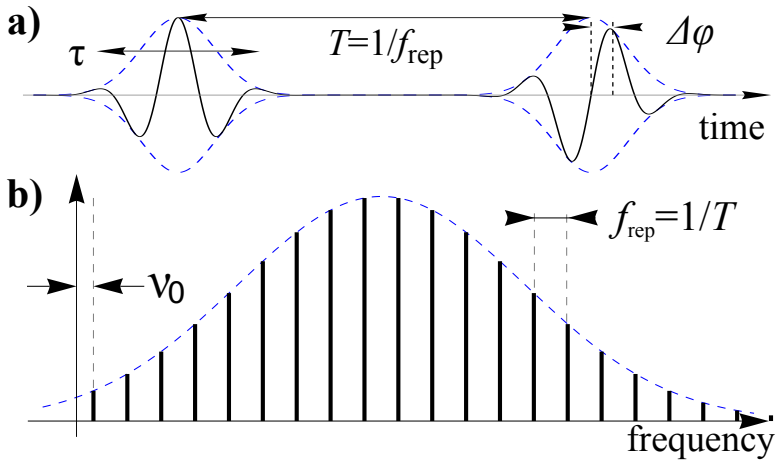

Figure 9.1: (a) Electric field amplitude (solid line) and envelope (dashed) of a pulsed laser with period T and pulse-to-pulse phase difference $\Delta\phi$. (b) Associated spectra: a broad peak for one pulse (dashed) and a modulated comb for a pulse train with repetition rate f_{rep} (solid). The frequency offset ν_0 depends on the pulse-to-pulse phase difference $\Delta\phi$.

several quantum algorithms, starting by a simple two-level protocol for consecutive pulses in a low intensity regime and also in a $\theta \simeq \pi$ regime. We further this study by introducing analogous protocols for delayed sequences of pulses which display an enhanced sensitivity. Afterwards, we describe equivalent protocols using Raman schemes which minimize spontaneous emission. Finally, we present a discussion of experimental errors and the achievable sensitivities in practical implementations. The resulting methods do not require an octave-spanning comb, broadening or frequency doubling. They are thus useful for a wide variety of lasers, demand less power, and may profit from the ever-growing precision in atomic interferometry.

Single-pulse unitary

We start by determining the unitary transformation experienced by an atom subject to a laser pulse, and how this unitary depends on the CEP, ϕ_n. Note that the interaction of multilevel atoms with a frequency comb was studied previously in the limit of many consecutive pulses [FL09], while in this section we are interested in the action of a single pulse. We model the atom interaction with a single laser pulse in the semiclassical limit

$$H = \frac{\omega_{at}}{2}\sigma_z + s(t)\cos(\bar{\omega}t + \phi_m)\sigma_x. \tag{9.2}$$

Here, m is the pulse index, $s(t) \geq 0$ is the pulse envelope, $\bar{\omega} = 2\pi\bar{\nu}$ is the comb carrier frequency, ω_{at} is the atomic transition frequency ($\hbar = 1$ throughout),

there is an unknown phase ϕ_m for each pulse, and $\sigma_{x,y,z}$ are the Pauli matrices. The evolution under this Hamiltonian is described by a unitary operator that satisfies the Schrödinger equation $i\frac{d}{dt}W(t) = H(t)W(t)$. We are going to extract the evolution with the spin operator σ_z as $W(t) = \exp(-i\bar{\omega}\sigma_z t/2)U(t)$. In the rotating frame, the remaining contribution to the unitary operator evolves now according to

$$i\frac{d}{dt}U = \frac{\omega_{at} - \bar{\omega}}{2}\sigma_z + s(t)(e^{i\bar{\omega}t+i\phi_m} + \text{c.c.})(e^{i\bar{\omega}t}\sigma^+ + \text{H.c.}). \tag{9.3}$$

Assuming that the Rotating Wave Approximation (RWA) is valid, in this Hamiltonian we can neglect the counter rotating terms, such as $e^{i2\bar{\omega}t+i\phi_m}\sigma^+$, and keep only those that are slowly varying. We obtain the Hamiltonian H_{RWA} in the Rotating Wave Approximation

$$H_{\text{RWA}} = \tfrac{1}{2}(\omega_{at} - \bar{\omega})\sigma_z + s(t)\left(e^{-i\phi_m}\sigma^+ + \text{H.c.}\right). \tag{9.4}$$

The RWA works for pulses which contain ≥ 30 periods of the carrier frequency, $\tau \geq 30/\bar{\nu}$, and allows us to explicitly write the pulse unitaries

$$U_m = \cos\left(\frac{\theta_m}{2}\right) + i\sin\left(\frac{\theta_m}{2}\right)\sigma_{\phi_m} = e^{-i\phi_m\sigma_z}U_0 e^{i\phi_m\sigma_z}, \tag{9.5}$$

in terms of the total Rabi flip angle of a single pulse, $\theta_m = 2\int_{-\tau/2}^{\tau/2} s(t)dt$, with $\sigma_{\phi_m} = \cos(\phi_m)\sigma_x + \sin(\phi_m)\sigma_y$. In the following sections, we assume that the comb is almost resonant, $\bar{\omega} \simeq \omega_{at}$, and has uniform intensity, i.e. $\theta_m = \theta$. These assumptions imply that we only need to stabilize the pulse-to-pulse phase difference $\Delta\phi$.

In order to study when the Rotating Wave Approximation is valid, we have performed numerical simulations of the evolution of the qubit under Eq. (9.2), varying the duration of the pulse or number of oscillations it contains, as well as the intensity and detuning. In Figure 9.3a we show the fidelity, F, of a resonant pulse, with a pulse area $\theta = \pi/2$, and a variable pulse length, τ. The validity of RWA is also challenged by the inaccuracy of the control parameters, and in particular the driving frequency: as Figure 9.3b shows, the unitary is affected by the detuning, and the differences between the RWA and the full model increase as the pulse length decreases. In practice this is not a problem, for we expect the detuning of the comb to be smaller than 1%. The main message is that for pulses above 30 oscillations, we are safe using the RWA Hamiltonian. On the other hand, we can still develop the MPQI protocols using the numerical expressions of the unitary operators when the RWA does not apply.

As a final check, we show in Figure 9.3c that the phase of the unitary is indeed proportional to the phase of the pulse. We obtain that $\phi_{\text{eff}} = \phi_m + \phi_{\text{AC}}$, where the carrier frequency appears in two different places: (i) determining the phase

of the pulse, $\phi_m \sim \bar{\omega} t_m + \phi_0 \sim \nu_0 \times m \times T + \phi_0 \,[\mathrm{mod}\, 2\pi]$, and (ii) in the AC Stark shift phase, ϕ_{AC}, that depends on the detuning $\omega_{\mathrm{at}} - \bar{\omega}$ and which becomes strictly zero for resonant pulses (see Figure 9.3c). In all other detuned cases, ϕ_{AC} will either be the same for all pulses, in which case it will be eliminated by our algorithms, which are based on phase differences, or we will be able to take it into account with the error analysis methods, by studying the fluctuations of the two-level frequency around the mean value ω_{at}.

Multipulse unitaries and protocols

We need protocols that efficiently detect the difference between a sequence of unequal pulses $U_{tot} = \prod_{i=1}^{N} U_i$, and the ideal case U_1^N. Let us first assume an ideal qubit, seeking an ordering of pulses with which the fidelity $|\mathrm{tr}(U_1^{N\dagger} U_{\mathrm{tot}})|$ decreases most rapidly with N. The simplest protocol (1A) applies N consecutive pulses (see Figure 9.3a) with low intensity ($\theta \ll 1$) on the qubit, and a uniform carrier-envelope frequency mismatch, $\phi_m = m\Delta\phi$. The combination of the unitaries for a sequence of pulses reads

$$\begin{aligned} U_{tot}^{(1A)} &= \prod_{m=1}^{N} e^{-i\phi_m\sigma_z} e^{i\theta/2\sigma_x} e^{+i\phi_m\sigma_z} \\ &= \cos\left(\frac{\theta}{2}\right) + i\sin\left(\frac{\theta}{2}\right) \sum_{m=1}^{N} e^{-i\phi_N\sigma_z} \sigma_x e^{i\Delta\phi\sigma_z} \\ &\simeq \mathbb{1} + i\frac{\theta}{2} e^{-i(N+1)\Delta\phi} \frac{\sin(N\Delta\phi)}{\sin(\Delta\phi)} \sigma^+ + \mathrm{H.c.} + \mathcal{O}(\theta^2) \end{aligned} \tag{9.6}$$

Note that in this context the pulse-to-pulse phase difference $\Delta\phi$ can be measured. It has the effect of a detuning, suppressing any excitation probability induced by the pulses of long trains and decreasing the amplitude of the Rabi oscillations. However, as we show later on, the functional dependence on $\Delta\phi$ implies a low sensitivity on the phase in practical implementations of the protocol.

We can do much better increasing the intensity to have a large pulse area $\theta = \pi$ (protocol 1B), so that each comb pulse can flip the state of the atom. Under these conditions, for an even set of pulses we get

$$U_{tot}^{(1B)} = \prod_{m=1}^{N} i e^{-i\phi_m\sigma_z} \sigma_x e^{+i\phi_m\sigma_z} \tag{9.7}$$

If we assume that the number of pulses is even, we can use the anticommutation rule $\sigma_x\sigma_z = -\sigma_z\sigma_x$ and

$$\begin{aligned} e^{-i\phi_m\sigma_z} \sigma_x e^{+i\phi_m\sigma_z} e^{-i\phi_{m-1}\sigma_z} \sigma_x e^{+i\phi_{m-1}\sigma_z} \\ = e^{-2i(\phi_m - \phi_{m-1})\sigma^z}, \end{aligned} \tag{9.8}$$

recovering the following expression

$$U_{tot}^{(1B)} = \prod_i U_i = \exp\left[-2i\sum_{k=1}^{N/2}(\phi_{2k} - \phi_{2k-1})\sigma^z\right], \tag{9.9}$$

which for constant $\Delta\phi$ implies $U_{tot}^{(1B)} = \exp(-iN\Delta\phi\sigma^z)$. Now $\Delta\phi$ can be interferometrically detected with an enhancement proportional to the number of pulses, N.

It is obvious that the sensitivity for the protocol in Eq. 9.9 increases by maximizing the phase difference between consecutive pulses. To profit from this, we design a set of protocols that extract a sequence of $N/2$ pulses from the original pulse train, and delay them a time $T_d \gg T$. This sequence is then intercalated with the original one, as seen in Figure 9.3b, so that $\phi_{2k} = k\Delta\phi + \Delta\phi\, T_d/T$ and $\phi_{2k-1} = k\Delta\phi$. Introducing this sequence in Eqs. (9.7, 9.9) we obtain respectively the unitaries corresponding to protocols 2A (for $\theta \ll 1$) and 2B ($\theta \sim \pi$). In particular, the unitary corresponding to protocol 2B is

$$U_{tot}^{(2B)} = \exp\left(-i\sigma^z\Delta\phi \times NT_d/T\right), \tag{9.10}$$

with an additional enhancement factor, $N_d = T_d/T$. This is optimal with respect to any rearrangement of the pulses, using each pulse only once.

Some optimality considerations

We now prove that the sequence for protocol 2B (2 sequence of pulses split from the original train with a time delay) is optimal when our only resource is the comb laser. As seen before, if we work around $\theta = \pi$ we obtain the analytical formula

$$U_{tot}^{(1B)} = \exp\left[-2i\sum_{k=1}^{N/2}(\phi_{2k} - \phi_{2k-1})\sigma^z\right] \tag{9.11}$$

and our protocol accumulates phase quite fast, about $\mathcal{O}(NN_d)$ for N pulses, where N_d depends on the delay. It is possible to prove that for any rearrangement of the same set of pulses (that is, with the same phases and intensity as before) this is the largest accumulation that can be detected.

If σ is a permutation for a certain arrangement of initial pulses, we can use the analytical expression for the arbitrary product of a train of pulses with different phases to compute product of the unitaries after the permutation

$$\prod_{i=1}^{M} U_{\sigma(i)} = e^{2i\sum_{i=1}^{M}(-1)^{\sigma(i)}\phi_{\sigma(i)}\sigma^z}\sigma_x^M \tag{9.12}$$

It is possible to find all permutations σ such that they maximize

$$|\sum_{i=1}^{M}(-1)^{\sigma(i)}\phi_{\sigma(i)}| \tag{9.13}$$

Suppose the original pulses are ordered in terms of their carrier-envelope phase ϕ_n, then it is quite straightforward to see how to construct optimal rearrangements of these pulses. Consider α a permutation of the first half of pulses and β a permutation of the second half of pulses. Then, the optimal set of rearrangements will be those formed by pulses labelled according to their carrier-envelope phase as $\{\phi_{\alpha(i)}, \phi_{\beta(N/2+i)}\}_{i\in\{1,\ldots,N/2\}}$ or of the form $\{\phi_{\beta(N/2+i)}, \phi_{\alpha(i)}\}_{i\in\{1,\ldots,N/2\}}$.

In particular, our proposed protocol corresponds to α and β being the identity permutation. This protocol accumulates the largest possible amount of phase after the action of the pulses onto the ion.

The fastest phase-accumulation protocol: phase referencing

If we allow for more gates, performing unitaries in between the pulses, we can measure not only the phase difference, but also the total sum of the carrier-envelope phases $\sum_i \phi_i$. In order to do so, the new set of gates and unitaries, considered in order, would be $\{\sigma_x, U(\phi_1), \ldots, \sigma_x, U(\phi_N)\}$, for which the overall product is

$$\begin{aligned}
&\prod_{i=1}^{M}\sigma_x U(\phi_{\sigma(i)}) = \prod_{i=1}^{M}\sigma_x e^{-i\phi_i\sigma_z}\sigma_x e^{i\phi_i\sigma_z} \qquad (9.14)\\
=\ &\prod_{i=1}^{M} e^{i\phi_i\sigma_z}\sigma_x^2 e^{i\phi_i\sigma_z} = \prod_{i=1}^{M} e^{i\phi_i\sigma_z}e^{i\phi_i\sigma_z}\\
=\ &\prod_{i=1}^{M} e^{2i\phi_i\sigma_z} = e^{2i\sum_i\phi_i\sigma_z}
\end{aligned}$$

where we use both $\sigma_x e^{-k\sigma_z} = e^{k\sigma_z}\sigma_x$ and $\sigma_x^2 = Id$.

Note however this protocol demands σ_x gates in between the pulses. Since the phase of these gates is stable, we can thus view this extra protocol as the referencing of the comb to the device that implements the σ_x gates, which can itself be a laser or a microwave beam, in the case of hyperfine qubits.

9.4 Analysis and performance of the protocols

We now transfer the information of the acquired phase to the measurable populations of the atomic states. For this, we complete the previous unitaries with

Implementation	$\theta \ll 1$ (A)	$\theta \simeq \pi$ (B)
2 levels, no delay (1)	$\sqrt{M}$	$N\sqrt{M}$
2 levels, with delay (2)	$N_d\sqrt{M}$	$NN_d\sqrt{M}$
Raman, 1 delay (1)	$N_d\sqrt{M}$	-
Raman, 2 delays (2)	$\lvert N_{d2} - N_{d1}\rvert\sqrt{M}$	$N\lvert N_{d2} - N_{d1}\rvert\sqrt{M}$

Table 9.1: Sensitivities, $\sigma^{-1}_{\Delta\phi,\theta}$, of a set of $2M$ two- or three-level atoms to the protocols described in the text (1A, 1B, 2A, 2B). N is the number of pulses in a sequence, which in the delayed cases are combined with N pulses from a later time, $T_d = N_d T$.

additional operations and measurements that enable estimating $\Delta\phi$ and θ. Out of $2M$ atoms, M are subject to the following steps (see Figure 9.3c): (i) initialization to the ground state, $|0\rangle$, (ii) apply a $\pi/2$ rotation (which could be either $\exp(i\sigma_x\pi/4)$ or a Hadamard gate) onto the ground state (iii) apply a reference phase ξ onto the level $|1\rangle$, (iv) let the atom interact with the comb as described before, (v) undo the $\pi/2$ rotation of step (i) and measure the state of the atom, $s \in \{0, 1\}$. The measurement outcome is described by the probability distribution, $P_1(s|\theta, \Delta\phi)$. For the remaining M atoms we skip (ii), obtaining the distribution $P_2(s|\theta, \Delta\phi)$. We remark that we need no phase coherence between the comb and the lasers that implement the $\pi/2$ rotations. The reference phase, ξ, is computed a priori to maximize the sensitivity of $P_{1,2}$ to the $\Delta\phi$.

The functions P_1 and P_2 convey all the information accessible in the lab: from the measurements of s in P_1 and P_2 experiments, one should compute different estimators and use them to infer the values of θ and $\Delta\phi$, with uncertainties σ_θ and $\sigma_{\Delta\phi}$. Using error propagation and the Fisher information we obtain fundamental lower bounds and practical estimates of the sensitivities ($\sigma^{-1}_{\Delta\phi}$ and σ^{-1}_θ) of each protocol. As summarized in Table 9.1, it is possible to build estimators of minimal variance for θ and $\Delta\phi$, which saturate the fundamental lower bounds. Moreover, we observe that all protocols but 1A improve over the standard statistical sensitivity, $\sqrt{M}$, thanks to the large number of pulses or to the use of pulses from well-separated times. In practice, both N and N_d span several orders of magnitude, providing a sensitivity comparable to the state of the art.

Fisher information and sensitivity

We are interested in estimating the sensitivity of the interferometric protocols that we have developed with respect to changes in the parameters they depend on. A measure of the information that one can extract about one or several parameters

from a given probability distribution is the so-called Fisher Information [Hel76, Hol11].

In our protocols, we want to estimate the intensity of each of the pulses θ (considered constant throughout the whole experiment) and the pulse-to-pulse phase difference $\Delta\phi$. They will be related to some physical observables which measure the population of the excited state after applying certain protocols. The precision of the parameters θ and $\Delta\phi$ is determined by the fluctuations of these observables and their variance can be obtained using standard error propagation theory. The Fisher Information will yield a measure of the available precision in the estimation of the parameters. Also, the variance of the estimation of a given parameter will be limited by the Cramer-Rao bound [Cra99], which sets the ultimate limit for the precision that we can achieve.

Let us see how to compute both the Fisher Information and the Cramer-Rao bound in the multivariate case [Rao45]. We consider $\vec{X} = (X_1, X_2, \ldots, X_i)^T$, a sample vector of observations with joint probability density function given by $f(\vec{X}|\vec{k})$, where $\vec{k} = (k_1, k_2, \ldots, k_i)^T$ is a parameter vector. We also define $h(\vec{k})$, a real valued function of $\vec{k}$ and $\mathbb{E}(\cdot)$ denotes the expectation value. Then, under suitable regularity conditions (see Refs. [Hel76, Hol11]) it holds that for any unbiased estimator $\hat{h}(\vec{X})$ of $h(\vec{k})$

$$\mathrm{Var}(\hat{h}) \geq D_h^T [I(\vec{k})]^{-1} D_h \tag{9.15}$$

where $I(\vec{k})$ is a matrix called the *Fisher Information matrix*

$$I_{ij}(\vec{k}) = \mathbb{E}\left(\frac{\partial}{\partial k_i} \log f(\vec{X}|\vec{k}) \frac{\partial}{\partial k_j} \log P(\vec{X}|\vec{k}) \right) \tag{9.16}$$

$$= -\mathbb{E}\left(\frac{\partial^2}{\partial k_i \partial k_j} \log f(\vec{X}|\vec{k}) \right) \tag{9.17}$$

and D_h is the vector of derivatives of $h(\vec{k})$

$$D_h = \left(\frac{\partial}{\partial k_1} h(\vec{k}), \frac{\partial}{\partial k_2} h(\vec{k}), \ldots, \frac{\partial}{\partial k_i} h(\vec{k}) \right). \tag{9.18}$$

We have used the standard error propagation theory and computed the Fisher Information as explained before in order to get fundamental lower bounds and practical estimates of each of the proposed protocols which, for $\Delta\phi$ and θ, as shown in Table 9.1.

9.5 Physical implementations

The protocols discussed admit many implementations. For concreteness, we focus on a setup with trapped ions, because of recent progress in connection with

ultrafast lasers [CMQ$^+$10, MSN$^+$13]. The long coherence times of ions, $t_{\rm coh} \sim 1\,$s [OYM$^+$07], allows to consider trains of up to $t_{\rm coh}/T \sim 10^8$ pulses from a typical comb with $f_{\rm rep} \sim 100\,$MHz [1]. In the Raman schemes, with one ion and one delay line, this allows to detect CEP fluctuations $\delta\Delta\phi \sim 10^{-8}$ rad and calibrate the comb offset below $\delta\Delta\phi/T \sim 1\,$Hz, a remarkable precision for 1 s interrogation time. The numbers improve with a 2-delay Raman scheme, reaching $\delta\Delta\phi \sim 10^{-15}$ where error sources become relevant. Precision decreases marginally, $\delta\Delta\phi \sim 10^{-5} - 10^{-10}$, using faster duty cycles with $\sim 1\,$ms of interrogation time.

Three-level Raman schemes

In real atoms, if the qubit states 0 and 1 are dipole-coupled by a comb, spontaneous emission may severely limit the total interrogation time. One solution is to use dipole-forbidden transitions restricted in practice to the $\theta \ll 1$ regime.

An attractive alternative is the Λ-scheme in Figure 9.4, where two long-lived states, $|0,1\rangle$, talk via an intermediate level, $|e\rangle$. Applying combs or other lasers with orthogonal polarizations on the legs of the Λ-scheme, we can create effective Rabi oscillations between $|0\rangle$ and $|1\rangle$ while keeping a small population in $|e\rangle$ so that spontaneous emission is negligible.

A simple way to minimize spontaneous emission is to turn the Λ- into a Raman scheme, detuning the lasers that couple $|0,1\rangle$ with $|e\rangle$. Such Raman processes mix well with our algorithms. Most easily, if we have already stabilized the phase of a CW laser, we can combine it with the pulses from the comb (see Figure 9.4a). This process enables an accurate determination of the CEP with respect to the cw source. The result is a sequence of effective unitaries with an average Rabi angle, θ', and a pulse phase $\phi'_m = \phi_m - \phi_{\rm ref}$, where $\phi_{\rm ref}$ is the phase of the stabilized source. The identifications $\theta \to \theta'$ and $\phi_m \to \phi'_m$ directly *translate all protocols above to this new setup.* Likewise, one may combine the FC with a stabilized one (see Figure 9.4b) and use our protocols to reconcile them.

A more interesting use of Raman transitions is to achieve self-referencing of the comb. For this, we use the scheme from Figure 9.4b, combining two pulses from the same comb, but with a relative delay, T_d, as in Figure 9.3b. This amounts to a self-referenced interferometric scheme based on time shifts, not requiring frequency shifting nor shearing [WD09]. The phases of both pulses effectively combine in a nontrivial way in the unitary associated to the Raman process, $\phi'_m = \phi_m - \phi_{m-N_d} = N_d\Delta\phi$. We can apply a sequence of N pulse pairs with an effective angle θ' that should optimally lie around $N\theta' \simeq \pi/2$,

$$U^{(1A,Raman)} = e^{-iN_d\Delta\phi\sigma_z} e^{iN\frac{\theta'}{2}\sigma_x} e^{iN_d\Delta\phi\sigma_z} \tag{9.19}$$

[1] We discuss the maximum number of phase-coherent consecutive pulses in.

and use Ramsey interferometry to measure both θ' and $\Delta\phi$. A generalization of protocols 2A and 2B is also possible using a linear optics circuit with two delay lines, so that each atom is hit by pairs of pulses with alternating phases $(\phi_m, \phi_{m-N_{d1}})$ and $(\phi_m, \phi_{m-N_{d2}})$. This leads to the sensitivities shown in the lower half of Table 9.1.

Note that using Raman schemes demands the setup to be interferometrically stable up to a fraction of a wavelength. When a single pulse interacts with a two-level atom it does not matter whether the delay is a multiple of the comb period, or fails by a small amount, $\delta T = T_d - N_d T$ ($|\delta T| < T$). This is so because only the CEP enters the unitary and this only contains information on $\nu_0 N_d T$. However, in Raman schemes, where two pulses overlap in time, their relative delay is a new parameter that influences the effective Rabi angle as well as the phase. In particular, the phase difference reads $\Delta\phi' = \Delta\phi + \omega\delta T$, with a contribution due to the interferometric path $c\delta T$, which must be separately stabilized.

To remove the need for interferometric stability, we can use a different approach in which the comb only interacts with one transition, $|1\rangle \to |e\rangle$, performing π rotations, while $|0\rangle$ is a dark state. The unperturbed and delayed pulses arrive closely in pairs, but without temporal overlap, implementing the sequence $|1\rangle \to -e^{i(\phi_m - \phi_{m-N_d})}|1\rangle$. Due to the lack of overlap, the delay errors drop from the equations and the effective operation is a phase gate in the qubit space. Spontaneous emission lowers the visibility and it is small because $|e\rangle$ is populated only a time $T_e = \mathcal{O}(\tau)$. Denoting by γ the spontaneous decay rate of $|e\rangle$, we may afford $N = -\log(\epsilon)/\gamma T_e$ pulses before the visibility decreases by ϵ. For a typical value $1/\gamma = 8$ ns and a safe $T_e = 100$ ps, visibility decreases just 10% for 200 pulses, sufficient to implement the last protocol in Table 9.1.

Raman transitions

Our Raman protocols are developed assuming that we can use ultrashort pulses to implement Raman transitions between two states, a and b, mediated by a third one, c, which remains unpopulated at the end of the pulse. (Due to the very short duration of the interrogation sequence, it is not necessary that c be unpopulated at all times, as is usual in STIRAP processes.) In particular, we need that such operations implement the same quantum gates and carry the same phase information as the original designs based on two-level systems. We are going to discuss both requirements and how they are achieved.

Note that Raman transitions with very short pulses have been demonstrated experimentally by the group of C. Monroe *et al.* in a series of works that implement quantum gates with trapped ions and pulsed lasers [HMM+10, MMM+06]. In these references, an interpretation based on Raman transitions induced by all the comb teeth is provided, but here we discuss a different one.

For us the key aspect of a Raman transition is the fact that the intermediate state, c, is completely depopulated at the end of the process. In order for this to happen, we need that the energy of the final state is similar to the energy of the original one. Intuitively, this implies that the inverse of the duration of the process has to be smaller than $\delta = \omega_{at} - \omega$, the detuning of the laser from the atomic transitions $\{a, b\} \leftrightarrow c$, but larger than the difference $|\omega_{ac} - \omega_{bc}|$. As shown in Figure 9.5, this qualitative appreciation remains true even for rather extreme cases. In those exaggerated plots, we see that pulses with a detuning $\delta \sim 0.2\omega_{at}$ work fine even when they only contain $10 - 20$ oscillations of the laser. In this regime the excited state c is significantly populated during the pulse, but it has a population of less than 10^{-3} at the end.

The other aspect we demand from these pulses is the fact that they must carry information on the phase of the laser. To check this, we analyze the interaction between the three-level atom and the light using a simple Hamiltonian,

$$\begin{aligned} H = {} & s(t)\cos(\omega t + \phi_1)\,|c\rangle\langle a| + \text{H.c.} \\ & + s(t)\cos(\omega t + \phi_2)\,|c\rangle\langle b| + \text{H.c} \\ & + \omega_{at}\,|c\rangle\langle c|\,, \end{aligned} \tag{9.20}$$

which under the RWA becomes

$$\begin{aligned} H_{RWA}(\phi_1, \phi_2) = {} & s(t)e^{i\phi_1}\,|c\rangle\langle a| + \text{H.c.} \\ & + s(t)e^{i\phi_2}\,|c\rangle\langle b| + \text{H.c} \\ & + (\omega_{at} - \omega)\,|c\rangle\langle c|\,. \end{aligned} \tag{9.21}$$

Note how $H_{RWA}(\phi_1, \phi_2)$ is related to $H_{RWA}(0, 0)$ through a unitary transformation $\exp(-i\phi_l\sigma^z_{ab})$ in the $\{a, b\}$ subspace, with the relative phase $\phi_l = \phi_2 - \phi_1$. In other words, according to the RWA the phase of the laser is mapped onto the relative phase between the states. The question is whether this behavior also follows from the original Eq. (9.20). We have performed numerical simulations of the three level system in Eq. (9.20) and the conclusions are: (i) There is always a small deviation between the real phase and the RWA approximation. (ii) This deviation decreases with decreasing detuning, as in the two-level system, an indication that it is due to the AC Stark shift effect. (iii) The actual phase experienced by the atom is a monotonic function of the laser phase, that is $\phi_s(\phi_l)$ grows with ϕ_l. These properties are exemplified in Figure 9.5c for a case with 2% detuning, where the deviations from the RWA are small, below 1%, but the nonlinear behavior is clear in the inset.

It would seem that, since we are striving for large accuracies in the stabilization protocol, errors of 1% would be enough to discard the protocols. However, we have to remember that we are not actually measuring the absolute phase, but the phase difference between pulses. Hence, stabilizing ϕ_s, which is a smooth, monotonic function of the laser phase, is equivalent to (and as accurate as) stabilizing ϕ_l.

9.6 Experimental errors

We can also account for AC Stark and Zeeman shifts in experiments. In both cases, the effect can be modelled as a random term in the Hamiltonian, $\epsilon(t)\sigma_z$, that makes the atomic levels fluctuate on timescales much longer than τ. This induces an uncertainty in $\Delta\phi$ of order $\sigma_\epsilon \times (t_{m+1} - t_m)$, where σ_ϵ is the standard deviation of $\epsilon(t)$ from its (zero) average, and t_m the arrival time of each pulse. This error is cancelled using spin-echo techniques [KAH64] or, more directly, in protocols 2A and 2B, by calibrating the delays so that consecutive pulses arrive closely spaced but without overlap, say 10 ps apart. A pessimistic AC Stark shift $\sigma_\epsilon \sim 100\,\mathrm{Hz}$ then induces an error $\leq 10^{-9}$ rad in $\Delta\phi$.

In all cases the effect is similar: a random term $\epsilon(t)\sigma_z$ makes the atomic levels fluctuate on a time scale much longer than τ. This induces a time-dependent uncertainty in $\Delta\phi$ of order $\sigma_\epsilon \times (t_{m+1} - t_m)$, where σ_ϵ is the standard deviation of $\epsilon(t)$ from its (zero) average, and t_m the arrival time of each pulse. This error is cancelled using spin-echo techniques [KAH64] or, more directly, in protocols 2A and 2B, by calibrating the delays so that the alternating pulses arrive closely spaced but without overlap, say 10 ps apart. A pessimistic AC Stark shift $\sigma_\epsilon \sim 100\,\mathrm{Hz}$ then induces an error $\leq 10^{-9}$ rad in the determination of $\Delta\phi$.

Another source of error is temperature: when atoms shake between pulses, they sample the laser's spatial variations of phase and intensity. We can eliminate such errors (i) working in a Raman configuration which transfers no net momentum to the atom and (ii) ensuring the lasers are not tightly focused. These techniques allow working with sympathetically Doppler cooled ions in fast experiments ($\sim 1 - 10\,\mathrm{ms}$ from ion reset to detection).

Dephasing

In this subsection, we would like to clarify with greater detail our estimates of the errors induced by small detunings and energy shifts. From the theoretical point of view we consider a general situation in which we split the energy levels of the atom into two contributions: the average spacing, ω_{at}, and random fluctuation of zero mean, $\epsilon(t)$, on top of it:

$$H = \frac{\omega_{at} + \epsilon(t)}{2}\sigma_z + s(t)\cos(\bar{\omega}t + \phi_m)\sigma_x. \tag{9.22}$$

We assume that $\epsilon(t)$ may be random but always smoothly varying, so that it will not only remain constant within a single pulse, but it will also change slowly between consecutive pulses, $\frac{d}{dt}\epsilon(t) \ll t_{m+1} - t_m$.

Evolution then splits into two consecutive operations. Before the arrival of the pulse, $s \simeq 0$, the atom evolves freely with fluctuating energy levels, while during the pulse $\epsilon(t) \simeq \epsilon_n$ and the external field is approximately constant. In

other words, the evolution after the waiting period and the pulse may be written as a product of two unitaries, $U_n = U_{\text{pulse},n}U_{\text{free},n}$. The free evolution is not significantly affected by the random fluctuations

$$U_{\text{free},n} = \exp\left(i\int_{t_{m-1}+\tau/2}^{t_m-\tau/2}[\omega_{at}+\epsilon(t)]dt\right) \simeq \exp(-i\omega_{at}T). \tag{9.23}$$

During the laser pulse, however, the interaction between the atom and the light is ruled by the equations 9.20 and 9.21. In previous sections we have seen that the effect of any detuning is (i) an extremely small change of the excitation probability, θ_n, and (ii) an equally small AC Stark shift that changes the effective phase seen by the atom.

If these deviations in the rotation angles remain constant within consecutive pulses, they will be taken into account and suppressed by our algorithms. In other cases, they will contribute to the errors in the estimation of the CEO. Assuming that we can bring the pulses close together, so that the time lapse between pulse arrivals is comparable or smaller than the timescale of the fluctuations, we will find that the difference between two consecutive Stark shifts is proportional to the difference in arrival times and to the standard deviation of such external field fluctuations, $\sigma_\epsilon \times (t_{m+1} - t_m)$.

Temperature

Temperature can also induce dephasing: if the atom is not still enough and it has time to move between pulses, it will see different phases of the pulse which depend on the distance traveled as $2\pi\Delta x/\lambda$. There are various ways to address this issue. We can make a simple estimate for a free atom in space, assuming that it is Doppler cooled. The temperature of the atom is

$$k_B T \simeq \hbar\Gamma, \tag{9.24}$$

where Γ is the natural linewidth of the cooling transition. Let us pessimistically assume that all this energy goes to the kinetic part, $\frac{1}{2}mv^2$, giving us an average velocity

$$v \simeq \sqrt{\frac{2k_BT}{m}} \simeq \sqrt{\frac{2\hbar\Gamma}{m}}. \tag{9.25}$$

From this we can estimate the phase errors as

$$\delta\phi \simeq \frac{2\pi}{\lambda}v(t_m - t_{m-1}). \tag{9.26}$$

We will adopt a pessimistic estimate, $\Gamma \simeq 200$ MHz, and a light atom such as Be, obtaining $v \sim 5$ m/s, which for a pulse separation of 10 ps gives 10^{-3} (or actually a bit larger if we consider the additional velocity due to the photon recoil).

The situation is very much improved when we arrange the lasers to work in a co-propagating Raman configuration such that there is no net momentum transfer to the atom. This is indeed a solution to the previous problem because the spatially dependent phase $\vec{k}\vec{x}$ acquired from one laser pulse is cancelled by that of the other laser $-\vec{k}\vec{x}$, making the whole process independent on the position of the atom. In this favorable circumstance, the only effect that temperature may have is when the intensity of the laser varies spatially. However, by using a laser beam which is not too tightly focused and confining the atoms to a small region, the effect of this inhomogeneity may be safely neglected.

9.7 Applications

In practical applications, the phase differences between pulses may be large. To avoid it wrapping around 2π, the number of pulses must be dynamically adjusted so that $N < 1/\Delta\phi$, increasing it only as the comb is better stabilized. Thus, measurement times cannot be longer than the typical time for the *random* fluctuations in ν_0. The precision limit is in practice set by the timescale at which we can provide useful feedback to the comb and not by the interferometric protocol.

We identify two frequency ranges where our protocol appears particularly useful. First, due to the technological and scientific interests of mid-infrared ($\lambda = 2.5 - 25$ μm) combs [SPH12], we propose to use Ba^+ ions (that feature several narrow transitions around 2 μm) to stabilize a visible or near-IR FC at $\Delta\phi = 0$ so that difference-frequency generation from two of its teeth can produce a stabilized mid-IR FC. Secondly, Mg^+ presents various transitions around 280 nm which could be used to stabilize combs in the near-UV, with application in high-harmonic generation and strong-field physics. We discuss in further details on current FC technologies, possible atom or ion stabilization systems, and a comparison between typical drift rates of an unlocked comb's frequency offset and the timescale of the atomic experiment.

Experimental sensitivities with trapped ions

As mentioned earlier, trapped atomic ions [LBMW03] constitute one of the most mature systems in the implementation of Quantum Information Processing and Communication (QIPC) protocols and technologies. Precision records have been achieved in the realization of single-qubit [BWC$^+$11] and two-qubit [BKRB08] unitaries and measurements [MSW$^+$08, BEO09], even reaching the threshold for fault-tolerant quantum error correction protocols [CLS$^+$04]. In the last couple of years, fantastic progress in the controlled interaction between trapped ions and ultrafast lasers has been achieved by the group of C. Monroe at U. Maryland, with the demonstration of two qubit entanglement in the weak-field ($\theta \ll 1$), many-pulses regime [HMM$^+$10], and also in the strong-field ($\theta \sim \pi$), few-pulses

f_{rep}(MHz)	T (ns)	τ (ps)	T_d (ps)
100	10	10	10-100

Table 9.2: Typical parameters of a frequency comb [CMQ$^+$10, MSN$^+$13].

regime [MSN$^+$13], where logic gates faster than the trap oscillation period become accessible [CMQ$^+$10, GRZC03]. Because of this, we think that the technology required to implement the phase-stabilization protocol that we propose is already available.

Typical parameters for the frequency comb are listed in Table 9.2. Pulses with a duration < 1 ps are nowadays easily accessible. On the other hand, one has to keep in mind that a pulse duration τ effectively limits the possible pulse delay times to $T_d > \tau$ in order to avoid an overlap of the electric fields corresponding to different pulses: depending on their polarizations, this may lead to several unwanted effects, from excitation of motional sidebands to total cancellation of the Raman transition [CMQ$^+$10]; in either case, the action of a pulse pair on the qubit would still be described by a unitary transformation U_i, but not the ones we have written down earlier, so that our model would break down. Therefore, we will stick to a comb with pulses of 1-10 ps.

In the following subsections, we present details of our calculations to estimate the achievable sensitivity enhancements for the protocols introduced in the main text of the article. At the end, we present an estimation of the ultimate sensitivity limit that can be reached with pulse shaping techniques.

Sensitivity enhancements with two-level protocols

Protocols 1A to 2B consider direct transitions induced only by the comb laser that we want to study. In practice, there are two ways that this can be achieved: dipole and quadrupole transitions. Dipole transitions are, for instance, the ${}^2S_{1/2}$–${}^2P_{1/2,3/2}$ lines in Yb$^+$ [MMM$^+$06]. These transitions have a typical linewidth of a few tens of MHz, which is comparable to f_{rep}. This implies that the time between consecutive pulses could be shorter than the lifetime of the excited state of the ion. A possible solution to this problem will be presented later on in this chapter.

An alternative is to rely on quadrupole transitions, as provided by the Ca$^+$ ion using as qubit states the electronic states $|S_{1/2}\rangle$ and $|D_{5/2}\rangle$ [HRB08]. The excited level now has a radiative lifetime $\tau_{\text{rad}} \sim 1$ s which is favorable to implement our ideas. The downside of quadrupole transitions is their lower coupling strength, which demands a more powerful laser to excite them. In practice, depending on the laser, this might imply that we have to work in the limit $\theta \ll 1$ (protocols

1A and 2A) but we will forget this in following discussion.

Following Table 9.2, let us consider a frequency comb composed of 10-ps pulses with $f_{\text{rep}} = 100$ MHz. This pulse duration is much shorter than the trap oscillation period (1 μs for a typical $\omega_{\text{trap}} = 2\pi \times 1$ MHz rf Paul trap) and allows us to disregard the motional state of the ion in the trap (cf. Eq. 9.2) as well as its micromotion, which may affect the performance of coherent protocols at longer times [MMM$^+$06]. Such a frequency comb, and a typical ion coherence time for the electronic qubit states of $^{40}Ca^+$, $\tau_{\text{coh}} \gtrsim 10$ ms [HRB08], allow $\tau_{\text{coh}} f_{\text{rep}} \gtrsim 10^6$ pulses to go through the ion before decoherence becomes relevant. We take a conservative estimate of $T_{\text{inter}} = 1\,\text{ms}$ for the time during which the ion is accumulating information on $\Delta\phi$. Then, the number of pulses interrogated is $N = T_{\text{inter}} f_{\text{rep}} = 10^5$. Using protocol 1B, this leads to an enhancement of the sensitivity by a factor $\chi_{1B} = N = 10^5$, which translates in a stabilization of the frequency offset down to $\delta\nu_0 \sim f_{\text{rep}}/N = 1/T_{\text{inter}} = 1\,\text{kHz}$.

This result can be improved by applying the protocols with two pulse sequences (2A,2B). To be specific, we can pair $N = 5 \times 10^4$ pulses with delays $N_d = 5 \times 10^4$ and reach, with protocol 2B, a resolution $\delta\nu_0 = f_{\text{rep}}/(NN_d) = 40\,\text{mHz}$. Let us note that duty cycles (i.e., the time required for ion Doppler cooling + probing $\Delta\phi$ + ion-state detection + ion-state reset) of ~ 1 ms have been reported [HGWS12], so assessing the precision using 1 ms for the interrogation time can be considered a conservative estimate.

Again, we remark that the numerical estimates in this chapter take into consideration only the coherence properties of trapped ions for the stabilization of an "ideal frequency comb", and technical issues inherent to currently available combs are not included in the calculations.

Sensitivity enhancement with self-referenced Raman schemes

Use of a Raman scheme lifts the restrictions related to the excited-state lifetime of the qubit as spontaneous decay is of no concern. Such a scheme has been implemented with various systems, e.g., Yb^+ with a qubit defined by the $^2S_{1/2}$ hyperfine states $|F = 1, m_F = 0\rangle = |1\rangle$ and $|F = 0, m_F = 0\rangle = |0\rangle$, which are split by $\omega_{at} = 12.642815$ GHz [CMQ$^+$10, MSN$^+$13]. For these states, coherence times larger than 1 second have been measured [OYM$^+$07].

Let us consider a pulse train of 1 ms, which provides 10^5 pulses at $f_{\text{rep}} = 100\,\text{MHz}$, and let us split this train on two lines. We seek to maximize the phase difference between them. To this end, we consider the available 10^5 pulses into sets of 10^4 and keep the first set, $\mathcal{S}_1 = \{1, \ldots, 10^4\}$, the set $\mathcal{S}_2 = \{10^4+1, \ldots, 2\times10^4\}$, and the last set, $\mathcal{S}_3 = \{9\times10^4+1, \ldots, 10^5\}$. The first set, $\mathcal{S}_1$, will be further split in two, so that half of the pulses are paired with those in $\mathcal{S}_2$ ($N_{d1} = 10^4$) and the other half with $\mathcal{S}_3$ ($N_{d2} = 9 \times 10^4$). Then, this optical setup yields a sensitivity

enhancement of order $\chi = N|N_{d2} - N_{d1}| = 8 \times 10^8$ or $\delta\nu_0 \sim 0.1\,\mathrm{Hz}$. If we allow ourselves a longer interrogation time of 1 s, the figures would improve down to a remarkable precision of $10^{-7}\,\mathrm{Hz}$.

We note that these high sensitivies are achievable almost independently of the underlying physical system used for the qubit: taking into account the continuum spectrum of each pulse, the only requirement is the proximity of ω_{at} and $\bar{\omega}$, a feature that can be engineered, and coherence times which are experimentally available.

Recursive refinement for large pulse-to-pulse phase shifts

In our studies we have found that the sensitivity of our metrology protocols can be written in the form $\sigma^{-1} \sim \chi(N)\sqrt{M}$, where the enhancement factor $\chi(N)$ arises from a clever accumulation of the phase. In practice, for a non-stabilized frequency comb with a large $\Delta\phi$ and an excessive number of pulses, the total accumulated phase, $\chi(N)\Delta\phi$, will wrap around the maximum measurable value, π, precluding a unique determination of $\Delta\phi$.

The appropriate way to deal with this situation is to do an iterative refinement of the phase measurement. As an example, let us consider a fiber-based frequency comb: these devices have an intrinsic width of the offset frequency of about 200 kHz. This means that, for $f_{\mathrm{rep}} = 100\,\mathrm{MHz}$, the phase ϕ_m may wrap around π in about $N = 500$ pulses. Hence, on the first iteration, it is meaningless to interrogate the laser for much longer than a few μs. This iteration allows us already to achieve a precision in $\Delta\phi$ of order $\sqrt{M}/500$ with protocol 1B. This initial value can be used to fed back to the laser setup, to lower $\Delta\phi$ and, on the next iteration, use a larger number of pulses.

Continuing with this example, a similar iterative refinement using protocol 2B and a fixed interrogation time $\sim 1\,\mu$s, would lead to an accuracy in the comb offset frequency of $\delta\nu_0 = f_{\mathrm{rep}}/(NN_d) = f_{\mathrm{rep}}/250^2 = 3\,\mathrm{Hz}$ using only one ion.

Ultimate precision limits with advanced pulse-shaping techniques

The protocols discussed so far achieve a great efficiency thanks to the number of pulses in a given interrogation time and possible delays among them. Note however, that the comb is mostly "empty": between every two pulses of about 10 ps, there is a waiting time $\sim 10\,\mathrm{ns}$ in which the ion is idle. It would seem that this empty time, combined with the coherence rates of the ions, set the ultimate limits for precision in our setup. However, if the laser has enough power, we can engineer a clever scheme to fill these empty gaps, increasing the effective repetition rate of the ion-laser interaction.

The trick here will be to "compress" the pulses so that a minimal time elapses between the end of one pulse and the beginning of the following one, but without modifying the phase of any one pulse. Such "compression" could be realized with an optical setup as depicted in Figure 9.6b. The key ingredient in this setup is an optical device which we call Beam Splitter and Delayer (BSD) that, given an intense ultrashort pulse, extracts a train of n replica pulses separated by a very short time Δt (see Figure 9.6a). An alternative BSD optical setup producing 8 replicas of an initial pulse has been recently implemented in [MSN+13].

We have analyzed these ideas in a particular application: doing metrology of the comb with a dipole transition. In this case the qubit of choice will not satisfy the condition $\tau_{\rm coh} \gg T$. Consider for example Ca^+ ions using the dipole-coupled $|S_{1/2}\rangle$ and $|P_{1/2}\rangle$ states for which $\tau_{\rm rad} \approx 7$ ns [ASC07]. In this setup we can still reach high precisions taking a relatively long pulse train of duration $\gg \tau_{\rm coh}$ as long as we ensure that all the pulses pass through the ion within a short time $\lesssim \tau_{\rm coh}$. On the other hand, we must still fulfill the requirement that different pulses do not overlap in time, that is $\Delta t \geq 2\tau$, which restricts us to use sets of up to $n \leq \min\{\tau_{\rm rad}, \tau_{\rm coh}\}/(2\tau) \sim 7$ ns/20 ps = 350 replica pulses. To be concrete, let us use the setup in Figure 9.6b to pick up two pulses with a relative delay of $T_d = N_d T = 10\,\mu$s —this corresponds to pulses 1 and $k = N_d = 10^3$ in the previous figure. The pulses will go through the BSD and be recombined, alternating replica pulses from each line. For a conservative $n = 4$ (not to lose too much power in each replica), $\Delta t = 4\tau$, and $N_d \approx 1000$, we obtain a phase sensitivity enhancement by a factor $nN_d \approx 4 \times 10^3$.

The same ideas can be applied to the Raman scheme by ensuring that the replica pulses from both lines arrive simultaneously to the ion. The result is an enhancement of the sensitivity by an additional factor n on top of the formulae derived in the main text of the paper.

We finally note that the very short probe times considered here, allow for the recollection of a large set of statistical data in a very short time. Together with the large sensitivity enhancements calculated, the presented schemes appear as very competitive protocols to measure and stabilize the carrier-envelope offset phase of frequency combs without the need for octave-spanning spectra.

Frequency comb technologies and candidate systems for their stabilization

To conclude, let us discuss in some more detail a couple of contexts where present frequency comb technology might benefit particularly from the protocol we propose.

The stabilization of frequency combs (FCs) in the optical frequency range (see Table 9.3) is nowadays quite well solved with several protocols, and there are also

Table 9.3: Regions of the electromagnetic spectrum where the phase stabilization protocol may be immediately applicable with the systems discussed.

Region	Wavelength	Energy	Interest
Near-UV	10-400 nm	3-124 eV	HHG, strong fields
Visible	390-750 nm	430-790 THz	Electronic transitions
Near-IR	0.8-2.5 μm	120-430 THz	Vibrational overtones
Mid-IR	2.5-25 μm	12-120 THz	Rot-vib structure

various technologies that enable their optical and spectral manipulations. The situation is not so advanced in other regions of the spectrum which nevertheless are of high relevance for several scientific and technological applications. For example, the mid-infrared (mid-IR) frequency range is where many characteristic molecular vibrational and rotational lines lie, which makes it of biological, chemical and physical interest for molecular detection and trace analysis. In addition, the atmosphere is relatively transparent at these wavelengths, which makes them valuable for astronomical studies. For these reasons, in the last years there is a growing interest in developing combs in this spectral region [SPH12]. Several technologies are being developed to realize these combs, such as mode-locked lasers, difference-frequency generation (DFG), optical parametric oscillators (OPOs), and microresonator-based Kerr combs [SPH12].

Let us focus on DFG, where one uses a nonlinear optical effect to transfer energy from the visible or near-IR into the mid-IR. For example, one can take a near-IR frequency comb with frequencies $\nu_n = nf_{\text{rep}} + f_{\text{ceo}}$ and mix it with a CW laser of frequency f_{cw}. Then, a new comb with frequencies $\nu_n^{\text{DFG}} = |\nu_n - f_{\text{ceo}}|$ is obtained. Achieving phase matching on all the desired bandwidth can be eased by using either two stabilized frequency combs, or two teeth of a single comb. One gets in the latter case $\nu_{n,m}^{\text{DFG}} = |n-m|f_{\text{rep}}$. It is clear that this approach can benefit from the protocol that we propose if one has access to a probe ion sensitive to mid-IR frequencies close to the desired range of $\nu_{n,m}^{\text{DFG}}$. A good candidate for this can be Ba^+, whose lower electronic states we show in Figure (a). We see that the transitions from the ground electronic state, $S_{1/2}$, to the long-lived, metastable $D_{3/2,5/2}$ states have wavelengths in the near-IR ($\lambda = 1760$, 2052 nm).

On the other side of the visible frequencies, there is also a growing number of laboratories working in the UV region of the spectrum, with research on strong-field physics, high-harmonic generation (HHG), ultra-fast processes, above-threshold ionization, and others. The well-known f-$2f$ technique has problems in the UV due to the difficulty of frequency-doubling at such high energies, for example because of the damage of the nonlinear material.

9.8 Conclusions and outlook

Summing up, in this chapter we presented several quantum inteferometric algorithms based on the idea that one atom may accumulate the effect of multiple laser pulses, computing their differences through the appropriate pulse ordering, intermediate gates and measurements. Multipulse quantum interferometry protocols provide a polynomial sensitivity enhancement with respect to conventional atom or Ramsey interferometry. MPQI can be used to detect temporal changes in the CEP of a frequency comb because the unitary implemented by a single pulse is sensitive to both the intensity and the CEP, and not to the pulse arrival time. The schemes presented are particularly suitable for non-octave spanning combs with a low intrinsic phase noise, such as high-power Ti:Sapphire lasers where significant phase noise is introduced by amplification stages.

A direct generalization our work would be extending our protocols beyond the rotating wave approximation, as we have already mentioned in Section 9.3. In addition to this, there are further properties of a frequency comb that could be studied using our methods, such as intensity fluctuations. This could be done by engineering different quantum algorithms that would help obtain other characteristics of the comb. The most interesting property of such device is the absolute phase or carrier-envelope phase (CEP). Characterizing the absolute phase would allow to correct each pulse of the train on its own, instead of relying on the pulse-to-pulse phase shift. This idea would give rise to stabilization methods which would significantly lower the time scale considered.

In contrast with standard interferometry, our methods allow to interrogate the probe several times and profit from the repetition, enhancing the measurement process. Our methods can be applied to improve the precision of other interferometric processes, in particular, we would like to explore the possibility of using MPQI to increase the precision of the LIGO experiment, which has been devised to detect gravitational waves.

On the other hand, we have assumed that the fluctuations for the dephasing are random but smoothly varying so we could also explore which are the weakest hypothesis that are needed to apply our method experimentally. We anticipate MPQI will enable new progress in fields as diverse as ultrafast science, frequency metrology and direct frequency-comb spectroscopy, or coherent control of molecular processes.

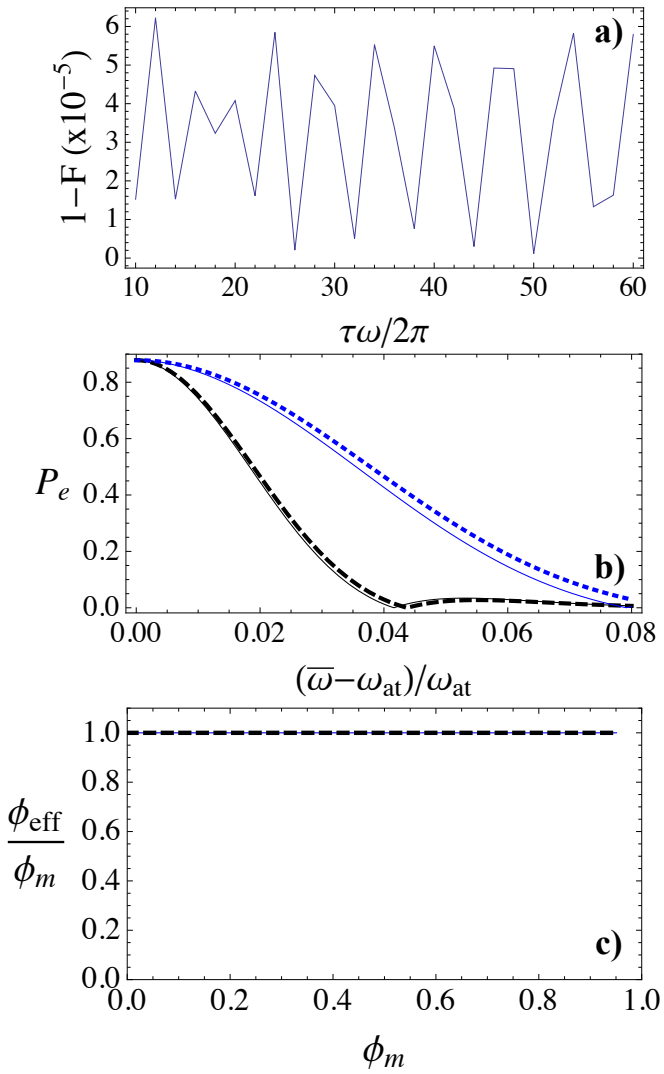

Figure 9.2: (a) Fidelity, F, between the unitary performed by the full model (9.2) and its description through the RWA (H_{RWA}), as a function of the pulse duration, τ, for a resonant pulse $\bar{\omega} = \omega_{at}$. (b) Qubit excitation probability for detuned pulses with $\tau = 30 \times 2\pi/\bar{\omega}$ (black) and $10 \times 2\pi/\bar{\omega}$ (blue), and comparable Rabi frequencies. We show the exact solutions (solid) and the RWA (dashed). (c) Effective phase, ϕ_{eff}, of the unitary U_m implemented by the full model (solid) and the RWA (dashed), as a function of the pulse phase, ϕ_m, for resonant pulses ($\bar{\omega} = \omega_{at}$.

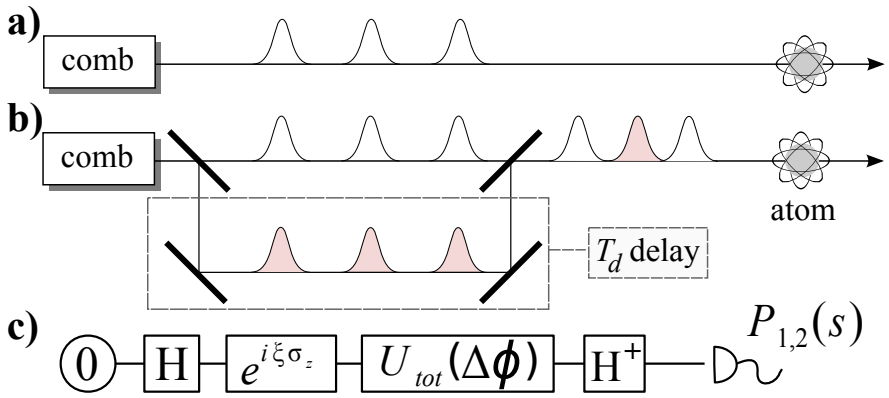

Figure 9.3: Comb phase measurement setups. A trapped atom interacts with (a) one train of pulses or (b) two trains with a delay T_d. (c) Additional gates and a final state interrogation build up a generalized Ramsey interferometry protocol to estimate $\Delta\phi$ and θ.

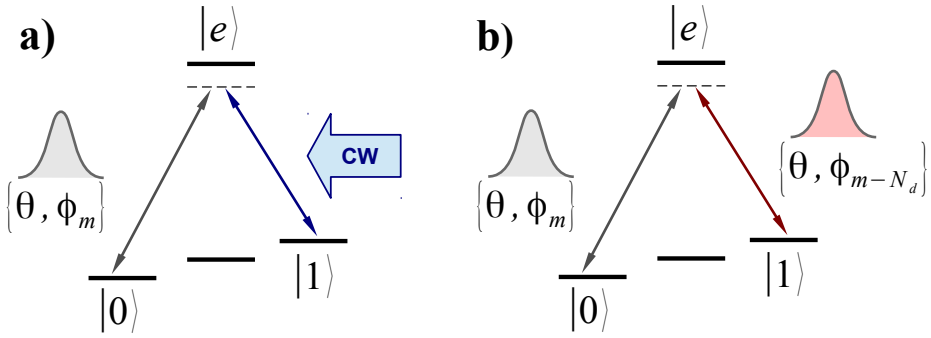

Figure 9.4: The m-th comb pulse interacts in a Raman setup with either (a) a CW laser signal or (b) another comb pulse. Controlling the polarization of the light and using the selection rules in atomic transitions we can ensure that each pulse or laser activates only one leg of the Λ scheme.

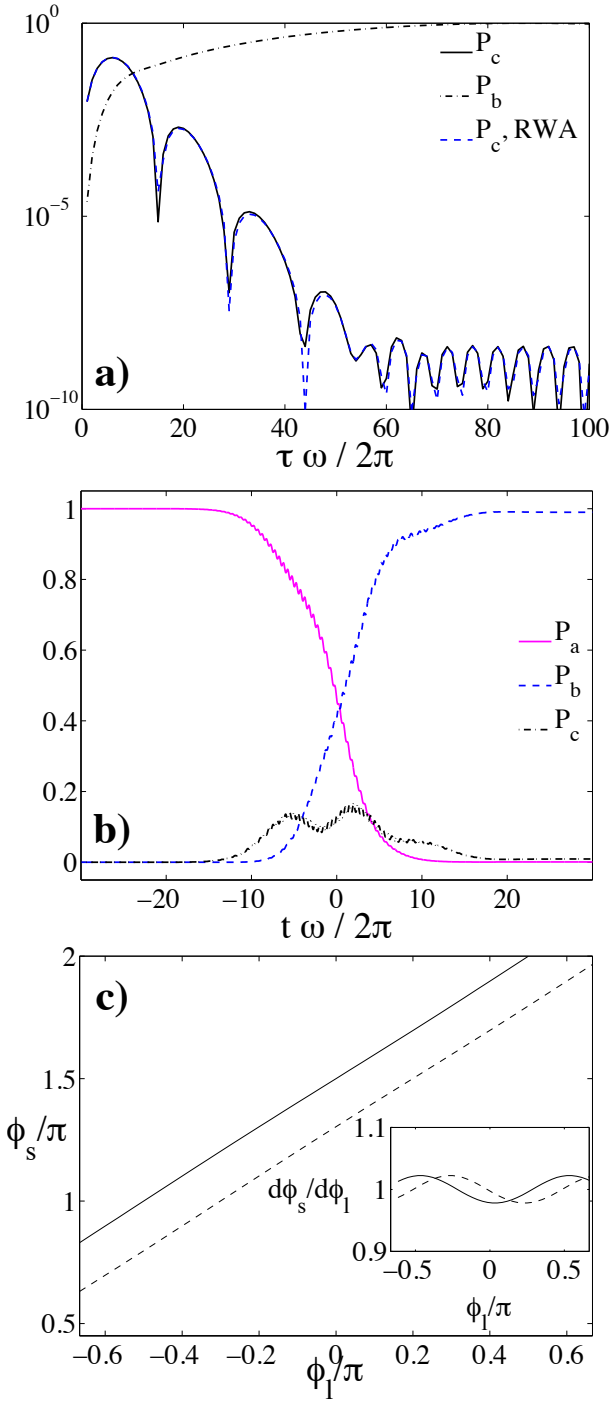

Figure 9.5: (a) Intermediate state population, P_c, and population of the state b, P_b, after a pulse of duration τ, for $\omega = 0.8\omega_{at}$ and Rabi frequency $\Omega = 0.033\omega_{at}$. (b) Evolution of the state populations during a pulse with $\Omega = 0.076\omega_{at}$, $\tau = 40\pi/\omega$ and $\omega = 0.8\omega_{at}$. (c) Relative phase between states b and a vs. the phase difference of the Raman pulse $\phi_l = \phi_2 - \phi_1$ in Eq. (9.20) for $\Omega = 0.016\omega$, $\omega = 0.98\omega_{at}$ and $\tau = 400\pi/\omega$. (Inset) Derivative $\frac{d\phi_s}{d\phi_l}$ confirming the monotonic behavior of ϕ_s.

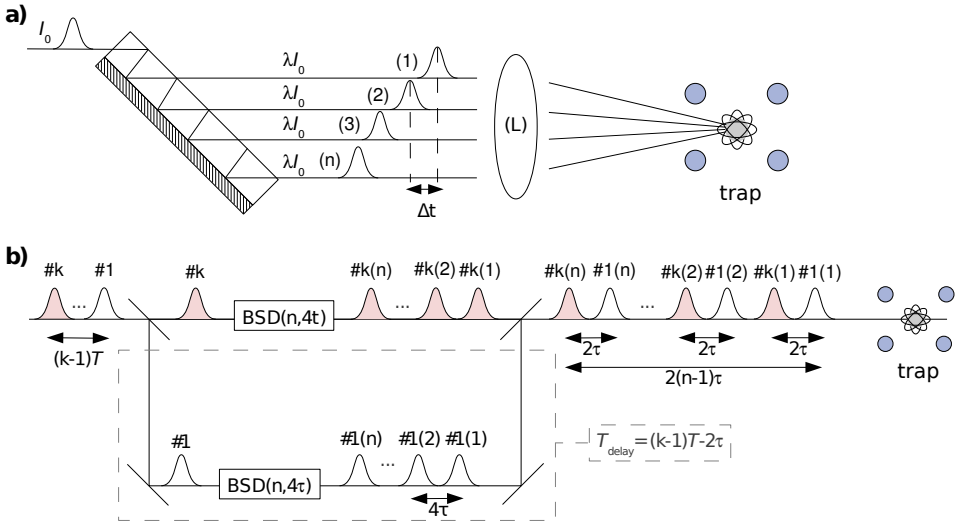

Figure 9.6: (a) A beam splitter and delayer (BSD) can be implemented by shining the laser pulse train into a semitransparent mirror facing a perfect mirror (shaded area). The incident angle of the beam determines the number, n, and delay, Δt, between the outgoing replica pulses, which are focused by a lens (L) onto the ion. (b) Optical setup with a delay line (dashed box) and two BSDs with delay $\Delta t = 4\tau$. This transforms the incident pulse train into a new train with interleaved pulses with a fixed phase difference between them and a total duration $2(n-1)\tau \ll kT$.

10 Conclusions and future work

In this chapter, we give a summary of the main conclusions and future lines of work discussed in this Thesis, which have also been presented and discussed in more detail in the last part of each chapter.

In Chapter 5, we have used matrix product states to quantify the entanglement between two disjoint regions of a one-dimensional system, in particular, a spin chain, in terms of the fractionalization in the magnetization of the chain. We have proved that a large fractional magnetization in such state must imply a large amount of entanglement in the system. In this line of work, it would be interesting to extend this result to higher dimensions using PEPS, or to perform numerical simulations to quantify the amount of entanglement in terms of the fractionalization of the magnetization in particular examples of spin chains.

In Chapter 6, we have shown that, for the state of a quantum spin chain, the impossibility of being well approximated by the ground state of a local Hamiltonian demands large entanglement. This backs up the physical intuition that when a system presents long-range interactions, any region of the state should be correlated to any other region and that this should imply a large amount of entanglement in the system. Formally, we have derived a lower bound for the entanglement entropy of a translationally invariant matrix product state which is not the ground state of any short-range gapped and frustration-free Hamiltonian and such that it is sufficiently far away from any other state with this property for any given interaction length. Furthermore, we show that the entanglement entropy scales with the range of the interaction and we obtain new bounds to approximate the reduced density matrix of the system using another reduced density matrix whose matrices have a smaller bond dimension. Following this line of research, it would be relevant to prove that a translational invariant matrix product state with a certain bond dimension D may be approximated using a translational invariant MPDO with a smaller bond dimension $\tilde{D} \leq D$ and such that the bound on the distance for the reduced density matrix for L particles scales linearly with the range of the interaction. This would allow us to give rigourous bounds on the accuracy of numerical algorithms for these types of states, such as the TEBD or the iTEBD, which rely on truncating the outcome of each infinitesimal evolution.

There are other interesting questions related to the tensor network representation of quantum many-body systems that we would like to explore in the future, such as whether it is possible to put forward efficient numerical methods to obtain the purifications of a given matrix product density operator using the sum of squares polynomial method.

In Chapters 7 and 8, we have derived new Lieb-Robinson bounds for a general model of finite dimensional systems interacting through a bosonic field that satisfies a Lieb-Robinson bound itself. We have applied these bounds to crystals of trapped ions and we have found out that the spread of spin correlations depends on the propagation speed of the phonons of the crystal as well as on the the efficiency with which the ions emit and reabsorb correlations from the phonons.

We have derived further Lieb-Robinson bounds in different regimes, such as the perturbative or the impulsive regime and we have obtained that the speed for the spread of correlations given by our bounds can be faster than the time scales in the experimental regimes currently considered. Finally, we have proposed an experimental scheme to measure retarded correlation functions via the crystal fluorescence, which allows to test the Lieb-Robinson bounds that we have derived in the impulsive regime.

To continue with this line of work, we would like to study further theoretical implications of these bounds, such as the efficiency of time-dependent density matrix renormalization group methods or the clustering of correlations.

On the other hand, a fruitful generalization of this work would be to extend these bounds to the continuous limit of the lattice and to prove whether the light cone implied by the Lieb-Robinson bound in the continuous is exacty the expected limit of the light cone obtained in the discrete case. This would allow us to address the propagation of quantum correlations in quantum field theories that are the uniform limit of discrete models of bosons interacting with fermions.

It would be also interesting to find other experimental schemes that could test the Lieb-Robinson bounds in different regimes. The most interesting regime would be the non-perturbative and non-impulsive (8.11), although we would also like to explore the perturbative regime, where the spread of correlations is slower.

In Chapter 9 we have presented several quantum inteferometric algorithms based on the idea that one atom may accumulate the effect of multiple laser pulses, computing their differences through the appropriate pulse ordering, intermediate gates and measurements. Multipulse quantum interferometry protocols provide a polynomial sensitivity enhancement with respect to conventional atom or Ramsey interferometry. MPQI can be used to detect temporal changes in the CEP of a frequency comb because the unitary implemented by a single pulse is sensitive to both the intensity and the CEP, and not to the pulse arrival time. The schemes presented are particularly suitable for non-octave spanning combs

with a low intrinsic phase noise, such as high-power Ti:Sapphire lasers where significant phase noise is introduced by amplification stages.

A direct generalization our work would be extending our protocols beyond the rotating wave approximation. In addition to this, there are further properties of a frequency comb that could be studied using our methods, such as intensity fluctuations. This could be done by engineering different quantum algorithms that would help obtain other characteristics of the comb such as the absolute phase or carrier-envelope phase (CEP). This idea would give rise to stabilization methods which would significantly lower the time scale considered.

In contrast with standard interferometry, our methods allow to interrogate the probe several times and profit from the repetition, enhancing the measurement process. Our methods can be applied to improve the precision of other interferometric processes, in particular, we would like to explore the possibility of using MPQI to increase the precision of the LIGO experiment, which has been devised to detect gravitational waves.

Bibliography

[AKLT87] I. Affleck, T. Kennedy, E. H. Lieb, and H. Tasaki. Rigorous results on valence-bond ground states in antiferromagnets. *Phys. Rev. Lett.*, 59(7):799–802, 1987.

[AKLT88] I. Affleck, T. Kennedy, E. H. Lieb, and H. Tasaki. Valence bond ground states in isotropic quantum antiferromagnets. *Commun. Math. Phys.*, 115(3):477–528, 1988.

[AKLV13] I. Arad, A. Kitaev, Z. Landau, and U. Vazirani. An area law and sub-exponential algorithm for 1D systems. *Proc. 4th Conf. Innov. Theor. Comput. Sci.*, page 18, 2013.

[Alt04] C. Altafini. Representing multiqubit unitary evolutions via Stokes tensors. *Phys. Rev. A*, 70(3):32331, 2004.

[ALV12] I. Arad, Z. Landau, and U. Vazirani. Improved one-dimensional area law for frustration-free systems. *Phys. Rev. B - Condens. Matter Mater. Phys.*, 85(19), 2012.

[ASC07] B. Arora, M. S. Safronova, and C. W. Clark. Blackbody radiation shift in a 43Ca+ ion optical frequency standard. *Phys. Rev. A*, 76(6):64501, 2007.

[BAA06] D. M. Basko, I. L. Aleiner, and B. L. Altshuler. Metal-insulator transition in a weakly interacting many-electron system with localized single-particle states. *Ann. Phys. (N. Y).*, 321(5):1126–1205, 2006.

[BBC+93] C. H. Bennett, G. Brassard, C. Crépeau, R. Jozsa, A. Peres, and W. K. Wootters. Teleporting an unknown quantum state via dual classical and Einstein-Podolsky-Rosen channels. *Phys. Rev. Lett.*, 70(13):1895–1899, 1993.

[BEO09] C. Burrell, J. Eisert, and T. Osborne. Information propagation through quantum chains with fluctuating disorder. *Phys. Rev. A*, 80(5):52319, 2009.

[BF04] H. Bruus and K. Flensberg. *Many-Body Quantum Theory in Condensed Matter Physics: An Introduction*. Oxford University Press, 2004.

[BHV06] S. Bravyi, M. B. Hastings, and F. Verstraete. Lieb-Robinson Bounds and the Generation of Correlations and Topological Quantum Order. *Phys. Rev. Lett.*, 97(5), 2006.

[BJKW00] O. Bratteli, P. E. T. Jorgensen, A. Kishimoto, and R. F. Werner. Pure states on Od. *J. Oper. Theory*, 43(1):97–143, 2000.

[BKRB08] J. Benhelm, G. Kirchmair, C. F. Roos, and R. Blatt. Towards fault-tolerant quantum computing with trapped ions. *Nat Phys*, 4(6):463–466, 2008.

[BOC+11] K. R. Brown, C. Ospelkaus, Y. Colombe, A. C. Wilson, D. Leibfried, and D. J. Wineland. Coupled quantized mechanical oscillators. *Nature*, 471(7337):196–199, 2011.

[Boh35] N. Bohr. Can quantum-mechanical description of physical reality be considered complete? *Phys. Rev.*, 48(8):696–702, 1935.

[BR01] H. J. Briegel and R. Raussendorf. Persistent Entanglement in Arrays of Interacting Particles. *Phys. Rev. Lett.*, 86(5):910–913, 2001.

[BSK+12] J. W. Britton, B. C. Sawyer, A. C. Keith, C.-C. J. Wang, J. K. Freericks, H. Uys, M. J. Biercuk, and J. J. Bollinger. Engineered two-dimensional Ising interactions in a trapped-ion quantum simulator with hundreds of spins. *Nature*, 484(7395):489–492, 2012.

[BUU+03] A. Baltuška, T. Udem, M. Uiberacker, M. Hentschel, E. Goulielmakis, C. Gohle, R. Holzwarth, V. S. Yakovlev, A. Scrinzi, T. W. Hänsch, and F. Krausz. Attosecond Control of Electronic Processes by Intense Light Fields. *Nature*, 421(6923):611–615, 2003.

[BW92] C. Bennett and S. Wiesner. Communication via one- and two-particle operators on Einstein-Podolsky-Rosen states. *Phys. Rev. Lett.*, 69(20):2881–2884, 1992.

[BW08] R. Blatt and D. Wineland. Entangled states of trapped atomic ions. *Nature*, 453(7198):1008–1015, 2008.

[BWC+11] K. R. Brown, A. C. Wilson, Y. Colombe, C. Ospelkaus, A. M. Meier, E. Knill, D. Leibfried, and D. J. Wineland. Single-qubit-gate error below 10ˆ-4 in a trapped ion. *Phys. Rev. A*, 84(3):30303, 2011.

[Car11] J. Cardy. Measuring Entanglement Using Quantum Quenches. *Phys. Rev. Lett.*, 106(15):150404, 2011.

[CBP+12] M. Cheneau, P. Barmettler, D. Poletti, M. Endres, P. Schausz, T. Fukuhara, C. Gross, I. Bloch, C. Kollath, and S. Kuhr. Light-cone-like spreading of correlations in a quantum many-body system. *Nature*, 481(7382):484–487, 2012.

[CEB+05] P. Cappellaro, J. Emerson, N. Boulant, C. Ramanathan, S. Lloyd, and D. G. Cory. Entanglement assisted metrology. *Phys. Rev. Lett.*, 94(2), 2005.

[CFIM12] E. Cuevas, M. Feigel'man, L. Ioffe, and M. Mezard. Level statistics of disordered spin-1/2 systems and materials with localized Cooper pairs. *Nat. Commun.*, 3:1128, 2012.

[CGW11] X. Chen, Z. C. Gu, and X. G. Wen. Classification of gapped symmetric phases in one-dimensional spin systems. *Phys. Rev. B - Condens. Matter Mater. Phys.*, 83(3), 2011.

[CHK+10] C. W. Chou, D. B. Hume, J. C. J. Koelemeij, D. J. Wineland, and T. Rosenband. Frequency comparison of two high-accuracy Al+ optical clocks. *Phys. Rev. Lett.*, 104(7):70802, 2010.

[CLS+04] J. Chiaverini, D. Leibfried, T. Schaetz, M. D. Barrett, R. B. Blakestad, J. Britton, W. M. Itano, J. D. Jost, E. Knill, C. Langer, R. Ozeri, and D. J. Wineland. Realization of quantum error correction. *Nature*, 432:602–605, 2004.

[CMPGR14] A. Cadarso, J. Mur-Petit, and J. J. García-Ripoll. Phase Stabilization of a Frequency Comb using Multipulse Quantum Interferometry. *Phys. Rev. Lett.*, 112:73603, 2014.

[CMQ+10] W. C. Campbell, J. Mizrahi, Q. Quraishi, C. Senko, D. Hayes, D. Hucul, D. N. Matsukevich, P. Maunz, and C. Monroe. Ultrafast Gates for Single Atomic Qubits. *Phys. Rev. Lett.*, 105(9):90502, 2010.

[CPHH15] L. Czekaj, A. Przysięza, M. Horodecki, and P. Horodecki. Quantum metrology: Heisenberg limit with bound entanglement. *Phys. Rev. A - At. Mol. Opt. Phys.*, 92(6), 2015.

[Cra99] H. Cramer. *Mathematical Methods of Statistics (PMS-9)*. Princeton Landmarks in Mathematics and Physics. Princeton University Press, 1999.

[CSE08] M. Cramer, A. Serafini, and J. Eisert. Locality of dynamics in general harmonic quantum systems. *Quantum Inf. many body quantum Syst.*, page 19, 2008.

[CSW+13] A. Cadarso, M. Sanz, M. M. Wolf, J. I. Cirac, and D. Pérez-García. Entanglement, fractional magnetization and long-range interactions. *Phys. Rev. B*, 87:035114, 2013.

[DCC+16] G. De las Cuevas, T. Cubitt, J. I. Cirac, M. M. Wolf, and D. Pérez-García. Fundamental limitations in the purifications of tensor networks. *J. Math. Phys.*, 57(071902), 2016.

[DKSV04] A. J. Daley, C. Kollath, U. Schollwöck, and G. Vidal. Time-dependent density-matrix renormalization-group using adaptive effective Hilbert spaces. *J. Stat. Mech. Theory Exp.*, 2004(2004):P04005, 2004.

[DSPGC13] G. De Las Cuevas, N. Schuch, D. Pérez-García, and J. I. Cirac. Purifications of multipartite states: limitations and constructive methods. *New J. Phys.*, 15(12):123021–123026, 2013.

[ECF+11] M. Endres, M. Cheneau, T. Fukuhara, C. Weitenberg, P. Schauß, C. Gross, L. Mazza, M. C. Bañuls, L. Pollet, I. Bloch, and S. Kuhr. Observation of Correlated Particle-Hole Pairs and String Order in Low-Dimensional Mott Insulators. *Science (80-.).*, 334(6053):200–203, 2011.

[ECP10] J. Eisert, M. Cramer, and M. B. Plenio. Area laws for the entanglement entropy. *Rev. Mod. Phys.*, 82(1):277–306, 2010.

[Eke91] A. K. Ekert. Quantum Cryptography Based on Bell's Theorem. *Phys. Rev. Lett.*, 67(6):661–663, 1991.

[EPR35] A. Einstein, B. Podolsky, and N. Rosen. Can Quantum-Mechanical Description of Physical Reality Be Considered Complete? *Phys. Rev.*, 47(10):777–780, 1935.

[FL09] D. Felinto and C. López. Theory for direct frequency-comb spectroscopy. *Phys. Rev. A*, 80(1):13419, 2009.

[FNW92] M. Fannes, B. Nachtergaele, and R. F. Werner. Finitely correlated states on quantum spin chains. *Commun. Math. Phys.*, 144(3):443–490, 1992.

[FRJ+04] T. M. Fortier, P. A. Roos, D. J. Jones, S. T. Cundiff, R. D. R. Bhat, and J. E. Sipe. Carrier-Envelope Phase-Controlled Quantum Interference of Injected Photocurrents in Semiconductors. *Phys. Rev. Lett.*, 92(14):147403, 2004.

[FSG+08] A. Friedenauer, H. Schmitz, J. T. Glueckert, D. Porras, and T. Schaetz. Simulating a quantum magnet with trapped ions. *Nat Phys*, 4(10):757–761, 2008.

[GH11] P. Griffiths and J. Harris. *Principles of Algebraic Geometry*. Wiley-Interscience, 2011.

[GHZ89] D. M. Greenberger, M. A. Horne, and A. Zeilinger. Going Beyond Bell's Theorem. *Bell's Theorem, Quantum Theory and Conceptions of the Universe*, 37(3):69–72, 1989.

[GK63] H. A. Gersch and G. C. Knollman. Quantum Cell Model for Bosons. *Phys. Rev.*, 129(2):959–967, 1963.

[GKZ+10] R. Gerritsma, G. Kirchmair, F. Zahringer, E. Solano, R. Blatt, and C. F. Roos. Quantum simulation of the Dirac equation. *Nature*, 463(7277):68–71, 2010.

[GLM04] V. Giovannetti, S. Lloyd, and L. Maccone. Quantum-enhanced measurements: beating the standard quantum limit. *Science (80- .)*., 306(5700):1330–6, 2004.

[GLM06] V. Giovannetti, S. Lloyd, and L. Maccone. Quantum metrology. *Phys. Rev. Lett.*, 96:010401, 2006.

[GLM11] V. Giovannetti, S. Lloyd, and L. Maccone. Advances in quantum metrology. *Nat. Photonics*, 5(4):222–229, 2011.

[GRZC03] J. J. García-Ripoll, P. Zoller, and J. Cirac. Speed Optimized Two-Qubit Gates with Laser Coherent Control Techniques for Ion Trap Quantum Computing. *Phys. Rev. Lett.*, 91(15):157901, 2003.

[GT07] N. Gisin and R. Thew. Quantum communication. *Nat. Photonics*, 1(3):165–171, 2007.

[Gur03] L. Gurvits. Classical deterministic complexity of Edmonds' Problem and quantum entanglement. In *Proc. thirty-fifth ACM Symp. Theory Comput. - STOC '03*, page 10, 2003.

[GW09] Z. C. Gu and X. G. Wen. Tensor-entanglement-filtering renormalization approach and symmetry-protected topological order. *Phys. Rev. B - Condens. Matter Mater. Phys.*, 80(15), 2009.

[Har77] R. Hartshorne. *Algebraic Geometry*. Springer-Verlag, 1977.

[Has06] M. B. Hastings. Solving gapped Hamiltonians locally. *Phys. Rev. B*, 73(8):85115, 2006.

[Has07a] M. B. Hastings. An area law for one-dimensional quantum systems. *J. Stat. Mech. Theory Exp.*, 2007(08):P08024, 2007.

[Has07b] M. B. Hastings. Entropy and entanglement in quantum ground states. *Phys. Rev. B*, 76(3):35114, 2007.

[Has07c] M. B. Hastings. Random unitaries give quantum expanders. *Phys. Rev. A*, 76(3):32315, 2007.

[Has09] M. B. Hastings. Locality in Quantum Systems. *Arxiv*, 1(3):1–26, 2009.

[Heg98] G. Hegerfeldt. Instantaneous spreading and Einstein causality in quantum theory. *Ann. Phys.*, 7(7-8):716–725, 1998.

[Hel76] C. W. Helstrom. *Quantum Detection and Estimation Theory*. Mathematics in Science and Engineering. Academic Press, 1976.

[HGWS12] B. Hemmerling, F. Gebert, Y. Wan, and P. O. Schmidt. A novel, robust quantum detection scheme. *New J. Phys.*, 14(2):23043, 2012.

[HHH96] M. Horodecki, P. Horodecki, and R. Horodecki. Separability of mixed states: necessary and sufficient conditions. *Phys. Lett. A*, 223(1-2):1–8, 1996.

[HHHH09] R. Horodecki, P. Horodecki, M. Horodecki, and K. Horodecki. Quantum entanglement. *Rev. Mod. Phys.*, 81:865, 2009.

[Hid94] K. Hida. Magnetic Properties of the Spin-1/2 Ferromagnetic-Ferromagnetic-Antiferromagnetic Trimerized Heisenberg Chain. *J. Phys. Soc. Japan*, 63(6):2359–2364, 1994.

[HK06] M. B. Hastings and T. Koma. Spectral Gap and Exponential Decay of Correlations. *Commun. Math. Phys.*, 265(3):781–804, 2006.

[HLB+11] M. Harlander, R. Lechner, M. Brownnutt, R. Blatt, and W. Hansel. Trapped-ion antennae for the transmission of quantum information. *Nature*, 471(7337):200–203, 2011.

[HMM+10] D. Hayes, D. N. Matsukevich, P. Maunz, D. Hucul, Q. Quraishi, S. Olmschenk, W. Campbell, J. Mizrahi, C. Senko, and C. Monroe. Entanglement of Atomic Qubits Using an Optical Frequency Comb. *Phys. Rev. Lett.*, 104(14):140501, 2010.

[HMM16] Z. Huang, C. Macchiavello, and L. Maccone. Usefulness of entanglement-assisted quantum metrology. *Phys. Rev. A - At. Mol. Opt. Phys.*, 94(1), 2016.

[Hol11] A. S. Holevo. *Probabilistic and Statistical Aspects of Quantum Theory*. Quaderni Monographs. Edizioni della Normale, 2011.

[HRB08] H. Häffner, C. F. Roos, and R. Blatt. Quantum computing with trapped ions. *Phys. Rep.*, 469(4):155–203, 2008.

[HS05] N. Hatano and M. Suzuki. Finding Exponential Product Formulas of Higher Orders. *Lect. Notes Phys.*, 679(4):37–68, 2005.

[HT13] P. Hauke and L. Tagliacozzo. Spread of Correlations in Long-Range Interacting Quantum Systems. *Phys. Rev. Lett.*, 111(20):207202, 2013.

[IEK+11] R. Islam, E. E. Edwards, K. Kim, S. Korenblit, C. Noh, H. Carmichael, G.-D. Lin, L.-M. Duan, C.-C. J. Wang, J. K. Freericks, and C. Monroe. Onset of a quantum phase transition with a trapped ion quantum simulator. *Nat. Commun.*, 2:377, 2011.

[ISC+13] R. Islam, C. Senko, W. C. Campbell, S. Korenblit, J. Smith, A. Lee, E. E. Edwards, C.-C. J. Wang, J. K. Freericks, and C. Monroe. Emergence and Frustration of Magnetism with Variable-Range Interactions in a Quantum Simulator. *Science (80-.).*, 340(6132):583–587, 2013.

[JCPG+13] J. Juenemann, A. Cadarso, D. Perez-Garcia, A. Bermudez, and J. J. Garcia-Ripoll. Lieb-Robinson bounds for spin-boson lattice models and trapped ions. *Phys. Rev. Lett.*, 111:230404, 2013.

[JDR+00] D. Jones, S. Diddams, J. Ranka, A. Stentz, R. Windeler, J. Hall, and S. Cundiff. Carrier-Envelope Phase Control of Femtosecond Mode-Locked Lasers and Direct Optical Frequency Synthesis. *Science (80-.).*, 288:635–640, 2000.

[KAH64] N. Kurnit, I. Abella, and S. Hartmann. Observation of a Photon Echo. *Phys. Rev. Lett.*, 13(19):567–568, 1964.

[KCK+10] K. Kim, M.-S. Chang, S. Korenblit, R. Islam, E. E. Edwards, J. K. Freericks, G.-D. Lin, L.-M. Duan, and C. Monroe. Quantum simulation of frustrated Ising spins with trapped ions. *Nature*, 465(7298):590–593, 2010.

[KGE14] M. Kliesch, D. Gross, and J. Eisert. Matrix-product operators and states: NP-hardness and undecidability. *Phys. Rev. Lett.*, 113(16), 2014.

[KKG+13] M. Knap, A. Kantian, T. Giamarchi, I. Bloch, M. D. Lukin, and E. Demler. Probing Real-Space and Time-Resolved Correlation Functions with Many-Body Ramsey Interferometry. *Phys. Rev. Lett.*, 111(14):147205, 2013.

[KPS+12] A. Khromova, C. Piltz, B. Scharfenberger, T. F. Gloger, M. Johanning, A. F. Varón, and C. Wunderlich. Designer Spin Pseudomolecule Implemented with Trapped Ions in a Magnetic Gradient. *Phys. Rev. Lett.*, 108(22):220502, 2012.

[Lau83] R. B. Laughlin. Anomalous Quantum Hall Effect: An Incompressible Quantum Fluid with Fractionally Charged Excitations. *Phys. Rev. Lett.*, 50(18):1395–1398, 1983.

[LBMW03] D. Leibfried, R. Blatt, C. Monroe, and D. Wineland. Quantum dynamics of single trapped ions. *Rev. Mod. Phys.*, 75(1):281–324, 2003.

[LHN+11] B. P. Lanyon, C. Hempel, D. Nigg, M. Müller, R. Gerritsma, F. Zähringer, P. Schindler, J. T. Barreiro, M. Rambach, G. Kirchmair, M. Hennrich, P. Zoller, R. Blatt, and C. F. Roos. Universal Digital Quantum Simulation with Trapped Ions. *Science (80-.).*, 334(6052):57–61, 2011.

[LKD02] H. Lee, P. Kok, and J. P. Dowling. A quantum Rosetta stone for interferometry. *J. Mod. Opt.*, 49(14-15):2325–2338, 2002.

[LR72] E. H. Lieb and D. W. Robinson. The finite group velocity of quantum spin systems. *Commun. Math. Phys.*, 28(3):251–257, 1972.

[LSM61] E. H. Lieb, T. Schultz, and D. Mattis. Two soluble models of an antiferromagnetic chain. *Ann. Phys. (N. Y).*, 16(3):407–466, 1961.

[Mac13] L. Maccone. Intuitive reason for the usefulness of entanglement in quantum metrology. *Phys. Rev. A - At. Mol. Opt. Phys.*, 88(4), 2013.

[Mag54] W. Magnus. On the exponential solution of differential equations for a linear operator. *Commun. Pure Appl. Math.*, 7(4):649–673, 1954.

[MMM+06] M. J. Madsen, D. L. Moehring, P. Maunz, R. N. Kohn, L.-M. Duan, and C. Monroe. Ultrafast Coherent Excitation of a Trapped Ion Qubit for Fast Gates and Photon Frequency Qubits. *Phys. Rev. Lett.*, 97(4):40505, 2006.

[MSL+04] A. Marian, M. C. Stowe, J. R. Lawall, D. Felinto, and J. Ye. United Time-Frequency Spectroscopy for Dynamics and Global Structure. *Science (80-.).*, 306(5704):2063–2068, 2004.

[MSN+13] J. Mizrahi, C. Senko, B. Neyenhuis, K. G. Johnson, W. C. Campbell, C. W. S. Conover, and C. Monroe. Ultrafast Spin-Motion Entanglement and Interferometry with a Single Atom. *Phys. Rev. Lett.*, 110(20):203001, 2013.

[MSW+08] A. Myerson, D. Szwer, S. Webster, D. Allcock, M. Curtis, G. Imreh, J. Sherman, D. Stacey, A. Steane, and D. Lucas. High-fidelity readout of trapped-ion qubits. *Phys. Rev. Lett.*, 100(20):200502, 2008.

[NC11] M. A. Nielsen and I. L. Chuang. *Quantum Computation and Quantum Information: 10th Anniversary Edition*. Cambridge University Press, 2011.

[NKD+11] M. Napolitano, M. Koschorreck, B. Dubost, N. Behbood, R. J. Sewell, and M. W. Mitchell. Interaction-based quantum metrology showing scaling beyond the Heisenberg limit. *Nature*, 471(7339):486–489, 2011.

[NOS06] B. Nachtergaele, Y. Ogata, and R. Sims. Propagation of Correlations in Quantum Lattice Systems. *J. Stat. Phys.*, 124(1):1–13, 2006.

[NRSS07] B. Nachtergaele, H. Raz, B. Schlein, and R. Sims. Lieb-Robinson Bounds for Harmonic and Anharmonic Lattice Systems. *Commun. Math. Phys.*, 286(3):1073–1098, 2007.

[NRSS09] B. Nachtergaele, H. Raz, B. Schlein, and R. Sims. Lieb-Robinson Bounds for Harmonic and Anharmonic Lattice Systems. *Commun. Math. Phys.*, 286(3):1073–1098, 2009.

[NS06] B. Nachtergaele and R. Sims. Lieb-Robinson bounds and the exponential clustering theorem. *Commun. Math. Phys.*, 265(1):119–130, 2006.

[NS10a] B. Nachtergaele and R. Sims. Lieb-Robinson Bounds in Quantum Many-Body Physics. *Contemp. Math.*, 529:141–176, 2010.

[NS10b] B. Nachtergaele and R. Sims. Much Ado About Something: Why Lieb-Robinson bounds are useful. *IAMP News Bull.*, pages 22–29, 2010.

[OFV10] J. L. O'Brien, A. Furusawa, and J. Vučković. Photonic quantum technologies. *Nat. Photonics*, 3(12):687–695, 2010.

[OGGS07] K. Osvay, M. Görbe, C. Grebing, and G. Steinmeyer. Bandwidth-independent linear method for detection of the carrier-envelope offset phase. *Opt. Lett.*, 32(21):3095–3097, 2007.

[OLA+08] C. Ospelkaus, C. E. Langer, J. M. Amini, K. R. Brown, D. Leibfried, and D. J. Wineland. Trapped-Ion Quantum Logic Gates Based on Oscillating Magnetic Fields. *Phys. Rev. Lett.*, 101(9):90502, 2008.

[Orú14] R. Orús. A practical introduction to tensor networks: Matrix product states and projected entangled pair states. *Ann. Phys. (N. Y).*, 349:117–158, 2014.

[OWC+11] C. Ospelkaus, U. Warring, Y. Colombe, K. R. Brown, J. M. Amini, D. Leibfried, and D. J. Wineland. Microwave quantum logic gates for trapped ions. *Nature*, 476(7359):181–184, 2011.

[OYA97] M. Oshikawa, M. Yamanaka, and I. Affleck. Magnetization Plateaus in Spin Chains: "Haldane Gap" for Half-Integer Spins. *Phys. Rev. Lett.*, 78(10):1984–1987, 1997.

[OYM+07] S. Olmschenk, K. C. Younge, D. L. Moehring, D. N. Matsukevich, P. Maunz, and C. Monroe. Manipulation and detection of a trapped Yb^+ hyperfine qubit. *Phys. Rev. A*, 76(5):52314, 2007.

[Par09] M. G. A. Paris. Quantum Estimation for Quantum Technology. *Int. J. Quantum Inf.*, 07(supp01):125–137, 2009.

[PBTO12] F. Pollmann, E. Berg, A. M. Turner, and M. Oshikawa. Symmetry protection of topological order in one-dimensional quantum spin systems. *Phys. Rev. B*, 85(7):075125, 2012.

[PC04] D. Porras and J. I. Cirac. Effective Quantum Spin Systems with Trapped Ions. *Phys. Rev. Lett.*, 92(20):207901, 2004.

[PC06] D. Porras and J. I. Cirac. Quantum Manipulation of Trapped Ions in Two Dimensional Coulomb Crystals. *Phys. Rev. Lett.*, 96(25):250501, 2006.

[Per96] Peres Asher. Separability Criterion for Density Matrices. *Phys. Rev. Lett.*, 77(August):1–3, 1996.

[PGSGG+10] D. Pérez-García, M. Sanz, C. E. González-Guillén, M. M. Wolf, and J. I. Cirac. Characterizing symmetries in a projected entangled pair state. *New J. Phys.*, 12(2):25010, 2010.

[PGVWC07] D. Pérez-García, F. Verstraete, M. M. Wolf, and J. I. Cirac. Matrix Product State Representations. *Quantum Inf. Comput.*, 7(5):401–430, 2007.

[PGW+01] G. G. Paulus, F. Grasbon, H. Walther, P. Villoresi, M. Nisoli, S. Stagira, E. Priori, S. De Silvestri, and Others. Absolute-phase phenomena in photoionization with few-cycle laser pulses. *Nature*, 414(6860):182–184, 2001.

[PGWS+08] D. Pérez-García, M. M. Wolf, M. Sanz, F. Verstraete, and J. I. Cirac. String Order and Symmetries in Quantum Spin Lattices. *Phys. Rev. Lett.*, 100(16):167202, 2008.

[PISK12] D. Porras, P. A. Ivanov, and F. Schmidt-Kaler. Quantum Simulation of the Cooperative Jahn-Teller Transition in 1D Ion Crystals. *Phys. Rev. Lett.*, 108(23):235701, 2012.

[PMCV10] B. Pirvu, V. Murg, J. I. Cirac, and F. Verstraete. Matrix product operator representations. *New J. Phys.*, 12:1–9, 2010.

[Pou10] D. Poulin. Lieb-Robinson Bound and Locality for General Markovian Quantum Dynamics. *Phys. Rev. Lett.*, 104(19):190401, 2010.

[PS95] M. E. Peskin and D. V. Schroeder. *An introduction to quantum field theory*. Advanced book program. Westview Press Reading (Mass.), Boulder (Colo.), 1995.

[PSHKMK09] I. Prémont-Schwarz, A. Hamma, I. Klich, and F. Markopoulou-Kalamara. Lieb-Robinson bounds for commutator-bounded operators. *Phys. Rev. A*, 81(4):5, 2009.

[PV05] M. B. Plenio and S. Virmani. An introduction to entanglement measures. *Quant. Inf. Comput.*, 7(1,2):1–51, 2005.

[Rao45] C. R. Rao. Information and the accuracy attainable in the estimation of statistical parameters. *Bull. Calcutta Math. Soc.*, 37:81–91, 1945.

[Rén61] A. Rényi. On measures of entropy and information. *Entropy*, 547(c):547–561, 1961.

[RGL+14] P. Richerme, Z.-X. Gong, A. Lee, C. Senko, J. Smith, M. Foss-Feig, S. Michalakis, A. V. Gorshkov, and C. Monroe. Non-local propagation of correlations in quantum systems with long-range interactions. *Nature*, 511(7508):198–201, 2014.

[RHUH99] J. Reichert, R. Holzwarth, T. Udem, and T. W. Hänsch. Measuring the frequency of light with mode-locked lasers. *Opt. Commun.*, 172(1-6):59–68, 1999.

[RLR+04] C. F. Roos, G. P. T. Lancaster, M. Riebe, H. Häffner, W. Hänsel, S. Gulde, C. Becher, J. Eschner, F. Schmidt-Kaler, and R. Blatt. Bell States of Atoms with Ultralong Lifetimes and Their Tomographic State Analysis. *Phys. Rev. Lett.*, 92(22):220402, 2004.

[RLR+08] C. Roos, G. Lancaster, M. Riebe, H. Haeffner, W. Haensel, S. Gulde, C. Becher, J. Eschner, F. Schmidt-Kaler, and R. Blatt. Tomography of entangled massive particles. *ArXiv*, (1):1–4, 2008.

[RLS+05] P. A. Roos, X. Li, R. P. Smith, J. A. Pipis, T. M. Fortier, and S. T. Cundiff. Solid-state carrier-envelope phase stabilization via quantum interference control of injected photocurrents. *Opt. Lett.*, 30(7):735–737, 2005.

[Rob29] H. P. Robertson. The Uncertainty Principle. *Phys. Rev.*, 34(1):163–164, 1929.

[Sch35] E. Schrödinger. Discussion of Probability Relations between Separated Systems. *Math. Proc. Cambridge Philos. Soc.*, 31(04):555–563, 1935.

[Sch11] U. Schollwock. The density-matrix renormalization group in the age of matrix product states. *Ann. Phys. (N. Y).*, 326(1):96–192, 2011.

[Sha48] C. E. Shannon. A Mathematical Theory of Communication. *Bell Syst. Tech. J.*, 27(3):379–423, 1948.

[SLRD13] J. Schachenmayer, B. P. Lanyon, C. F. Roos, and A. J. Daley. Entanglement Growth in Quench Dynamics with Variable Range Interactions. *Phys. Rev. X*, 3(3):31015, 2013.

[SM10] K.-A. B. Soderberg and C. Monroe. Phonon-mediated entanglement for trapped ion quantum computing. *Reports Prog. Phys.*, 73(3):36401, 2010.

[SPGC11] N. Schuch, D. Pérez-García, and I. Cirac. Classifying quantum phases using matrix product states and projected entangled pair states. *Phys. Rev. B - Condens. Matter Mater. Phys.*, 84(16), 2011.

[SPGWC10] M. Sanz, D. Pérez-García, M. M. Wolf, and J. I. Cirac. A quantum version of Wielandt's inequality. *IEEE Trans. Inf. Theory*, 56(9):4668–4673, 2010.

[SPH12] A. Schliesser, N. Picqué, and T. W. Hänsch. Mid-infrared frequency combs. *Nat. Photonics*, 6:440, 2012.

[SPS12] C. Schneider, D. Porras, and T. Schaetz. Experimental quantum simulations of many-body physics with trapped ions. *Reports Prog. Phys.*, 75(2):24401, 2012.

[Sre93] M. Srednicki. Entropy and area. *Phys. Rev. Lett.*, 71(5):666–669, 1993.

[SRL+05] P. O. Schmidt, T. Rosenband, C. Langer, W. M. Itano, J. C. Bergquist, and D. J. Wineland. Spectroscopy using quantum logic. *Science*, 309(5735):749–752, 2005.

[SRW+14] R. C. Sterling, H. Rattanasonti, S. Weidt, K. Lake, P. Srinivasan, S. C. Webster, M. Kraft, and W. K. Hensinger. Fabrication and operation of a two-dimensional ion-trap lattice on a high-voltage microchip. *Nat. Commun.*, 5:3637, 2014.

[STG99] H. L. Stormer, D. C. Tsui, and A. C. Gossard. The fractional quantum Hall effect. *Rev. Mod. Phys.*, 71(2):S298—-S305, 1999.

[SWL09] R. Schmied, J. H. Wesenberg, and D. Leibfried. Optimal Surface-Electrode Trap Lattices for Quantum Simulation with Trapped Ions. *Phys. Rev. Lett.*, 102(23):233002, 2009.

[SWPGC09] M. Sanz, M. M. Wolf, D. Pérez-García, and J. I. Cirac. Matrix product states: Symmetries and two-body Hamiltonians. *Phys. Rev. A*, 79(4):42308, 2009.

[SWVC08] N. Schuch, M. M. Wolf, F. Verstraete, and J. I. Cirac. Entropy scaling and simulability by matrix product states. *Phys. Rev. Lett.*, 100(3), 2008.

[SZ97] M. Scully and M. Zubairi. *Quantum Optics*. Cambridge, 1997.

[Ter00] B. M. Terhal. Bell inequalities and the separability criterion. *Phys. Lett. Sect. A Gen. At. Solid State Phys.*, 271(5-6):319–326, 2000.

[TGB+13] T. R. Tan, J. P. Gaebler, R. Bowler, Y. Lin, J. D. Jost, D. Leibfried, and D. J. Wineland. Demonstration of a Dressed-State Phase Gate for Trapped Ions. *Phys. Rev. Lett.*, 110(26):263002, 2013.

[TH00] B. M. Terhal and P. Horodecki. A Schmidt number for density matrices. *Phys. Rev. A*, 61:040301(R), 2000.

[TSG82] D. C. Tsui, H. L. Stormer, and A. C. Gossard. Two-Dimensional Magnetotransport in the Extreme Quantum Limit. *Phys. Rev. Lett.*, 48(22):1559–1562, 1982.

[UHH02] T. Udem, R. Holzwarth, and T. W. Hänsch. Optical frequency metrology. *Nature*, 416(6877):233–237, 2002.

[VC04] F. Verstraete and J. I. Cirac. Renormalization algorithms for Quantum-Many Body Systems in two and higher dimensions. *arXiv Prepr. cond-mat/0407066*, pages 1–5, 2004.

[VC06] F. Verstraete and J. I. Cirac. Matrix product states represent ground states faithfully. *Phys. Rev. B - Condens. Matter Mater. Phys.*, 73(9), 2006.

[VGRC04] F. Verstraete, J. J. García-Ripoll, and J. I. Cirac. Matrix product density operators: Simulation of finite-temperature and dissipative systems. *Phys. Rev. Lett.*, 93(20), 2004.

[Vid03] G. Vidal. Efficient Classical Simulation of Slightly Entangled Quantum Computations. *Phys. Rev. Lett.*, 91(14):147902, 2003.

[Vid04] G. Vidal. Efficient Simulation of One-Dimensional Quantum Many-Body Systems. *Phys. Rev. Lett.*, 93(4):40502, 2004.

[Vid07] G. Vidal. Entanglement renormalization. *Phys. Rev. Lett.*, 99(22), 2007.

[WD09] I. A. Walmsley and C. Dorrer. Characterization of ultrashort electromagnetic pulses. *Adv. Opt. Photon.*, 1:308–437, 2009.

[Wer89] R. F. Werner. Quantum states with Einstein-Podolsky-Rosen correlations admitting a hidden-variable model. *Phys. Rev. A*, 40(8):4277–4281, 1989.

[WF04] S. R. White and A. E. Feiguin. Real-time evolution using the density matrix renormalization group. *Phys. Rev. Lett.*, 93(7), 2004.

[WHH+09] T. Wittmann, B. Horvath, W. Helml, M. G. Schätzel, X. Gu, A. L. Cavalieri, G. G. Paulus, and R. Kienberger. Single-shot carrier–envelope phase measurement of few-cycle laser pulses. *Nat. Phys.*, 5(5):357–362, 2009.

[Whi92] S. R. White. Density matrix formulation for quantum renormalization groups. *Phys. Rev. Lett.*, 69(19):2863–2866, 1992.

[Whi93] S. R. White. Density-matrix algorithms for quantum renormalization groups. *Phys. Rev. B*, 48(14):10345–10356, 1993.

[WJK+10] W. Wasilewski, K. Jensen, H. Krauter, J. J. Renema, M. V. Balabas, and E. S. Polzik. Quantum Noise Limited and Entanglement-Assisted Magnetometry. *Phys. Rev. Lett.*, 104(13):133601, 2010.

[WL11] D. J. Wineland and D. Leibfried. Quantum information processing and metrology with trapped ions. *Laser Phys. Lett.*, 8(3):175–188, 2011.

[WMK+11] A. L. Wolf, J. Morgenweg, J. C. J. Koelemeij, S. A. van den Berg, W. Ubachs, and K. S. E. Eikema. Direct frequency-comb spectroscopy of a dipole-forbidden clock transition in trapped Ca+40 ions. *Opt. Lett.*, 36(1):49–51, 2011.

[Wol12] M. M. Wolf. *Quantum Channels and Operators: A Guided Tour*. Niels-Bohr Institute, 2012.

[WvdBUE09] A. Wolf, S. van den Berg, W. Ubachs, and K. Eikema. Direct Frequency Comb Spectroscopy of Trapped Ions. *Phys. Rev. Lett.*, 102(22):223901, 2009.

[WZU+05] S. Witte, R. T. Zinkstok, W. Ubachs, W. Hogervorst, and K. S. E. Eikema. Deep-ultraviolet quantum interference metrology with ultrashort laser pulses. *Science (80-.).*, 307(5708):400{\textendash}403, 2005.

[XSP+96] L. Xu, C. Spielmann, A. Poppe, T. Brabec, F. Krausz, and T. W. Hänsch. Route to phase control of ultrashort light pulses. *Opt. Lett.*, 21(24):2008–2010, 1996.

[YC05] J. Ye and S. T. Cundiff. *Femtosecond optical frequency comb: principle, operation, and applications*. Springer Verlag, 2005.